POLITECNICO DI TORINO
Repository ISTITUZIONALE

Head length's impact on taper junction stability in total hip prosthesis

Original
Head length's impact on taper junction stability in total hip prosthesis / Bologna, F.A., Putame, G., Audenino, A., Terzini, M.. - ELETTRONICO. - (2023). (18th International Symposium on Computer Methods in Biomechanics and Biomedical Engineering Paris (France) 3-5 May 2023).

Availability:
This version is available at: 11583/2978377 since: 2023-05-07T16:11:15Z

Publisher:
CMBBE Symposium Secretariat c/o Codan Consulting

Published
DOI:

Terms of use:

This article is made available under terms and conditions as specified in the corresponding bibliographic description in the repository

Publisher copyright

(Article begins on next page)

25 November 2026



CMBBE 2023 SYMPOSIUM

18th International Symposium on Computer Methods in Biomechanics and Biomedical Engineering

3 - 5 May 2023, Paris, France

CHALLENGES IN COMPUTATIONAL BIOMECHANICS FOR TOMORROW'S HEALTHCARE SYSTEMS

ABSTRACT BOOK POSTER PRESENTATIONS

www.cmbbe-symposium.com

Arts et Métiers Institute of Technology

Cardiff University / Prifysgol Caerdydd

société de BIOMECANIQUE



MORPHING THE LEFT ATRIUM TO COMPARE AND CLASIFFY THE LEFT ATRIAL APPENDAGE STASIS PATTERNS ACROSS PATIENTS

Jorge Dueñas-Pamplona*(1), Javier García (1),
José Sierra-Pallares (2), Javier Goicolea (3), Francisco Castro (2)

1. Departamento Ingeniería Energética. ETSII Universidad Politécnica de Madrid, Spain;
2. Departamento Ingeniería Energética y Fluidomecánica. EII Universidad de Valladolid, Spain;
3. Hospital Universitario Puerta de Hierro Majadahonda, Spain

1. Introduction

Atrial fibrillation (AF) is the most common type of cardiac arrythmia. During an episode of AF, the atrium contracts irregularly and ineffectively, increasing the risk of intra-cardiac thrombosis [1]. These thrombi can travel to the brain, which can then be the cause of stroke. Although the left atrial appendage (LAA) is known to be the most frequent site of intracardiac thrombosis, the mechanistic link between thrombus formation, flow patterns, and morphological parameters is not fully understood [2].

Our approach to this work, based in rigging and parameterisation of patient-specific atrial geometries [3], allows an extensive analysis of different parameters that are known to affect LAA stasis under extreme AF conditions, quantifying their influence on the formation of a dead volume within the LAA. To illustrate this approach, an extended Design of Experiments (DoE) has been proposed, seeking to determine how parameters such as LAA volume, number of lobes, and relative position are linked with stroke risk for a particular patient and how common stasis patterns can be observed in the different patients under study.

2. Materials and Methods

Atrial CT images of 3 cardiac patients have been segmented, reconstructing atrial geometries. Then, a 'morphing' methodology [3] was applied to each of the geometries: the first step, or 'rigging', provided each geometry with an armature, which was designed to apply plausible variations of the geometric parameters. The second step, called 'skinning', linked each of the bones to a group of nodes on the atrial surface, distributing the weights by using the envelope technique.

A tetrahedral volumetric mesh was then constructed from each of the generated geometries, allowing us to perform CFD atrial parametric simulations departing from patient-specific geometries and boundary conditions.

3. Discussion and Conclusions

We present a parametric study with extended DoE exploring the relationship between several geometric parameters and blood stasis in the LAA, within a physiological range in the absence of atrial contraction due to AF. The approach allowed us to take it a step further from previous atrial parametrical works, allowing us to quantify and compare stasis and dead volume when applying geometrical variations to patient-specific geometries. Furthermore, the approach provided us with a framework to identify common stasis patterns while applying morphological variations between different patient-specific geometries, illustrating some interesting features associated with thrombi formation.

4. References

1. Wolf PA et al., Stroke. 22(8):983-988 (1991)
2. García-Villalba M. et al., Fron. Physiol., 12:596596 (2021)
2. Dueñas-Pamplona J et al., Appl. Math. Model.; 108:27-45 (2022)

Acknowledgements:
This work was supported by the 'Ministerio de Ciencia, Innovación y Universidades' of Spain under the **DPI2017-83911-R** contract. The 'Programa Propio de la Universidad Politécnica de Madrid', and the 'Programa de Excelencia para el Profesorado Universitario de la Comunidad de Madrid' are acknowledged.

CMBBE2023
18th International Symposium on Computer Methods in Biomechanics and Biomedical Engineering
3 - 5 May 2023, Paris, France
Arts et Métiers Institute of Technology
Institut de Biomécanique Humaine Georges Charpak
155 boulevard de l'Hôpital 75013 Paris France
www.cmbbe-symposium.com

COMPARING THE SURFACE PROPERTIES OF THE TRAPEZOID METACARPAL JOINT WITH DIFFERENT TREATMENTS

Lin Fu (1), Lukasz Kaczmarek (1), Yaodong Gu (2)

1. Institute of Materials Science and Engineering, Lodz University of Technology, Lodz, Poland

2. Faculty of Sports Science, Ningbo University, Ningbo, China

1. Introduction

Hand injury is going to be a major clinical problem for people, especially hand osteoarthritis (OA). Titanium, considering as one of the most attractive materials in the area of aerospace, energy, shipbuilding, and medical applications [1-3], due to the favorable mechanical properties and corrosion resistance. More and more imlants designers are focusing on extending the service life of implants and reducing the risks of cartilage inflammation. We aim to consider about the mechanical properties in the joint of trapeziod metarcapal (TMC).

2. Materials and Methods

CT image data of TMC were obtained with dominant hands of male (age/45year, weight/67kg). The tested material Ti6Al4V (Grade 5, wt%: 6Al, 4V, 0.25Fe, 0.2O, 89.75%Ti) was applied in our experiments. All specimens were treated by thermal chemical treatment with oxygen and nitrogen.

Table 1: Parameters for different treatments of specimens

Treatments	Temperature	Gas flow
Nitrided	950℃	10sccm
Oxidized	900℃	6sccm

Finite element method was used in all subjects to analyze the deformation and strain of the cartilage between two bones.

Figure 1: The protype modelling with finite element method



3. Results

Figure 2: The deformation and strain distribution of cartilage

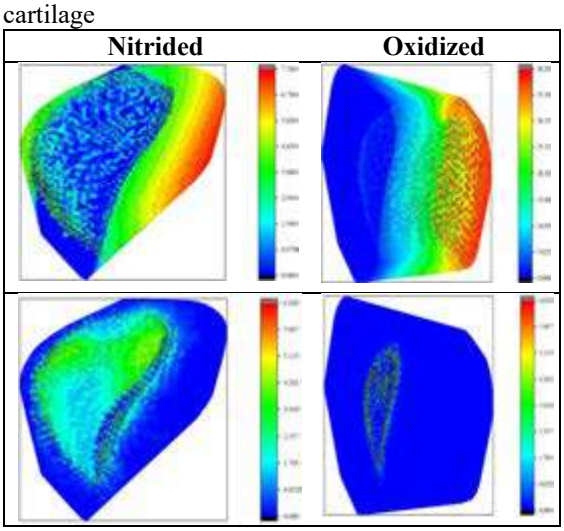

Note: First column represents the deformation of cartilage; the second column represents the strain of the cartilage.

Obvious deformation was observed at the edge of the contact surface. Oxidized sample showed less strain but more deformation, comparing to nitrided sample.

4. Discussion and Conclusions

Chemical surface treated samples represented better mechanical properties. Less strain could be found with oxidized sample. Patient-specific implant technology will enhance the function and life service of implants.

5. References

1. Brusa, E., Sesana, R., & Ossola, E. (2017). Procedia Structural Integrity, 5, 753-760.
2. Cimenoglu, H., Gunyuz, M., Kose, G. T., Baydogan, M., Uğurlu, F., & Sener, C. (2011). Materials Characterization, 62(3), 304-311.
3. Niinomi, M., Liu, Y., Nakai, M., Liu, H., & Li, H. (2016). Regenerative biomaterials, 3(3), 173-185.

CMBBE2023
18th International Symposium on Computer Methods in Biomechanics and Biomedical Engineering
3 - 5 May 2023, Paris, France
Arts et Métiers Institute of Technology
Institut de Biomécanique Humaine Georges Charpak
155 boulevard de l'Hôpital 75013 Paris France
www.cmbbe-symposium.com

Determination of the Activity Limitation Period after Plate Removal of Forearm Diaphyseal Fractures : The Bone Strength Evaluation Using Patient Specific CT Based Finite Element Analysis

Yusuke Matsuura(1), Tomoyuki Rokkaku(2), Seiji Ohtori(1)

1. Graduate school of medicine, Chiba university, Japan; 2. Chiba Aoba Municipal Hospital, Japan

1. Introduction

Bone atrophy of the forearm occurs after a plate-fixed forearm diaphysis fracture[1]. Therefore, it is necessary to prevent re-fracture after plate removal. We used finite element analysis(FEA) to evaluate patient-specific bone strength over time after plate removal to decide when to return to sports/work.

2. Materials and Methods

A consecutive series of 41 forearm fracture was investigated for evaluation of bone strength before and after forearm plate removal. Patients who were included underwent plate fixation for forearm diaphyseal fractures and who were scheduled for plate removal. Computed tomography (CT) scans of the entire length of the bilateral forearms were taken by follow protocol. (Fig.1)

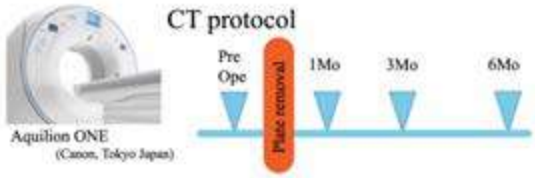

Figure 1: CT protocol

Patient-specific CT-based FEA was used to predict the forearm bone fracture strength against axial load (N), which was defined as the bone strength[2]. Bone strength was estimated by patient-specific CT-based FEA at each time point.

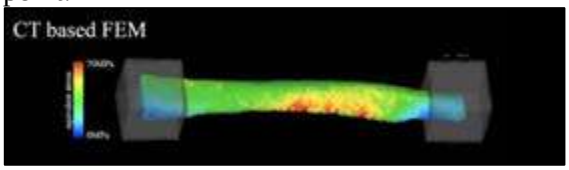

Figure 2: Measured bone strength by CT baced FEA

After plate removal, sports and physical labor were restricted, but restrictions were lifted individually based on the degree of bone strength recovery.

3. Results

The mean age of the patients was 37.3 years. The mean time between plate fixation and removal was 25.4 months. Bone strength before removal was estimated as reduced to 48% of that of the uninjured side. This was constant regardless of age group, involvement of the radius or ulna, AO classification, open fracture, or type of plate. Bone strength at 1, 3, and 6 months after removal was estimated to be 66%, 84%, and 97%, respectively. The bone strength of the distal ulna was weaker than that at the other sites in the forearm and showed delayed recovery.

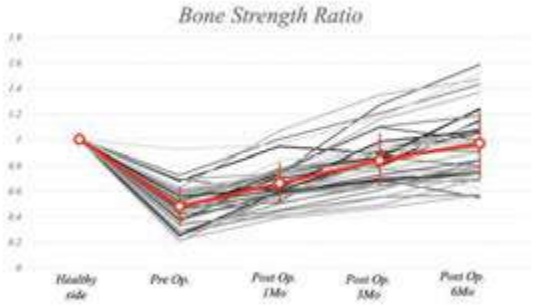

Figure 3: Bone strength ratio after plate removal

4. Discussion and Conclusions

Bone strength after plate removal showed recovery within 3-6 months and was fully recovered by 6 months. The degree of recovery of bone atrophy varies from site to site, and patients should be careful about refracture after removal. Therefore, we use patient specific CT based FEM to determine the bone strength of the individual patient's forearm in real time and use this data as an adjunct to the decision to allow the patient to return to sports or work.

5. References

1. Matsuura Y et al., J Hand SurgAm.; 42(8):659.e1-659.e9 (2017)
2. Matsuura Y et al., Comput Methods Biomech Biomed Engin.;18(16):1811-7(2015)



DEVELOPMENT OF A 3D STATISTICAL SHAPE MODEL OF THE HUMAN MANDIBLE

Giorgio Biesso (1, 2), Kilian Richthofer (1), Vincenzo Orassi (1), Özgür Cebeci (3), Carsten Rendenbach (2), Sara Checa (1)

1. Berlin Institute of Health at Charité – Universitätsmedizin Berlin, Julius Wolff Institute, Germany; 2. Charité – Universitätsmedizin Berlin, Freie Universität Berlin, Humboldt-Universität zu Berlin and Berlin Institute of Health, Department of Oral and Maxillofacial Surgery, Berlin, Germany; 3. IAT Ingenieurgesellschaft fuer Automobiltechnik mbH, Berlin, Germany.

1. Introduction

Computational models are a powerful tool to support surgical planning and manufacturing processes of patient-specific fixation systems. Such models allow simulating different clinical conditions and identifying biomechanical parameters that influence the healing outcome. They have been already introduced to maxillofacial applications [1], however, their development is time-consuming. Statistical shape models (SSMs) create parameterized 3D geometries reflecting anthropometric characteristics. Therefore, this project aims to develop a 3D SSM of the human mandible to accelerate the build-up of patient-specific *in silico* models.

2. Materials and Methods

The external surfaces of four mandibles were segmented from CT scans and, subsequently, 3D meshes of those surfaces were created. Among them, one was selected as the target mesh while the remaining three were used as sources. Initial meshes were pre-aligned in space and then, through a morphing procedure [2], a point correspondence between the meshes was obtained (Fig. 1). The morphed meshes were analyzed in terms of geometrical fit to the target, consistency, and mesh quality. A Procrustes transformation was used to align the mandibles in space, allowing the nodal coordinates to be compared.



Figure 1: Comparison between source and target mesh before (left) and after morphing (right).

Through a principal component analysis, an average shape (AVG) and principal components (PCs) were determined. Eventually, morphological changes caused by each PCs were analyzed.

3. Results

The meshes obtained through the morphing presented a mean Hausdorff distance of 0.11 mm. The 1st PC (PC1) was responsible for size changes, the 2nd (PC2) influenced the cross-sectional shape and the 3rd (PC3) affected inclination and twisting (Fig. 2).

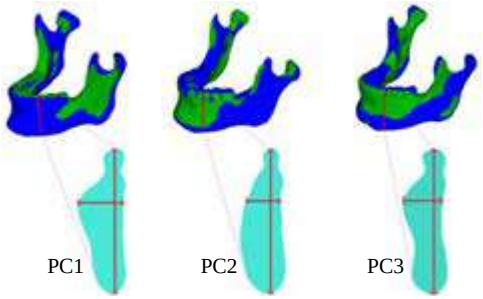

Figure 2: PCs mode 1-3. Visualization of the average shape (green) and the -2 standard deviation (blue) with detail on the cross-sectional views.

4. Discussion and Conclusions

A meaningful statistical shape model was generated with results comparable to other studies [3]. Next steps aim to increase the training dataset and apply this method to build *in silico* models of reconstructed mandibles.

5. References

1. Orassi et al., front. in bioeng. and biotech., 2021
2. Beillas et al., J. Crash Prev. Injury Control., 2017
3. Vallabh et al., biomech. model in mechano., 2020.

Acknowledgements:
This study was funded by the German Research Foundation (CH 1123/10-1).

CMBBE2023
18th International Symposium on Computer Methods in Biomechanics and Biomedical Engineering
3 - 5 May 2023, Paris, France



Arts et Métiers Institute of Technology
Institut de Biomécanique Humaine Georges Charpak
155 boulevard de l'Hôpital 75013 Paris France
www.cmbbe-symposium.com

MATHEMATICAL MODELING IN PROBLEMS OF OPTIMIZING THE PLACEMENT OF VASCULAR BYPASSES

Kuianova Iulia O (1), Dubovoy Andrey (1,2), Bervitsky Anatoly (1,2), Chupakhin Alexander (1); Parshin Daniil (1)

1. LIH SB RAS, Russian Federation, 2. Federal Neurosurgical Center (Novosibirsk)

1. Introduction

Shunting is widely used in the treatment of cardiovascular pathologies. The surgeon faces a number of non-trivial tasks: the need for a bypass as such, the optimal angle of its installation, the optimal shape of the docking window, and others. From the point of view of hydrodynamics and mechanics, this corresponds to a number of specific problems, the solution of which was proposed in the papers [1,2,3].

2. Materials and Methods

As part of the task of determining the optimal angle of installation of the vascular anastomosis during a neurosurgical operation, the hydrodynamics of the tee was studied. Four possible installation angles were considered: $\pi/6$, $\pi/4$, $\pi/3$ и $\pi/2$. An electrical circuit (Fig.1) For the recirculation of large cerebral vessels was constructed based on the configurations of the circle of Willis of real patients, the optimal parameters of which (the best graft position and graft morphology) were determined numerically using swarm intelligence methods. Also, various options for connecting the recipient vessel were considered from the point of view of the optimality of the stress concentrator zones arising during the articulation with the donor vessel.

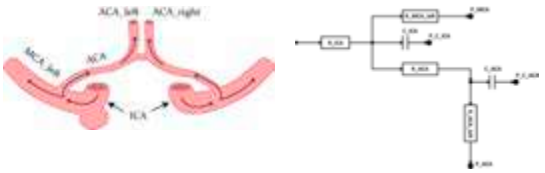

Figure 1: Electrical analogue of anterior brain circulation compartment.

3. Results

It was shown that the bypass angle $\pi/3$ is optimal, the angle $\pi/4$ is the least favorable. Based on the results of the study, a computer program was developed and registered, which allows, according to the data of a real patient, using the electrical analogy of the circulatory system, to suggest the optimal location for the installation of a vascular bypass. The optimal arteriotomy angle was found as 10deg. It is shown that the obtained results are in good agreement with the practice of real operations.

4. Discussion and Conclusions

The results obtained in the course of the cycle of works significantly expand the fundamental knowledge of vascular bifurcations, as well as provide answers to practical questions of clinical surgeons.

5. References

1. O. Kuyanova, S.S. Presnyakov, A.V. Dubovoi, A.P. Chupakhin, D.V. Parshin. Journal of Applied Mechanics and Technical Physics, 2019, Vol. 60, No. 6, pp. 1038–1045
2. Yu.O. Kuyanova, A.V. Dubovoi, A.V. Bervitskii, D.V. Parshin., Journal of Applied Mechanics and Technical Physics, 2022, Vol. 63, No. 4, pp. 606–613
3. Igor I. Tagiltsev, Daniil V. Parshin and Alexey V. Shutov Math. Model. Nat. Phenom. 17 (2022) 20

Acknowledgements:
This study was supported by a grant from Russian Science Foundation (No 20-71-10034)



VIRTUAL COHORT GENERATION FOR *IN SILICO* TRIALS OF TRANSCATHETER AORTIC VALVE IMPLANTATION

Sabine Verstraeten (1), Martijn Hoeijmakers (2), Frans van de Vosse (1), Wouter Huberts (1,3)

1. Eindhoven University of Technology, The Netherlands; 2. ANSYS, The Netherlands; 3. Maastricht University, the Netherlands

1. Introduction

In silico clinical trials are a promising method to increase the efficiency of the development of transcatheter aortic valve implantation (TAVI) devices. With an *in silico* trial, devices can be tested on virtual patients which are computer models that realistically mimic the physiological response induced by TAVI implantation. The domain of interest of each patient of the virtual cohort for TAVI evaluations is represented by a synthetic aortic valve geometry. Two important aortic valve morphologies to include are: (1) the shape of the left ventricular outflow tract (LVOT), either convergent or divergent, and (2) the angle between the LVOT and the ascending aorta ($\angle \mathrm{LVOT} - \mathrm{AA}$) (Fig. 1). These morphologies are key features when evaluating TAVI devices as they influence the occurrence of complications, such as conduction problems, and paravalvular leakage. The aim of this research is to develop a framework to generate synthetic aortic valve geometries, that (1) are physiologically plausible, and (2) allow for selection of the aforementioned morphologies.

2. Materials and Methods

Non-parametric statistical shape modeling (SSM) [1] was used to extract the mean shape and shape variance (shape modes) from a set of 97 stenotic aortic valve geometries. Each geometry within or outside this data set was approximated by adding a weighted combination of 24 shape modes to the mean shape. With the SSM 500 synthetic geometries were generated by sampling new weight combinations from an inferred distribution [2]. Logistic regression and linear regression models were used to filter synthetic geometries on LVOT morphology and ∠LVOT-AA respectively.

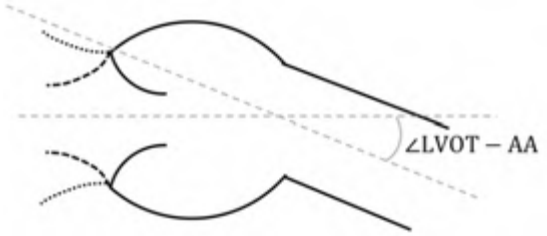

Figure 1: Schematic overview of important morphologies: convergent (dashed line), and divergent (dotted line) LVOT, and angle between LVOT and ascending aorta.

3. Results

A non-parametric multivariate ANOVA test revealed that the 500 synthetic geometries did not differ significantly from the set of 97 real patient geometries ($p = 0.47 > 0.05$). The LVOT shape filter and the ∠LVOT-AA filter successfully selected the aforementioned morphologies with a sensitivity of 97% and 94% respectively.

4. Discussion and Conclusions

These results demonstrate that the framework developed in this study, (1) succeeded in generating synthetic geometries that are physiologically plausible, and (2) makes it possible to select geometries with certain morphologies. Consequently, this framework has the potential to generate synthetic data sets for *in silico* TAVI trials.

5. References

1. Bône A et al., LNCS (2018).
2. Romero P et al., Front. Physiol., (2021).

Acknowledgements:

We acknowledge the European Union's Horizon 2020 research and innovation programme (grant agreement No 101017578) for their financial support.

CMBBE2023
18th International Symposium on Computer Methods in Biomechanics and Biomedical Engineering
3 - 5 May 2023, Paris, France



Arts et Métiers Institute of Technology
Institut de Biomécanique Humaine Georges Charpak
155 boulevard de l'Hôpital 75013 Paris France
www.cmbbe-symposium.com

PATIENT-SPECIFIC BOUNDARY CONDITIONS ADAPTATION FOR COMPUTATIONAL HEMODYNAMICS IN THE LEFT VENTRICLE USING THE CIRCADAPT MODEL

Agathe Bedoux (1), Daniel Curnier (2), Maja Krajinovic (2), Caroline Laverdière (2), Daniel Sinnett (2), Delphine Périé (1)
1. Polytechnique Montréal, Canada; 2. Université de Montréal, Canada

1. Introduction

Personalised computational hemodynamics in the left ventricle may help to identify patients at risk of heart failure [1]. Here, we propose a method for personalisation of boundary conditions, namely aortic pressure (outlet) and blood speed at the mitral valve (inlet).

2. Materials and Methods

Sixty-six Acute Lymphoblastic Leukemia survivors having received cardiotoxic chemotherapy were included in this study. CMR acquisitions were performed at rest on a Siemens Skyra 3T MR system using a 18-channel phased array body matrix and included an ECG-gated cine TruFISP. A segmentation of the left ventricle (LV) was performed using a semi-automatic procedure (CIM v8.1, University of Auckland). Heart rate, diastolic and systolic aortic pressure and cardiac output were monitored at rest using a cardiac hemodynamic monitoring (PhysioFlow, Manatec Biomedical). The CircAdapt model [2], a lumped model of the heart and circulation, was used to simulate patient-specific blood speed at the mitral valve (inlet) and aortic pressure (outlet). To do so, a sensitivity analysis based on the Morris method was performed in order to identify the most impacting inputs on three outputs: the LV volume, blood speed at the mitral valve and aortic pressure. The segmented and simulated LV volumes used to reverse-optimise the identified inputs.

3. Results

Among the seven first most impacting inputs, LV volume and blood speed at the mitral shared five, and LV volume and aortic pressure shared six. Three of these inputs were monitored: heart rate, cardiac output and mean aortic pressure. Therefore, LV volume was considered an appropriate output to reverse-optimise the three remaining inputs. Reverse-optimisation gave acceptable results for fifty-three of the participants, meaning simulated LV volume was sufficiently close to the segmented LV volume (Figure 1).

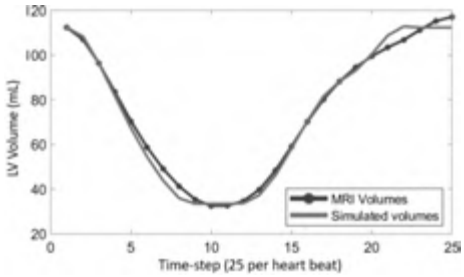

Figure 1: Evolution of the segmented and simulated LV volumes obtained for one patient.

Blood speed at the mitral valve and aortic pressure could then be retrieved using the personalised optimised inputs for the CircAdapt model. For ALL survivors, blood speed was in the range of physiological values, however slightly slower.

4. Discussion and Conclusions

CMR-based computational hemodynamics in the LV allows for a non-invasive analysis of the cardiac function. The proposed method allows to further personalise blood flow simulation by offering personalised boundary conditions and may help to identify early biomarkers of heart failure.

5. References

1. Doost, S.N. et al. Heart blood flow simulation: a perspective review. BioMed Eng OnLine 15, 101 (2016).
2. Walmsley J et al. Fast Simulation of Mechanical Heterogeneity in the Electrically Asynchronous Heart Using the MultiPatch Module. PLoS Comput Biol 2015;11:e1004284.

Acknowledgements:
We thank FRQNT, Polytechnique Montréal and researchers from the PETALE study.



ANALYSIS OF THE MECHANICS OF BIORESORBABLE WIRE-BRAIDED STENTS IN A PATIENT SPECIFIC SCENARIO

Agnese Lucchetti (1), Alissa Zaccaria (2), Thomas Gries (1), Ted J. Vaughan (3)

1. Institut für Textiltechnik of RWTH Aachen University, Germany; 2. Consorzio Intellimech, Via Stezzano 87, Bergamo 24126, Italy; 3. Biomechanics Research Centre (BMEC), School of Engineering, University of Galway, Ireland

1. Introduction

Bioresorbable stents are a promising alternative to permanent metallic devices since they provide vessel support for the time needed and are subsequently naturally degraded. Open challenges are still present with polymeric devices mainly concerning the mechanical performance that is still lower with respect to the metal stents [1]. Finite element models (FEM) are nowadays widely spread since they allow to obtain an insight on the device mechanical performance in relative time and cost-effective way. In literature there is a distinct lack of data describing the behaviour of bioresorbable wire-braided stents in patient specific scenarios. Therefore, the present work aims to computationally replicate the deployment procedure of different newly developed bioresorbable wire-braided stents and analyse their performance in an artery reconstructed from clinical imaging.

2. Materials and Methods

Different poly-L-lactic acid (PLLA) wire-braided stents featuring different braiding patterns and number of wires, based on in-house manufactured stents, were reconstructed by means of a Matlab Code provided by Zaccaria et al. [2] and imported into Abaqus/Explicit software as orphan meshes of Timoshenko beam elements. PLLA was modelled as an elastoplastic material and its mechanical properties were determined from tensile testing of filaments. The artery was reconstructed from patient specific images and meshed with hexahedral elements. Its material properties were modelled as hyperplastic. The geometrical features and material properties of the delivery system were taken from commercially available catheter and literature, respectively. The simulation was subdivided in different steps namely: (1) stent loading on the delivery system, (2) guidewire insertion in the artery, (3) morphing of stent-catheter system and (4) stent deployment. The contact pressures of the stent on the artery as well as the conformability of the different stent geometries to the anatomic shape of the lesion were considered to evaluate the performance of the different stents.

3. Results

The reconstructed stents well represented the geometrical and mechanical features of physical prototypes. All the different stents simulated could be successfully loaded on the delivery system and deployed at the lesion site.

4. Discussion and Conclusions

The model presented in the present work allowed the study of the mechanics of different stent geometries in a complex scenario such that of a patient specific vessel that would have been not possible just by physical bench tests. The same model could be easily adapted to other braided devices and/or materials and applied in the development of next generation bioresorbable braided stents.

5. References

1. Wu et al, Expert review of medical devices, 18 (4): 351–365, 2021.
2. Zaccaria et al, J Biomech, 2020.

Acknowledgements:

This project has received funding from the European Union's Horizon 2020 research and innovation programme under grant agreement No 813869. This publication reflects only the author's view and the REA is not responsible for any use that may be made of the information it contains. The authors would like also to thank Boston Scientific Ltd., Co. Galway, Ireland for their support and collaboration on this work.

CMBBE2023
18th International Symposium on Computer Methods in Biomechanics and Biomedical Engineering
3 - 5 May 2023, Paris, France
Arts et Métiers Institute of Technology
Institut de Biomécanique Humaine Georges Charpak
155 boulevard de l'Hôpital 75013 Paris France
www.cmbbe-symposium.com

A WORKFLOW FOR GENERATING COMPUTATIONAL MODELS OF KNEE JOINT CONTACT USING INPUTS FROM LOADED MRI SCANS

Brett D. Steineman (1), Kalle Chastain (1), Sean Letendre (1), Erin Leatherman (2), Thomas Santner (3), Joshua Leadem (4), Madison Lang (4), Kate Lindsey (4), Erin Argentieri (1), Amanda Wach (1), Ashley Pekmezian (1), Matthew Koff (1), Amy Lerner (3), Scott Rodeo (4), Suzanne Maher (1)

1. Hospital for Special Surgery, USA; 2. Kenyon College, USA; 3. The Ohio State University, USA; 4. University of Rochester, USA

1. Introduction

Partial meniscectomies (PMs) are widely performed with relief of symptoms, but some patients develop degeneration within 6-12 months postop and force distribution may drive variability [1,2]. Finite element (FE) knee models are powerful tools to study joint contact forces and statistical methods can help capture the effect of unknowns such as individual tissue properties. Models capable of predicting force distribution following PMs based on loaded knees during MRI would help inform treatment. Our goal was to create a statistically augmented computational workflow for the generation of FE models to investigate knee contact forces.

2. Materials and Methods

MRIs were acquired of four cadaver knees in an unloaded and a 50% bodyweight loaded condition [3,4]. Menisci and cartilage surfaces were segmented from unloaded scans and finite element models were created to replicate the loaded MRI condition. A 'small' and 'large' PM were created in the posterior medial meniscus. A maximin space-filling design was constructed using ranges of cartilage and meniscal material properties found in the literature to provide 70 knee simulation scenarios [2]. After scanning, the knees were mounted on a robotic test system designed to mimic the loaded condition. Meniscectomies were created in the cadavers to mimic the two PMs created in the FE models. An electronic pressure sensor was used to measure joint pressure and calculate percent force through the medial meniscus [5]. The differences between the FE simulations results for the PM conditions relative to the intact condition were calculated and compared to sensor outputs.

3. Results

Experimental pressure sensor output was unavailable for both PM conditions of one knee and the small PM condition for a second knee (Fig. 1). The change in percent force through the medial meniscus decreased 2% and 22% for the remaining two knees for the small PM condition. The change in perfect force decreased from 22% to 48% for the large PM condition. The median percent force through the medial meniscus calculated from the FE model simulations of small and large PMs was an average of 12% ± 4% away from the experimental output.

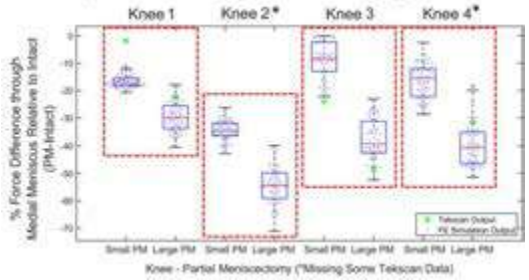

Figure 1 – Percent force difference through medial meniscus relative to intact.

4. Discussion and Conclusions

The workflow of using loaded MRI scans to develop FE models of different PMs provided representative distributions of forces through the medial meniscus in comparison with pressure sensor outputs. This method has promise to be useful to inform PM treatment.

5. References

[1] Souza et al., *Knee Surg Sports Traumatol Arthrosc* 2015 [2] Guo et al., *J Orthop Res* 2017 [3] Wang et al., *J Biomech* 2015 [4] Maher et al., *J Orthop Res* 2017 [5] Santner TJ et al., 2018.

Acknowledgements:

The authors would like to thank the National Institutes of Health (NIH 5R01AR075523) for providing financial support to this project.

CMBBE2023
18th International Symposium on Computer Methods in Biomechanics and Biomedical Engineering
3 - 5 May 2023, Paris, France



Arts et Métiers Institute of Technology
Institut de Biomécanique Humaine Georges Charpak
155 boulevard de l'Hôpital 75013 Paris France
www.cmbbe-symposium.com

EVENT-RELATED CONTROL OF FUNCTIONAL ELECTRICAL STIMULATION USING OPEN-SOURCE PYTHON LIBRARIES

Amedeo Ceglia (1), Kevin CO (1), Teddy Caderby (2), Mickael Begon (1)
1. Université of Montréal, Canada; 2. University of la Réunion, France

1. Introduction

Functional electrical stimulation (FES) is an effective method for physical rehabilitation after a stroke [1]. It can be used for movement dysfunction in daily tasks such as walking, reaching, and grasping. We developed an open-source event-related python method to control and interface the Rehastim2 stimulator (HASOMED, Germany) synchronized with various devices to trigger the electrical stimulation.

2. Materials and Methods

We developed two Python open-source libraries: (i) *pyScienceMode2*[1] to operate the rehastim2 device using Python coding. As the rehastim2 comes with the MOTOmed (RECK, Germany), we also interfaced the MOTOmed command through the rehastim2. (ii) *Biosiglive*[2] to stream and process data in real-time from research and clinical devices and display visual feedback. We implemented three applications of FES, highlighting the versatility of our algorithms. Nexus (Vicon, Oxford, US) was used to stream stimulation data. A healthy participant was equipped and asked to perform different movements and tasks in each case.

(1) *Hand Cycling*: equipped with eight electrodes (four per arm), the participant was instructed to pedal at 30 RPM on the MOTOmed viva 2. *pyScienceMode2* was used to retrieve the angle from the MOTOmed in real-time, allowing muscle stimulation at predetermined angles (Fig. 1).

(2) *Walking*: equipped with two electrodes on the *Soleus*, the participant was asked to walk at his preferred speed on an instrumented treadmill (BERTEC, United States). Force data were recorded using Nexus 2.11 (Vicon, Oxford, UK). Each foot strike was detected using *Biosiglive*. After a 300-ms delay, a stimulation was sent to improve propulsion.

(3) *Reaching task*: equipped with two electrodes on the right biceps brachii and triceps brachii and six skin markers, the participant was placed on a passive exoskeleton arm (Kinova robotics, Canada) and asked not to drive the movement. The aimed task was to reach, with a finger, a certain distance and come back. Markers trajectories were recorded using Nexus and streamed in *Biosiglive*, to define the events for the stimulation.

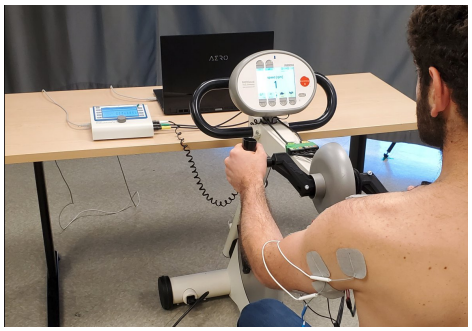

Figure 2: MOTOmed hand cycling with stimulation.

3. Results

For each application, we successfully controlled the stimulation based on events coming from different devices.

4. Discussion and Conclusions

We have shown that our libraries are fast and robust enough to provide relevant stimulation for a given task and deliver the stimulation according to the experimental conditions. A restricted number of examples were presented, but the algorithm can be used in many more contexts (grasping, foot pedaling, etc.). In future work, we would like to optimize the stimulation during a hand cycling task using the pedal data feedback.

5. References

1. Rushton DN. Functional electrical stimulation and rehabilitation-an hypothesis. Med Eng Phys. 2003 Jan;25(1):75-8.2.

[1] *https://github.com/s2mLab/pyScienceMode2*

[2] *https://github.com/pyomeca/biosiglive*

CMBBE2023
18th International Symposium on Computer Methods in Biomechanics and Biomedical Engineering
3 - 5 May 2023, Paris, France



Arts et Métiers Institute of Technology
Institut de Biomécanique Humaine Georges Charpak
155 boulevard de l'Hôpital 75013 Paris France
www.cmbbe-symposium.com

STANDARDISING FRAME ALIGNMENTS TO ALLOW FOR CONSISTENT KINEMATIC INTERPRETATION: PART I

Ariana Ortigas Vásquez (1, 2), Adrian Sauer (1, 2), Allan Maas (1, 2), William R. Taylor (3), Thomas M. Grupp (1, 2)

1. Research and Development, Aesculap AG, Tuttlingen, Germany;
2. Department of Orthopaedic and Trauma Surgery, Musculoskeletal University Center Munich (MUM), Campus Grosshadern, Ludwig Maximilians University Munich, Munich, Germany;
3. Laboratory for Movement Biomechanics, ETH Zurich, Switzerland

1. Introduction

Kinematic patterns characterising joint motion are often compared to determine whether significant differences can be associated with different pathologies *versus* measurement systems. Such comparisons rely on the fundamental assumption that the kinematics resulting from different sources or analysis techniques result in a consistent outcome. However, a lack of consensus in the use and interpretation of approaches can lead to substantially different outcomes [1], hence posing the question: Given kinematic data, how can a consistent and clinically meaningful conclusion be attained?

2. Materials and Methods

Knee kinematics were replicated in a joint simulator and assessed using inertial measurement units (IMUs), allowing the ground truth to be compared against the measured data [2]. After establishing kinematic differences between the two datasets, we aimed to determine whether a minimisation of cross-talk could result in a more consistent interpretation of the kinematic outcome. Here, a least squares approach to derive a set of malalignment compensation parameters was employed. These parameters were then used to rotate the IMU-based segment frames and obtain a new set of aligned IMU-based kinematics. Kinematic errors between approaches were then calculated as root-mean-square errors (RMSEs) from the ground truth.

3. Results

Compensation parameters to execute rotations of the IMU-based segment frames by up to 5.2° resulted in a decrease in RMSEs from an initial range of 0.4-1.6° to 0.0-0.4° (Figure 1).

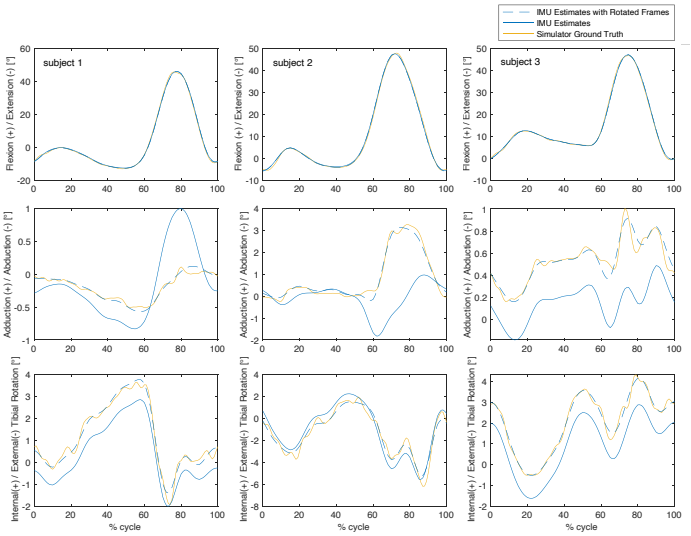

Figure 1: Knee angles for three sample subjects for level-walking showing simulator-, IMU- and optimised IMU-based kinematics.

4. Discussion and Conclusions

To address the clinical challenge of ensuring consistent interpretation of kinematic datasets, this study has demonstrated that kinematic errors can be explained and corrected by addressing differences in frame alignment. Here, the method used to calculate knee kinematics from inertial data [3] provides extremely accurate estimates, as long as differences in frame alignment are accounted for, a challenge that is addressed in Part II of this abstract.

5. References

1. Postolka et al., J Biomech; 17:144, (2022)
2. Ortigas Vásquez et al., in review, (2022)
3. Versteyhe et al., Sensors; 20(6):1683, (2020)

CMBBE2023
18th International Symposium on Computer Methods in Biomechanics and Biomedical Engineering
3 - 5 May 2023, Paris, France
Arts et Métiers Institute of Technology
Institut de Biomécanique Humaine Georges Charpak
155 boulevard de l'Hôpital 75013 Paris France
www.cmbbe-symposium.com

STANDARDISING FRAME ALIGNMENTS TO ALLOW FOR CONSISTENT KINEMATIC INTERPRETATION: PART II

Adrian Sauer (1, 2), Ariana Ortigas Vásquez (1, 2), Allan Maas (1, 2), William R. Taylor (3), Thomas M. Grupp (1, 2)

1. Research and Development, Aesculap AG, Tuttlingen, Germany;
2. Department of Orthopaedic and Trauma Surgery, Musculoskeletal University Center Munich (MUM), Campus Grosshadern, Ludwig Maximilians University Munich, Munich, Germany;
3. Laboratory for Movement Biomechanics, ETH Zurich, Switzerland

1. Introduction

Part I of this work demonstrated that when comparing rotational kinematics, aligning the orientations of segment frames is necessary to achieve consistent interpretation of movement data. However, the previously presented approach required the availability of a ground truth signal for which the underlying segment frame orientations are assumed to be optimal. In almost all practical applications, however, no ground truth signal is available. The aim of this study was therefore to build on the frame alignment optimisation method (presented in Part I) and develop an approach that is able to establish whether two datasets differ through alignment errors or whether the underlying kinematic signal is fundamentally different.

2. Materials and Methods

Previously, rotational kinematics based on inertial measurement unit (IMU) data were compared to a ground truth simulator signal for six subjects [1]. A self-contained mathematical optimisation method allowing standardisation of both the IMU- and simulator-based kinematics was developed that minimised cross-talk parameters in each dataset independently.

3. Results

The optimisation resulted in a rotation of 3.32° ± 1.24° of the segment frames around the associated screw axis. This led to a decrease in root-mean-square error between IMU-derived and simulator-based out-of-sagittal-plane rotations from 0.79° ± 0.30° to 0.29° ± 0.30°. The magnitude and characteristics of the ab/adduction and int/external rotation curves then fundamentally changed and converged on a consistent set of kinematic data across all axes. Importantly, the optimised kinematic patterns remained fundamentally different between subjects (Figure 1).

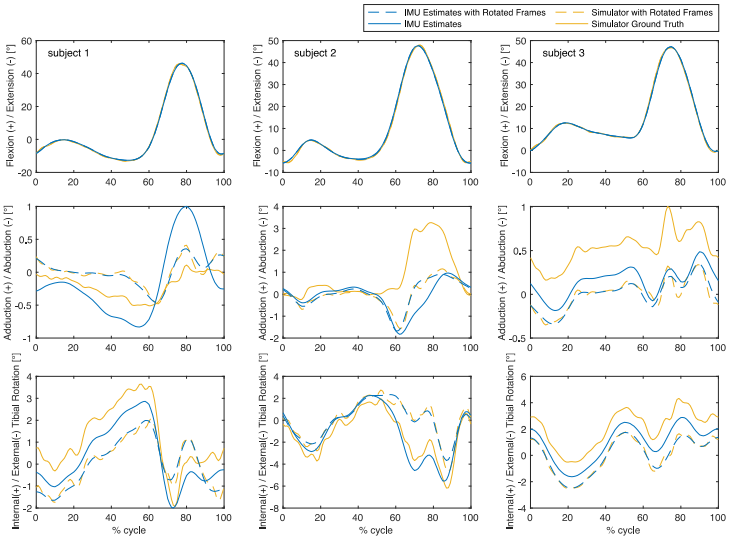

Figure 1: Knee angles for three sample subjects for level-walking showing simulator-, optimised simulator-, IMU- and optimised IMU-based kinematics.

4. Discussion and Conclusions

Optimisation of the orientations of segment frames may lead to sufficient changes to allow convergence on a consistent kinematic signal. This standardisation protocol therefore provides a basis for independently realigning segment frames and avoiding errors associated with sensor malalignment. Even in the absence of a ground truth signal, this standardisation method allows a consistent comparison of kinematic datasets.

5. References

1. Ortigas Vásquez et al., in review, (2022)

CMBBE2023
18th International Symposium on Computer Methods in Biomechanics and Biomedical Engineering
3 - 5 May 2023, Paris, France



Arts et Métiers Institute of Technology
Institut de Biomécanique Humaine Georges Charpak
155 boulevard de l'Hôpital 75013 Paris France
www.cmbbe-symposium.com

EXERCISE CAN IMPROVE CARDIAC DYSFUNCTIONS MEASURED BY ECHOCARDIOGRAPHY IN CHILDHOOD CANCER SURVIVORS

Maxime Caru (1,2), Pierre Dubois (1), Daniel Curnier (2,3), Gregor Andelfinger (2,4), Maja Krajinovic (2,4), Caroline Laverdière (2,4), Daniel Sinnett (2,4), and Delphine Périé (1,2)
1. Department of Mechanical Engineering, Polytechnique Montreal, Canada; 2. Sainte-Justine Research Center, Canada; 3. School of Kinesiology and Physical Activity Sciences, Faculty of Medicine, University of Montreal, Canada; 4. Department of Pediatrics, University of Montreal, Canada

1. Introduction

Children exposed to anthracycline agents are at high risk of cardiac abnormalities. In fact, childhood acute lymphoblastic leukemia (ALL) survivors are seven times more likely to die from cardiovascular complications than their healthy peers [1]. Thus, it is important to consider alternative therapies to prevent the onset of anthracycline-induced cardiotoxicity such as regular physical activity. Therefore, we aimed to explore the association between physical activity levels, cardiorespiratory fitness and cardiac parameters measured by echocardiography.

2. Materials and Methods

216 childhood ALL survivors underwent a maximal cardiopulmonary exercise test to assess their cardiorespiratory fitness (peak of oxygen consumption) and self-reported their daily minutes of moderate-to-vigorous physical activity. Participants underwent a complete transthoracic echocardiographic assessment. Systolic and diastolic function analysis, and strain images analysis were performed. The associations were studied through the preventive fraction (examined with univariate crude and adjusted logistic regression models) of regular physical activity (≥150min/week) and adequate cardiorespiratory fitness levels (above the median ≥32.0mL.kg-1.min-1) on cardiac parameters.

3. Results

Crude analysis shows that regular physical activity was associated with a significant preventive fraction in mitral E/A ratio (56%; p=0.013), while adjusted analyses highlighted a non-significant reduction of 74% to 37% in the prevalence of cardiac parameters associated with physical activity. Similar associations of adequate cardiorespiratory fitness on cardiac parameters were observed. Adjusted analyses revealed a non-significant reduction of 7% to 86% in the prevalence of cardiac parameters associated with cardiorespiratory fitness.

4. Discussion and Conclusions

This study reports that regular physical activity and adequate cardiorespiratory fitness were associated with a higher preventive fraction. Thus, engaging in physical activity prevents childhood ALL survivors' cardiac dysfunctions [2]. These findings are novel and clinically relevant in pediatric cardio-oncology and provide additional evidence to strengthen the benefits of exercise as long-term care in childhood cancer survivors.

5. References

1. Armstrong GT, Liu Q, Yasui Y, Neglia JP, Leisenring W, Robison LL, et al. Late mortality among 5-year survivors of childhood cancer: a summary from the Childhood Cancer Survivor Study. J Clin Oncol. 2009;27(14):2328-38
3. Lemay V, Caru M, Samoilenko M, Drouin S, Alos N, Lefebvre G, et al. Prevention of Long-term Adverse Health Outcomes With Cardiorespiratory Fitness and Physical Activity in Childhood Acute Lymphoblastic Leukemia Survivors. J Pediatr Hematol Oncol. 2019;41(7):e450-e8.

Acknowledgements:

This work was supported by the Institute of Cancer Research of the Canadian Institutes of Health Research, in collaboration with C17 Council, Canadian Cancer Society, Cancer Research Society, Garron Family Cancer Centre at the Hospital for Sick Children, Ontario Institute for Cancer Research and Pediatric Oncology Group of Ontario



IN SILICO ANALYSIS OF AUXETIC INSPIRED STENT GRAFTS FOR ENDOVASCULAR ANEURYSM REPAIR

Rahul Vellaparambil (1,2), Woo-Suck Han (1), Pierluigi Di Giovanni (2), Stephane Avril (1)

1.Mines Saint-Etienne, Univ Lyon, Univ Jean Monnet, Etablissement Francais du Sang, INSERM, U 1059 Sainbiose, Centre CIS, F - 42023 Saint-Etienne, France ; 2.R&D Department, HSL S.R.L, Trento, Italy

Corresponding Author's email: rahul.vellaparambil@emse.fr

1. Introduction

Stent-grafts (SGs) involved in endovascular aneurysm repair (EVAR) are plagued by kinks & device migration which has been linked to insufficient SG flexibility [1,2] during deployment in tortuous arteries. Auxetic designs have been recently analysed for coronary stents with their unique properties of fracture toughness & indentation resistance among others to combat kinking/mal apposition [3]. In this work, the bending behaviour of auxetic inspired SG designs are numerically simulated and contrasted with results of a commercial SG (Zenith ® Low Profile) published in literature [4].

2. Materials and Methods

Using the geometrical features of commercial SG Zenit ® Low Profile (Cook Medical Europe) from Demanget et al.,2013[4] as a template, finite element (FE) models of 3 auxetic designs such as re-entrant (RE), chiral-re-entrant(CRE), chiral-star(CSTAR) & three novel auxetic hybrid designs (RE-Diamond , CRE-Diamond & CSTAR-Diamond) are constructed on Simulia Abaqus software(v2020) with Timoshenko B31 beam elements for stents & 4-node quadrilateral S4 shell elements for the graft. The bending behaviour of all SG models were assessed using a computational benchmark comprising of bending until 180° and pressurization at 150mmHg as per Demanget et al.,2013[4]. The SG flexibility & durability was evaluated using the maximal luminal reduction rate, maximal stresses in stents & maximal strains in fabric [4]. Furthermore, as SGs with a low delivery profile are prioritised, all SG models were crimped to 60% of their original diameter and evaluated using crimping strain attributes.

3. Results

Auxetic stent-graft designs such as RE, CSTAR& CRE which possess stent-rings that are linked to each other, are observed to suffer high stresses & severe kinks in comparison to Zenith stent. Hybrid auxetic inspired designs (unlinked) such as RE-Diamond, CSTAR-Diamond & CRE-Diamond are recorded with lower stent stresses & kink deformations in contrast to the Zenith stent. While evaluating the crimp test for above mentioned hybrid designs, CRE-Diamond emerged as the best performing candidate.

4. Discussion and Conclusions

Preliminary results have found promising auxetic inspired SG designs that can match or surpass Zenith SG in terms of its flexibility & durability characteristics. Future computational studies will be undertaken to assess the sealing effect of auxetic inspired designs in aortic aneurysms post in-vivo deployment.

5. References

1. Umscheid, T, and W J Stelter. Journal of endovascular surgery : the official journal of the International Society for Endovascular Surgery vol. 6,1 (1999): 17-32
2. Carroccio, Alfio et al., Journal of vascular surgery vol. 36,4 (2002): 679-84
3. Xue, Huipeng et al., Frontiers in bioengineering and biotechnology, Vol. 8, Page 736 (2020).
4. Demanget, Nicolas et al., Journal of endovascular therapy : an official journal of the International Society of Endovascular Specialists vol. 20,4 (2013): 523-3

Acknowledgements:

This work was supported by grant 859836 from the European Union's Horizon 2020 research and innovation programme.

CMBBE2023
18th International Symposium on Computer Methods in Biomechanics and Biomedical Engineering
3 - 5 May 2023, Paris, France
Arts et Métiers Institute of Technology
Institut de Biomécanique Humaine Georges Charpak
155 boulevard de l'Hôpital 75013 Paris France
www.cmbbe-symposium.com

SIMULTANEOUS SIMULATION OF COLD FLOW AND IMPINGEMENT IN POLYETHYLENE LINER OF HIP PROSTHESIS

Changhee Cho

The University of Kitakyushu, Japan

1. Introduction

Wear and failure of ultra-high-molecular-weight polyethylene (UHMWPE) component after total joint replacement cause serious clinical and biomechanical reactions [1], thus restricting the longevity of artificial joints. In retrieved UHMWPE liners of hip prostheses, catastrophic wear and failure are frequently observed as shown in Figure 1 [2].

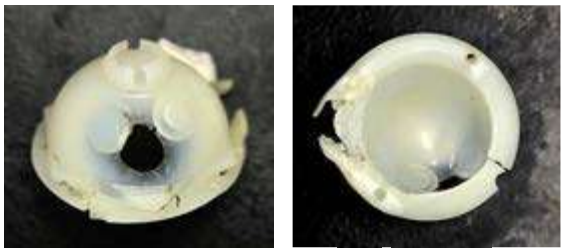

Figure 1: Retrieved UHMWPE liner showing catastrophic wear and failure (290 months *in vivo*).

2. Materials and Methods

The purpose of this study is to investigate the cause of catastrophic wear and failure of the retrieved UHMWPE liner of hip prosthesis shown in Figure 1. Simultaneous simulation of cold flow and impingement in the UHMWPE liner of the retrieved hip prosthesis by using the finite element method (FEM) was performed to investigate the mechanical states of the liner. Finite element model of the retrieved hip prosthesis is shown in Figure 2.

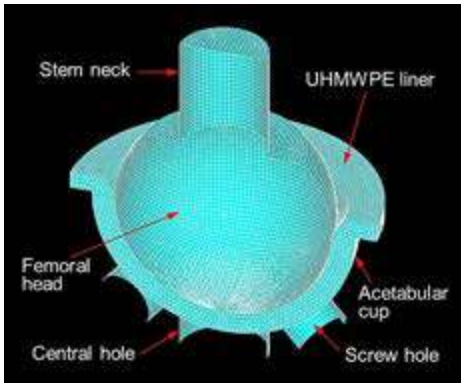

Figure 2: Finite element model of hip prosthesis.

Metallic components were modelled as rigid bodies. UHMWPE liner was modelled as an elasto-plastic body. The finite element analysis (FEA) was performed by using the ANSYS.

3. Results

The FEA simulation result is shown in Figure 3. The distribution of contact stress generated in the UHMWPE liner due to the simultaneous occurrence of cold flow and impingement corresponds to the catastrophic wear and failure sites observed in the retrieved UHMWPE liner.

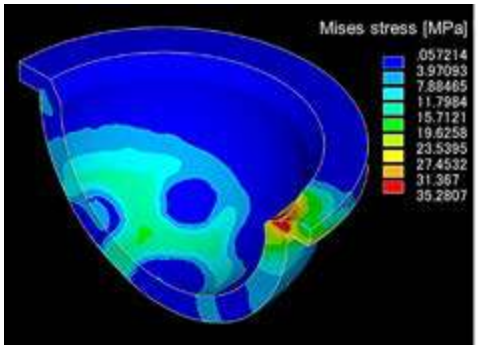

Figure 3: Contour plot of contact stress of the retrieved UHMWPE liner shown in Figure 1.

4. Discussion and Conclusions

The results of this study suggest that change in mechanical states due to the simultaneous occurrence of cold flow and impingement in hip prosthesis is the cause of catastrophic wear and failure of the retrieved UHMWPE liner.

5. References

1. Ingham E, Fisher J, Proc Instn Mech Engrs; 214 (Part H): 21-37 (2000).
2. Cho C, Mori T and Kawasaki M, CMBBE 2019 Conference Proceedings: 539-549 (2020).

Acknowledgements:

This work was supported by JSPS KAKENHI Grant Number JP21K12689. The authors would like to thank the Dept. of Orthop Surg, UOEH for providing the retrieved artificial hip joints.

CMBBE2023
18th International Symposium on Computer Methods in Biomechanics and Biomedical Engineering
3 - 5 May 2023, Paris, France



Arts et Métiers Institute of Technology
Institut de Biomécanique Humaine Georges Charpak
155 boulevard de l'Hôpital 75013 Paris France
www.cmbbe-symposium.com

A NEW CONCEPT FOR MONITORING PATIENT ACTIVITY USING AN ENERGY-AUTONOMOUS TOTAL HIP ENDOPROSTHESIS STEM

Franziska Geiger[1], Henning Bathel[2], Sascha Spors[2], Rainer Bader[1], Daniel Kluess[1]

1. University Medical Center Rostock, Germany; 2. University of Rostock, Germany

1. Introduction

A recently presented total hip replacement stem with an integrated piezoelectric energy harvesting system [1] could be a new opportunity for monitoring daily activities without external energy supply [2]. The present study aimed to determine the maximum force on the energy-autonomous total hip replacement stem during different activities via the electrical voltage output.

2. Materials and Methods

Hip joint contact forces of different activities [2] were applied to the energy-autonomous hip stem with a uniaxial testing machine. Synchronously, an oscilloscope was used to record the electrical voltages generated (Fig.1). Forces acting on the piezoelectric element were calculated using the voltage output and the formula of Safaei et al. [3]. The maximum predicted forces on the hip stem were then determined by linear regression and compared to the real forces exhibited by the testing machine.

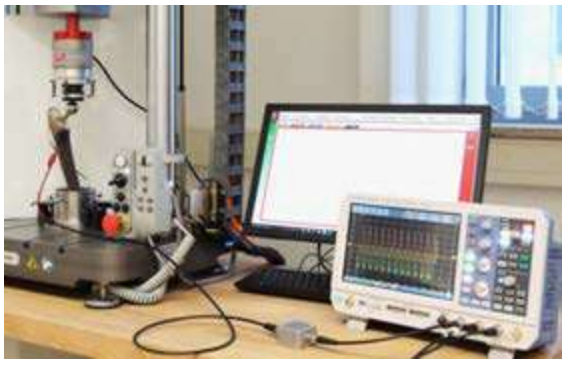

Figure 1: Experimental measurement setup- Application of different force profiles to the energy-autonomous hip implant.

3. Results

For all activities, the median is close to zero. The 25th and 75th percentiles of walking, jogging, stance, stand up, stairs up and stairs down are between median to 5 and median to -5 percent deviation. For the activities cycling, sitting down and knee bend the first quartiles range from 5 to 10 and the third quartiles are between -5 to -10 percent deviation (Fig. 2).

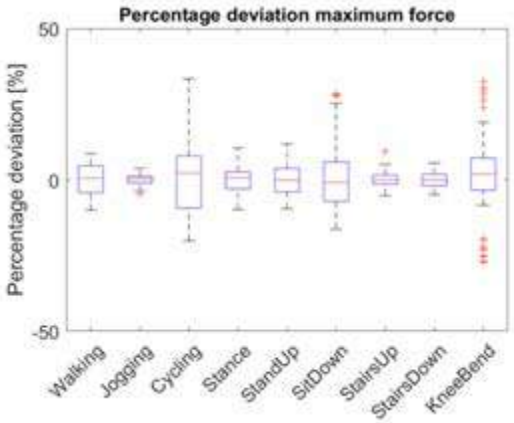

Figure 2: Percentage deviation of the actually applied maxima and the calculated maxima to the energy-autonomous hip implant.

4. Discussion and Conclusions

The maximum force on the energy-autonomous implant can be predicted with little percentage deviation for most of the activities. Next, an activity detection algorithm will be created. This could provide a new way to permanently determine patients' daily activities with total hip replacements in situ.

5. References

1. Lange et al., Materials, 14(18):5151, 2021.
2. Bergmann et al., PloS One, 11(5):e0155612, 2016.
3. Safaei et al., J Intell Mater Syst Struct, 30(20):3163-3175, 2019.

Acknowledgements:
This research was supported by the German Research Foundation (Deutsche Forschungs-gemeinschaft, DFG) within the Collaborative Research Centre 1270 ELAINE.

CMBBE2023
18th International Symposium on Computer Methods in Biomechanics and Biomedical Engineering
3 - 5 May 2023, Paris, France



Arts et Métiers Institute of Technology
Institut de Biomécanique Humaine Georges Charpak
155 boulevard de l'Hôpital 75013 Paris France
www.cmbbe-symposium.com

USE OF ELECTRICAL MUSCLE STIMULATION TO ENHANCE PROPULSION DURING WALKING IN ABLE-BODIED ADULTS

Thomas Aout (1), Baptiste Jégou (1), Mickaël Begon (2), Nicolas Peyrot (1,3), Teddy Caderby (1)

1. Laboratoire IRISSE, Le Tampon, La Réunion ; 2. Laboratoire de Simulation et Modélisation du Mouvement, Laval, Canada ; 3. Laboratoire Motricité Interactions Performance, Le Mans, France

1. Introduction

Functional electrical stimulation (FES) consists in applying a small electrical current to neuromuscular tissue, usually from electrodes placed on the skin, to reproduce functional movements. FES was initially developed to improve mobility in people with neuromuscular disorders, such as hemiplegics [1] and paraplegics [2]. Nevertheless, FES could also be a potential solution to assist gait in able-bodied individuals, but this remains to be proven. In this study, we tested the hypothesis that electrical muscle stimulation could enhance propulsion during walking in healthy adults.

2. Materials and Methods

Twenty-one healthy young adults (24 ± 4 years) performed a series of walking trials at their self-selected preferred speed on a 5-meter walkway in two randomized conditions: with and without electrical stimulation of the triceps surae of the dominant leg (Fig. 1). The stimulation was applied during the push-off phase of gait using a portable electrical stimulator coupled with an inertial measurement unit. The stimulation intensity corresponded to the maximum intensity tolerated by the subject (just below the pain threshold). A motion capture system and two force plates were used for kinematic and dynamic gait analysis.

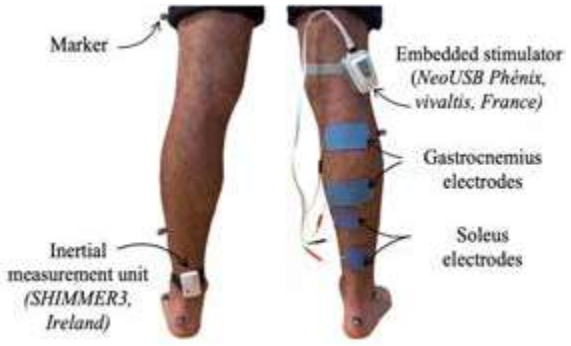

Figure1: Experimental device

Student's t-tests for paired samples ($P<0.05$) were used to evaluate the effect of electrical muscle stimulation on gait parameters.

3. Results

Electrical muscle stimulation resulted in a significant increase in the peak propulsive force ($P<0.05$; Table 1), peak mechanical ankle power at push-off ($P<0.05$) and walking speed ($P<0.01$).

Table 1: Results of studied parameters.

	With stimulation	Without stimulation
Propulsive force (N)	154 ± 32	147 ± 35
Ankle power (W/kg)	4.0 ± 0.6	3.5 ± 0.9
Walking speed (m/s)	1.17 ± 0.07	1.14 ± 0.07

4. Discussion and Conclusion

Previously, authors have reported that FES may modify gait pattern in healthy adults [3,4]. Nevertheless, to our knowledge, this is the first study to show an improvement in ankle propulsive function during walking in this population, as evidenced by the increase in mechanical ankle power (16%). This improvement contributed to an increase in propulsive force and walking speed in our participants. Future studies should investigate whether this benefit can be transferred to elderly.

5. References

1. Liberson WT, Holmquest HJ, Scot D & Dow M., Arch Phys Med Rehabil; 42, 101–105 (1961).
2. Thrasher TA & Popovic MR., Annales de Réadaptation et de Médecine Physique ; 51, 452–460 (2008).
3. Meng L, Porr B, Macleod CA & Gollee H., Proc Inst Mech Eng H; 231, 315–325 (2017).
4. Rane L & Bull AMJ., Arthritis Res Ther; 18, 255 (2016).



A comparative clinical trial to evaluate the effect of a lumbar belt on the kinematics of the spine

Aicha Errabity[1,2], *Rébecca Bonnaire*[3], *Woo-Suck Han*[1], *Reynald Convert*[2], *Romain Pannetier*[2], *Paul Calmels*[4], *Jérôme Molimard*[1]

[1]*Mines Saint-Etienne, Univ Jean Monnet, INSERM, U 1059 Sainbiose, Centre CIS, Saint-Etienne France ;* [2]*Thuasne, BP243, 92307 Levallois-Perret cedex, France ;*
[3]*Institut Clément Ader (ICA), Université de Toulouse, CNRS, IMT Mines Albi, INSA, ISAE-SUPAERO, UPS Campus Jarlard, F-81013 Albi, France ;* [4]*Hôpital Nord, CHU de Saint-Etienne, France ;*

Corresponding author. Email: aicha.errabity@emse.fr

1. Introduction

Low back pain (LBP) is a very common health problem that has a significant socio-economic impact. it remains the leading cause of disability worldwide. Many studies have evaluated spinal kinematics to predict the level of disability in patients with LBP and have reported that altered spinal motion patterns are common in individuals with LBP [1]. The lumbar belt is a widely used therapeutic tool for LBP with the assumption that it can have a positive effect on trunk movements. It can either prevent extreme movements or improve body postures. However, only a few studies have reported the biomechanical results of different movements with a lumbar belt, leaving the impact of these devices on the spine kinematics incomplete. The objective of this work, which is part of a full clinical trial, is to evaluate the effect of a lumbar belt on the spine kinematics during different movements in people with and without LBP, using an in-house IMU-based system [2].

2. Materials and Methods

In a preclinical study, two IMU sensors were placed at L1 and L5 to assess lumbar spine kinematics with and without a lumbar belt on 10 healthy subjects. Then, the clinical study involved 16 people LBP pain and 16 matched controls. Three IMU sensors were placed at T1, T12, and S1 to analyse spinal kinematics.

Considered positions were neutral standing, anterior flexion, lateral flexion, extension and sit-to-stand. Lumbar lordosis, thoracic kyphosis, pelvic tilt, and range of motion of the lumbar and thoracic spine were calculated during each movement.

The Wilcoxon signed rank test was performed to evaluate the effect of wearing a commercial lumbar belt on each variable.

3. Results

Results of the pre-clinical study are presented in Figure 1. Initial statistical results showed an effect of wearing the belt on almost all measured variables, except for the maximum hip extension angle.

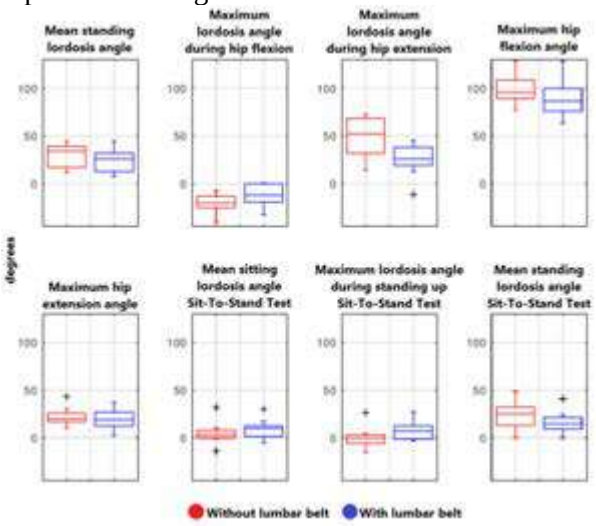

Figure 1: Boxplot of each measured variable with and without the lumbar belt

4. Discussion and Conclusions

This study showed the relevance of using IMUs in measuring belt effect on lumbar kinematics, with statistical differences for almost all parameters. Further results and conclusions on LPB patients will be given after the inclusion of all individuals in the clinical trial.

5. References

1. Laird, R.A. et al. BMC Musculoskelet Disord 15, 229 (2014).
2. Molimard, J. et al., arXiv preprint arXiv : 2104.03565 (2021).

CMBBE2023
18th International Symposium on Computer Methods in Biomechanics and Biomedical Engineering
3 - 5 May 2023, Paris, France
Arts et Métiers Institute of Technology
Institut de Biomécanique Humaine Georges Charpak
155 boulevard de l'Hôpital 75013 Paris France
www.cmbbe-symposium.com

LOWER LIMB PROSTHESIS: COMPUTER METHODS FOR DESIGNING MATAMATERIAL LINER

Vasja Plesec (1), Gregor Harih (1)

1. *Faculty of Mechanical Engineering, University of Maribor, Slovenia*

Corresponding author: Vasja Plesec, Laboratory for Intelligent CAD Systems, Faculty of Mechanical Engineering, University of Maribor, Smetanova ulica 17, Maribor 2000, Slovenia. Email: vasja.plesec@um.si

1. Introduction

The development of a socket-liner system for lower limb amputees is demanding due to the non-linear nature of the biological tissue and the complex geometry of the residual limb. The current common solution uses a homogeneous silicone liner to alleviate the pressure between the soft tissue and the stiff definitive socket. Although silicone liners can reduce stress concentrations, they are far from ideal because they are poorly customisable, and their low thermal conductivity can lead to limb overheating [1]. Adaptability of 3D-printed metamaterials can be used to overcome the listed shortcomings and thus further improve the liner. In the current study, different metamaterial designs are evaluated (both numerically and experimentally) for custom-made prosthetic liners, and the best designs for reduction of contact pressure and increase in stability are proposed.

2. Materials and Methods

Samples of various cellular structures were 3D printed using a low-cost FDM printer with TPU filament (Figure 1a,b). The thickness of the samples was 6 mm, corresponding to the thickness of a typical silicone liner [2]. Measurements of compressive tests were carried out with the Tinius Olsen H10KT testing machine. Material properties were extracted from the experimental tests and used in the FEA. The material models for the prosthetic liner were evaluated in numerical simulation on the previously developed and validated generic transtibial model (Figure 1c). Three different loading conditions were included in the simulation, namely: donning of the socket, one-legged stance, and static proof test according to ISO 10328.

3. Results

The peak contact pressure and the relative deformation of the liner were the main criteria for the evaluation of the metamaterial liners. The numerical results were compared with the results of a conventional silicone liner in which the peak contact pressure at the limb-liner interface was 67 kPa, 106 kPa, and 318 kPa for donning, one-legged stance, and proof test, respectively.

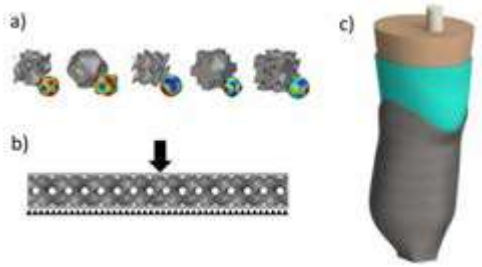

Figure 1: Metamaterial unit cells (a), compression test (b), numerical model of the transtibial limb (c).

4. Discussion and Conclusions

The results obtained indicate that 3D-printed metamaterials can be used to reduce stress concentrations without compromising stability. By adjusting the mechanical properties of the metamaterials, a tailored biomechanical response can be achieved that reduces stress peaks while maintaining the stability of the prosthesis.

5. References

1. Paterno L et al., IEEE Trans Biomed Eng; 65(9): 1996-2010, 2018.
2. Cagle J et al., J Prosthet Orthot; 30(4): 187-199, 2018.

Acknowledgements:
The authors acknowledge the financial support from the Slovenian Research Agency (research core funding No. P2-0063).

CMBBE2023
18th International Symposium on Computer Methods in Biomechanics and Biomedical Engineering
3 - 5 May 2023, Paris, France
Arts et Métiers Institute of Technology
Institut de Biomécanique Humaine Georges Charpak
155 boulevard de l'Hôpital 75013 Paris France
www.cmbbe-symposium.com

HEAD LENGTH'S IMPACT ON TAPER JUNCTION STABILITY IN TOTAL HIP PROSTHESIS

Federico A. Bologna (1,2), Giovanni Putame (1,2), Alberto L. Audenino (1,2), Mara Terzini (1,2)

1. Department of Mechanical and Aerospace Engineering, Politecnico di Torino, Turin, Italy
2. Polito^{BIO}Med Lab, Politecnico di Torino, Turin, Italy

1. Introduction

Despite their widespread use in joint deficiencies treatment, hip prostheses still present issues related to the establishment of relative micromotions between coupled components, which can lead to a fretting-corrosion process generating cytotoxic metal debris and ions. It is proven that micromotions at the junction interface are affected by different parameters, such as head diameter, neck length, head length, and taper angle mismatch [1]. In this study, a biomechanical analysis, combining finite elements (FE) and multibody (MB) simulations, was carried out to evaluate the effect of specific geometric features on micromotions and contact pressures generated during walking at the head-neck taper junction of a parametrized hip prosthesis.

2. Materials and Methods

Firstly, a FE model (Abaqus, Dassault Systèmes, France) of the head-neck junction assembly was implemented (Figure 1a) by simulating the dynamic insertion of the head on the neck using a 4 kN applied force [2]. Secondly, MB derived loads (Figure 1b) were imposed as reference boundary conditions in a FE dynamic simulation to estimate the contact pressure distribution (CPRESS) on the taper surface and the micromotions as the relative slip (CSLIP) between the contacting surfaces (Figure 1c) during a walking cycle. In detail, the MB model of a lower limb was created (Adams View, MSC Software, USA) including a parametrized hip prosthesis which allowed to obtain seven sets of boundary conditions by varying the femoral head diameter (32 ± 4 mm), neck length (38 ± 4 mm), and head length (19.7 ± 4 mm) of the implant. Thereafter, as many FE models were realized by replicating the varied implant geometry.

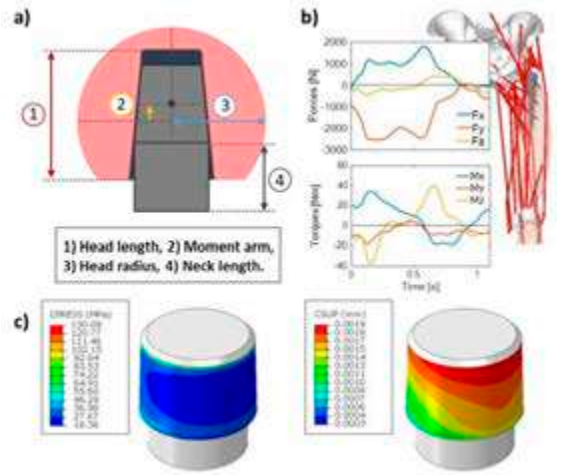

Figure 1: a) Geometric features of interest; b) multibody model with estimated hip reaction forces and torques; c) explanatory results (CPRESS and CSLIP) from the FE analysis.

3. Results

Main results revealed that, among the considered geometric features, the head length variation causes important alterations of both CPRESS and CSLIP, as consequence of the generation of a moment arm between head centre and centre of pressure, which leads to an increase in contact pressure greater than 10%.

4. Discussion and Conclusions

The described computational workflow might represent a powerful tool to improve implant design, thus reducing the risk of implant failures, and, in the long run, to support clinical decision-making processes.

5. References

1. Falkenberg A et al, J Biomech; 98 (2020).
2. English R et al, Wear; 338-339 (2015) 210-220.

Acknowledgements:
This work was funded by MIUR PRIN 2017 "BIONIC" project.



FRACTURE TOUGHNESS IN HUMAN CORTICAL BONE FROM INDIVIDUALS WITH AND WITHOUT TYPE 2 DIABETES MELLITUS

Eva M Wölfel (1), Jasmin Koldehoff (2), Sofie Dragoun Kolibova (1), Felix N Schmidt (1), Benjamin Ondruschka (3), Hans Jelitto (2), Gerold Schneider (2), Björn Busse (1)

1. Department of Osteology and Biomechanics, University Medical Center Hamburg-Eppendorf, Germany; 2. Institute Advanced Ceramics, Hamburg Technical University, Germany; 3. Department of Legal Medicine, University Medical Center Hamburg-Eppendorf, Germany

Corresponding author address: Lottestr. 55A, 22529 Hamburg, Germany; b.busse@uke.de

1. Introduction

Diabetes mellitus is a metabolic disease that affects 537 million individuals worldwide, the majority suffering from type 2 diabetes mellitus (T2DM) [1]. Patients with T2DM experience an increased fracture risk, which is assumed to be linked to an impaired bone quality as bone quantity is similar or higher compared to non-diabetics. Thus, fracture risk assessment which is exclusively based on bone mineral density fails to predict diabetic patients at risk. Therefore, we set out to perform a comprehensive bone quality assessment in combination with fracture toughness measurements to deepen the understanding of fracture characteristics with type 2 diabetes mellitus.

2. Materials and Methods

Human cortical bone from male individuals was obtained during autopsy at the Department of Legal Medicine (IRB approval present) from 15 individuals with T2DM and 19 healthy controls to measure fracture toughness in a three-point bending set-up. Rectangular bone samples of 3 x 2 x 12mm were prepared and polished. The mineralization degree was analysed with quantitative backscattered electron imaging, while biomechanical properties at the nano-level were assessed with nanoindentation. Three-point bending tests were performed at ambient environmental conditions with imaging of crack propagation to determine fracture toughness. Using micro-computed tomography, the samples were scanned with 6µm resolution and cortical bone and vessel microstructure were determined.

3. Results

Bone quality indices of the mineral phase showed similar degree of mineralization, hardness, and elastic modulus in the T2DM group compared to controls. Accordingly, resistance to fracture testing revealed similar behaviour in cortical bone from individuals with and without T2DM for fracture initiation and propagation toughness. The unchanged fracture toughness was in line with unchanged microstructure of cortical bone volume and vessel characteristics.

4. Discussion and Conclusions

In a first step, we performed fracture toughness tests on human cortical bone from male individuals with T2DM and healthy controls in combination with bone quality assessment. In the tested cohort, in which both groups presented with similar degrees of mineralization, hardness, and elastic modulus also the fracture initiation and propagation toughness were unchanged. Next, we will perform fracture risk assessment in bone tissue from individuals with significantly different bone quality indices to evaluate if the mechanisms driving fracture risk in T2DM are rather related to collagen characteristics [1-4].

5. References

1. IDF Atlas, 2021; 10th edition
2. Wölfel et al., Bone 2020; 140: 115556
3. Wölfel et al., Bone 2022; 165: 116546
4. Wölfel et al., JBMR 2022 (Epub ahead of print)

Acknowledgements:

The authors acknowledge support of the Interdisciplinary Center for Interface Research (ICCIR) and the Forum of Medical Technology Hamburg.

CMBBE2023
18th International Symposium on Computer Methods in Biomechanics and Biomedical Engineering
3 - 5 May 2023, Paris, France



Arts et Métiers Institute of Technology
Institut de Biomécanique Humaine Georges Charpak
155 boulevard de l'Hôpital 75013 Paris France
www.cmbbe-symposium.com

THEORETICAL DYNAMIC MODEL OF WRIST PROSTHESIS WITH OPTIMIZED MAGNETORHEOLOGICAL BRAKE

Rina Dutra (1,2), Guilherme Rúbio (2), Rafhael de Andrade (3) and Claysson Vimieiro (2)

1. Department of Telecommunications and Mechatronics Engineering, UFSJ, Brazil; 2. Graduate Program in Mechanical Engineering, UFMG, Brazil; 3. Department of Mechanical Engineering, Graduate Program in Mechanical Engineering, UFES, Brazil.

1. Introduction

The resistive actuators of currently available prostheses may not provide sufficient torque for an adequate weight, present difficulties in controlling position and velocity or have low response time and limitation of postural changes in rapid wrist movements [1]. These factors demand excessive effort from the user, whose bodily compensations can lead to muscle and joint injuries, contributing to users abandoning prostheses [2]. This work proposes analyzing the theoretical dynamic model of a fist with a magnetorheological (MR) brake. It is believed that the validation of the geometric optimization of the brake through the dynamic model offers an alternative to resistive actuators in upper prosthetic limbs.

2. Materials and Methods

The dimensioning of magnetorheological brakes is described in previous works [3]. A particle swarm algorithm, PSO, optimized the geometric dimension of the MR brake. The optimized results were validated through the theoretical dynamic model of the MR brake, whose block diagram is shown in Fig 1a. Considering the physical limitations of the MR brake, a saturation block was introduced to limit the current in the coil. The manufacturer Lord Corporation of the MRF-140CG fluid provides the experimental curve of the product.

3. Results

The torque curve as a function of current, Fig.1b, shows that the dynamic model is consistent with the results obtained in the MR brake design and compatible with the biomechanics of wrist rotation.

4. Discussion and Conclusions

The analyzes developed in the mechanical design ensure that the device has been adequately designed. Magnetorheological fluid actuators are gaining popularity in prosthetic applications due to their fast response, large force/torque capacity, simplicity, and compact design [4]. These features meet users' demands by supplying the actuators' limited functionality. Therefore, the MR brake is a promising alternative for resistive actuators in upper prosthetic limbs as it provides better torque density when compared to other resistive actuators such as DC and ultrasonic motors.

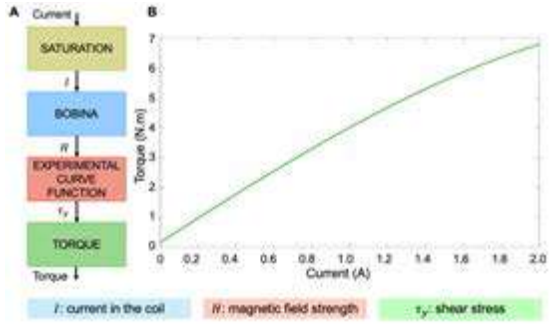

Figure 1: Theoretical dynamic model of MR Brake. A) Block diagram, B) Current x torque curve.

5. References

1. Damerla R et al., IEEE Trans on Med Robotics and Bionics; 4(2): 502-519 (2022).
2. Legrand M et al., ICRA 2020 conference; 2020. p. 2763-2769.
3. Dutra R M A et al., ICORR 2022 conference; 2022. P.1-6.
4. Liu G et al., Smart Mater. Struct.; 31(043002): (2022).

Acknowledgements:
The authors would like to thank the FINEP (Grant no: 01.21.0101.00, Ref. 2790/20], FAPES (Grant no: 2021-8GJZ6, 2021-L7SZ4), Capes (Grant no: 001) and CNPq (Grant no: 200250/2021-3) for providing financial support to this project.



MECHANICAL IMPACT OF CAVITY DESIGN OPTIMIZATION (CDO) IN INLAY FABRICATION INLAY DESIGN: FINITE ELEMENT APPROACH.

Bilal Balbzioui [1], Frederic Heichelbech[1], Christophe Noiret[3], Olivier Etienne [1 2 3]

1 Faculty of Dental Medicine, Universitée de Strasbourg, Strasbourg, France ; 2 INSERM Biomaterials and 2 Bioengineering ; 3 Hexagon France

1. Introduction

The advent of adhesive techniques has led to a paradigm shift in restorative and prosthetic dentistry. Inlays, whether made of resin composite or ceramic are parts of these techniques used as a biomimetic approach to restore the decayed teeth. Whether composite or ceramic, a bonding resin allows the assembly of the inlay to the the inlay to the dental tissue. Caries decay can lead to clinical situations where tissue conservation is achieved by by filling in the undercuts with plastic materials.

This approach is called Cavity Design Optimization (CDO) allows to modify the design of the cleaned carious cavity, in undercut to give it a shape that is favorable for inlay insertion.

Dentin substitutes such as hybrid composite resins, glass- ionomer cements or flow composites are used to fill in these undercuts. these undercuts. This choice of material is likely to have an impact on the mechanical behavior of the of the tooth and the inlay.

2. Materials and Methods

The study was conducted using the 3D finite element method (FEM). Two models were built-up to mimic 2 different clinical situations involving either a large (LCDO) or a small CDO (sCDO). Each of these 2 models was studied using 3 different dentin substitute material (Fuji II LC GC, EverX postGC, SDR flowdensply sirona) associated to 2 types of inlay (ceramic (Emax Press) or composite (Cerasmart)).

The maxillary premolar model was obtained from a natural Tooth CBCT scan. Enamel and dentin were separated using invesalius software. The inlay, the resin cement layer as well as the dentin substitutes were modelized with mesh mixer. The 3D FE Models were built-up and an axial chewing load was simulated using APEX software. The stress distribution for all groups was first studied with colorimetric graphs. Then, the mean of maximal modified von Mises stresses (mvM) was calculated at the enamel/CDO interface for all groups.

3. Results

For The LCDO and sCDO models the lowest mvM were measure using fuji IILC as dentine substitute for the two types of inlay. For the LCDO model the EverX post and SDRflow dentine substitute showed an increase in mvM of +34,69% and +52,80% respectively. For the sCDO model the EverX post and SDRflow dentine substitute showed an increase in mvM of +9,23% and + 68,46% respectively.

4. Discussion and Conclusions

This study does not take into account the reality of dental adhesion. Withing the limits of these study the best biomechanical option for the dental clinician would be using fujyIILC as dentin substitute for SCDO and LCDO.

5. References

Acknowledgements: The authors would like to thank Hexagon for their logistical support.



A Dynamic Finite Element Model of the Reconstructed Mandible With Body and Ramus Defect for Stress Analysis During Chewing

H. Aftabi(1), J. Lloyd(1), E. Prisman(1), A. Hodgson(1), S. Fels(1)
(1) University of British Columbia, Canada;

1. Introduction

Advanced head and neck cancers involving the mandible often require the removal of the diseased part of the mandible and replacement of it with donor tissue (e.g., fibula bone) to recreate the form and function of the premorbid jaw. Surgeons frequently use virtual surgical plans (VSP) to predict the outcome of surgery. Although using VSP approaches has been shown to help surgeons reduce surgical time and better reach the desired jaw shape, the bone non-union or partial union rate can still be high. The absence of a gap, the level of stress in the reconstructed parts and mandibular movement are known to affect bone healing [2]. In this study, we present a dynamic finite element model of the reconstructed mandible to examine the stress distribution in the reconstructed components throughout a chewing cycle.

2. Materials and Methods

We collected computed tomography (CT) images of a patient with a mandible tumour that involves the mandible ramus and body. We used 3D Slicer software to segment the CT image, define the cut plane for mandible resection, and convert the bone elements (mandible and fibula bones) to 3D meshes. To develop the reconstructed model, Ramer–Douglas–Peucker (RDP) algorithm was used in the Artisynth software, based on which the number of donor segments and the deformation of the reconstruction plate were obtained [2]. We converted the donor segments and reconstruction plate to volumetric finite element meshes using the TetGen library. Finally, we assembled all rigid bodies, constraints, and finite element components and added twenty muscles (excluding those attached to the resected part) to our model in Artisynth. Muscle properties, such as activation, insertion, and origin points, were obtained based on the literature [3].

3. Results

Figure 1 illustrates the dynamic finite element model of the reconstructed mandible. The von Mises stress distribution in donor segments of the model is presented for three frames of one chewing cycle (beginning, middle, and end). The donor segments were attached to the mandible using a plate and screws. The preliminary results show higher stress in mandible-donor interaction compared to donor-donor. This finding suggests that more consideration needs to be taken into account when designing plates for attaching donors.

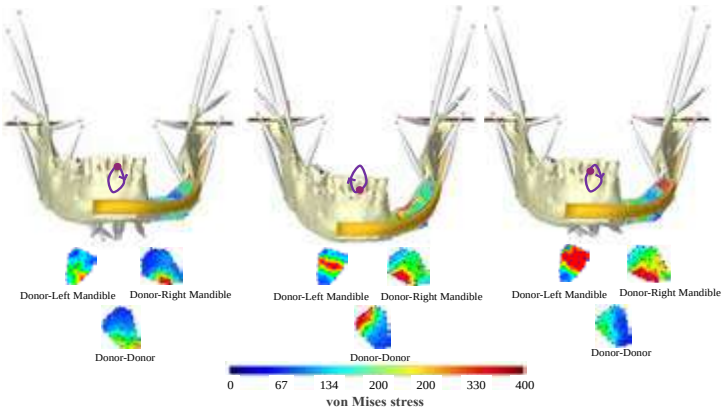

Figure 1: Stress distrubution in donor segments for three frames of one chewing cycle

4. Discussion and Conclusions

This modeling approach could possibly enable surgeons to preoperatively evaluate the success of mandible reconstruction surgery, especially during mastication, and supplement other criteria, such as clinical experience and intuition, in order to predict and minimize the negative consequences of such surgeries.

5. References

1. Nobuhiro Yoda et al. In: Medical engineering & physics 56 (2018), pp. 1–8.
2. Shkedy Yotam et al. In: The Laryngoscope 130(2020)pp E619--E624.
3-. Alan G Hannam et al. In: The Journal of Prosthetic Dentistry 104.3 (2010), pp. 191–198.

CMBBE2023
18th International Symposium on Computer Methods in Biomechanics and Biomedical Engineering
3 - 5 May 2023, Paris, France



Arts et Métiers Institute of Technology
Institut de Biomécanique Humaine Georges Charpak
155 boulevard de l'Hôpital 75013 Paris France
www.cmbbe-symposium.com

AXIAL TENSION/COMPRESSION AND TORSIONAL LOADING OF LATTICE STRUCTURES: SIMULATION AND EXPERIMENT

Anatolie Timercan, Patrick Terriault, Vladimir Brailovski

Department of Mechanical Engineering, École de technologie supérieure, 1100 Notre-Dame West, Montreal, Quebec H3C1K3, Canada

Corresponding author: A. Timercan – anatolie.timercan.1@etsmtl.net

1. Introduction

Lattice structures are increasingly used in biomedical implants, requiring a better understanding of their behavior for the different types of loading they undergo during application [1].

2. Materials and Methods

Strut-based diamond and sheet-based gyroid structures with porosity levels of 50, 60, 70 and 80% and an identical pore size of 750 µm were manufactured from Ti6Al4V alloy on an EOS M280 system. Structures were CT-scanned and tested experimentally in axial tension and compression, and in torsion. Concurrently, analogous numerical models were built and simulated numerically.

3. Results

The manufactured structures were within 5% of the targeted porosity. Numerical simulations overestimated the experimental stiffness and strength of the structures by an average of 25%, likely due to the presence of manufacturing defects, especially in the higher porosity lattices.

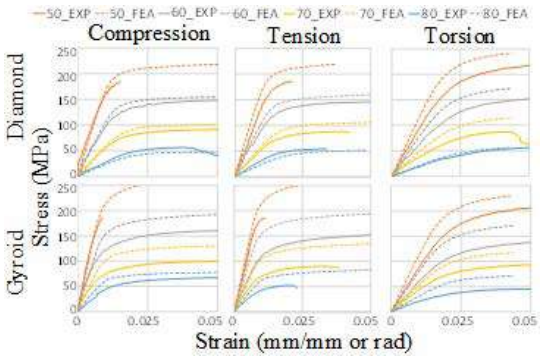

Figure 1: Comparison of the experimental and FEA stress-strain diagrams of 50-80% porous structures

Experimental and numerical results showed that the structures have quasi-identical mechanical properties in compression and in tension with elastic moduli ranging from 3-22 GPa and yield stresses ranging from 48-186 MPa. However, a comparison of the torsion and axial results indicated that conventional bulk material failure theories such as the von Mises limitation criterion do not apply to the apparent properties of lattice structures.

4. Discussion and Conclusions

To achieve defect-free lattice structures, the printing parameters must be adapted to the lattice type, but also to the porosity level, while considering that this might negatively affect the material microstructure and the mechanical properties. The validated numerical models were used for an exploratory study to assess the benefits of using more compliant materials for the manufacture of lattice structures for biomedical applications. As compared to the Ti6Al4V 60% gyroid, the geometrically equivalent superelastic TiNi structures must offer higher reversible displacements (3 vs. 1%) with lower stiffness (2.8 vs. 17.6 GPa), and lower stresses applied to the surrounding tissues (83 vs. 160 MPa). Experimental validation of these calculations is currently under study.

5. References

1. Mahmoud D, M Elbestawi. JMMP MDPI 1(2): 13. (2017).

Acknowledgements

This work was funded by the Fonds de Recherche du Québec - Nature et Technologies (272262); the Natural Sciences and Engineering Research Council of Canada and the Fonds de Développement de l'ÉTS.

CMBBE2023
18th International Symposium on Computer Methods in Biomechanics and Biomedical Engineering
3 - 5 May 2023, Paris, France



Arts et Métiers Institute of Technology
Institut de Biomécanique Humaine Georges Charpak
155 boulevard de l'Hôpital 75013 Paris France
www.cmbbe-symposium.com

DEVELOPMENT AND CHARACTERIZATION OF 3D PRINTED BONE SUBSTITUTES MIMICKING TRABECULAR BONE ARCHITECTURE

Fanny Leborgne (1), Laëtitia Caillé (1), Christophe Tromas (1), Donatien Campion (2), Mathieu Séveryns (1,3), Paul Danty (4), Patricia Pascaud-Mathieu (4), Valéry Valle (1)

1. Institut Pprime UPR 3346, CNRS - Université de Poitiers - ISAE-ENSMA, France; 2. Marle Group, France; 3. Orthopaedic Surgery and Traumatology department, Clinique Chirurgicale Porte Océane, France; 4. IRCER UMR 7315, CNRS – Université de Limoges

1. Introduction

Additive manufacturing (AM) opens new opportunities in producing complex shape medical devices compared to conventional processes. It is relevant when dealing with trabecular bone microstructure to fill bone gaps during surgical procedures such as Valgus Tibial Osteotomy (VTO). Particularly, it allows to control pore size and interconnectivity to promote mechanical strength, bone regeneration and tissue revascularization [1].
In this study, the mechanical properties of a 3D printed trabecular bone substitute produced by laser powder bed fusion (L-PBF) are analysed from both experimental and digital standpoints.

2. Materials and Methods

A cubic centimeter trabecular bone sample was harvested from the proximal epiphysis of a human tibia and scanned with a microCT scan (Ultratom RX Solutions, Institut Pprime). The images were then segmented (Simpleware Scan IP v2018.03 Synopsys, 3D Medlab) in order to reconstruct a numerical model of the bone segment compatible with the 3D printing technique resolution (M290 EOS, 3D Medlab). A multiscale characterization of the printed sample mechanical properties was performed through nanoindentation, 3-points bending and compression tests to assess the influence of the porosity at micro- and macro- scales. The 3D strain fields were assessed by Digital Volume Correlation (DVC) [2] (X-DVCorrel, Pprime Institute) and compared to Finite Element Analysis (FEA).

3. Results

The mechanical test results gathered in Table 1 evidence that both the micro- and macro-porosities decrease the elastic properties of the printed samples.

Mechanical test	Elastic modulus (GPa)
Nanoindentation	124 ± 6
3-points bending	107,6 ± 3
Compression	0.505

Table 1: Multiscale mechanical properties of Ti-6Al-4V printed samples.

Figure 1 highlights similar 3D strain distributions for the tibial trabecular bone and its 3D printed replica under compression, meaning that the microstructure drives bone strain behaviour. The elastic modulus measured through DVC reach 0.056 GPa and 0.505 GPa for the trabecular bone and the Ti-6Al-4V printed sample respectively.

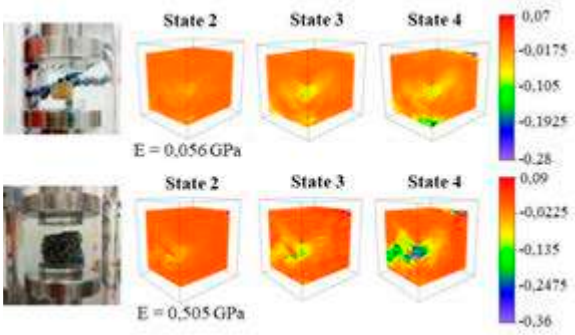

Figure 1: DVC analysis of trabecular bone (top) and Ti-6Al-4V bone substitute (bottom) 3D strain fields.

4. Discussion and Conclusions

AM is a valuable and promising tool to produce bone substitutes with an interconnected pores network. These preliminary data will be compared to ongoing FEA.

5. References

1. Yang et al, Int J Bioprint, 5, 2018
2. Bokam et al, Comput Methods Biomech Biomed Engin, 22:S42-S44, 2019

Acknowledgements:
This work was supported by the Nouvelle-Aquitaine region.

CMBBE2023
18th International Symposium on Computer Methods in Biomechanics and Biomedical Engineering
3 - 5 May 2023, Paris, France



Arts et Métiers Institute of Technology
Institut de Biomécanique Humaine Georges Charpak
155 boulevard de l'Hôpital 75013 Paris France
www.cmbbe-symposium.com

IDENTIFICATION OF A VISCO-HYPERELASTIC MODEL FOR THE MANDIBULAR PERIOSTEUM

Alexandre Hamma (1), Vincent Serantoni (1), Jeremy Dallard (1), Natacha Kadlub (1), Jean Boisson (1)

1. UME, ENSTA-Paris, Institute Polytechnique of Paris, 828 Boulevard des Maréchaux, Palaiseau, France

1. Introduction

The periosteum is a thin bi-layered fibrous connective tissue covering most of the bones, that plays a significant role in bone regeneration and growth, and participates in the transmission of blood and nutrients to bones. [1,2]

The work presented here is an identification method to select the combination of visco-hyperelastic laws that best characterize a soft tissue mechanically. This method is applied to model the mechanical behavior of the mandibular periosteum based on different laws extracted from the literature.

2. Materials and Methods

The model parameters are determined using stress-strain curves of five human's mandibular periosteums. Each harvested sample is divided in two and tested, at two different speeds, either longitudinally or transversely to the main direction of the supposed collagen fibers.

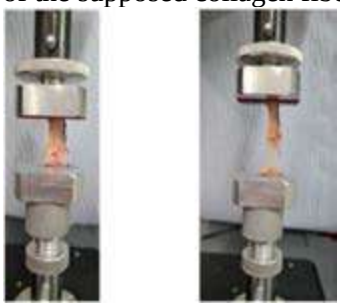

Figure 1: A. Sample set in the jaws - B. Sample after breakage.

The isotropic contributions of this tissue are extracted on the tests performed transversely, while the anisotropic contributions are extracted longitudinally on the other half of the samples. In a second step, the identified global law is validated using twelve samples tested only in the longitudinal direction.

3. Results

The selected combination uses the simplified 2nd order Rivlin law [1] to model the hyperelasticity of the cell matrix. For the other contributions, the Kulkarni law [2] was found to be the most relevant.

The equation (1) is the combined strain energy density function of the identified models for the mandibular periosteum. Material constants are $C_{01}, C_{20}, \mu_1, q, \mu_2, n_1, \mu_3, n_2$. I_1, I_2, K_4 are invariant of $\boldsymbol{C}$ and J_2, J_5 are invariant of $\dot{\boldsymbol{C}}$

$$W = C_{01}(I_2 - 3) + C_{20}(I_1 - 3)^2 + \mu_1(K_4 - 7)^q + \frac{1}{2}\mu_2 J_2 (I_1 - 3)^{n_1} + \mu_3 J_5 (K_4 - 7)^{n_2} \quad (1)$$

4. Discussion and Conclusions

This law can be then implemented in a numerical code to model the behavior of the mandibular periosteum during a maxillary distraction. The objective is to identify for a given patient the least stretched and constrained areas so that the device can be optimally positioned on him/her. Furthermore, it has been shown that bone regeneration during osteogenic distraction is improved by mechanical stimulation. These simulations could therefore potentially provide a better understanding of the mechanism of bone remodeling related to the periosteum.

5. References

1. Evans and al, 2013. Tissue Engineering Part B: Reviews 19,147–159.
2. Kanno and al, 2005. Journal of Oral and Maxillofacial Surgery 63, 499–504.
3. Dallard and al, 2019. Comput. Methods Biomech. Biomed. Eng. 22 (sup1), S39–S41.
4. Kulkarni and al, 2016. Math. Mech. Solids 21 (6), 747–770.

Acknowledgements:

We thank l'École de Chirurgie du Fer à Moulin, (AP-HP), its headmaster Pr Pascal Frileux, his associate Djamel Taleb and all the staff, as they kindly supported all anatomic experiments . We also thank, the NARTMF association for the support of A. Hamma. V. Serantoni is supported by the french Defense Innovation Agency (AID-SIMFACE Project).



NUMERICAL SIMULATION OF ACOUSTIC WAVES IN A SIMULATED HUMAN TOOTH FOR ROOT FRACTURE DETECTION

Si Yen Ng [1], Chi-Lun Lin [2]

[1,2] Department of Mechanical Engineering, National Cheng Kung University, Taiwan

1. Introduction

Diagnosis of dental root fractures is challenging and complicated for many dentists. Nowadays, conventional films, intraoral digital imaging systems, and cone-beam computed tomography (CBCT) are the diagnostic imaging used in the clinic. CBCT has the highest imaging resolution among the clinically available diagnosis methods; still, it cannot visualize cracks smaller than 150μm and require the patient to be exposed to radiation [1]. Therefore, a non-radiation and non-invasive approach to fast screen the existence of dental root fracture is needed. This paper uses a numerical simulation of acoustic waves in the simulated human tooth to investigate the ultrasound probing parameters before the miniature ultrasound transducer is developed in-house.

2. Materials and Methods

This numerical simulation employed the Acoustics Module of the COMSOL Multiphysics® 6.0 software, the elastic waves, and the time-explicit physics interface to model the propagation of the sinusoidal burst wave in simulated human teeth with and without a crack. The acoustic wave was transmitted from a miniature conical point contact ceramic piezoelectric transducer, detecting the presence of a crack using the pulse-echo method. Density, longitudinal acoustic velocity, and transverse acoustic velocity of Build-It™ LC light cure core material were measured in experiments and were used to calculate Young's modulus and Poisson's ratio of the simulated tooth model.

3. Results

For the three source signal frequencies simulated in our study, the crack can be identified from the change in the temporal response of average pressure over the transducer's surface (Figure 1). The crack's width insignificantly affects the response signal (Figure 2a). The signal response to the crack can be observed most clearly when the source signal is placed at the root region (Figure 2b).

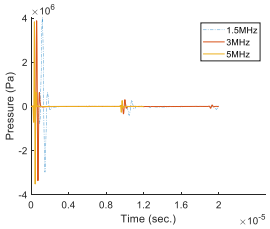

Figure 1: Effect of the source signal with different frequencies on the 150μm-width crack.

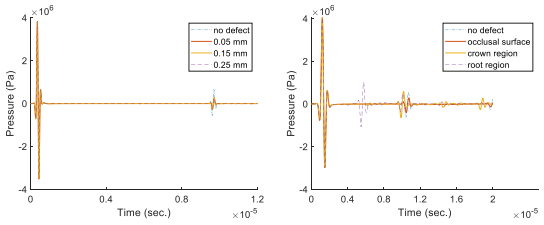

(a) (b)

Figure 2: Signal responses of (a) 5MHz sine burst wave on different widths of cracks and (b) 1.5MHz sine burst wave on the 150μm-wide crack detected from different locations.

4. Discussion and Conclusions

We employed numerical simulation to study the feasibility of using acoustic waves in detecting dental cracks and evaluated the ultrasound probing parameters. Our results suggested the probing location being placed at the root region, which best visualizes the crack in the response signal and avoids the attenuation of high-frequency ultrasound waves along a long propagation travel path.

5. References

1. Makeeva IM et al., International endodontic journal. 2016;49(10):980-989.

Acknowledgments:

This research is supported by the Ministry of Science and Technology, Taiwan, under funding no. 111-2221-E-006-038.

CMBBE2023
18th International Symposium on Computer Methods in Biomechanics and Biomedical Engineering
3 - 5 May 2023, Paris, France
Arts et Métiers Institute of Technology
Institut de Biomécanique Humaine Georges Charpak
155 boulevard de l'Hôpital 75013 Paris France
www.cmbbe-symposium.com

IMAGING OF MUSCULOSKELETAL TISSUES BY ULTRASONIC TOMOGRAPHY - PROSPECTS FOR CHILDREN LIMB IMAGING

Elise Doveri (1), Luis Espinosa (2), Vadim Monteiller (1), Régine Guillermin (1), Laurent Sabatier (1), Vincent Long (1), Cécile Baron (3), Philippe Lasaygues (1)

1. Aix Marseille Univ, CNRS, Centrale Marseille, LMA UMR 7031, Marseille, France
2. Univ. Toulouse 3 - Paul Sabatier, Institut Clément Ader, Tarbes, France
3. Aix Marseille Univ, CNRS, Centrale Marseille, IRPHE UMR 7342, Marseille, France

1. Introduction

B-mode ultrasound (US) has long been a first-line examination for the diagnosis of many musculoskeletal diseases in children [1]. The other modalities, such as X-ray or magnetic resonance imaging, are associated with inconveniences that are constraining for pediatric applications. Because the large acoustic impedance contrast between echogenic bony structures, and the adjoining soft tissues, US can only see the outer surface of bony structures, and not what lies within. In that context, the ultrasound computed tomography (USCT), with an adapted filtering and signal processing algorithm [2], allows to visualize with a good resolution ($\lambda/10$) and contrast, the different morphologies of small organs (skin, muscles, tendons, nerves, vessels, fat and bony structures). But the method fails to provide quantitative images.

2. Materials and Methods

In this work, a new nonlinear approach to USCT is proposed using the full waveform inversion (FWI) algorithm [3], [4], based on a full numerical modeling of the wave propagation in the media, and on the minimization of the difference between recorded and simulated waveforms based on the iterative resolution of the inverse problem. The method requires only one set of recorded signals.

A USCT prototype has been developed, consisting of a crown (300 mm) of 8 1MHz-transducers distributed every 45°. A wavelet-based coded excitation method (WCE) has been adapted to this device [5] allowing to map the inter- or centro-diaphyseal areas, and thus reducing the low-pass filtering effect influencing the contrast-to-noise (CNR).

3. Results

Experiments were conducted on a newborn arm phantom containing blood vessels, single and joined bones (Fig. 1), and on a chicken drumstick with skin, different muscles, fat, tendons, nerves, tibia and fibula (Fig. 2).



Figure 1: X-ray, linear and non-linear USCT of a newborn arm phantom (True Phantom™, CA).

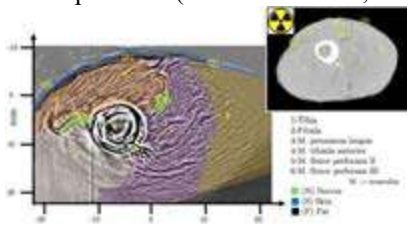

Figure 2: USCT of a chicken drumstick

4. Discussion and Conclusions

The algorithm for CNR and gain calculation is detailed in [2] and [4]. The performance of the method is presented in the following table.

Target	CNR	Gain (%)
Arm	1.3 (1.1)	1784
Chicken	1.1 (1)	175

Table 1: Control-to-noise ratio (average and standard deviation) and gain (%) of the USCT of musculoskeletal tissues

5. References

[1] J. F. Griffith, 2nd Edition. Salt Lake City: Amirsys Publishing, 2019.
[2] E. Doveri et al., *Appl. Sci.*, vol. 11, no. 20, p. 9368, 2021.
[3] S. Bernard et al., *Phys. Med. Biol.*, vol. 62, no. 17, pp. 7011–7035, 2017.
[4] L. Espinosa et al. *Ultrason. Imaging*, vol. 43, no. 2, pp. 88–99, 2021.
[5] M. Loosvelt and P. Lasaygues, *Ultrasonics*, vol. 51, no. 3, pp. 325–339, 2011.

Acknowledgements:
Centre de Calcul Intensif d'Aix-Marseille is acknowledged for granting access to its high-performance computing resources.

CMBBE2023
18th International Symposium on Computer Methods in Biomechanics and Biomedical Engineering
3 - 5 May 2023, Paris, France
Arts et Métiers Institute of Technology
Institut de Biomécanique Humaine Georges Charpak
155 boulevard de l'Hôpital 75013 Paris France
www.cmbbe-symposium.com

PREDICTING LIVER RESECTION COMPLEXITY FROM CT SCANS WITH A MACHINE LEARNING FRAMEWORK

Omar Ali (1-4), Alexandre Bône (1), Caterina Accardo (5), Omar Belkouchi (5), Marc-Michel Rohe (1), Eric Vibert (3,4,5), Irene Vignon-Clementel (2)

1. Guerbet Research, France; 2. Inria (Saclay, IdF), France; 3. Inserm U1193, France; 4. Paris-Saclay University; 5. Paul Brousse Hospital – APHP, France;

1. Introduction

The preoperative evaluation of liver resection complexity (LRC) is essential to avoid the risk of postoperative complications. We introduce an automated image-based machine learning pipeline for LRC prediction from preoperative CT scans based on imaging biomarkers. First, the segmentations of the liver anatomy are generated by deep learning models. Second, a liver vessel pruning algorithm defines the hepatic central zone (HCZ). Third and last, a machine learning model predicts the LRC.

2. Materials and Methods

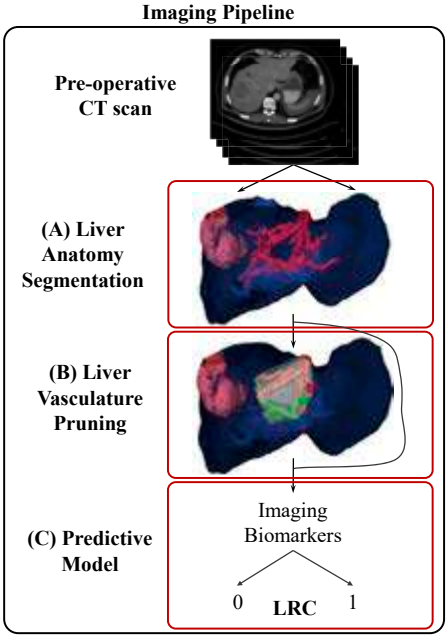

Figure 1: Proposed imaging pipeline

The segmentations of the liver, tumors, and hepatic venous vessels are generated from preoperative CT scans using 3D convolutional neural networks (Fig. 1A) [1]. Then, the predicted vessel segmentation masks are skeletonized and converted to a graph with branches and edges [2]. The liver vasculature is mainly constituted of two distinct venous structures: the portal and the hepatic trees. The extremities of the branches with the largest diameters are obtained for each tree after computing the distance transform of the original vessel segmentation mask. From these extremities, the different branches are exploited and pruned, only keeping the major liver vessels. The convex volume around these remaining major vessels defines the HCZ, the region where surgical resections are known to be complex (Fig. 1B). The liver volume, number of tumors, and volume of tumors are imaging biomarkers directly extracted from the raw segmentations. They are complemented by a newly proposed imaging biomarker B_{HCZ}, defined to be the nonzero relative volume of occupancy of the tumor inside the HCZ, or the negative of the minimal distance from the tumor to the pruned vessels when the tumor is outside the HCZ. A logistic regression model is finally trained with these features to predict the LRC (Fig. 1C).

3. Results

The dice score reaches 96.0%, 71.6% and 79.1% for the segmentation of the liver, tumors, and hepatic venous vessels respectively. The results also show that the best configuration to predict the LRC combines B_{HCZ} with the volume and number of tumors. This configuration achieves an accuracy, F1 score and AUC of 0.77, 0.75 and 0.84 respectively.

4. Discussion and Conclusions

The results highlight the importance of analyzing the position of the tumors inside the liver with respect to the HCZ and the major vessels.

5. References

1. Isensee F. et al, Nat Methods; 18:203-211 (2021).
2. Nunez-Iglesias J. et al, PeerJ; 6:e4312 (2018).

Acknowledgements of funding support: work supported by Île-de-France, Guerbet and Inria.



AVERAGE 3D CORNEAL MODEL TO ANALYSE ENDOTHELIAL TRANSPLANT SURGERY

Julia Talajic (1,2), Antoine Sylvestre-Bouchard (1,2), Étienne Bénard-Séguin (1,3), Arnaud Polette (4), Zachary M Mayko (5,6), Michael D Straiko (5,6), Mark A Terry (5,6), Jean Meunier (7), Isabelle Brunette (1,2)

1. Dept of Ophthalmology, U. of Montreal, Canada, 2. Maisonneuve-Rosemont Hospital Research Center, Canada, 3. School of Medicine, Queen's University, Canada, 4. ENSAM, France, 5. Lions VisionGift, Portland, USA, 6. Devers Eye Institute, Portland, USA, 7. DIRO, U. of Montreal, Canada

1. Introduction

The 3D corneal surfaces of a patient can be measured with a medical imaging device called corneal topographer. However, comparison between individual corneal shapes is limited due to large inter-subject variabilities. Consequently, we previously proposed different strategies to generate an average 3D model (atlas) of the cornea from a set of topographies to characterize a specific population [1]. In this paper we investigate a similar approach to assess two corneal transplant surgeries: Descemet's membrane endothelial keratoplasty (DMEK) and Descemet's Stripping Automated Endothelial Keratoplasty (DSAEK). These interventions are used to restore the anatomical 3D shape of the cornea in patients with Fuchs endothelial corneal dystrophy (FECD).

2. Materials and Methods

A dataset of topographies (Pentacam HR, Oculus, Arlington, WA) from 193 DMEK and 52 DSAEK (before and after surgery) as well as 96 normal subjects was approved by the institutional review boards. Each topography consists of three arrays (anterior surface elevation, posterior surface elevation and corneal thickness or pachymetry) of 141 x 141 points evenly spaced every 0.1 mm over 14 mm x 14 mm. An elevation map gives the height of a surface relative to a reference plane perpendicular to the line of sight. The proposed average model (atlas) construction follows 5 steps: *Step 1*. Limit the computation to the central 10.0-mm-diameter zone to avoid various issues with peripheral data (e.g., missing points due to lashes, lid borders, and surface irregularities). *Step 2*. Alignment of all anterior surfaces along the elevation axis to minimize their distances in the least square sense. The anterior surface was used as the reference surface since there is no significant change in anterior elevation in FECD eyes [2]. *Step 3*. The same (anterior) translations are applied to the corresponding posterior surfaces to treat the cornea as one entity. *Step 4*. Once aligned, anterior and posterior surfaces are averaged. *Step 5*. Pachymetry maps are averaged directly.

3. Results

Using these average maps, various comparisons of populations can be performed (Fig. 1). By displaying the average 3D corneal shape before and after surgery in patients with FECD and comparing to normal corneas our results show that DMEK was better and faster at restoring the normal morphology of the cornea than DSAEK as anticipated. However, the post-DMEK corneal model had an increased central corneal thinning compared to healthy controls.

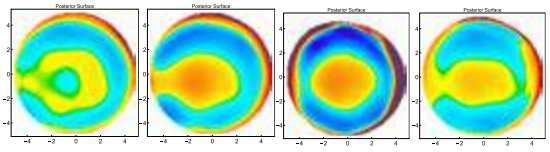

Figure 1: 3D corneal atlas of the posterior surface. From left to right: FECD, DMEK, DSAEK, Normal.

4. Discussion and Conclusions

This research demonstrates that average 3D corneal models offer a unique way to investigate the effect of corneal transplant on the 3D corneal shape.

5. References

1. Laliberté, JF *et al.*, Invest. Ophthalmol. Vis. Sci. 48, 1072–1078 (2007).
2. Brunette, I *et al.*, Invest. Ophthalmol. Vis. Sci. 52, 206–214 (2011).

Acknowledgements:
The authors thank the Quebec Vision Health Research Network for financial support.



MICROGROOVE SUBSTRATES AS A PLATFORM FOR CANCER CELL DEFORMATION

Bettina Roellinger (1), Claire Leclech (2), Abdul I. Barakat (3)

LadHyX, CNRS, Ecole Polytechnique, Institut Polytechnique de Paris, Palaiseau, France

1. Introduction

What triggers cancer cells to migrate through the body during the process of metastasis is of great importance in the comprehension of the disease. Metastatic activity is indeed one of the hallmarks of cancer cells [1] and is responsible for 90% of cancer deaths. Several studies suggest that cancer cells are more deformable than normal cells, and the mechanobiological basis of this observation has received growing interest [2]. We are interested in developing new microenvironment engineering tools and image analysis techniques that can bring new insight into the mechanics of cells in general and cancer cells in particular. The specific tool of interest here is microgroove substrates on which cells can be cultured and that induce significant cellular deformations.

2. Materials and Methods

Fabrication of microgroove substrates. To fabricate the microgroove substrates on which the cells were cultured, liquid PDMS was spin coated at 1500 rpm for 30 s on a PDMS mold composed of 8 µm deep microgrooves with sizes in width varying from 5 to 10 µm.

Cell lines used. The following cell lines were used: normal breast epithelial cells (MCF10A), moderately invasive breast cancer cells (MCF7), highly invasive breast cancer cells (MDA-MB-231), and two mutated breast epithelial cell lines (MCF10A-BRAFV600E and MCF10A Rac1Q61L).

Image processing and data analysis. 2D images were analysed using the image processing packages Fiji and scikit-image developed in Python. Cell nuclear segmentation was performed through deep learning tools based on the u-net architecture. Data analysis was based on conformational classification of the nuclei and morphological parameters associated to classification.

3. Results

Using the microgroove substrate, we have shown significant deformation and morphological differences among the three breast cancer cell lines MCF10A, MCF7 and MDA-MB-231. We also detected significant differences between the two cell lines with targeted mutations. More specifically, the fraction of nuclei deformed on the microgroove substrate was significantly higher for MCF10A cells than for either the Rac1Q61L or BrafV600E cells.

4. Discussion and Conclusions

These preliminary findings suggest that microgroove substrates combined with deep learning-based image analysis algorithms constitute a promising tool for characterizing mechanical deformations of different cell types pertinent to cancer. These results open avenues for improved understanding cell mechanical properties and their role in certain pathologies.

5. References

1. Hanahan, D., & Weinberg, R. A. (2000). The hallmarks of cancer. cell, 100(1), 57-70.
2. Alibert, C., Goud, B., & Manneville, J. B. (2017). Are cancer cells really softer than normal cells?. Biology of the Cell, 109(5), 167-189.

CMBBE2023
18th International Symposium on Computer Methods in Biomechanics and Biomedical Engineering
3 - 5 May 2023, Paris, France
Arts et Métiers Institute of Technology
Institut de Biomécanique Humaine Georges Charpak
155 boulevard de l'Hôpital 75013 Paris France
www.cmbbe-symposium.com

A METHOD TO ASSESS CHANGES IN MECHANICS IN PROGRESSIVE ADOLESCENT IDIOPATHIC SCOLIOSIS PATIENTS

Corey Fry (1), Maria Antico (1), J Paige Little (1)

1. Biomechanics and Spine Research Group, School of Mechanical, Medical and Process Engineering, Queensland Uni of Technology, Australia.

1. Introduction

Adolescent idiopathic scoliosis (AIS) is a 3D deformity of the spine. While AIS aetiology has been linked to biomechanical, biochemical, and genetic factors [1], progression of the deformity is associated with biomechanical drivers [2, 3]. Attempts have been made to explore the progressive changes in joint biomechanics [3,4], but no prior study has explored the 3D change in joint centre of mass, as the AIS spinal deformity progresses with growth. Using magnetic resonance imaging (MRI) of AIS patients, this study sought to develop a reliable and quick method to extract the 3D location of the vertebral centre of mass in the AIS spine, with a view to future evaluation of change in biomechanical loading over time.

2. Materials and Methods

MRI data (3T, T1-weighted, 0.5mm cubic voxels) for an AIS patient who was imaged sequentially (4 months apart) over three occasions during the course of their pre-operative treatment (HREC #14/88/AM03) was utilised. The dataset included the major structural curve - T5 to T12. A previously published convolutional neural network (CNN) [5] was used to automatically create a binary 3D DICOM stack (same resolution as MRI) of the thoracic vertebrae. Stack was auto-segmented in Amira (Vsn6.0.0, Thermo Fischer Scientific, USA), the reconstruction smoothed and surface artefacts removed using Geomagic Wrap (2022, 3D systems, USA), and the vertebral body isolated using anatomical landmarks on the posterior vertebral surface (Fig 1a).

3. Results

Using the CNN, a 3D dataset of a thoracic spine spanning T5-T12 could be reconstructed, smoothed and cleaned (Fig 1a). Following image processing, the vertebral body COV were calculated and registered to the centroid of T12 in Scan 1. The 3D location of all vertebral COV were tracked between scans, showing change with progressive deformity (Fig 1b,c). Using this CNN-based workflow, a thoracic spine can be reconstructed from 3D MRI and biomechanically relevant landmarks created in approximately 90-120 minutes.

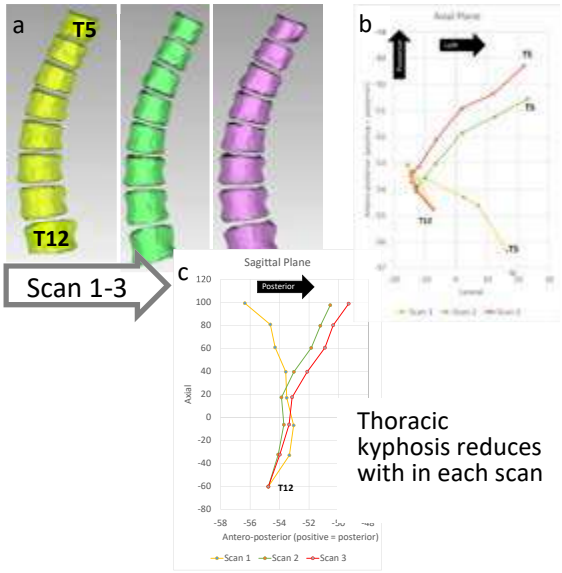

Figure 1: a. 3D reconstructions; Vertebral centroids in the axial (b) and sagittal (c) plane.

4. Discussion and Conclusions

3D reconstruction of vertebral anatomy from MRI is typically carried out using manual segmentation, which is time-consuming and impractical for large datasets. But the use of MRI is preferable for paediatric populations due to the lack of ionising irradiation. The current study presents a reliable and highly promising approach to enable exploration of the biomechanical drivers relating to AIS progression in the developing spine.

5. References

1. Goldberg et al. Pediatric Surg Int, 24 (2008).
2. Stokes et al. Scoliosis, 1:16 (2006).
3. Keenan et al Scoliosis, 10:35, (2015)
4. Adam et al, Spine, 33(2), E30, (2008).
5. Antico et al, IEEE Access, 9, p86811, (2021).



FEATURE EXTRACTION OF FMRI FOR AUTISM BY REINFORCEMENT LEARNING

Hung-Ming Chi
Department of Computer Science, College of Computer Science, National Yang Ming Chiao Tung University, Taiwan

1. Introduction

Autism Spectrum Disorder (ASD) is diagnosed as having deficits in social interaction and repetitive behaviors and exhibits the impairment of brain function [1,2]. Although the brain region of ASD has been investigated, the neural mechanism is still unclear. The objective of this study is to extract the main brain regions of ASD from functional Magnetic Resonance Imaging (fMRI) data by using reinforcement learning.

2. Materials and Methods

The resting-state fMRI data of cortical thickness from the open-access Autism Brain Imaging Data Exchange [3] was used to explore the brain regions of 6–64 years old ASD and healthy control (HC) groups. To collect the Wechsler Abbreviated Scale of Intelligence scores, the Caltech, NYU, Pitts, SDSU, Stanford, UCLA, and USM datasets [3] were selected for follow-up analysis. A total of 101 brain regions as input information were applied to the Extended Classifier System with continuous real-coded variables (XCSR).

The XCSR, one kind of reinforcement learning method [4], was used to classify and extract important features between the ASD and HC groups. The parameter setup of XCSR was based on the previous study [5], and the epoch and population size were 100 and 4,000, respectively. The reward of XCSR for HC and ASD were 0 and 1,000, respectively. The XCSR classifiers showed a reward of 1,000 and a numerosity over one for analyzing the brain features. The data processing was carried out in the LabVIEW environment of the 2019 version.

3. Results

This study deleted the missing data and then analyzed the fMRI data of 233 ASD (17.5 ± 8.4 years old; 207 men) and 275 HC (16.6 ± 7.3 years old; 225 men). Fig. 1 illustrates the classification accuracy (%) for 25,400 iteration numbers by the moving average per 50 exploitations and the average of 30 replications. For feature extraction, the left hippocampus, left medial orbitofrontal, right rostral anterior cingulate, right medial orbitofrontal, right entorhinal, and left lingual are the dominant brain regions.

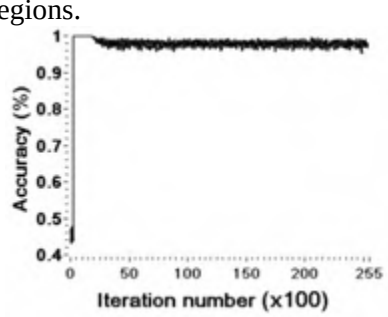

Figure 1: Classification accuracy

4. Discussion and Conclusions

This study proposed a novel method to extract the important brain regions of ASD. The result support previous research into the group differences in brain regions [2]. However, this study had not investigated the age differences. Notwithstanding this limitation, this study offers a way to observe the mechanism of ASD.

5. References

1. Belmonte MK et al., J Neurosci; 24(42):9228-9231 (2004).
2. Zielinski BA et al., J Neurol; 137(6):1799-1812 (2014).
3. Craddock C et al., Neuroinformatics 2013
4. Wilson SW. 1813 of Lecture Notes in Artificial Intelligence; 2000. P. 209–219
5. Ji HM et al., GECCO 2019

Acknowledgements:
The author would like to thank the Taiwan Ministry of Science and Technology (Grant no: MOST 110-2222-E-A49-010) for providing financial support to this project and L.Y. Chen for providing the code of XCSR.



FROM THE MICRO- TO THE MESOSCALE 3D RECONSTRUCTION OF THE HUMAN LIVER ARCHITECTURE

Mathieu de Langlard (1,2), Olivier Trassard (2,3,4), Jiří Pešek (1,2), Antonietta Messina (2,5), Nassima Benzoubir (2,5), Anne Dubart-Kupperschmitt (2,5), Jean-Charles Duclos-Vallée (2,5), Catherine Guettier-Bouttier (2,3,5), Irene Vignon-Clementel (1,2), Dirk Drasdo (1,2)

1. Inria (Saclay IdF), France; 2. Fédération Hospitalo-Universitaire Hépatinov, Hôpital Paul Brousse, Villejuif, France; 3. UMS44, Inserm-Paris-Saclay University, Le Kremlin-Bicêtre, France ; 4. Pathology Unit, Bicêtre Universitary Hospital, Assistance Publique-Hôpitaux de Paris, Le Kremlin-Bicêtre, France ; 5. UMR_S1193, Inserm-Paris-Saclay University, Villejuif, France.

1. Introduction

2D histopathology is a common technic for the diagnosis and study of diseases of the liver tissue. However, the complexity of the liver organization calls for richer and more consistent data representation, hence leading to spatially resolved 3D visualization and analysis. It would enable better understanding and earlier diagnosis of liver diseases.

We here report on an automatic pipeline of 3D histology reconstruction based on image registration and segmentation to analyse large and consistent liver sample volumes from the micro- to the mesoscale. Morphological quantifications emerging from such an analysis can furthermore inform computational models permitting to probe the possible functional consequences of architectural alterations.

2. Materials and Methods

A tissue of approximately $14 \times 9 \times 0.9\text{mm}$ is taken from a patient liver following orthotopic liver transplantation at the Paul-Brousse Hospital. After fixation and paraffin inclusion, 300 serial sections of 3µm thick are individually labelled with the antibodies anti-EpCAM for the bile ducts and anti-CD31 for the vessels, and stained with haematoxylin for the nuclei.

Due to the physical sectioning, misalignment and deformations of the tissue occur. The fundamental step of the image analysis pipeline is therefore the registration of the 300 images, which mainly consists of i) *a pre-alignment*: centres of mass alignment and best rotation search using the cross-correlation metric, ii) *a global registration*: a rigid followed by an affine transformation, and iii) *a local registration*: application of the well-known diffeomorphic Demons algorithm [1].

The obtained volume is further segmented and post-processed with local thresholding and mathematical morphology techniques. Besides, the liver primary units, called *lobules*, are reconstructed with the morphological watershed algorithm; the segmentation function considers geometrical and topological constraints based on the liver structures.

3. Results

A statistically representative number of entire lobules and their inter-lobular structures (portal veins and hepatic arteries, central veins, bile ducts) are automatically reconstructed and morphologically quantified (e.g. see Fig. 1).

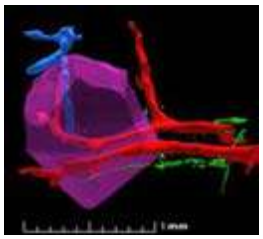

Figure 1: Example of a reconstructed lobule (magenta) with its surrounding structures: afferent vessels (red), central vein (blue) and bile ducts (green).

4. Discussion and Conclusions

For the first time, a large liver tissue volume is automatically reconstructed in 3D and morphologically quantified from 2D histological images i.e. from the micro- to the mesoscale.

5. References

1. Vercauteren, T., et al., NeuroImage, 45(1), p. 61-72, (2009).

Acknowledgements of funding support:
Agence Nationale de la Recherche (iLite project ref 16-RHUS-0005) and the European Research Council under the European Union's Horizon 2020 research and innovation program (No. 864313).

CMBBE2023
18th International Symposium on Computer Methods in Biomechanics and Biomedical Engineering
3 - 5 May 2023, Paris, France



Arts et Métiers Institute of Technology
Institut de Biomécanique Humaine Georges Charpak
155 boulevard de l'Hôpital 75013 Paris France
www.cmbbe-symposium.com

PLANNING SOLUTION FOR SEMI-AUTONOMOUS ASPIRATION OF POPLITEAL CYSTS

Adam Ciszkiewicz (1), Jacek Lorkowski (2), Grzegorz Milewski (1)

1. Department of Applied Mechanics and Biomechanics, Cracow University of Technology, Poland;
2. Central Clinical Hospital of the Ministry of the Interior and Administration in Warsaw, Poland

1. Introduction

A popliteal cyst, also known as a Baker's cyst, is a pathological fluid structure located near a kneepit or in its direct vicinity – Fig. 1. As the classical surgery is undeniably the most common solution, an increasing interest can be observed in the field of computer-aided and robotic surgery [1]. While many different medical conditions have already been considered, there is a lack of work describing a software-hardware platform dedicated to Baker's cysts treatment. The presented solution provides the ability for simple, safe, collision-free and quick aspiration of Baker's cysts during a preliminary diagnosis.

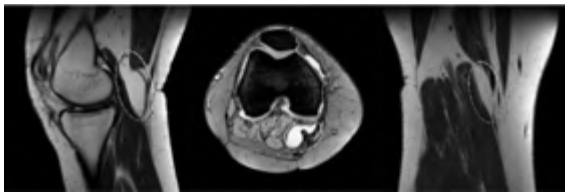

Figure 1. Baker's cysts as seen in different projections and sequences obtained using magnetic resonance (MRI).

2. Methods

The proposed method described in detail in [2] is based on a transverse plane MRI scan of a symptomatic knee. The radiologist/surgeon picks two locations of the needle's tip. The first location is to be inside the cyst and determines the suction position, while the second stands for the incision angle. Then, the computed control data is outputted to the robot and the surgery is performed autonomously with the patient still on the MRI scanner's table. The hardware scheme assumes a gantry-type structure for the simply surgical robot with three translational joints and an additional revolute joint for orienting the needle. The programming trial consists of the DICOM image analyses with the custom software written in Python as well as the vector and matrix transformation analyses for determination of the orientation and insertion angle of the needle.

3. Results

The system was proven to be effective in four numerical scenarios based on real-life cases. The example of the computed needle's orientation and trajectory is shown in Fig. 2.

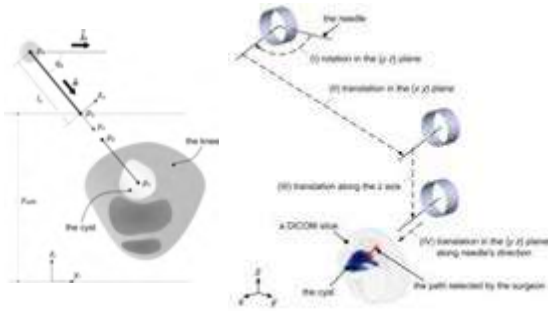

Figure 2: The collision free needle's trajectory approach oriented to the robot's reference frame.

4. Conclusions

The presented solution provides automatic cyst segmentation, estimation of cyst volume and suction time, inverse position analysis and collision-free positioning of the robot for fast and secure emergency aspiration of the liquid content of the cysts. The time delay between the scan and the procedure is reduced to a minimum.

5. References

1. Moustris GP, et al., Evolution of autnomous and semi-autnomous robotic surgical systems: a review of the literature. Int J Med Robotics 7(2011), 375–392.
2. Ciszkiewicz A, Lorkowski J, Milewski G., A novel planning solution for semi-autonomous aspiration of Baker's cysts, Int J Med Robotics Comput Assist Surg. 2018;e1882.



UNCERTAINTY QUANTIFICATION OF HEMODYNAMIC RUPTURE RISK PARAMETERS FOR INTRACRANIAL ANEURYSMS

Florian Hellmeier (1), Jan Brüning (1), Adriano Schlief (1), Leonid Goubergrits (1,2)

1. Institute of Computer-Assisted Cardiovascular Medicine, Charité – Universitätsmedizin Berlin, Berlin, Germany; 2. Einstein Center Digital Future, Berlin, Germany

Correspondence to: Florian Hellmeier, florian.hellmeier@charite.de

1. Introduction

Unruptured intracranial aneurysms (IAs) affect a relevant part of the population and deciding on an optimal surveillance or treatment strategy for incidental IAs remains a challenging task given the substantial morbidity and mortality associated with both IA rupture and treatment [1,2]. While a large number of hemodynamic rupture risk parameters has been proposed, clinical adoption has yet to take place. Besides the ability to identify IAs at risk of rupture, arguably the second most important feature for any rupture risk parameter to be viable is robust computability. To address the later aspect, this study examines the effect of image segmentation on a set of hemodynamic rupture risk parameters.

2. Materials and Methods

A previous study by Voß et al. examined the influence of image segmentation on five hemodynamic rupture risk parameters based on segmentations of five IAs from 26 groups obtained during the Multiple Aneurysms AnaTomy CHallenge 2018 (MATCH) on which 73 computational fluid dynamics (CFD) simulations were performed [3]. Based on that CFD data, this study analyzed a set of 25 hemodynamic rupture risk parameters from three parameter groups (IA wall, IA neck, IA volume). Rupture risk parameters were spatially and temporally averaged where necessary, to obtain scalar quantities for rupture risk assessment.

3. Results

Evaluation of results is still ongoing as of the writing of this abstract. Analysis will include segmentation-induced relative uncertainties and deviations of individual rupture risk parameters, inter-parameter correlations, and histograms to assess parameter distributions. Detailed results will be presented at CMBBE 2023.

4. Discussion and Conclusions

The results will allow assessment of the sensitivity of different hemodynamic rupture risk parameters to image segmentation. Additionally, intra-parameter correlations will help in identifying which parameters capture similar aspects of aneurysmal hemodynamics. This information can be used to identify sets of hemodynamic rupture risk parameters and/or parameter groups that are robust and capture as many hemodynamic features as possible, while hopefully also providing insight into what distinguishes robust parameters.

5. References

1. UCAS Japan Investigators: Morita A et al. N Engl J Med. 2012;366(26):2474-82
2. Kotowski M et al. J Neurol Neurosurg Psychiatry. 2013;84(1):42-8
3. Voß S, Beuing O, Janiga G, Berg P. PLoS One. 2019;14(5):e0216813

Acknowledgements

The authors would like to thank PD Dr.-Ing. Philipp Berg and Dr.-Ing. Samuel Voß (both Laboratory of Fluid Dynamics and Technical Flows, University of Magdeburg, Germany) for providing the CFD data.

Publication of results

Once published, the complete results will be linked to here:

CMBBE2023
18th International Symposium on Computer Methods in Biomechanics and Biomedical Engineering
3 - 5 May 2023, Paris, France



Arts et Métiers Institute of Technology
Institut de Biomécanique Humaine Georges Charpak
155 boulevard de l'Hôpital 75013 Paris France
www.cmbbe-symposium.com

QUANTIFYING JOINT CONGRUENCE WITH AN ELASTIC FOUNDATION

Charles B. Burson-Thomas*, Alex S. Dickinson, and Martin Browne

University of Southampton, UK
**c.b.burson-thomas@soton.ac.uk*

1. Introduction

The level of congruence (or geometric conformity) between the articulating surfaces of a synovial joint can vary substantially between people. It has been hypothesised that a more incongruent instance of a joint could be more at risk of developing osteoarthritis. However, previous methods of quantifying congruence have required detailed mathematical descriptions of the articulating surfaces and their relative position [1,2]. In this talk, we will share our recently published new method of measuring joint congruence [3], directly from the 3D segmented points clouds.

2. Materials and Methods

First, a finite element (FE) simulation of an elastic layer compressed between each set of segmented bones is performed. The results of this are then interpreted using the elastic foundation model (Figure 1), enabling an equivalent, but simpler, contact geometry to be identified. From this, the equivalent radius (quantification of joint congruence) is found. This defines the radius of a sphere contacting plane (or "ball on flat") that produces an equivalent contact to that in each joint. The minimal joint space width (in this joint position) can also be estimated from the FE simulations. The new method has been applied to ten healthy instances of the thumb metacarpophalangeal (MCP) joint.

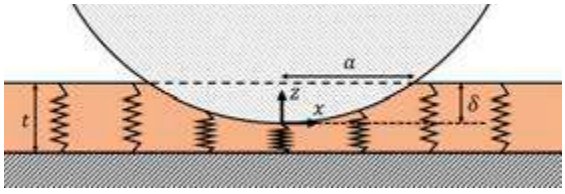

Figure 1: Elastic foundation model: an elastic layer between two rigid surfaces is modelled as a set of independent springs. [3]

3. Results

The ten thumb MCPs had similar levels and variability of congruence as the other diarthrodial joints that have been characterized previously and showed no relationship between congruence and joint space width (Figure 2).

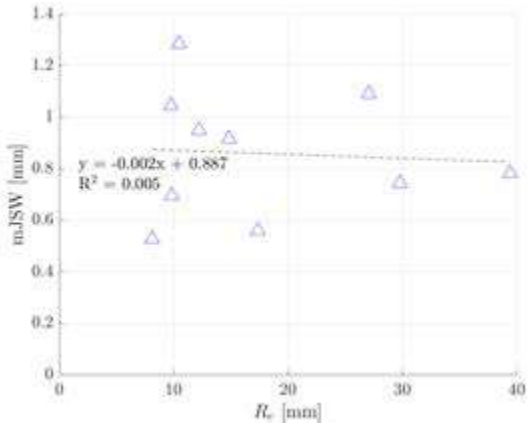

Figure 2: Relationship between minimal joint space width (mJSW) and equivalent radius (R_e). [3]

4. Discussion and Conclusions

The new method enables efficient quantification of congruence directly from CT- or MRI-derived bone geometry in any relative orientation, lending itself to large data sets and coupling with kinematic models.

5. References

1. Ateshian G et al., J of Biomech Eng.; 25(6):591-607 (1992).
2. Connolly KD et al., J of Biomech Eng.; 131(12):124503 (2009).
3. Burson-Thomas CB et al., J of Biomech Eng.; 144:101003 (2022).

Acknowledgements:
This research was conducted as part of the APRICOT project, which has received funding from the European Union's Horizon 2020 research and innovation program under grant agreement No. 863183.

CMBBE2023
18th International Symposium on Computer Methods in Biomechanics and Biomedical Engineering
3 - 5 May 2023, Paris, France



Arts et Métiers Institute of Technology
Institut de Biomécanique Humaine Georges Charpak
155 boulevard de l'Hôpital 75013
Paris France
www.cmbbe-symposium.com

DEEP LEARNING AS A TOOL FOR AUTOMATICALLY CREATING PATIENT-SPECIFIC SPINE MODELS

Ivanna Kramer (1), Sabine Bauer (2), Manuel Hun (1), Martin George (1), Dietrich Paulus (1)

1. Institute for Computational Visualistics, University of Koblenz, Koblenz, Germany; 2. Institute of Medical Technology and Information Processing, University of Koblenz, Germany

1. Introduction

Building complex patient-specific spinal biomechanical models that incorporate hundreds of parameters is often done manually. Even partial automation of this process would help eliminate possible manual errors and save a lot of effort and time. In this study, we present two deep learning approaches that facilitate the construction of multibody simulation (MBS) models of the spine by automatically reconstructing the spine and its essential parts from patient data.

2. Materials and Methods

In order to automatically extract the vertebrae from the Magnetic Resonance Images (MRI) of the lumbar spine (Figure 1), a 3D-Unet [1] was adapted and trained. Once the vertebrae are segmented, we calculate the centroid of the intervertebral disc as a middle point of the cubic spline that connects the centers of the extracted vertebral bodies (Figure 1 (c)).

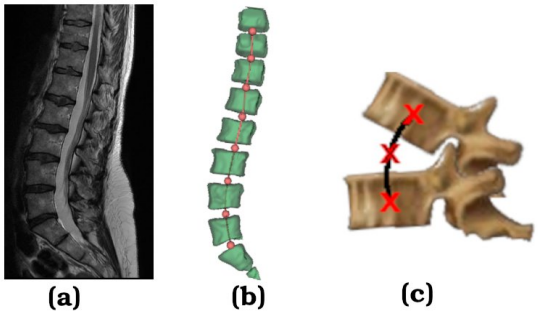

Figure 1: Input MRI (a) is segmented by applying 3D-Unet neural network. The result of the segmentation is shown in (b). Subsequently, the centroids of the intervertebral discs are estimated using the spline constructed between the centers of the adjacent vertebral bodies.

For the localization of the ligament attachments, a fully connected neural network (FCN) was trained to find 77 points on the vertebrae's surface (Figure 2(a)). The initial dataset containing 17 verterae was enlarged using mesh deformation methods.

3. Results

The experimental results show that the trained Unet exceeds state-of-the-art performance on the chosen datasets with an accuracy of 98.79±(0.23)% and DICE of 88.63 ± (1.08)%. The FCN demonstrates good results with an average euclidean distance of approx. 0.665mm between ground truth and predicted

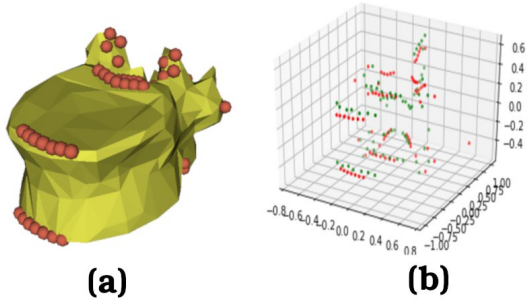

points (see example prediction in Figure 2(b)).

Figure 2: 3D mesh of T11 with annotated attachment points of the ligaments (a), 77 ligament points predicted by the proposed FCN (green) and corresponding ground truth (red).

4. Discussion and Conclusions

We could show, that deep learning methods successfully extract structures from patient data and, therefore, can be effectively applied in automatically building the spinal MBS models.

5. References

1. Çiçek, Ö., Abdulkadir, A., Lienkamp, S. S., Brox, T., & Ronneberger, O. (2016, October). 3D U-Net: learning dense volumetric segmentation from sparse annotation. In International conference on medical image computing and computer-assisted intervention (pp. 424-432). Springer, Cham.



ON THE FEASIBILITY OF USING FE-BASED DIGITAL VOLUME CORRELATION TO MAP BREAST DEFORMATION

T. Lavigne (1), A. Mazier (1), A. Perney (1,2) , S. P.A. Bordas (1) , F. Hild (3) , J. Lengiewicz (1,4)

1. Institute of Computational Engineering, University of Luxembourg, Luxembourg; 2. Centre des Materiaux, Mines ParisTech, PSL University, France; 3. Laboratoire de Mecanique Paris-Saclay, France; 4. Institute of Fundamental Technological Research, Polish Academy of Sciences, Poland

Correspondence: Thomas.lavigne@uni.lu

1. Introduction

In vivo soft tissue displacement field measurement is key for validating numerical models. For breast conservative surgery, the surgeon needs to mentally assess the tumor position from prone to supine stances [1]. This study aims to demonstrate the feasibility of using Digital Volume Correlation (DVC) to measure hard/soft tissue deformations of a female quarter thorax between two scans.

2. Materials and Methods

Each scan was segmented, and a multipart mesh composed of bone, cartilage, and tissue, was created. In the absence of intermediate scans, a 3-step DVC pipeline was implemented. The displacement field was computed based on external biomarkers placed on the skin. Homogeneous and regularized DVC on mask images provided a more accurate displacement field. High elastic contrasts between the soft tissue and the bones (10^6) and cartilage (10^4) were introduced to run heterogeneously regularized DVC.

3. Results

The large displacement field, including the inframammary fold, was recovered by the proposed method (Fig. 1). A final RMS residual equal to 18.3 gray levels was achieved when using a regularization length of 4 voxels (i.e., 1.4 mm). An a posteriori standard strain uncertainty was found to be less than 5×10^{-3}.

4. Discussion and Conclusion

The present study showed the capacity of FE-based DVC to faithfully capture large deformations of hard/soft tissues. However, only one sample was studied, and the gravitational forces were not included in the regularization scheme. Further study is thus required to consider the same method using MRI-scans, more samples and including gravity. Further details are provided in Ref. [2].

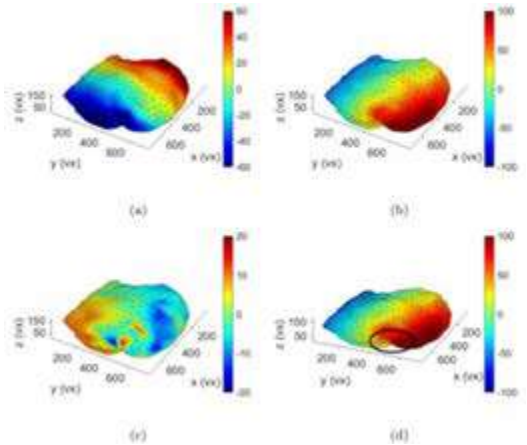

Figure 1 Displacement fields expressed in voxels (1 voxel ≡ 0.34 mm). (a) $\boldsymbol{u_x}$, (b) $\boldsymbol{u_y}$ and (c) $\boldsymbol{u_z}$. (d) $\boldsymbol{u_y}$ from another point of view and inframammary fold; after Ref. [2].

5. References

1. Mazier, A. et al., Journal of Biomechanics 128; ISSN 1751-6161, 2021
2. Lavigne T. et al., Journal of the Mechanical Behavior of Biomedical Materials 136; ISSN 0021-9290, 2022.

Acknowledgements:

This study was supported by the EU Horizon 2020 research and innovation program under grant No 811099 & 800150, 764644, and the FNR Project No. C20/MS/14782078/QuaC. The medical images were obtained at Hospital Arnaud de Villeneuve and AnatoScope. The authors thank Synopsys for the courtesy of the meshes.



POLYCHROMATIC POLARIZED LIGHT MICROSCOPY FOR DYNAMIC TENDON AND 3D PRINTED SCAFFOLD IMAGE ANALYSIS

Devin von Stade (1), Samuel Winston (1), Tia Tedford (1)
Ben Gadomski (1), Daniel Regan (1), Kirk McGilvray (1)

1. Orthopaedic and Bioengineering Research Laboratory, Colorado State University, Fort Collins, Colorado, United States of America

Corresponding Author: Devin von Stade Email: vonstade@colostate.edu
Colorado State University, 0912 Campus Delivery, Dairy Building Fort Collins, CO 80523, USA

1. Introduction

Polychromatic Polarized Light Microscopy (PPM) is an advanced microscopy technique that correlates hue of transmitted light with the direction of anisotropic polarization by a subject and intensity of birefringence with brightness [1]. As the degree of birefringence and anisotropy are both related to molecular organization, patterns of colour and light intensity can inform on changes in molecular organization during mechanical loading allowing inference of the effects of this loading on the material. Herein we describe our investigation of this image analysis technique for use in rotator cuff tendon and a 3d printed, melt-electrowritten scaffold (MEW) undergoing uniaxial mechanical loading.

2. Materials and Methods

Imaging was performed using a BX40 Olympus microscope modified with a PPM light generator and analyzer,and taken at 400X magnification. Unstained sections of ovine rotator cuff tendon (paraffin-embedded fixed infraspinatus; 2x1cm and 200um thick) were deparaffinized and soaked in mineral oil prior to mounting on a mechanical tester. 3D printed scaffolds were similarly mounted and imaged in 3 regions of interest, defined by woven geometry. All samples were loaded uniaxially in the direction of the fibers (collagen or MEW). The open-source image analyser ImageJ was used to assign topology scores based on hue and saturation patterns. Topology scores were compared across mechanical loading and between tendon and the 3d printed scaffold.

3. Results

Sections of tendon demonstrate shifts in the characteristic crimping pattern of the tendon collagen bundles demonstrated by hue shifts from purple to green (Fig.1-left). Scaffold sections demonstrate the bunching of the woven fibers with a shift in hue characterizing their alignment (Fig.1-right). This is similar to the shift in crimping observed in the tendon.

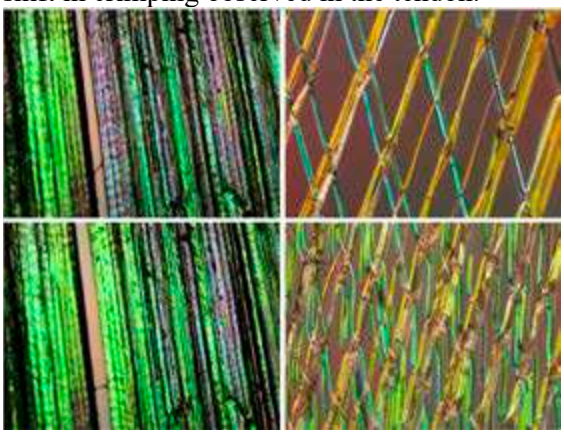

Figure 1: Tendon (left) and scaffold (right) at relaxed and tensed states imaged using PPM. Scaffold fiber diameter is 10-15um (400X mag).

4. Discussion and Conclusions

These proof-of-concept techniques demonstrate changes in fiber alignment in both an implantable scaffold and its tissue target that can infer sub-microscopic shifts in molecular organization. In this way, we hope to expand our ability to assess the mechanical characteristics of tissues and their scaffold/ implant counterparts, better informing medical device designs and tissue responses.

5. References

1. Shribak, M. Scientific Reports; 5(1), 17340 (2015).

CMBBE2023
18th International Symposium on Computer Methods in Biomechanics and Biomedical Engineering
3 - 5 May 2023, Paris, France
Arts et Métiers Institute of Technology
Institut de Biomécanique Humaine Georges Charpak
155 boulevard de l'Hôpital 75013 Paris France
www.cmbbe-symposium.com

CORRESPONDENCE-BASED STATISTICAL ANALYSIS OF SUBJECT-SPECIFIC HIP BIOMECHANICS

Penny R. Atkins (1), Alan Morris (1), Shireen Y. Elhabian (1), Andrew E. Anderson (1)

1. University of Utah, USA

1. Introduction

While finite element analysis has become a staple method in biomechanics, statistical analysis of these data remains rudimentary and rooted in descriptive statistics of arbitrarily defined regions. Recently, statistical parametric mapping (SPM) has been adopted for similar surface-based analyses; however, the spatial relationships of the data are often ignored. We propose a related inference-based method that respects subject-specific variation and accounts for the spatial connectivity of the data. To demonstrate feasibility, we applied our approach to a previously published dataset comparing acetabular cartilage contact stress between control subjects and patients with acetabular dysplasia [2].

2. Materials and Methods

We leveraged correspondence-based shape modelling (CSM), which automatically optimizes the placement of a dense set of corresponding particles (i.e., landmarks) across any population of shapes, for our analysis. Here, a CSM (ShapeWorks, shapeworks.sci.utah.edu) of the acetabular chondrolabral surface was generated. Spatially varying contact stress data was interpolated for each particle on the articulating surface (303 of 768 particles). We then compared these values using a two-way ANOVA with consideration of a between-subject factor of Group (control vs. dysplastic) and a within-subject factor of Activity (heel-strike of ascending and descending stairs, heel-strike and mid-stance of level walking). The spm1d python library (spm1D, spm1d.org) was used for the initial statistical analysis and for 1D-SPM, while custom Python scripts were used to apply correspondence network based statistical inference, considering spatial connectivity of correspondences [2]. Both analyses used 10,000 permutations for inference and a p-value <0.05 for significance.

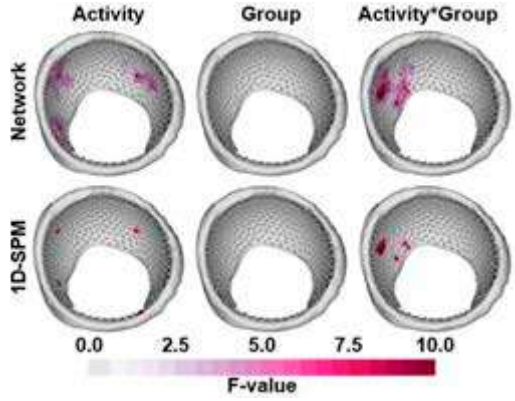

Figure 1: The network-based approach (top) identified similar, but larger regions of significance compared to 1D-SPM (bottom).

3. Results

Activity and Activity-Group interaction effects were identified using both methods. The network method identified three broad regions significantly related to activity (64 particles), whereas 1D-SPM identified four isolated particles, three of which overlapped with the network results. The network method identified one broad region significantly related to the interaction effect (48 particles), whereas 1D-SPM identified three smaller regions (8 particles) within the same area.

4. Discussion and Conclusions

The proposed correspondence-based network analysis method identified interpretable regions of significant effects without loss of subject-and spatial-specificity.

5. References

1. Henak CR et al., Osteoarthritis Cartilage; 22(2):210-7 (2014).
2. Gatti AA et al., MAGMA; 35(5):861-73 (2022).

Acknowledgements:

The authors would like to thank the National Institutes for Health (Grants R01EB016701, U24EB029011, R01AR076120) for providing financial support to this project.



CRYOGENIC CONTRAST-ENHANCED MICROCT ENABLES 3D HISTOPATHOLOGY OF SOFT BIOLOGICAL TISSUES

Arne Maes[1,2,3], Camille Pestiaux[2,3], Alice Marino[4], Tim Balcaen[2,3,5], Lisa Leyssens[2,3], Sarah Vangrunderbeeck[2,3,5], Grzegorz Pyka[2,3], Wim M. De Borggraeve[5], Luc Bertrand[4], Christophe Beauloye[6], Sandrine Horman[4], Martine Wevers[1], Greet Kerckhofs[1,2,3,7]

[1] Department of Materials Engineering, KU Leuven, Belgium [2] Biomechanics lab, IMMC, UCLouvain, Belgium [3] Pole of Morphology, IREC, UCLouvain, Belgium [4] Pole of Cardiovascular Research, IREC, UCLouvain, Belgium [5] Molecular Design and Synthesis, Department of Chemistry, KU Leuven, Belgium [6] Division of Cardiology, University Hospital Saint-Luc, Belgium [7] Prometheus, Division for Skeletal Tissue Engineering, KU Leuven, Belgium

Correspondence information: arne.maes@kuleuven.be

1. Introduction

Visualization of the tissue's microstructure is crucial to fully understand their functioning, as well as the impact of diseases and treatments. However, classical 2D histology only partially reveals the complex 3D microstructure of tissues. In this regard, X-ray based 3D histology, using contrast-enhanced microCT (CECT), can provide important complementary information [1]. Here, we present an extension to conventional CECT, termed cryogenic contrast-enhanced microCT (cryo-CECT), which substantially improved the 3D visualization of individual tissue constituents, such as muscle and collagen fibers [2].

2. Materials and Methods

Cryo-CECT combines sample staining, using a contrast-enhancing staining agent (CESA), with subsequent freezing at an optimal freezing rate. Next, the sample is imaged by microCT in the frozen state, using an *in situ* cryo-stage.

3. Results

Cryo-CECT was first optimized in terms of CESA and freezing rate using bovine muscle tissue (Fig. 1 a-d). To demonstrate the added value of cryo-CECT to histopathology, we then applied cryo-CECT on murine hearts that underwent transverse aortic constriction (TAC) surgery, a well-established animal model for pressure overload-induced cardiac hypertrophy. Cryo-CECT allowed to analyze, in an unprecedented manner, the orientation and diameter of the individual muscle fibers in the entire heart (Fig. 1 e), as well as the 3D localization of fibrotic regions within the myocardial layers.

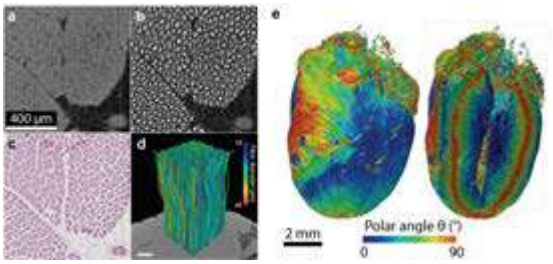

Figure 1: **Cryo-CECT allows histo(patho)logical assessment of skeletal and cardiac muscle tissues. a-b**, MicroCT images of the same bovine muscle sample stained with Hf-WD POM, acquired with conventional CECT (a) and with cryo-CECT (b). **c**, Matching 2D histological section (H&E staining) **d**, Fiber model based on (b). Color scale indicates fiber diameter. Scale bar = 500 µm. **e**, 3D spatial graph of the cardiac muscle fiber orientation of a TAC heart. Color scale indicates fiber orientation.

4. Discussion and Conclusions

In this study, we presented a novel approach to CECT, termed cryo-CECT, which enables nondestructive 3D histo(patho)logy of various individual soft tissue constituents by imaging the stained sample in its frozen state. The application of cryo-CECT to murine hearts that underwent TAC surgery demonstrated the histopathological potential and added value of this new technique.

5. References

1. De Bournonville S et al., Contrast Media and Molecular Imaging (2019).
2. Maes A et al., Nature Communications (2022).



COMPARISON OF THE MORPHOLOGY AND HEMODYNAMICS OF THE HUMAN, PORCINE, AND OVINE PULMONARY ARTERY

Jan Brüning (1), Nina Krüger (1), Pavlo Yevtushenko (1), Leonid Goubergrits (1)

1. Institute of Computer-assisted Cardiovascular Medicine; Charité – Universitätsmedizin Berlin; Germany

1. Introduction

Animal models play a crucial role in clinical and biomedical research, as well as development of medical devices. They are commonly used as pre-clinical tool towards human clinical trials. In this study, we investigate the similarity of porcine, ovine, and human pulmonary artery (PA) geometries with respect to anatomic and hemodynamic parameters. The study aims to support translation of findings from animal models to human trials to assess safety and efficacy of cardiovascular devices implanted within the PA.

2. Materials and Methods

Using computed tomography data, the subject-specific anatomy of 14 ovine, 41 porcine, and 48 human PAs was reconstructed. Reconstruction was performed manually using region flood-fill and brush tools implemented in ZIBAmira (v2015.28, Zuse Institute Berlin). Surface geometries were subsequently smoothed and truncated at the main pulmonary artery as well as all branching vessels of the left and right PA. The vascular tree centreline was calculated automatically and used to assess anatomical parameters, such as diameters, segment lengths, bifurcation angle and the curvature.

To also assess the subject-specific hemodynamics within these anatomies, computational fluid dynamics (CFD) simulations were performed using STAR-CCM+ (v. 17.04, Siemens PLM). Blood was modelled as non-Newtonian fluid using a Carreau-Yasuda model, whereas turbulence was modelled using a k-ω SST model. Transient simulations using pulmonary artery volume flow waveforms, measured using 4D velocity encoded MRI, as inlet boundary condition, were conducted. Zero-pressure outlets were used as outlet boundary conditions, as no patient-specific information on either the pulmonary resistance or the flow split towards the left and right pulmonary artery was available. Hemodynamic parameters commonly used in thrombus prediction models, such as oscillation shear indices and wall shear stresses were evaluated.

3. Results

Evaluation of the results is still ongoing and only preliminary results are available. However, already relevant differences between anatomical parameters, such as the bifurcation angle between left and right PA, as well as the diameters, lengths, and curvatures of these vessels, were found for the different species. Thus, differences between the hemodynamic parameters of interest are also to be expected and will be reported.

4. Discussion and Conclusions

The anatomy of relevant cardiovascular structures and their respective hemodynamics differ markedly between humans and different animal models. In-silico studies are a promising approach to assess these differences and provide additional crucial information necessary to improve the translation from animal to human trials. Furthermore, as capabilities of numerical models are ever increasing, in-silico clinical trials might allow to reduce pre-clinical trials and better incorporate the inter-species differences in the future.

Acknowledgements:

This work has been funded under the European Union's Horizon 2020 research and innovation programme under grant agreement N° 101017578.

CMBBE2023
18th International Symposium on Computer Methods in Biomechanics and Biomedical Engineering
3 - 5 May 2023, Paris, France



Arts et Métiers Institute of Technology
Institut de Biomécanique Humaine Georges Charpak
155 boulevard de l'Hôpital 75013 Paris France
www.cmbbe-symposium.com

VALIDATION OF ABDOMINAL AORTIC ANEURYSM MOTION TRACKING WITH SIMULATED ULTRASOUND CINE-LOOPS

Marta Irene Bracco (1,2), Marco Biancolini (3), Stephane Avril (1), Laurence Rouet (2)

1. Mines Saint-Étienne, France; 2. Philips Research, France; 3. University of Tor Vergata, Italy

Corresponding author: Marta Irene Bracco, marta.bracco@emse.fr

1. Introduction

Current management of abdominal aortic aneurysms (AAA) cannot reliably assess the disease severity and the risk of rupture as it fails to characterize the mechanical aspects of the disease. A promising approach consists in extracting the cyclic strains in the AAA wall from time resolved ultrasound (US) sequences. Our aim is to validate the fast Sparse Demons tracking algorithm for this application.

2. Materials and Methods

Data acquisition: Five AAA 2D US b-mode cine-loops (frame rate 30-40 Hz) were acquired.
US simulation: The MUST toolbox was employed to obtain realistic time resolved 2D b-mode US simulations using real images as templates [1]. Simulation is based on the convolution of a pressure field with a map of scatterers, i.e. monopole sources of US echoes. Scatter coefficients were calculated from the pixel intensity in the corresponding locations on the template. The scatter map was updated at each frame to impose fictitious displacements in the wall from a mechanical simulation of its motion to use as a ground truth, similarly to a previous validation for myocardial strain [2].
Wall motion analysis: A regular circular grid with a thickness of 2 mm and a resolution of 1 mm was placed on the AAA wall. The Sparse Demons tracking algorithm [3] was then applied to the grid nodes. The mean and maximum errors in each frame were calculated as the distance to the ground truth.

3. Results

Boxplots of mean and maximum frame errors in each sequence are shown in Figure 1. The mean error found was always below the average image resolution (0.2 mm). However, maximum values up to 1.2 mm were found.

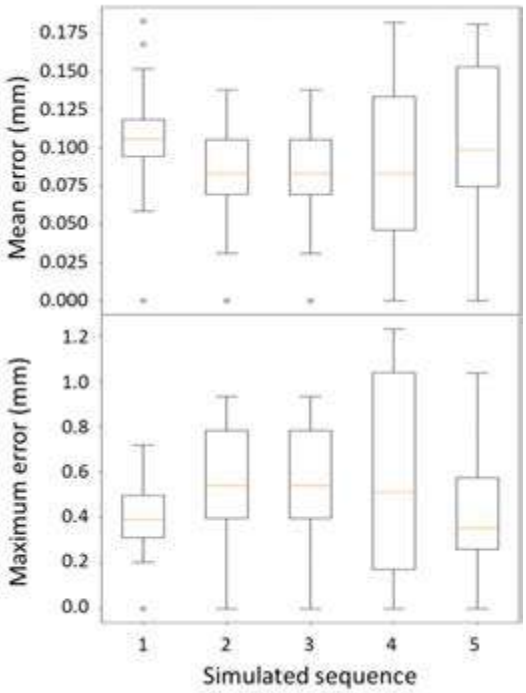

Figure 1: Boxplots of mean (top) and maximum (bottom) frame errors in each US sequence.

4. Discussion and Conclusions

The presented work shows that the sparse demons tracking algorithm was able to reconstruct the overall displacement field in the AAA wall, although localized error peaks are present, likely due to low image quality.

5. References

1. Rodriguez-Molares, Alfonso, et al. 2017 IEEE IUS. IEEE, 2017. p. 1-4
2. Alessandrini, M. et al., IEEE Trans. Ultrason. Ferroelectr. Freq. Control, 65(3):411-422 (2018).
3. Somphone O et al., 2013 IEEE 10th ISBI: IEEE; 2013. p. 1182-1185

Acknowledgements:
This project has received funding from the European Union's Horizon 2020 grant 859836.



AUTOMATIC ESTIMATION OF CENTER OF MASS FROM MULTI-CAMERA VIDEO SYSTEM

T. Goyallon (1,2), B.K. Lahkar (3), P. Marrec (1,2), R. Dumas (3), L. Reveret (1,2), A. Muller (3), T. Robert (3)

1. LJK, CNRS UMR 5224, Université Grenoble Alpes, France ; 2. INRIA Grenoble Rhône-Alpes, France ; 3. Univ Lyon, Univ Eiffel, Univ Claude Bernard Lyon 1, LBMC UMR_T9406, France

Corresponding author: T. Robert (thomas.robert@univ-eiffel.fr)

1. Introduction

Estimation of Center of mass (CoM) is essential in analysing human movement and posture, and is widely estimated using anthropometric tables (AT) [1]. These tables are, however, based on a population of normal weights, without accounti -ng for high variability in age and body shapes. Alternatively, body segments' volume can not only provide reliable estimation of subject-specific CoM, but also take into account segme -nt deformability. Here we propose an automatic method for estimating CoM from 3D meshes of body envelope computed with a multi-camera video system in different posture.

2. Materials and Methods

Three subjects participated in this study, with mean age: 26.7±2 years and mean BMI: 28±1.8 kg/m^2. Data collection was performed using a calibrated markerless video camera system (10 RGB full HD cameras, 60 fps). Participants were asked to perform a T-pose and a squat-pose. The multi-stage approach for recovering 3D human meshes from the video-data are: (i) *2D keypoints estimation,* (ii) *Person re-identification*, (iii) *Silhouette extraction,* and (iv) *3D pose and shape estimation*. On the recovered meshes, a predefined segmented template (16 body-segments with anatomical landmarks (AL) as in [1]) was used. Segment coordinate systems (SCS) were defined from the AL [1]. Assuming homogeneous density (1 g/cm3), CoM positions were estimated from volumetric data of each segment derived from the meshes, and expressed in respective SCS. Whole-body CoM was also computed. They were compared to segmental and whole-body CoM positions estimated based on AT [1].

3.Results

In T-pose, CoM differences for all segments (except Pelvis) remain in the range 0-3 cm, indicating good shape approximation from the silhouette. For the squat pose, these differences remain similar except abdomen (~5cm) and thighs (~7cm along SI), possibly due to erroneous pelvis pose (too large pelvis tilt) that should be further investigated. Nevertheless, less than 1.5 cm of difference was observed for the whole-body CoM.

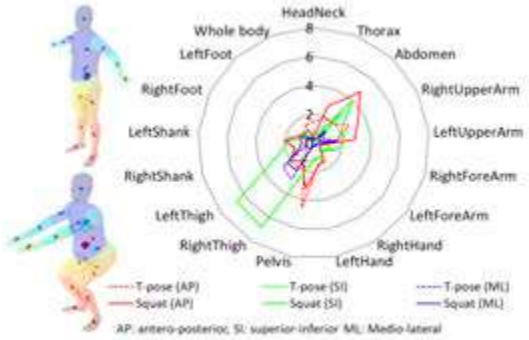

Figure 1: Mean absolute difference between CoM positions (in cm) obtained with volume-based and AT-based method, across all subjects.

4. Discussion and Conclusions

As a first study, we proposed an approach for automatic estimation of CoM positions obtained with volumetric-based method and assessed with classical AT. Preliminary results are promising, yet further investigation is necessary to confirm these results with larger population.

5. References

1. Dumas and Wojtusch, Handbook of Human Motion; 47-77 (2018).

Acknowledgements:

This study was partly funded by the project PerfAnalytics, ANR 20-STHP-0003



VIRTUAL REALITY AS A MEANS TO IMPROVE THE COMMUNICATION AMONG USERS AND ARTIFICIAL HANDS

Joaquín Cerdá-Boluda (1), Marta C. Mora (2), José V. García-Ortiz (2)

1. Instituto de Instrumentación para Imagen Molecular, Universitat Politècnica de València, Spain;
2. Dept. of Mechanical Engineering and Construction, Universitat Jaume I, Spain

1. Introduction

Advanced anthropomorphic hand prostheses are a reality in the present, but the use of these devices is limited due to their high cost and lack of functionality and comfort [1]. One important factor for comfort is the control performance. It turns out that communicating the user with the hand in a natural way is a very complicated problem. A correct and fast interpretation of the user' intention is essential.

From a clinical perspective, an important limitation of myoelectric prostheses is that offline successful performance does not necessarily translate to successful on-subject performance [2]. As a result, occupational therapies have a dramatic impact in the adaptation of subjects to their prostheses. In this context, the introduction of technologies based on virtual reality (VR) and augmented reality (AR) can reinforce the adaptation process and make it less traumatic. Some initiatives were developed years ago but with a very limited range of application due the difficulty of having equipment of enough performance [3]. Lately, the field of VR and AR has experienced an exponential increase, due to the appearance of devices with high computing capacities at affordable prices for the general public.

In this work, a preliminary VR environment for the adaptation of prosthetic hands is presented.

2. Materials and Methods

A VR environment has been developed using Unity3D (see Figure 1), where 3D hand models have been integrated and the teleoperation and communication with these models has been implemented through different input devices, allowing the actuation of the different degrees of freedom of the hand. This environment uses hand models obtained both by 3D scan and 3D modelling using several programs such as blender 3D. A Leap Motion Controller obtains direct estimation of physical hand gesture.



Figure 1: Virtual reality environment.

3. Results

The environment maps physical to virtual hand postures. It senses the hand posture while obtaining other signals, such as myoelectric information, to implement a natural control. In a first approximation, a direct mapping of the hand degrees of freedom has been developed.

4. Discussion and Conclusions

This VR environment offers a first step for the development of a complete solution for prosthetic hand control training that merges several information sources.

5. References

1. Smail LC et al., Disabil Rehabil-Assi; 16(8): 821-830 (2021).
2. Roche AD et al., Curr Surg Rep 7, 5 (2019).
3. Hargrove et al., EMBS conference: IEEE; 2007. p. 4842-5.

Acknowledgements:
The authors would like to thank the Spanish Ministry (Grant no: PID2020-118021RB-100) for providing financial support to this project.



INTEGRATION OF IMAGE-BASED STRAIN MEASUREMENT IN THE FEBIO STUDIO ENVIRONMENT

Elana Lapins[1,2], Steve Maas[2], Michael Herron[2], Jeffrey A. Weiss[1,2]

1. *Department of Biomedical Engineering, University of Utah, United States of America*
2. *Scientific Computing and Imaging Institute (SCI Institute), United States of America*

1. Introduction

Image-based strain measurement methods such as fiducial tracking, image correlation, and deformable image registration are commonly used in biomechanics to measure full-field strain. Digital image correlation (DIC) matches a unique pattern between a series of 2D images taken through deformation, while digital volume correlation (DVC) applies the same algorithms to 3D image data. Combining DIC/DVC with finite element (FE) software would provide users with the ability to validate FE models, map displacement and strain fields directly to FE models, and determine specimen material properties through inverse FE in an integrated environment [1,2]. Current DIC software is either expensive or limited in capabilities. The objective of this work was to develop an interactive open-source framework for DIC/DVC within FEBioStudio and extend the algorithms for applications in biomechanics and mechanobiology.

2. Materials and Methods

We implemented a FE-based DIC approach. The initial image is split into equal sub-regions, called subsets. A pixel-matching algorithm using the normalized sum of squares differences matches each reference subset with its corresponding location in the deformed image. The best match location determines nodal point displacements of a rectilinear grid. Bilinear shape functions interpolate nodal displacements across each subset and are used to calculate the strain. DVC considers voxels rather than pixels. DIC/DVC results can be analyzed in FEBioStudio, an interactive workspace for FEBio, an open-source FE solver created at the University of Utah [3]. We validated our DIC implementation against results from the commercial software VIC-2D [4]. A gold standard was created by warping an image of lung tissue based on the displacement field from a FE model simulating uniaxial stretch. Displacement and strain fields were compared between the DIC implementations.

3. Results

Compared to the FE gold standard model, the normalized mean average error (NMAE) for x and y displacement data was 1.20% and 1.11% for FEBioDIC, and 0.650% and 0.800% for VIC-2D. NMAE between VIC-2D and FEBioDIC x and y displacement data was 0.940% and 1.23%.

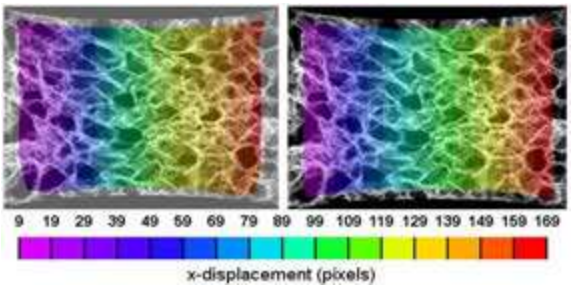

Fig.1: DIC x-displacement results obtained using FEBioStudio (left) and VIC-2D (right).

4. Discussion and Conclusions

Both codes demonstrate excellent agreement with the FE model. Although VIC-2D errors were slightly lower, we think this is likely because we are not currently utilizing the same post-processing methods to eliminate noise. Our future developments include adding similar tools. FEBioDIC will offer users reliable open-source tools to perform DIC and use the results to validate FE models, estimate material coefficients with FEBio optimization modules, and map displacement and strain fields to prescribed boundary conditions for FE analysis.

5. References

1. Lava P et al., Strain 2020;56:e12350. 2. Moerman KM et al., J Biomech 2009; 42(8):1150-1153; 3. Maas SA et al., J Biomech 2012; 134:011005. 4. CorrelatedSolutions,correlatedsolutions.com/vic-2d

Acknowledgments: NIH #R01GM083925



AUTOMATED LABEL-FREE CELL PHENOTYPING FOR DYNAMIC STUDY OF IMMUNE-CANCER CELL INTERACTIONS

Brian Quartey(1),Pratik Kayastha(1),Aavishkar Gautam(1),Jiranuwat Sapudom(1),Jeremy Teo(1)

1. Laboratory for Immuno Bioengineering Research and Applications, Division of Engineering, New York University Abu Dhabi, Abu Dhabi, UAE

Corresponding author: Prof. Dr. Jeremy Teo (Jeremy.teo@nyu.edu, +97126286689)

1. Introduction

Tumor microenvironment comprises a mass of heterogenous cell types including immune cells, along with cancer cells and live imaging is essential to study and understand the interactions of these different cell types. Hence, an automated framework to distinguish the various cell types is necessary. Using fluorescent imaging to identify cells poses unique challenges as dyes have been shown to be potentially cytotoxic, limiting long-term study of cells. Here, we utilize Detectron2, a next generation object detection and instance segmentation library [1] to develop a computational framework for studying dynamic interactions of immune-cancer cell from bright-field live imaging.

2. Materials and Methods

Live imaging of macrophages and MDA-MB-231 cancer cells was performed using a brightfield microscope equipped with an incubation chamber. Initial training dataset of each cell type was generated by manual annotation of > 500 each for macrophages and cancer cells using VGG annotator. Dataset of each cell type was subsequently used to train separate models to automatically generate and compile the final dataset consisting of 77,113 cells from 2576 live images. A validation dataset which was used to determine average precision (AP) and generate confusion matrix to evaluate the model performance.

3. Results

In general, the performance of deep learning models is highly dependent on the quality and quantity of the training dataset used. To ensure that our compiled dataset is generalized and representative, we first sought to determine if microscope magnification at which image data is collected would impact model performance. To do this, a model trained with MDA-MB-231 images taken under 10x magnification was validated on images taken at 20x magnification and vice versa. Our results show that microscope magnification of image data does not significantly affect model performance. Following training of our final model, evaluation shows that our trained model can accurately segment and classify the cell types with AP value for an IoU threshold of 0.75 at 78.8. The confusion matrix also shows that our trained model accurately segments and classifies macrophages with 84.3% accuracy and cancer cells with 87.6% accuracy. Figure 1 presents a sample detection using our framework, showing accurate detection of interaction between macrophage and cancer cell compared to staining with fluorescent dye.

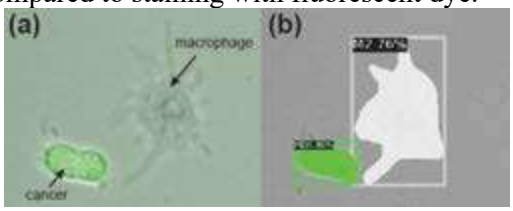

Figure 1: (a) Fluorescently labelled cancer cell and (b) model detection of macrophage and cancer cell.

4. Discussion and Conclusions

Our workflow for automated dataset generation allows us to overcome the challenge of generating large quantity and quality training datasets for our image segmentation model. Overall, this computational framework eliminates the tedious processes and challenges that comes with cell staining, allowing for long term and real-time study of immune-cancer cell interactions.

5. References

1. Wu, Yuxin, et al. "Detectron2." (2019): 2019
2. Dutta, Abhishek, and Andrew Zisserman. "The VIA annotation software for images, audio and video." Proceedings of the 27th ACM international conference on multimedia. 2019.

CMBBE2023
18th International Symposium on Computer Methods in Biomechanics and Biomedical Engineering
3 - 5 May 2023, Paris, France
Arts et Métiers Institute of Technology
Institut de Biomécanique Humaine Georges Charpak
155 boulevard de l'Hôpital 75013 Paris France
www.cmbbe-symposium.com

AI-BASED TRANSVAGINAL ULTRASOUND IMAGE SEGMENTATION ENABLES AUTOMATED CERVICAL LENGTH MEASUREMENT

Alicia B Dagle (1), Yucheng Liu (2), David Crosby (3), Helen Feltovich (4), Michael House (5), Sachin Jambawalikar (2), Kristin M Myers (1)

1. Columbia University, United States of America, 2. Columbia University Irving Medical Center, United States of America, 3. National Maternity Hospital and University College Dublin, Ireland, 4. Intermountain Healthcare, United States of America, 5. Tufts Medical Center, United States of America

kmm2233@cumc.columbia.edu

1. Introduction

Preterm birth (PTB), defined as delivery before 37 weeks of gestation, is the leading cause of perinatal death [1] and is difficult to predict [2]. Thus far, only ultrasound-measured cervical length (CL) has clinical significance as a stand-alone, reproducible factor that can be predictive of PTB [3]. In this work, a deep learning-based model is proposed to automate segmentation and measure CL from transvaginal ultrasound (TVUS) images.

2. Materials and Methods

A 2D Residual UNet [4] generated pixel-level labels of the cervix and surrounding anatomy from TVUS images of 29 term patients [5]. Python scripts automated CL measurement between anatomical internal and external os. Prediction and ground truth were compared by reporting Dice similarity coefficient and differences in CL measurement.

3. Results

The model (Figure 1) achieved a Dice score of 0.80 and 0.82 for the anterior and posterior cervix respectively. The algorithm-reported CL was larger than the manual caliper-reported CL, by an average value of 0.2 cm (N=27).

4. Discussion and Conclusions

In this work, a fully automatic, deep learning-based model generated anatomy labels and CL measurements from TVUS images. Validation on out-of-distribution images suggests the model is generalizable to multiple hospitals and ultrasound systems. This automated workflow may increase sonographer confidence, save clinician time, and promote increased adoption of CL screening in low resource settings.

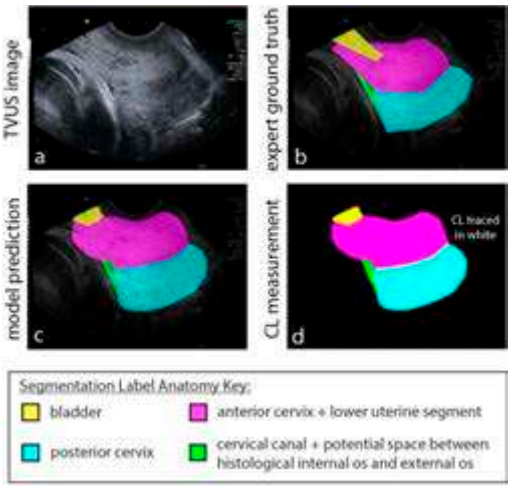

Figure 1: TVUS images (a) were labeled (b) according to 4 segmentation classes. A deep learning model [5] was trained on images submitted to the CLEAR training program for CL screening, and corresponding expert labels. This trained model was applied to an out-of-distribution dataset [6] to generate predicted labels (c). These anatomy labels were then used to automatically measure CL (d).

5. References

1. World Health Organization (2018).
2. Wood NS et al. Arch Dis Child Fetal Neonatal Ed; 90(2): (2005).
3. Mella MT et al. Seminars in Perinatology; 33(5):317-324 (2009).
4. Dagle AB et al., MICCAI 2022 Conference: PIPPI 13575:48-59 (2022).
5. Louwagie EM et al., PLoS ONE;16(1): (2021).

Acknowledgements:

The authors thank the National Science Foundation (Grant no: DGE-2036197) and CU SEAS Interdisciplinary Research Seed grant for providing financial support, the Perinatal Quality Foundation for supplying TVUS images, and Keri Johnson of Intermountain Health for labeling images.

CMBBE2023
18th International Symposium on Computer Methods in Biomechanics and Biomedical Engineering
3 - 5 May 2023, Paris, France



Arts et Métiers Institute of Technology
Institut de Biomécanique Humaine Georges Charpak
155 boulevard de l'Hôpital 75013 Paris France
www.cmbbe-symposium.com

PRELIMINARY RESULTS OF TRACKING CCTA CENTERLINE USING DDQN COMBINED WITH CNN

Wei-Yu Chiu (1), Liang-Yu Chen (2), Hong-Ming Chi (2) and Tzu-Chien Hsiao(2)

1. Institute of Biomedical Engineering, College of Electrical and Computer Engineering, National Yang Ming Chiao Tung University, Hsinchu, Taiwan, ROC.
2. Department of Computer Science, College of Computer Science, National Yang Ming Chiao Tung University, Hsinchu, Taiwan, ROC.

1. Introduction

The coronary artery stenosis and plaque identification from coronary computed tomography angiography (CCTA) requires the extraction of precise centreline [1]. Centerline extraction needs to be performed by an experienced specialist to avoid artificial lesions [2]. In this study, Double Deep Q-learning Network (DDQN) combined with Convolutional Neural Network (CNN) system was developed to track the coronary centreline.

2. Materials and Methods

The data used in this study was the medical imaging database of the National Center for High-performance Computing (NCHC) in Taiwan. This preliminary study adopted the data of 22 subjects, with a total of 3,247 images. Each CCTA image was downscaled to a size of 300x300 pixels as input. Each CCTA image has centreline points marked by professional physicians as output label. The DDQN was responsible for direction tracking, and CNN was responsible for tracking the step size. The structure of the model is shown in Figure 1. The evaluation indicators of the model tracking results adopted the coefficient of determination (R^2) and the Root Mean Square Error (RMSE).

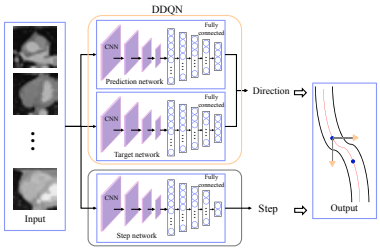

Figure 1: network structure

3. Results

Table 1 lists the results of R^2 and RMSE for the X and Y coordinates, respectively. The results showed that the centreline extracted by DDQN and CNN have high correlation and small errors compared with the ground truth. Figure 2 shows the tracking results, where the red line is the ground truth and the blue line is the prediction result.

Table 1: The results of R^2 and RMSE

	X coordinate	Y coordinate
R^2	0.94	0.99
RMSE	1.09	0.28

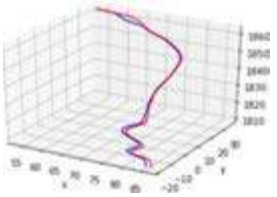

Figure 2: Ground truth and tracking results.

4. Discussion and Conclusions

Preliminary results showed that DDQN combined with CNN to track the centreline of CCTA images can achieve effectively. The RMSE is about 1 millimeter compared to the ground truth. The tracking results are also highly correlated with the ground truth. In the future, the complete CCTA image database will be used to verify the generalization and tracking capabilities of the model. Rule-based reinforcement learning is then employed to interpret what the model has learned [3].

5. References

1. Zhang P, Wang F, Zheng Y. MICCAI 2018 conference: Springer; 2009. p. 755-763
2. Leipsic J et al., J. Cardiovasc Comput Tomogr; 8(5):342-358 (2014).
3. Chen L.-Y et.al., GECCO 2015 conference: ACM; 2015. p. 973-980

Acknowledgements:
This study was supported by the Taiwan Ministry of Science and Technology (MOST109-2221-E009-117-MY3). Dataset access rights obtained from NCHC approval (MIAI-2021-M9-01)

CMBBE2023
18th International Symposium on Computer Methods in Biomechanics and Biomedical Engineering
3 - 5 May 2023, Paris, France



Arts et Métiers Institute of Technology
Institut de Biomécanique Humaine Georges Charpak
155 boulevard de l'Hôpital 75013 Paris France
www.cmbbe-symposium.com

COLORECTAL CANCER STAGE PREDICTION USING MACHINE LEARNING ALGORITHMS

Elçin Güveyi (1), Zeyneb Kurt (2), Nizamettin Aydın (1)

1. Department of Computer Engineering, Yildiz Technical University, Turkey;
2. Department of Computer and Information Sciences, University of Northumbria, UK

Corresponding author: Elçin Güveyi, eguveyi@yildiz.edu.tr

1. Introduction

Colorectal cancer is one of the deadliest types of cancer in the world. There are many studies in the literature investigating genes related to CRC with machine learning approaches [1,2]. In this study, we used machine learning algorithms to predict the stage of cancer patients based on gene expression data. The commonly used staging system has four cancer stages, from 1 to 4. Staging of cancer patients enables clinicians to plan appropriate treatment.

2. Materials and Methods

The GSE39582 [3] dataset was used in the study as it has more samples than any other general gene expression dataset. The dataset includes the gene expression values of colorectal cancer patients and control (normal) samples. Normal samples without tumours were excluded as we aimed to estimate the cancer stage of the patients. Also, samples labelled as stage 0 were excluded. Finally, the dataset was obtained with 562 patients (sample) and 17639 genes (features).

Pre-processing is an important step in machine learning research. Reducing the number of features increases the success of the machine learning model. In this study, DGE analysis was applied as a feature selection method to find discriminative genes between cancer stages. For DGE analysis, *limma* package was used in the RStudio environment. After DGE analysis, up and down regulated genes were determined for each stage. Total of 843 unique genes were obtained.

SMOTE is an algorithm which provides equal distribution between the classes. It produces synthetic samples based on real data points. It has been used in machine learning studies based on gene expression data [4]. Initially, the dataset classes from stage 1 to stage 4 contained 33, 264, 205 and 60 samples, respectively. The number of instances in each class has been balanced and set to 264 after SMOTE. After the pre-processing steps, the dataset was made ready to be trained on machine learning models with 1056 (264*4) samples and 843 features. Three different widely used algorithms were chosen for the study: *Quadratic Discriminant Analysis (QDA)*, *Random Forest (RF)*, and *Support Vector Machine (SVM)*.

3. Results

The dataset is divided into two parts: 80% of the data was used for training and the other part was used for testing. QDA, Random Forest and SVM methods were applied to the dataset. The training, testing, and 10-fold cross-validation accuracy results are shown in Table 1.

Table 1: Success of the models (%)

Model	Train acc.	Val. acc.	Test acc.
RF	100	82	85
QDA	100	84	85
SVM	98	82	83

4. Discussion and Conclusions

Machine learning techniques provide important results such as identifying important genes in diseases. In this study, we predicted cancer stages of CRC patients using gene expression data. In this way, patients can be grouped more accurately and appropriate treatment can be applied.

5. References

1. Liu, J., Dong, C., Jiang, G. et al. BMC Med Genomics 13 (Suppl 9), 135 (2020).
2. Maurya, N.S., Kushwaha, S., Chawade, A. et al. Sci Rep 11, 14304 (2021).
3. Marisa, Laetitia et al. PLoS medicine vol. 10,5 (2013).e1001453.
4. S. Roy, R. Kumar, V. Mittal, D. Gupta, Sci Rep. 10 (2020) 4113.



SYNTHETIC DATA AUGMENTATION STRATEGY FOR THE AORTIC SEGMENTATION FROM PC-MRI SMALL DATASET

Simone Garzia (1,2), Martino Andrea Scarpolini (1,3), Simona Celi (1)

1. BioCardioLab, Fondazione Toscana G. Monasterio, Massa, Italy; 2. Department of Information Engineering, University of Pisa, Pisa, Italy; 3. Department of Industrial Engineering, University of Rome "Tor Vergata", Roma, Italy

1. Introduction

Phase contrast magnetic resonance imaging (PC-MRI) is a modern non-ionizing imaging technique, that can be used to extract functional and morphological information as well as to set up computational models. However, it is characterized by complex data post-processing and the availability of patients' images for research purposes is still challenging in the context of data-driven techniques such as deep learning (DL). In fact, segmenting these images is not trivial, especially for DL algorithms without either enough data or exploiting data augmentation [1]. This work aims to assess the feasibility of a pipeline for the generation of synthetic PC-MRI images to improve the segmentation of thoracic aorta images through DL from small datasets.

2. Materials and Methods

Synthetic high-resolution (HR) 4D velocity images were obtained by analysing 100 computational fluid dynamic velocity maps from both healthy and pathological subjects. The corresponding models were also processed to obtain the masks for the models (Fig. 1a). To generate high-fidelity low resolution (LR) images (Fig.1d) a four-steps procedure [2] was applied. Firstly, a fast Fourier transform (FFT) was used to convert images from spatial domain to the frequency one, then high-frequency information was selected along all three axes to obtain half-dimension data and a zero-mean white gaussian noise was added. It was characterized by a standard deviation (σ) signal proportional to the desired signal-to-noise ratio. Finally, an inverse FFT was applied to revert to the spatial domain. A specific 3DU-Net was set up and trained with different 3D PC magnetic resonance angiography (PC-MRA) datasets combing both synthetics (100) and real (30) cases. A total of 5 real PC-MRA were used as test set and the effect on the DICE score was evaluated by including (DICEsynt) and non-including (DICEnosynt) the synthetic data.

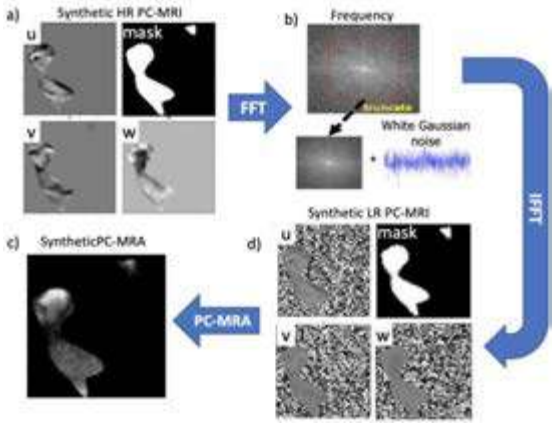

Figure 1: Workflow for the generation of the synthetic PC-MRI and PC-MRA.

3. Results

The results obtained from the trained 3DU-Net, reported as DICE score values, show an improvement in the segmentation performance in all 5 test set cases. Indeed, the ratio between DICEsynt and DICEnosynt was 0.90/0.77, 0.89/0.59, 0.83/0.77, 0.86/0.86, and 0.75/0.55 for P1, P2, P3, P4, and P5 respectively.

4. Discussion and Conclusions

Results suggest the advantages of the adoption of synthetic data augmentation for the 3DU-Net. Additional tests will be performed by increasing the synthetic dataset and by using new synthetic data generation strategies.

5. References

1. Taylor L et al., IEEE SSCI; p. 1542-1547 (2018).
2. Ferdian, E et al., Front. Physics 138 (2020).

Acknowledgements:

MeDiTaTe Project has received funding from the EU's Horizon 2020 research (No. 859836).



AUTOMATIC VIEW CLASSIFICATION OF FOCUSED CARDIAC ULTRASOUND VIDEOS

Catarina Rodrigues (1,2,3), Bárbara Malainho (1,2,3), Ana Cláudia Tonelli (4, 5), André Santanchè (6), Marco A. Carvalho-Filho (7), Jaime C. Fonseca (3), Sandro Queirós (1,2)

1. Life and Health Sciences Research Institute, School of Medicine, University of Minho, Braga, Portugal; 2. ICVS/3B's – PT Government Associate Laboratory, Portugal; 3. Algoritmi Center, School of Engineering, University of Minho, Guimarães, Portugal; 4. Department of General Internal Medicine, Hospital Clínicas de Porto Alegre, Brazil; 5. Department of Medicine, Unisinos University, São Leopoldo, Brazil; 6. Institute of Computing, University of Campinas, São Paulo, Brazil; 7.Univeristy Medical Center Groningen, University of Groningen, Groningen, The Netherlands.

1. Introduction

For any automated processing of focused cardiac ultrasound (FoCUS) videos, the first step is the identification of the imaged cardiac view. So far, most state-of-the-art algorithms were trained on conventional echocardiography images, which have higher image quality and far less instability than those of FoCUS.

2. Methodology

This work proposes a method to automatically classify which of the seven cardiac views a FoCUS video belongs to. The approach is based on four components: (1) a preprocessing routine that standardises each video; (2) a convolutional neural network based on the ResNet-18 [1] and the blur block [2], that simultaneously processes multiple frames of the input video; (3) a training scheme with a flexible loss function and random video augmentations that integrate domain knowledge; and (4) a video-level inference strategy that averages the prediction over multiple clips of the original video.

3. Results

A dataset of 4029 videos from 713 patients was used in the development of the algorithm. The annotation of the cardiac view was performed by a FoCUS expert. The patients were randomly split into 6 groups of equal proportion, with five used for training and validation (5-fold cross validation) and the remaining one used as a held-out test set. The results of the proposed method are presented in Table 1, together with those achieved by a 2D network variant or a plain multi-frame version (*i.e.* without the blur block and training scheme).

Table 1: MCC and F1-scores of the proposed model and its counterparts

Set	Models	MCC	F1 Macro	F1 Micro
Validation	2D	0.9156	0.8949	0.9300
	Plain multi-frame	0.9184	0.9042	0.9323
	Proposed	0.9276	0.9110	0.9400
Test	Proposed	0.9244	0.9147	0.9372

4. Discussion and Conclusion

The results prove that incorporating temporal information by considering a video clip input leads to a significant performance gain over its frame-level counterpart (2D). Interestingly, a synergy is observed when further combined with task-oriented training scheme and the blur block. Finally, the comparison between validation and test sets' results demonstrates the model's generalisation to unseen data.

5. References

1. K. He et al., IEEE/CVF Computer Vision and Pattern Recognition; 2016, p.770-778.
2. N. Park and S. Kim, Int. Conference on Machine Learning (ICML); 2022, 162:17390-17419.

Acknowledgements:

The authors acknowledge the financial support provided by National funds, through the Foundation for Science and Technology (FCT, Portugal; PTDC/EMD-EMD/1140/2020 and UMINHO/BIM/2021/64), and the donation of a RTX A6000 GPU by NVIDIA (USA).



EFFECT OF THE REDUCTION OF CONE-BEAM CT ARTEFACTS BY CGAN ON THE DIAGNOSIS OF ENDODONTIC COMPLICATIONS

Candemil Amanda (1,2), Gatti Filippo (2), Macedo Gabriel (3), Salmon Benjamin (4), Florindo João (3), Oliveira Matheus (5), Mazzi-Chaves Jardel (1), Vennat Elsa (2), Sousa-Neto Manoel (1)

1. Department of Restorative Dentistry, School of Dentistry of Ribeirão Preto, University of São Paulo, Brazil; 2. CentraleSupélec-ECP Laboratoire de Mécanique de Paris Saclay UMR 9026, France; 3. Institute of Mathematics, Statistics and Scientific Computing - University of Campinas; 4. Orofacial Pathologies, Imaging and Biotherapies Lab, Université de Paris, URP2496, France; 5. Division of Oral Radiology, Department of Oral Diagnosis, Piracicaba Dental School, University of Campinas, Brazil.

1. Introduction

Cone-beam computed tomography (CBCT) is an imaging exam widely used by health professionals to diagnosis diseases and evaluate internal root anatomy. However, one of its limitations is the presence of artifacts that hampers the diagnostic efficacy [1]. Previous studies introduced different techniques to overcome this limitation, however, sufficient image quality has not been achieved yet [2]. Several deep learning techniques have been developed in the last years to successfully reduce the presence of artifacts in CBCT images [3]. However, at present, its impact on the diagnostic accuracy of clinical tasks has not been investigated so far. As a better image quality does not always reflect high diagnostic accuracy, this study aimed to evaluate the applicability of deep learning in a clinical scenario.

2. Materials and Methods

We adopted the conditional Generative Adversarial Network (cGAN) proposed by Ghani & Karl [4] to reduce artifacts arising from high-density materials and low X-ray dose, based in a large number of CBCT scans. A custom-made imaging phantom with a partially edentulous macerated human mandible was introduced. One hundred extracted human teeth were endodontically instrumented and then divided in two steps: in step one, 40 instrumented and filled teeth were used to simulate artifacts from high-density materials (scattering, beam hardening, starvation and blooming) to train the cGAN. In step two, 60 teeth were divided in three groups (n=20) in accordance with the proposed endodontic complication: vertical root fracture, root perforation and control. Each teeth group was positioned individually in an empty socket of the human mandible and CBCT scans were obtained with a field of view of 5 × 5 cm at two resolution protocols (high and low). Additional scans were obtained from the teeth of interest in the empty sockets of the mandible to a clinical condition with two dental implants in both sides of the teeth.

3. Results

The cGAN successfully removed the artifacts, generating CBCT images with higher diagnostic accuracy.

4. Discussion and Conclusions

The cGAN is effective increase the diagnostic accuracy of endodontic complications.

5. References

1. Patel SBJ, Semper MAF, Mannocci F. European Society of Endodontology position statement: Use of cone beam computed tomography in Endodontics: European Society of Endodontology (ESE) developed by. Int Endod J 2019; 52(12):1675-1678.
2. Candemil AP et al. Are metal artifact reduction algorithms effective to correct cone beam CT artifacts arising from the exomass? Dentomaxillofac Radiol 2019; 20180290.
3. Liang K et al. Metal artifact reduction for practical dental computed tomography by improving interpolation-based reconstruction with deep learning. Med Phys 2019; 46(12): 823-834.
8. Ghani MU, Karl WC. Fast Enhanced CT Metal Artifact Reduction Using Data Domain Deep Learning. IEEE Transactions on Computational Imaging 2019; 6:181-193.

Acknowledgements:

The authors gratefully acknowledge financial support from São Paulo Research Foundation, FAPESP nº 2021/01623-8.



SPINOPEVIC ANATOMICAL PARAMETER EXTRACTION USING A NOVEL DEEP LEARNING PHYSICS-INFORMED MODEL (LAN-DET)

AliAsghar MohammadiNasrabadi (1), John McPhee (1)

1. Department of Systems Design Engineering, University of Waterloo, Canada.

1. Introduction

Surgeons measure spinopelvic parameters to evaluate spinopelvic alignment preoperatively. Automatic extraction of these parameters saves time and provides consistent measurements. In this paper, a new approach for landmark detection is introduced in which landmarks are considered as objects. A novel model (Lan-Det) is introduced in which anatomical parameter errors are considered in the loss function being minimized. The model has a global understanding of images and the relations between landmarks (i.e., anatomical parameters), which improves the deep learning model accuracy to detect the desired landmarks.

2. Materials and Methods

In total, 750 lateral spine X-ray images were collected and labelled. The dataset was divided into training (80%), validation (10%), and test (10%) sets. Landmarks were considered as objects and the coordinates of a landmark were considered at the center of a bounding box [1] in the training. In the labelled dataset, 10 classes of landmark objects were defined (femoral heads, anterior/posterior points of S1, L1, C7 superior end plates, and L5 inferior endplate). The model is an object detection model based on yolov5 algorithm, which detects each object individually without any global intuition of the image and the relationship that objects might have. To provide this global understanding for the model, the loss function is modified as below:

$$Loss = l_{box} + l_{obj} + l_{cls} + \sum_{i=1}^{n} \boldsymbol{w_i}.\boldsymbol{l_{prt}} \quad (1)$$

where l_{box} is the Intersection of Union (IoU) loss for bounding boxes, and l_{obj}, l_{cls} are abjectness and class losses based on Binary Cross Entropy loss. The term " $\sum_{i=1}^{n} w_i.l_{prt}$ " is the weighted combination of parameter losses using regression loss approach.

3. Results

The spinopelvic parameters (SS, PT, PI, LL, and SVA) are calculated using detected landmarks (Figure 1). The results are presented in Table 1 where the accuracy of Lan-Det for parameter extraction are compared to yolov5.

Table 1: Comparison of Lan-Det prediction (PR) accuracy and error to yolov5 model.

Parameter	PR Error (%)		PR Accuracy (%)	
	yolov5	Lan-Det	yolov5	Lan-Det
SS°	5.9	5.1	87.1	88.8
PT°	2.9	2.2	85.0	88.7
PI°	6.5	6.2	88.7	89.3
LL°	9.9	8.9	80.3	84.3
SVA (cm)	0.77	0.71	84.7	86.3

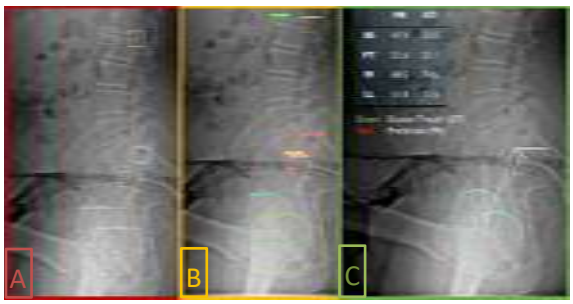

Figure 1: A: Manual labelling of landmarks; B: Trained model output, bounding boxes with different confidences; C: Spinopelvic parameter calculation.

4. Discussion and Conclusions

Using an object detection approach to detect landmarks addresses the drawbacks of heatmap-based regression (e.g., overlapping signals) [2]. In addition, based on the novel idea of connecting these landmarks and providing global intuition for the model, the accuracy of spinal parameter extraction has been improved.

5. References

1. MohammdiNasrabadi A et al., MIDL, 2022
2. Korez R et al., ESJ, 2020; (29-9), pp.2295.

Acknowledgements:

This research was funded by the Natural Sciences and Engineering Research Council of Canada (NSERC) and Intellijoint Surgical.

CMBBE2023
18th International Symposium on Computer Methods in Biomechanics and Biomedical Engineering
3 - 5 May 2023, Paris, France



Arts et Métiers Institute of Technology
Institut de Biomécanique Humaine Georges Charpak
155 boulevard de l'Hôpital 75013 Paris France
www.cmbbe-symposium.com

EVALUATING ANTICIPATORY CONTROL FOR STEP-DOWN PERTURBATIONS IN SIMULATIONS OF HUMAN WALKING

Daniel D.B. Haeufle (1,2), Lucas Schreff (3,4), Roy Müller (3,4)

1. Hertie Institute for Clinical Brain Research, University of Tübingen, Germany, 2. Institute for Modelling and Simulation of Biomechanical Systems, Univeristy of Stuttgart, Germany, 3. Department of Neurology/Department of Orthopedic Surgery, Klinikum Bayreuth GmbH, Germany, 4. Bayreuth Center of Sport Science, University of Bayreuth, Germany

Correspondence to Daniel Haeufle: daniel.haeufle@uni-tuebingen.de

1. Introduction

Experimental results indicate that human locomotion is a result of feedback, feed-forward and anticipatory control components [1]. With neuro-muscular models and computer simulation it is possible to investigate the role of these control components in dealing with ground-level perturbations. We propose a combination of feedback and feed-forward [2] and a high-level anticipatory strategy augmenting a low-level muscle-reflex control to anticipate step down perturbations [3].

2. Materials and Methods

We built our simulation studies on a planar walking model with seven muscle-tendon units per leg (Fig. 1) and a low-level reflex-based controller [4]. We extended the controller by a feed-forward and an anticipatory control strategy. The anticipatory strategy directly changes the gain of the reflex control exclusively during the last contact prior to a drop in ground level. By applying the strategy to different reflex pathways, we investigated the capability to cope with step-down perturbations.

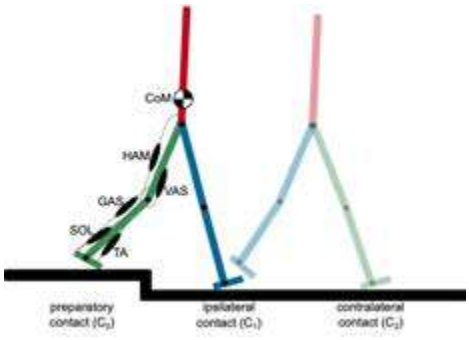

Figure 1: Model of human walking anticipating step down perturbations. Figure taken from [3].

3. Results

Our simulations show that especially the anticipatory reduction of soleus activity and the increase of hamstrings activity result in higher robustness. The best results were obtained when the change in stimulation of the soleus muscle occurred 300 ms after the heel strike of the contralateral leg. This enabled the model to descend perturbation heights up to − 0.21 m and the resulting kinematic and dynamic adaptations are similar to the experimental observations [3].

4. Discussion and Conclusions

This proves that the anticipatory strategy observed in experiments has the purpose of increasing robustness. Furthermore, this strategy outperforms other reactive strategies, e.g., pure feedback control [4] or combined feedback and feed-forward control [2].

5. References

1. Müller, R., Vielemeyer, J., & Häufle, D. Journal of Biomechanics, 113, 110121 (2020).
2. Haeufle, D. F. B., Schmortte, B., Geyer, H., Müller, R., & Schmitt Syn. Frontiers in Computational Neuroscience, 12, 80. (2018)
3. Schreff, L., Haeufle, D., Vielemeyer, J., & Müller, R., Scientific Reports, 12, 1. (2022).
4. Geyer, H., & Herr Hugh. IEEE Transactions on Neural Systems and Rehabilitation Engineering, 18, 263–73. (2010).

Acknowledgements:
We acknowledge funding of DFG (MU 2970/4-2 to L.S. and R.M. and Ministry of Science, Research, and the Arts Baden-Württemberg (Az: 33-7533.-30-20/7/2). We thank Johanna Vielemeyer for her contribution!

CMBBE2023
18th International Symposium on Computer Methods in Biomechanics and Biomedical Engineering
3 - 5 May 2023, Paris, France



Arts et Métiers Institute of Technology
Institut de Biomécanique Humaine Georges Charpak
155 boulevard de l'Hôpital 75013
Paris France
www.cmbbe-symposium.com

REAL-TIME BIOFEEDBACK OF HUMAN KINEMATICS AND MUSCLE FORCES BASED ON EMG-MARKER DATA FUSION

Amedeo Ceglia (1), François Bailly (2), Mickael Begon (1)

1. Faculté de médecine, Université de Montréal, Canada; 2. INRIA, Université de Montpelier, France

1. Introduction

Real-time biofeedback based on measurements (kinematics, electromyography (EMG)) has improved the rehabilitation of post-stroke patients [1]. Muscle forces should give clinicians more representative information as they can differ from EMG. To estimate muscle forces in real-time, we have developed a method using trajectory optimization and moving horizon estimation (MHE) based on bio-signals (markers trajectories and EMG). Visual feedback of muscle forces and kinematics is displayed to the participant and the experimenter.

2. Materials and Methods

One healthy right-handed male was involved in this feasibility study and equipped with 10 EMG sensors to record muscular activity (2 kHz) and 16 skin markers. A 12-camera motion capture system (Vicon, Oxford, UK) was used to record marker trajectories (100 Hz). The participant performed ten maximal voluntary contractions to normalize EMG signals. A 10-degree-of-freedom upper-limb model actuated by 31 muscles was used for the computation. An optimization algorithm leveraging the MHE formulation was used to find the closest optimal trajectories of the model to recorded biosignals. The implementation was done using Bioptim [2], a library dedicated to solving biomechanical optimal control (OC) problems. A succession of short overlapping OC subproblems was solved forward in time. Muscle activations and markers trajectories were tracked. An open-source library (biosiglive) has been developed to stream and process experimental data in real-time. Each time a problem was solved, the 31 estimated muscle forces and 3D kinematics were displayed in real-time (Fig. 1). Optimization and data processing were performed on two computers to improve real-time performance.

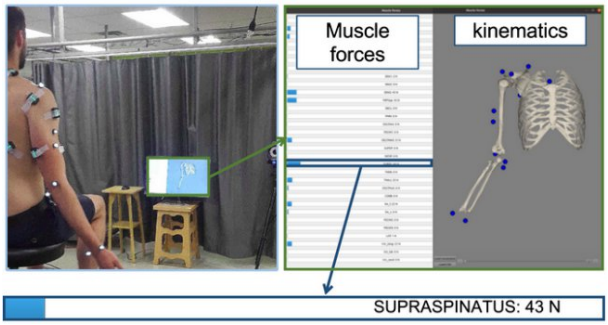

Figure 1: Subject fully equipped with visual biofeedback.

3. Results

The algorithm estimated muscle forces and kinematics with a refresh/solving frequency of 30 Hz (almost three times faster than standard real-time [3]). Feedback was provided with a total delay of 110 ms compared to the actual motion, which is low enough for rehabilitation [4]. Estimated values were consistent with average marker errors of 25 mm and average EMG phase errors of 8 %.

4. Discussion and Conclusions

These results demonstrate the relevance of using forward approaches combined with optimization in real-time for a complex model using the MHE formulation. Results provide a consistent estimation of human movement and muscle forces. We want to improve this method by calibrating the muscle parameters and applying the method for a hand cycling rehabilitation task.

5. References

1. Brodland GW, Veldhuis JH. PLoS One. 2012;7(9):e44281 (2012).
2. Michaud, B. et al., Systems, Man, and Cybernetics: Systems, 2022, 2168-2216
3. O.A. kannape and O.Blank, Journal of neurophysiology, 2013, 110(8), 1837-1847.
4. Thomas Waltemate et al., VRST 2016 conference: p. 27-35



Multi-modal registration for Adolescent Idiopathic Scoliosis subject specific avatar creation

Nicolas Comte (1, 2), Sergi Pujades (1), Olivier Daniel (3), François Faure (2), Jean-Sebastien Franco (1), Aurélien Courvoisier(3), Edmond Boyer (1)

1. UGA, INRIA, CNRS, INP, LJK, France; 2. Anatoscope, France; 3. Grenoble Alps Scoliosis and Spine Center-Grenoble Alps University Hospital, SPM-TIMC-IMAG, France

1. Introduction

Adolescent Idiopathic scoliosis (AIS) is a progressive disease of the spine evolving throughout the period of growth. Beside the 3D analysis of the spine with X-Rays, there is a great interest to characterise scoliosis using motion capture. Unfortunately there is yet no consensus in the literature based on the superficial analysis of the torso. Therefore we propose a protocol and a workflow to create a subject-specific biomechanical model that is able to capture both the external (back surface) and internal (vertebrae) specificities of the patient, towards the goal of motion-based scoliosis characterisation.

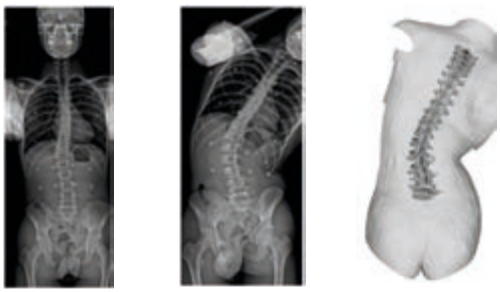

(a) (b) (c)

Figure 1: Coronal views in bi-planar radiographs of the patient in standing (a) and bending (b). The resulting 3D avatar of the patient in bending (c).

2. Materials and Methods

The torso motion reveals information about the biomechanics of the body. We propose to build a model from multimodal data that include a static surface scan of the back, a 3D reconstruction of the spine with the SterEOS platform [2] and mocap trajectories with Codamotion. Patients wear the same radio-opaque mocap markers throughout all the acquisitions (Fig. 1a and 1b), allowing sparse correspondences of the skin surface across the different modalities. In contrast to [1], we propose to use low-dose imaging sources and to avoid the spinous palpation task during the placement of the markers.

Our model is composed of 18 articulated rigid-bodies with stiffness constraints [3], and mapped meshes. With an optimization, it captures anatomical characteristics of the patient. To validate the precision of the spine motion, we can then optimize the pose of the avatar to match the 3D markers in the bending biplanar images (Fig 1b).

3. Results

We tested our workflow on one patient. The avatar captured its anatomy with an average 3D error in vertebrae positions of 1.8mm (std: 1.2mm) and 2.1° (std: 2.3°) in orientations on the three anatomical planes. The average 3D error of the markers is 4.1mm (std: 2.6mm).
In bending (Fig 1c), as preliminary results, our biomechanical model is able to fit the superficial markers with an average 3D error in vertebrae positions of 1.1cm (std: 0.3) and 4.8° (std: 3.7°) in the vertebrae orientations on each anatomical plane.

4. Discussion and Conclusions

We presented a workflow to create a 3D articulated avatar of the patient torso. By further adjusting the biomechanical properties of the patient-specific model with the mocap trajectories, we foresee to improve the fidelity of the motion of the spine inside of the body.

5. References

1. Overbergh T et al. J. of Biomechanics; 2020.
2. Humbert L et al. Med Eng & Physics; 2009
3. Ignasiak et al. J. of Biomechanics; 2015

Acknowledgements:
The authors would like to thank the ANRT for providing financial support to this project.



QUANTIFYING THE ROLE OF THE FORCE-VELOCITY RELATION IN SIMULATED PERTURBED HOPPING

Fabio Izzi (1,2,*), An Mo (2), Matthew Araz (1), Alexander Badri-Spröwitz (2), Daniel F. B. Haeufle (1,3)

1. Hertie-Institute for Clinical Brain Research, University of Tübingen, Germany; 2. Dynamic Locomotion Group, Max Planck Institute for Intelligent Systems, Germany; 3. Institute for Modelling and Simulation of Biomechanical Systems, University of Stuttgart, Germany

** Corresponding author*: izzi@is.mpg.de

1. Introduction

Muscle fibre force depends on muscle fibre contraction velocity (Fig 1b). Little is known about the function of this force-velocity relationship. One hypothesis is that it enables muscles to react to unexpected perturbations with zero latency [1-2]. A quantitative evaluation of this hypothesis is still missing.

2. Materials and Methods

We quantified the force produced by the force-velocity relation via computer simulations of a simplified hopper (Fig.1a). Rewriting the formulation of the muscle fibre force (F_{CE}) as in

$$\begin{aligned} F_{CE} &= F_{CE}^{V} + F_{CE}^{L} + F_{CE}^{A} + F_{CE}^{0} \\ F_{CE}^{V} &= \int_{t_{TD}}^{t_x} \frac{\partial f_{CE}}{\partial v_{CE}} dv_{CE} \\ F_{CE}^{L} &= \int_{t_{TD}}^{t_x} \frac{\partial f_{CE}}{\partial l_{CE}} dl_{CE} \\ F_{CE}^{A} &= \int_{t_{TD}}^{t_x} \frac{\partial f_{CE}}{\partial a} da \end{aligned} \qquad (1)$$

permits to separate the contribution of the force-velocity relation (F^{V}_{CE}) from muscle fibre elasticity (F^{L}_{CE}), excitation (F^{A}_{CE}) and prestimulation level (F^{0}_{CE}). We measured the contribution of the force-velocity relation when rejecting changes in ground height, with different feedforward stimulation strategies (constant vs. ramp signals).

3. Results

The force-velocity relation can adapt muscle fibre force and dissipated energy in response to variations in ground height. This regulating capacity depends on the muscle fibre velocity at touch-down: large impact velocities produce negligible force correction due to the flat side of the force-velocity relation. In addition, feedforward stimulation can tune and amplify the force-velocity relation's contribution.

4. Discussion and Conclusions

The force-velocity relation facilitates rejecting ground perturbations through a zero-delay response, but it requires low-level control for best effectiveness. Hill-type muscle models, which have limited validity in eccentric contraction, are limitations in current research on the force-velocity relation's functionality. We intend to generalize our findings to more complex biomechanical models and in-vitro muscle fibre experiments.

5. References

1. Haeufle D.F.B. et al., Bioinspir Biomim; 5, 016004; 10.1088/1748-3182/5/1/016004 (2010)
2. Gerritsen K.G. et al., Motor Control; 2, 206-220 (1998).

Acknowledgements:
Funding: Deutsche Forschungsgemeinschaft (DFG) – 449912641; Max Planck Society; Max Planck Research School for Intelligent Systems (IMPRS-IS); China Scholarship Council (CSC).

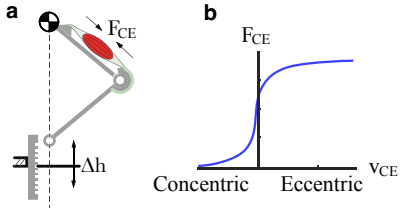

Figure 1: (a) Simulation hopper. (b) Force-velocity relation.

CMBBE2023
18th International Symposium on Computer Methods in Biomechanics and Biomedical Engineering
3 - 5 May 2023, Paris, France



Arts et Métiers Institute of Technology
Institut de Biomécanique Humaine Georges Charpak
155 boulevard de l'Hôpital 75013 Paris France
www.cmbbe-symposium.com

MUSCLE FORCE RESPONSE TO PERTURBED LOCOMOTION: IN-VITRO EXPERIMENTS VS. HILL-TYPE MUSCLE MODEL

Matthew Araz (1*), Sven Weidner (2), Fabio Izzi (1,3), Alexander Badri-Spröwitz (3), Tobias Siebert (2) Daniel Haeufle (1,4)

1. Hertie-Institute for Clinical Brain Research, University of Tuebingen, Germany; 2. Motion and Exercise Science, University of Stuttgart, Germany; 3. Dynamic Locomotion Group, Max-Planck Institute for Intelligent Systems, Germany; 4. Institute for Modelling and Simulation of Biomechanical Systems, University of Stuttgart, Germany

**Corresponding Author: matthew.araz@uni-tuebingen.de*

1. Introduction

Initial viscoelastic muscle reaction to sudden perturbations is assumed to stabilize locomotion [1]. However, many previous studies are based on Hill-type muscle models which inadequately represent muscle force during eccentric contractions [2]. Here, we investigate how muscle fibers adapt their force response to stretch velocities due to perturbed locomotion.

2. Materials and Methods

To generate realistic boundary conditions for in-vitro muscle fiber experiments (Fig.1B) and isolated contractile element (CE) simulations (Fig.1C), we simulated level and perturbed single leg hopping (Fig.1A). In hopping simulation, we gathered CE length and contraction velocity data of one hopping cycle for each perturbation. We kept the stimulation in the first 30 ms constant, which presents the preflex time after touchdown. Hence, during preflex, muscle force is only influenced by elastic and viscous properties. We also conducted quasistatic experiments to separate viscous and elastic force contributions during hopping speed experiments for each lengthening profile.

3. Results

We found that muscle intrinsic properties adapt the force response with respect to the perturbation condition, in the preflex phase. Such an adaptation is not visible in the Hill-type CE simulation due to the saturation in force-velocity (F-v) relation. Despite the dynamic differences between both, the mechanical work estimation of Hill-type model is found close to muscle fibers. In the slow contraction conditions, both the dynamic and the energy response of the Hill-Type model were found to be close to muscle fibers.

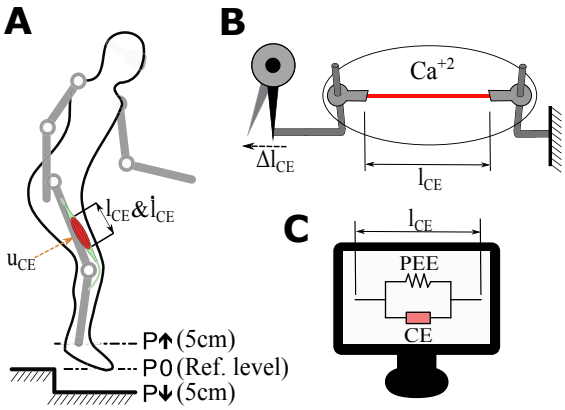

Figure 1 : (A) Hopping simulation with perturbation levels, (B) Wet lab muscle fiber experiment set-up, (C) Isolated contractile element simulations

4. Discussion and Conclusions

While the Hill-Type model accurately predicts the mechanical work done by fibers in the extreme conditions of perturbed locomotion, the details of the eccentric F-v relation need to be modified and also the short-range stiffness needs to be included in Hill-type muscle models to predict better force response.

5. References

1. Wochner I. et al., arxiv.org/abs/2207.03952v1 (2022)
2. Till O. et al., J Theor Biol., 225(2):176-87 (2008)

Acknowledgements: This work was funded by the Deutsche Forschungsgemeinschaft (DFG, German Research Foundation) - 449912641



THE INFLUENCE OF SENSORY FEEDBACK ON HUMAN WALKING

Elsa K. Bunz (1), Syn Schmitt (1)

1. Institute for Modelling and Simulation of Biomechanical Systems, University of Stuttgart, Germany
Corresponding author: Elsa K. Bunz, elsa.bunz@imsb.uni-stuttgart.de

1. Introduction

Human walking relies on sensory feedback. Geyer and Herr [1] showed that a network of reflexes is enough to generate human-like walking, providing a basis to study the influence of sensory feedback on human walking. More specific additional reflexes can be examined. With this for example the effects of preactivation, i.e. activation of muscles before landing can be evaluated. Experimental results suggest that preactivation causes higher co-contraction preparing the landing and thereby increasing the robustness.

2. Materials and Methods

We add preactivation to the walking model of [1] by introducing a length reflex to one muscle at a time. We then subject the model to unexpected step-down perturbations to determine the maximally rejected step height $h_{s,max}$ and analyze the changes caused by preactivation. The model of [1] without adaptations can cope with steps of $h_{s,max}$ = 3 cm.

3. Results

The addition of preactivation increases the robustness to unexpected step-down perturbations when added to certain muscles (see Table 1). An addition to Ham destabilizes the model such that no walking is possible. The best improvement is found when adding preactivation to the biarticular Gas. Analyzing the resulting gait on flat terrain, we find that overall the time course of the muscular activation is still similar to human activation. The activation

[cm]	Hfl	Glu	Ham	Vas	Gas	Ta	Sol
$h_{s,max}$	3	4	-	6	10	5	7

Table 1: Maximally rejected step height $h_{s,max}$ for preactivation added to one muscle (Hfl: hip flexors, Glu: gluteus, Ham: hamstrings, Vas: vastus, Gas: gastrocnemius, Ta: tibialis anterior, Sol: soleus).

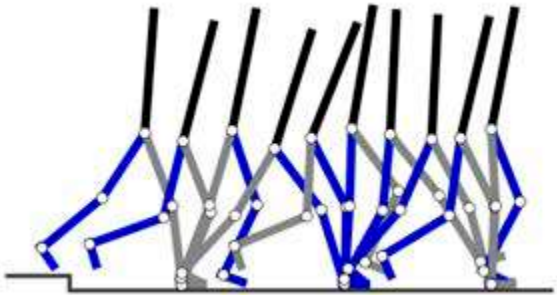

Figure 1: Step encounter (h_s = 10cm) of model with preactivation to gastrocnemius. The contralateral (blue) leg performs a large countering step.

of some muscles is increased in the late swing and early stance phase w.r.t. the original model leading to a higher co-contraction and changed ankle and knee kinematics. Selectively turning on preactivation of specific steps reveals that, preactivation is not needed during but prior the step encounter. Namely, changed knee kinematics of the contralateral leg allow the model to perform a large step countering the falling and thereby stabilizing the model (see Fig. 1).

4. Discussion and Conclusions

Sensory feedback is crucial for human walking and its role can be analyzed leveraging neuromusculoskeletal models. As one example, preactivation can be caused by sensory feedback. We show that it is a strategy to increase robustness in unknown terrains as it markedly increases the robustness to unexpected step-down perturbations due to changed knee kinematics.

5. References

1. Geyer & Herr, IEEE TNSRE (2010).

Acknowledgements:
This work was funded by DFG (GRK 2198/1 and 390740016 EXC 2075 (SimTech)). E.K.B was supported by IMPRS-IS and the German Academic Scholarship Foundation.



INTERACTION EFFECTS OF LIFTING TECHNIQUES AND LOAD POSITION/ASYMMETRY ON SPINAL AND KNEE LOADS

Sajjad Daroudi (1), Mahdi Mohseni (1), Navid Arjmand* (1)

1. Department of Mechanical Engineering, Sharif University of Technology, Tehran, Iran

**Corresponding author: Prof. Navid Arjmand, Ph.D., Tehran, 11155-9567, Iran, arjmand@sharif.edu*

1. Introduction

Low-back and knee injuries are the most common musculoskeletal disorders that can be caused by lifting tasks [1]. Several task-related parameters as well as adapting different lifting techniques (LT) may affect knee/spinal loads [2, 3]. Here, we aim to investigate the effects of LTs and its interaction effects with the hand-load weight (LW)/horizontal distance (HD)/ vertical distance (VD)/asymmetry angle (LA) on knee/spinal loads in various lifting activities.

2. Methods

Motion data from nine individuals (71.2±7.6 kg, 176±5.5 cm, and 24.5±1.7 years) was collected via the Vicon motion capture system. Each subject performed 24 two-handed lifting tasks at two HDs (30 and 60 cm from the feet), two VDs (0 and 30 cm from the floor), and two LAs (0 and 45° from the sagittal plane) while adapting three LTs (stoop, semi-squat, and full-squat). Subject-specific musculoskeletal models were developed using the AnyBody Modeling System v.7.3 with/without a 5 kg hand load. L5-S1 and knee loads were estimated by the models. Repeated measures analysis of variance was implemented to evaluate the main effect of LT and its interaction effects with the task-related parameters on spine/knee loads. Fisher's least significant difference post-hoc tests were used to identify the differences.

3. Results

LT significantly affected the L5-S1 and knee loads (Table 1). All the investigated task-related parameters, except LW for all spine/knee loads as well as VD for the resultant knee load, had significant interaction effects with the LT on the spine/knee loads (Table 1). According to the post-hoc analyses, the semi-squat LT generated the largest spinal loads and the stoop LT generated the largest knee loads.

Table 1: P-values for the main effects of LT and also its interaction effects with HD, VD, LA, and LW on knee and L5-S1 loads. Significant effects (p-value<0.05) are presented in bold.

Joint loads	LT	LT*HD	LT*VD	LT*LA	LT*LW
L5-S1 compression	**0**	**0.02**	**0**	**0.04**	0.13
L5-S1 shear	**0**	**0**	**0**	**0**	0.28
Knee compression	**0**	**0**	**0**	**0**	0.11
Knee shear	**0**	**0**	**0.02**	**0**	0.18
Resultant knee load	**0.02**	**0**	0.17	**0**	0.09

4. Discussion and Conclusions

The adapted LT had a significant effect on all L5-S1 and knee loads. Semi-squat, as the most adapted LT by workers [4], generated the largest L5-S1 loads and thus calling for precautionary measures in occupational workplaces. Note that while stoop LT produced the largest knee resultant load, the risk of knee stress and injury cannot be discussed here as the knee joint load-bearing contact area changes in different knee flexion angles [5]. This should be investigated in future studies using a detailed finite element analysis of load-bearing contact area changes in different LTs.

5. References

1. Thiese M et al., *BMC Musculoskelet. Disord.*, vol. 15, no. 1, pp. 1–11 (2014).
2. Mohseni M et al, *J. Biomech.*, vol. 131, 110921 (2022).
3. Dehghan P, Arjmand N, *Hum. Factors J. Hum. Factors Ergon. Soc.*, in press (2022)
4. Straker L, *Int. J. Ind. Ergon.*, vol. 31, no. 3, pp. 149–160 (2003).
5. Walker P, Hajek J, *J. Biomech.*, vol. 5, no. 6, pp. 581–589 (1972).



INTERACTIONS BETWEEN EEG AND EMG FREQUENCY BANDS ASSOCIATED WITH VISUAL PERTURBATIONS

Fatimah Alani (1), Ahsan H. Khandoker (1,2), Herbert F. Jelinek (1,2,3)

1. Department of Biomedical Engineering, Khalifa University, UAE; 2. Health Engineering Innovation Center, Khalifa University, UAE; 3. Biotechnology Center, Khalifa University, UAE.

1. Introduction

Posture is maintained by an integrative control system that involves multiple sensory inputs, cognitive perception, and coordinated motor output to maintain balance [1,2]. Cognitive and motor coordination aspects have been investigated [3,4], but the neuromuscular interactions in postural balance have not been quantified. The current research investigated activations and interactions among EEG and EMG signals associated with visual perturbations. Interactions were measured through a non-linear transfer entropy (TE) model pre-and post-perturbation.

2. Materials and Methods

Twenty right-dominant females (age mean ± SD; of 20.2 ± 3.8 years) were exposed to visual perturbations using an HTC-Vive Pro virtual reality headset that induced 20–70-degree expected and unexpected rotations during different postures, bilateral and single-leg stances. All subjects provided written informed consent. The experimental protocol was approved by Khalifa University Institutional Review Board (H21-040). EEG signals were recorded from Cz. Muscle activity was recorded using surface EMG electrodes on the tibialis anterior and gastrocnemius medialis muscles. Transfer entropy [5] was used to study neuromuscular interactions. EEG signals were decomposed into the delta, theta, alpha, beta, and gamma bands. EMG signals were decomposed into two frequency ranges corresponding to frequency activation ranges of slow-twitch and fast-twitch muscle fibers [6]. Transfer entropy was computed cross-frequencies on three-time intervals [-1000 0] ms pre-perturbation, [0 1000] ms, and [1000 2000] ms post-perturbations.

3. Results

Transfer entropy results showed that interaction between EEG and EMG is mainly modulated by beta and alpha EEG bands. Perturbation onsets had a significant opposing effect on TE values in the low-frequency and high-frequency bands of the EMG signal ($p=0.012$). TE values in expected perturbations were immediate and transient in expected perturbations but were delayed and of longer latency in unforeseen conditions.

4. Discussion and Conclusions

TE results showed that in trials of less postural demands, balance is maintained via activations of low-frequency muscle fibers. However, in trials of more considerable postural difficulty, the activation of high-frequency muscle fibers is preferred. Comparing TE values across the expectancy of perturbation suggests that the nervous system can use predictive information about upcoming perturbations to modulate an earlier response for maintaining balance. TE identified neuromuscular interactions that could assess impaired balance and assist in understanding underlying dysfunctionalities in movement disorders.

5. References

1. Kleiner A et al., Revista Neurociencias; 19(2):349-357 (2011).
2. Shaffer S et al., Physical Therapy; 87(2):194-307 (2007).
3. Peterson SM et al, eNeuro; 5(4):ENEURO.0207 (2018).
4. Frances, T. Master's Theses and Capstones; 1280 (2019).
5. Spinney R et al., Physical Review, 95(3):32319 (2017).
6. Sipp A et al., Journal of Neurophysiology, 110(9):2050-2060 (2013).

CMBBE2023
18th International Symposium on Computer Methods in Biomechanics and Biomedical Engineering
3 - 5 May 2023, Paris, France



Arts et Métiers Institute of Technology
Institut de Biomécanique Humaine Georges Charpak
155 boulevard de l'Hôpital 75013 Paris France
www.cmbbe-symposium.com

PLANTAR FLEXOR MUSCLE WEAKNESS ALTERS CONTRIBUTION OF ACCELERATED BODY MASSES TO FORWARD PROGRESSION

Jérémie Begue (1), Félicie Pommerell (2), Nicolas Peyrot (1,2), Georges Dalleau (1), Teddy Caderby(1)

1.Laboratoire IRISSE, Le Tampon, La Réunion ; 2. Motricité Interactions Performance, Le Mans, France

1. Introduction

Ankle plantar flexor muscles (PF) play a major role in forward propulsion during walking [1]. Evidence suggests that PF weakness, such as induced by aging or pathology, results in reduced propulsive forces and preferred speed during walking [2,3]. These PF weakness-related changes may be associated with modifications in body segment accelerations and their contribution to forward propulsion, since the net external force is equal to the sum of the body segment masses multiplied by their respective acceleration [4]. However, to date, little is known about the influence of PF weakness on accelerated body masses during walking. The purpose of this study was to assess how fatigue-induced PF weakness influences the contribution of accelerated body masses to forward progression in able-bodied adults.

2. Materials and Methods

Eleven able-bodied volunteers (22 ± 2 years) performed a series of gait trials at their preferred speed along a 7-meter walkway in three different conditions, presented in the following order: before PF fatigue (Pre-Fatigue condition), after a 5-min rest period (Control) and after PF fatigue (Post-Fatigue). Fatigue protocol consisted of performing concentric-eccentric contractions of the ankle plantar flexors from a standing position (standing heel raises) until exhaustion. During gait trials, full-body kinematics and ground reaction forces were collected from a motion capture system and a force-plate, respectively. For each condition, trial was validated if the gait speed was within ± 2.5% of the preferred speed.

The contribution of the trunk (sum of the instantaneous mass-acceleration products of the head, torso and pelvis), legs (thighs, shanks and feet) and arms (upper-arms, forearms and hands) during the stance phase of the dominant leg was determined as follows:

$$Contribution_i = 100 * \frac{\int |m_i a_i|}{\int (\sum_{i=1}^{3} |m_i a_i|)}$$

Where m_i and a_i are the mass and the anteroposterior acceleration of the *i-th* segment group, respectively.

3. Results

ANOVAs revealed a significant Fatigue effect for the trunk, arm and leg contributions (Table 1).

Contribution (%)	Pre-Fatigue	Control	Post-Fatigue
Trunk	53.4(3.2)[a]	53.2(3.4)[b]	55.5(3.1)[a,b]
Arms	7.1(1.4)[a]	6.8(1.3)[b]	7.9(1.6)[a,b]
Legs	39.5(3.3)[a]	40(3.4)[b]	36.6(3.3)[a,b]

Table 1: Mean (SD) contribution of the three segment groups in the three conditions. Means with similar letters differ significantly ($P < 0.05$).

4. Discussion and Conclusions

Our findings revealed that fatigue-induced PF weakness altered the contribution of accelerated body masses to forward progression. Specifically, we found that PF weakness decreased leg contribution and conversely, increased trunk and arm contribution to forward progression. These results are consistent with the distal-to-proximal redistribution of joint kinetics induced by weakness associated with aging [2].

5. References

1. Neptune RR et al., Journal of Biomechanics 34, 1387-1398 (2001).
2. Franz JR. Exercise and Sport Sciences Reviews 44, 129-136 (2016).
3. Nadeau S et al., Clinical Biomechanics 14, 125-135 (1999).
4. Gillet C et al., American Journal of Physical Medicine & Rehabilitation 82,101-109 (2003).

Acknowledgements:
Thanks to Ms Margo Zamère for her technical support.

CMBBE2023
18th International Symposium on Computer Methods in Biomechanics and Biomedical Engineering
3 - 5 May 2023, Paris, France
Arts et Métiers Institute of Technology
Institut de Biomécanique Humaine Georges Charpak
155 boulevard de l'Hôpital 75013 Paris France
www.cmbbe-symposium.com

PRECISION OF PHYSICS-INFORMED INTERVERTEBRAL DISC SURROGATE MODELS

Maria Hammer (1,2), Tizian Wenzel (2,3), Gabriele Santin (4), Bernard Haasdonk (2,3), Syn Schmitt (1,2)

1. Institute for Modelling and Simulation of Biomechanical Systems, University of Stuttgart, Germany;
2. Stuttgart Center for Simulation Science (SC SimTech), University of Stuttgart, Germany;
3. Institute for Applied Analysis and Numerical Simulation, University of Stuttgart, Germany;
4. Digital Society Center, Bruno Kessler Foundation, Trento, Italy

Correspondence: Maria Hammer, maria.hammer@imsb.uni-stuttgart.de

1. Introduction

Computer simulation is a key technique for research in spine biomechanics. In multibody (MB) spine models, intervertebral discs (IVDs) are typically implemented linear spring-damping elements [1], disregarding the non-linear characteristics. In contrast, more complex models do either neglect mutual influences of degrees of freedom or violate energy balance. To tackle both issues and provide a precise surrogate model valid even for large and multidirectional deformations, we developed a physics-informed algorithm in [2] combining the conservation of mechanical energy with kernel approximation techniques [3]. The aim of the current study is to evaluate the errors and biomechanical effects of different IVD modelling approaches on the same (artificial) dataset.

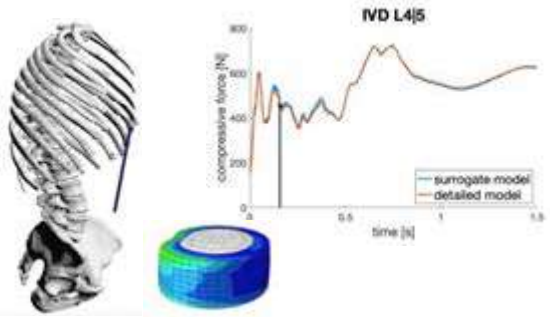

Figure 1: Kernel surrogates of detailed FE IVD models can predict patient-specific elastic disc responses in spinal movement simulations.

2. Methods

Following the procedure presented in [4,5], finite element (FE) and MB models of a healthy, subject-specific spinal anatomy were built. Load simulations of the thoracolumbar FE IVD models provided coupled force-displacement data used to train surrogate models of different types. To account for energy conservation, we create surrogate models for the force potential of individual IVDs, from which the respective force and torque components can be derived. Finally, these IVD models were included in the MB spine model and predicted elastic IVD responses of different surrogate types were compared with respect to their accuracy for simulated movement kinematics.

3. Results

The kernel surrogates clearly outperform the commonly used linear spring-damper elements and exhibit a high precision not only for training but even for unseen data (see Fig. 1). This observation especially applies for multi-dimensional displacements as in full spine bending movements.

4. Discussion and Conclusions

With the established algorithm, we improve the prediction of the non-linear characteristics of subject-specific IVDs in MB simulations. This approach can equally be applied to in vivo data of elastic IVD responses or other passive soft tissue elements in the human body.

5. References

1. Christophy et al. (2013). *Multibody Syst Dyn*, **30**: 413-432.
2. Hammer et al. *In preparation*.
3. Wenzel et al. (2021), *J Approx Theory*, **262**:105508.
4. Little et al. (2009). *Spine*, **34**:E76-E82.
5. Meszaros-Beller et al. *Under review.*

Acknowledgements:
Funded by Deutsche Forschungsgemeinschaft (DFG, German Research Foundation) under Germany's Excellence Strategy - EXC 2075 – 390740016.

CMBBE2023
18th International Symposium on Computer Methods in Biomechanics and Biomedical Engineering
3 - 5 May 2023, Paris, France
Arts et Métiers Institute of Technology
Institut de Biomécanique Humaine Georges Charpak
155 boulevard de l'Hôpital 75013 Paris France
www.cmbbe-symposium.com

A POTENTIAL FIELD APPROACH TO DETERMINE THE JOINT KINEMATICS OF A HUMAN UPPER EXTREMITY

Iman Soodmand(1), Maeruan Kebbach(1), Eric Kleist(2), Annika Volpert(1), Hannes Wackerle(3), Robert Grawe(2), Peter Augat(3), Rainer Bader(2), Christoph Woernle(3), Sven Herrmann(1)

1. Department of Orthopaedics, University Medicine Rostock, Germany 2. Chair of Technical Dynamics, University of Rostock, Germany 3. Institute for Biomechanics, BG Unfallklinik Murnau, Germany

1. Introduction

Multibody kinematic optimisation has been frequently used to effectively translate measured marker trajectories to joint kinematics at the position level while reducing errors from soft tissue artefacts (STA) [1]. However, calculating consistent velocities and accelerations by some methods is challenging, influencing subsequent dynamic analysis. This work aimed to introduce a potential field method applied to a multibody model of the upper extremity that directly generates the complete kinematics from marker trajectories.

2. Materials and Methods

The upper extremity model of one healthy subject was built in the SIMPACK software, consisting of clavicle, scapula, humerus, ulna, radius, and hand bones with 13 joint coordinates, whereby the thorax was assumed to be fixed. The kinematic chain is closed by two holonomic constraints allowing the scapula to glide over the ellipsoid of the thorax [2]. Since the inertial forces disturb the tracking accuracy, the inertia properties of bones were set to small unit values. The potential field is constructed by spring-damper force elements connecting the moving skin markers to segment-fixed model points, where a sensitivity analysis determined spring and damping constants. When the measured marker trajectories are applied to the skin markers in the model, the motion is transferred through the potential field to segment-fixed points, ending in the motion of bone segments. Five motion cycles of arm flexion and abduction were simulated. Results were compared to the in vivo measurements with cortical bone pins [3]. As a second evaluation, the least-square method [1] was implemented for the same motion scenarios from the same subject.

3. Results

The model consistently tracked the marker trajectories for both motion scenarios. Comparison to the least-square method and bone pin measurements [3] shows overall good agreement in the kinematics of the clavicle and humerus bones during arm abduction (Fig. 1).

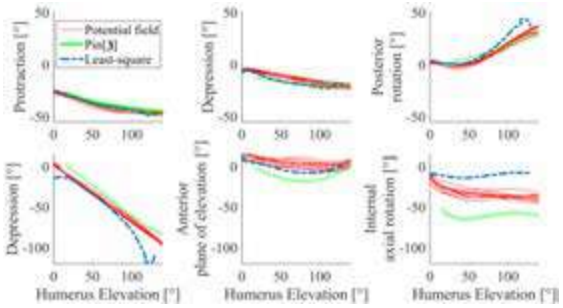

Figure 1: Evaluating kinematics of clavicle (above) and humerus (below) bones during arm abduction.

4. Discussion and Conclusions

Deviations can be attributed to model scaling errors, STA, and inter-study variations in motion execution. Also, our proposed potential field approach generates comparable results to the least-square method and is efficient. Advantages are direct calculation of velocities and accelerations required for inverse dynamics without formulating an optimization problem. On this basis, skeletal motions for various daily activities could be identified and used in subsequent dynamic analyses.

5. References

1. Begon M et al., J biomech eng. 2018; 140(3)
2. Herrmann et al., Multibody Dyn: Springer; 2020
3. Ludewig et al., J Bone Joint Surg Am. 2009; 91

Acknowledgements

The German Research Foundation (DFG, WO 452/11-1, BA 3347/14-1 and HE 7885/1-1) supported this work.

CMBBE2023
18th International Symposium on Computer Methods in Biomechanics and Biomedical Engineering
3 - 5 May 2023, Paris, France



Arts et Métiers Institute of Technology
Institut de Biomécanique Humaine Georges Charpak
155 boulevard de l'Hôpital 75013 Paris France
www.cmbbe-symposium.com

CLASSIFICATION OF AUTISM AND CONTROL GAIT IN CHILDREN USING JOINT KINETIC AND TEMPORAL-SPATIAL FEATURES

Victoria Chester (1), Ashirbad Pradhan (2), Karansinh Padhiar (1)

1. Kinesiology, University of New Brunswick, Canada; 2. Engineering, University of Waterloo, Canada

1. Introduction

Autism spectrum disorder (ASD) is a developmental disorder associated with atypical gait patterns. To further understand gait patterns in children with ASD versus neurotypical controls, there has been a recent increase in the number of studies using machine learning (ML) tools for classification. While few ML studies have investigated kinetic gait parameters in ASD [1-3], differences in joint kinetics have been found previously [1]. Further research is needed to better understand mechanics of gait in ASD to provide optimal treatment plans. The purpose of this study was to investigate the classification of gait patterns in children with ASD using 3D joint moment and power data (Kinetic) and temporal-spatial (TS) data.

2. Materials and Methods

Nineteen children (n=19) diagnosed with autism between the ages of 6-15 years participated in the study (16 males, 3 females; age=10.47±2.91 years; height: 1.42±0.15 m; weight: 41.20±17.00 kg) and compared to a neurotypical control group consisting of twenty-one children (n=21) between the ages of 6-16 years (11 males, 10 females, age=11.38±2.91 years; height: 1.49±0.14 m; weight: 44.32±16.36). A 12 camera Vicon T160 motion capture system (Oxford Metrics Group Ltd.), sampling at a 100Hz, was used to track the three-dimensional trajectories of 32 reflective markers placed on the participant's skin as they walked at a self-selected speed. Six force plates (Kistler Instruments, Winterthur, Switzerland), embedded in the lab floor, measured the three-dimensional forces and moments during gait, sampling at 1000Hz. Hip, knee, and ankle kinetic data were computed using an inverse dynamics approach. The features extracted from the kinetic waveforms included maximum and minimum hip, knee and ankle joint moment and power during key gait events. The features extracted from TS data included cycle time, step length, walking velocity, single and double limb support time, time to toe-off (TO), cadence, and stride length. The kinetic and TS features, individually and combined, served as input to a support vector machine (SVM) classifier with radial basis function (RBF) kernel.

3. Results

Using a SVM with RBF, the individual joint (hip, knee, ankle) kinetics gave an average classification accuracy of 78.8%. Combining all joints showed a significant increase in accuracy (92.5%). The combination of kinetics and TS resulted in the highest accuracy of 93.8% with only 17 features (out of 44 features).

Table 1: Classification performance evaluation

Segment	#Features	Accuracy	Precision	Recall	F1
TS + Kinetics	17	93.8	92.3	94.7	93.5
Kinetics	14	92.5	90.0	94.7	92.3
Knee	6	83.8	87.9	76.3	81.7
Hip	10	83.8	82.1	84.2	83.1
Ankle	3	68.8	74.1	52.6	61.5
TS	2	68.8	68.6	63.2	65.8

4. Discussion and Conclusions

Gait patterns in children with autism can be classified with a high accuracy of 93.8% with both kinetic and TS features combined using a SVM with RBF. Similar results were obtained using kinetic features alone (92.5%). These results are similar to past work that achieved a high classification accuracy of 95.8% by combining kinematic, ground reaction force (GRF), and TS features using a SVM classifier [3] and joint kinetic data (82.5%) using LDA [1]. This study is the first to show high classification rates using joint kinetic and TS data without kinematic and GRF data. Joint kinetic data are critical to treatment planning. Further studies may lead to a better understanding of atypical gait patterns in ASD and improved treatments.

5. References

1. Hasan et al. (2017). JAEBS, vol. 7, p. 150-156.
2. Zakaria et al. (2020). IJETER, 9, p. 3995–4005.
3. Ilias et al. (2016). ISCAIE, p. 52-56.



PREDICTIVE SIMULATIONS OF ADAPTIVE TREADMILL GAIT

Kayla Pariser, Jill Higginson

Department of Mechanical Engineering, University of Delaware, USA

1. Introduction

Adaptive (ATM) or self-paced treadmills that update belt speed based on user gait mechanics are an emerging rehabilitation tool [1-2]. While stroke survivors can tolerate walking on ATMs responses are mixed [1], perhaps due to lack of customization to target patient-specific impairments that hinder walking function. Predictive simulations using direct collocation optimal control methods have been employed to test responses to new rehabilitation protocols prior to experiments, which may improve rehabilitation efficacy [3]. The purpose of this study is to develop and validate a predictive simulation framework to estimate changes in ground reaction forces, joint kinematics, and step length on various ATM controllers.

2. Materials and Methods

The ATM controller updates the belt speed as the weighted sum of the current speed and intermediate speeds due to user step length (SL), propulsive impulse (PI), and position on the treadmill [4]. Unitless gains α and γ define the importance of changes in step length and propulsive impulse on belt speed. For this study one young adult walked at their self-selected speed on the ATM with γ=α and γ=1.75α. Kinematic and kinetic data were recorded.

We scaled a 2D fixed speed treadmill gait model [5] and modified it to make treadmill motion a free parameter. Using OpenSim Moco [3], a tracking problem established an initial guess for the predictive simulation. The tracking cost function minimized effort and the error between reference and simulated states. The predictive cost function minimized effort (a^3) and a tracking error to promote a constant belt velocity of scalable speed ($e_{vel}{}^2 * c$), and maximized PI and SL, Eq. 1. Bilateral periodicity and zero average speed of the center of mass relative to ground were constraints. We will vary gains w_1 and w_2 to mimic experimental ATM conditions and compare predicted solutions to experimental results.

$$J = w_1 PI_{max,goal} + w_2 SL_{max,goal} + \int_{t_0}^{t_f} (w_3 \|a^3\| + w_4 \|e_{vel}{}^2 * c\|) dt \quad (1)$$

3. Results

The ATM simulation framework successfully varies belt speed and predicts gait mechanics depending on selected weights and cost functions. As the velocity scaling term (c) increased from 0.5 to 1, predicted average belt speed increased from 0.6 m/s to 1.2 m/s and peak hip extension, knee flexion, and ankle dorsiflexion angle also increased, Fig 1.

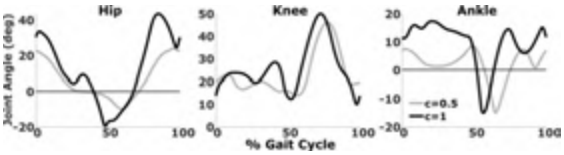

Figure 1: Predicted joint angles, c=0.5 and c=1.

4. Discussion and Conclusions

We developed the first predictive simulation framework to estimate changes in gait patterns and self-selected speed on an adaptive treadmill that match experimentally observed trends [1]. Future work will seek to remove the bilateral periodicity constraint and impose unilateral muscle weakness to predict the response of stroke survivors on custom ATMs.

5. References

(1) Ray et al., J Biomech 101:109643 (2020). (2) Oh et al., J Neuroeng Rehabil 18(1):60 (2021). (3) Dembia et al., PLoS Comput Biol 16(12):e1008493 (2020). (4) Pariser et al., J Biomech 133:110971 (2022). (5) Pariser et al., J Biomech Eng 144(11):114505 (2022).

Acknowledgements: Nick Bianco, NSFGRFP 1940700, NIH P30 GM103333, UD Helwig Fellowship, Delaware Space Grant Consortium, and UD Dissertation Fellowship.



SOFT PIEZOELECTRIC ACTUATOR FOR HAPTIC FEEDBACK: A PRELIMINARY STUDY OF DISPLACEMENT

António Diogo André (1), Pedro Martins (2,3), Majid Taghavi (4)

1. INEGI, Portugal; 2. INEGI-LAETA, Portugal; 3. i3A, University of Zaragoza, Spain; 4. Imperial College London, United Kingdom

1. Introduction

On-skin sensors and stimulators have received significant interest in healthcare and human-machine interfaces, due to their excellent performance and wearability [1]. Stimulators used for haptic feedback in rehabilitation, for example, can be used to perform sensory re-education interventions, critical for the recovery of patients with mobility impairments. The sensation of touch provided by these devices can activate numerous mechanoreceptors in the human skin, depending on the actuation frequency, displacement and pressure [2]. Polyvinylidene fluoride (PVDF) has been widely used as a compliant piezoelectric actuator [3]. As an electrically stimulated material, PVDF can change its shape when subjected to an electrical stimulus. This study presents a new approach to investigate the suitability of PVDF ionic film for future implementations in haptic feedback devices.

2. Materials and Methods

PVDF/Ionic Liquid (IL) composite was used to develop the actuation films. The ionic liquid (Pmim-TSFI) induces the creation of β phase content in the film which is mainly responsible for the electroactive properties of PVDF [4]. The IL was mixed with DMSO in a proportion of 40/60% w/w (IL/PVDF). After that, the PVDF was added to the solution in a ratio of 12/88% w/w (PVDF/DMSO). After achieving a homogenous solution, it was cast into a glass for total solvent evaporation in the oven (1 hour at 85ºC). Both sides of the PVDF films ($30x6x0.06mm^3$) were then coated with thin layers of gold using a hot press. 18 samples were developed and tested for displacement using a laser displacement when activated by a sinusoidal wave of 20V at 0.2 Hz.

3. Results

Table 1 shows the mean displacements ($\bar{x}$) measured for each sample, as well as their standard deviation (STD, σ). The maximum displacement achieved was 3.70 ± 0.51 mm while the minimum was 1.34 ± 0.03 mm.

Table 1: Mean displacement and STD.

#	$\bar{x} \pm \sigma$ (mm)	#	$\bar{x} \pm \sigma$ (mm)	#	$\bar{x} \pm \sigma$ (mm)
1	2.42 ± 0.11	7	1.61 ± 0.05	13	1.60 ± 0.05
2	1.28 ± 0.08	8	3.45 ± 0.35	14	2.33 ± 0.13
3	1.94 ± 0.19	9	3.70 ± 0.51	15	1.47 ± 0.06
4	2.57 ± 0.25	10	3.13 ± 0.07	16	1.54 ± 0.17
5	3.07 ± 0.26	11	3.51 ± 0.56	17	1.64 ± 0.05
6	1.34 ± 0.03	12	2.37 ± 0.09	18	1.98 ± 0.09

4. Discussion and Conclusions

When one end of the PVDF ionic film is fixed, the other end moves in a direction perpendicular to the beam axis. This preliminary study confirms the periodic movement of the film when a sinusoidal voltage with a peak voltage of 20V is applied to both sides of the film. The displacement obtained is adequate for future applications of these films in haptic feedback solutions that will be investigated in our future work.

5. References

1. Guo et al., Adv Mater Technol, 7:2100452 (2022).
2. Seo et al., J. Mech. Sci. Technol; 32(2):631-636 (2018).
3. Ruan et al., Polymers; 10(3):228 (2018).
4. Correia et al., J. Phys. Chem. C; 123(20):12744−12752 (2019).

Acknowledgements:

A.D.A. and P.M. gratefully acknowledge funding from FCT, Portugal, under grant SFRH/BD/147807/2019 and the research unit LAETA. M.T. acknowledges Imperial College Research Fellowship.



REAL-TIME CONTINUOUS AUDITORY FEEDBACK FOR GAIT RETRAINING FROM PRESSURE SHOE INSOLES

Ariane P Lallès (1, 2), Luisa Cedin (2), Christopher B Knowlton (2), Markus A Wimmer (2)

1. Ecole normale supérieure de rennes, Bruz, France; 2. Rush Univ Med Ctr, Chicago, IL, USA

Corresponding author: Ariane P Lallès ariane.lalles@ens-rennes.fr

1. Introduction

A biomechanical marker for knee osteoarthritis progression is an increase of dynamic joint load at the medial knee compartment [1]. A surrogate measure of medial load is the knee adduction moment (KAM), and gait retraining is a simple and non-expensive strategy to reduce it. Recent studies used various wearable devices with visual, auditory, or haptic feedback. On average, participants managed to reduce KAM, but not all were responders. These systems generally provided negative and invariable feedback, which can be difficult to interpret and limit motivation [2]. Movement sonification is more engaging, and informs if the movement is properly executed and how it is performed. The goal of this study was to build a KAM modifying system based on an existing pressure shoe insole and musical software, which delivers real-time continuous auditory feedback by creating or modifying sounds.

2. Materials and Methods

Real-time plantar pressure and total force were obtained at 100 Hz with the Insole3 (Moticon GmbH, Munich, Gemany), a 16-sensor pressure insole with an embedded six-axis inertial measurement unit controlled by a smartphone app via Bluetooth connection. Data was transmitted to the Moticon Science software (Moticon GmbH, Munich, Gemany) in real-time across Wi-Fi, and was internally transmitted to Max 8/MSP (Cycling '74, San Francisco, CA, USA) using the User Datagram Protocol (UDP) (Figure 1).



Figure 1: Data transmission from the insoles to the phone and computer.

3. Results

We successfully built a KAM reducing system and followed two different approaches to medialize the center of pressure (CoP). In the first one, we used Musical Instrument Digital Interfaces (MIDI) to generate chord pairs for the right and left foot. A 50 N threshold triggered chords from heel strike to toe-off while walking at a self-selected pace. When the CoP was too lateral, a percussion sound occurred, and the piano chords stopped playing. Each progressive step played a different chord pair cycling through a specific chord sequence (C Major, G Major, A minor, E minor, F major). Each side could be muted or set to its own instrument (e.g. acoustic grand piano). In the second set up, we continuously played a music piece, and only monitored CoP. As the user was moving away from acceptable CoP progression lines, music was progressively muffled. Both approaches provided targeted feedback to reduce KAM, while enriching the users' training experience.

4. Discussion and Conclusions

This new and adaptable shoe-integrated training system can be used in the community for a wide range of activities (once portable), and it will provide improved information and exercise feedback for both patient and clinician. The gamification of exercising should help with patient adherence. Future steps include building a portable and suitable system for home training via the development of a smartphone application and demonstrating the efficacy and reliability in KAM reduction.

5. References

1. Kumar, et al., Osteoarthritis and cartilage, 2013
2. Sigrist et al., Psychonomic bulletin review, 2013

CMBBE2023
18th International Symposium on Computer Methods in Biomechanics and Biomedical Engineering
3 - 5 May 2023, Paris, France
Arts et Métiers Institute of Technology
Institut de Biomécanique Humaine Georges Charpak
155 boulevard de l'Hôpital 75013 Paris France
www.cmbbe-symposium.com

A LINKAGE-BASED PROSTHETIC ANKLE WITH MR-DAMPER

Sachin Kumar (1), Sujatha Srinivasan (2), Sujatha Chandramohan (3)

† Machine Design Section, Department of Mechanical Engineering, Indian Institute of Technology Madras, Chennai-600036, India,

Email: sachinkumarit4@gmail.com[1], sujsree@iitm.ac.in[2], sujatha@iitm.ac.in[3]

1. Introduction

Prosthetic feet may be passive, active, and semi-active based on the actuation system. Since passive devices are incapable of providing adequate ankle energy during walking, increased emphasis has recently been placed on adding active features to the prosthetic foot [1]. Although powered prostheses can enhance a prosthesis user's mobility, they require large actuators to provide the required push-off force. In this work, a four-bar mechanism actuated by a semi-active magnetorheological (MR) fluid damper is designed to bridge these objectives.

2. Methodology

A semi-active prosthetic ankle using a 4-bar linkage actuated by an MR damper has been designed. The design goal was to imitate normal ankle range of motion during the stance phase of gait. A 3-D model of the ankle design is shown in Figure 1. The pivot between the blue and brown links functions as the ankle.

The planar four-bar linkage was synthesized using function generation [2], which correlates prescribed rotations of the input link(green) with the rotation of the output link (brown) attached to the foot.

The fundamental idea behind this design is to use a four-bar mechanism to provide mechanical advantage to enable the use of a smaller actuator, and match the linearity of the stiffness at the human ankle during stance. In this design (see Fig. 1), the MR damper provides a moment at the ankle joint. Utilizing the standard four bar analysis, moment at ankle has been calculated and plotted in Fig 2.

A comparison of the stiffness with the human ankle, a passive ankle and the new semi-active ankle (Fig. 2) showed the the four-bar mechanism could produce a maximum plantarflexion moment of 1.5 Nm/kg, which is higher than the 1 Nm/kg produced by the single axis passive ankle [2].

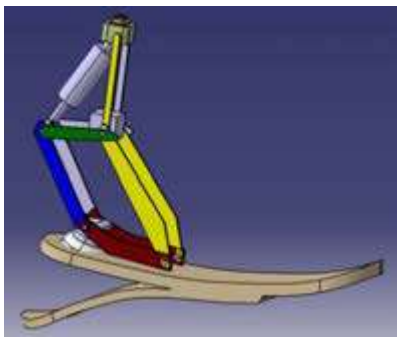

Figure 1: 3-D prosthetic ankle model

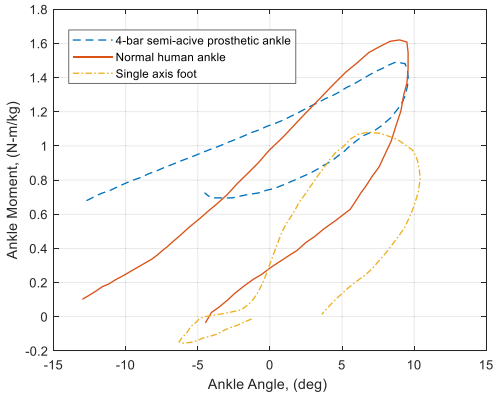

Figure 2: Ankle stiffness comparison plot.

3. Results

The new design enables the desired ankle range of motion of 20˚ plantarflexion and 10˚ dorsiflexion, and produces higher ankle moments via the semi-active damper.

4. Discussion and Conclusions

Using a four-bar mechanism and an MR damper to achieve an ankle joint's desired range of motion provides better stiffness characteristics and mechanical advantage than a passive single-axis prosthetic ankle joint.

5. References

1. Versluys R *et al.* : State of the art review and the importance of human ankle-foot biomechanics.
2. Sandor, G.N and Erdman, A.G.: Advanced Mechanism Design: Analysis and Synthesis, vol. II. Prentice Hall, New Jersey (1984).



DAILY ACTIVITIES KINEMATICS AND KINETICS IN SUBJECTS WITH EXTERNAL FIXATOR: PRELIMINARY TESTS

Rosanna Viglialoro (1), Andrea Di Pietro (2), Lorenza Mattei (2,3), Stefano Marchetti (1), Marco Gesi (2,3), Elisabetta Rosellini (2), Francesca Di Puccio (2,3),

1. Department of Translational Research and New Technologies In Medicine And Surgery, University of Pisa, Italy;

2. Department of Civil and Industrial Engineering, University of Pisa, Italy;

3. Center for Rehabilitative Medicine "Sport and Anatomy", University of Pisa, Italy

1. Introduction

Complex long-bone fractures are widely treated with external fixation devices, which stabilize the fracture, partially support load and thus promote the healing. Although their beneficial effects are proved, such devices can cause a significant change of the biomechanics of motor tasks execution. In particular, patients with tibial fractures treated with Ilizarov have shown gait adaptation strategies with abnormal joint angles and asymmetric loading patterns of the fixated/healthy leg [1,2]. Fixator weight and size can thus determine musculoskeletal issues that can affect the healing process.

The aim of the present study is to evaluate the biomechanics of patients treated with Ilizarov fixator, during the healing process and after fixator removal in order to i) assess the healing process in quantitative and non-invasive way [3,4]; ii) improve fixator design.

2. Materials and Methods

The study was conducted at the Biomechanics Laboratory of the "Sport and Anatomy Centre" of the University of Pisa, where a Vicon motion analysis system (Oxford Metrics Ltd., Oxford, UK) with eight infrared cameras @100 Hz is installed. Ground reaction forces were recorded by two 3-dimensional AMTI OR6–7-1000 force plates at a sampling frequency of 1000 Hz. The adopted marker-set is composed by 24 passive markers (ϕ 14 mm): 16 markers were attached to anatomical landmarks according to the Lower body Plug-in-Gait model, 4 additional markers were placed to the femur and knee, and 4 markers were placed on the fixator frame as shown in Figure 1 left. The selected patient wore an Ilizarov fixator. Four motor tasks were performed during the trial, with three repetitions each one: posture, gait, going up and down a step, and sit-to-stand.

3. Results

Preliminary results are in agreement with the literature [1,2] and demonstrate the adaptation of motor tasks in presence of a fixator. A comparison of joint flexion-extension angles at the hip, knee and ankle joints between fixated and healthy legs are provided in Fig. 1 right. Results also support the use of motion analysis technique to quantify the healing process.

In the next months, other follow ups of the same patient are scheduled before and after fixator removal. Additionally, other subjects will be analysed, with circular and unilateral fixator to compare the outcomes of the two solutions.

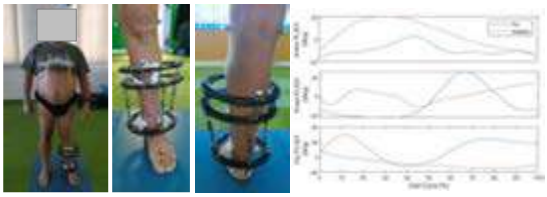

Figure 1 (left): An example of marker-set;
(right): Preliminary results of joint kinematics.

4. References

1. Layton R et al. Proc Inst Mech Eng H; 232(6): 628-636 (2018).
2. Besh L et al. J Foot Ankle Surg; 47(1):19-25 (2008).
3. Di Puccio et al. J Mech Behav Biomed; 121: 104619 (2021).
4. Mattei et al. J R Soc Interface; 15(142): 20180068 (2018).

Acknowledgements:

The authors would like to thank the University of Pisa for providing financial support to this project (PRA_2020_55).

CMBBE2023
18th International Symposium on Computer Methods in Biomechanics and Biomedical Engineering
3 - 5 May 2023, Paris, France



Arts et Métiers Institute of Technology
Institut de Biomécanique Humaine Georges Charpak
155 boulevard de l'Hôpital 75013 Paris France
www.cmbbe-symposium.com

EFFECTS OF JUMPING EXERCISES TO PREVENT OSTEOPOROSIS GAINED FROM ACCELERATION DATA

Lukas Reinker (1)(2), Sebastian Dendorfer (1)(2)

1. OTH Regensburg, Germany; 2. Regensburg Center of Biomedical Engineering, Germany

1. Introduction

The prevalence of osteoporosis has increased significantly in recent years. In earlier studies scientists tried to figure out how high-impact exercises (e.g., running, jumping, drop jumps) affect bone mineral density (BMD) especially of the femur. Results showed a positive correlation between a minimum number of movements with specific high accelerations and an increased BMD in examined regions which leads to prevention of osteoporosis. [1,2] To offer prevention programs it is necessary to monitor the accelerations the body undergoes during these exercises and to understand the preventive mechanisms and impacts on the femur. The intention of this study is to clarify at which segments or body regions such impacts on the lower extremities can best be recorded during these exercises.

2. Materials and Methods

49 subjects performed different jumping tasks five times each, containing Squad Jumps (SJ), Countermovement Jumps (CMJ) and Drop Jumps (DJ). These jumps were recorded at 60 Hz using 17 inertial motion capture sensors (MVN Awinda, Xsens Technologies B.V., NL) for full-body setup, comprising a 3-axial accelerometer, 3D gyroscope and a 3D magnetometer (see Figure 1).

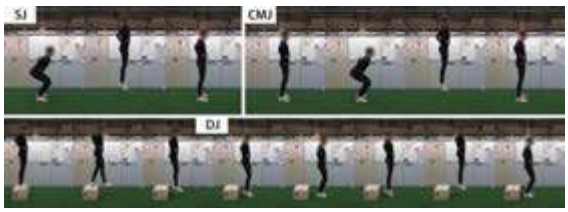

Figure 1: Step by step execution of the different high-impact exercises SJ, CMJ and DJ.

3. Results

Comparing the maximum accelerations for each exercise, the medians for DJ are the highest, followed by CMJ. Pearson's correlation matrix over the whole time series shows that the measured correlate very well for all exercises between pelvis sensor and sensors at the upper body. Here, all correlation coefficients are above a value of 0.87. For the thighs, the correlation with the pelvis sensor is also above 0.83. Accelerations in the lower leg correlate less well with the pelvis. The coefficients here take values between 0.66 and 0.74. The foot sensors do not correlate with the upper body with values below 0.3.

4. Discussion and Conclusions

The maximum accelerations at the different sensor positions show, that the impact of the jumping exercises can be measured on all parts of the body. These results can be used as a basis for the prevention of osteoporosis and for monitoring of movement using accelerometers. The study shows that the accelerations measured at the pelvis during jumping exercises can be tracked very well on the upper body and upper extremities. This includes the locations where smart devices are typically worn, such as the wrist (smart watch) or sternum (chest strap). The impact and effects of these exercises on the legs is difficult to deduce from the accelerations on the upper body. Here, a more far-reaching consideration is necessary considering the acting joint and muscle forces for a validation, in order to analyze further statements around the preventive mechanisms and impacts on the femur. In the next steps, the forces occurring in the femur will be determined using the measured kinematic data via musculoskeletal simulations. The forces and their points of attachment on the bone will serve as the basis for investigation at the micro level with finite element analyses.

5. References

1. A. Vainionpää et al., Osteoporosis; 16(2):191–197 (2005).
2. D. Vlachopoulos et al., Archives of osteoporosis; 13(1):128 (2018)

CMBBE2023
18th International Symposium on Computer Methods in Biomechanics and Biomedical Engineering
3 - 5 May 2023, Paris, France



Arts et Métiers Institute of Technology
Institut de Biomécanique Humaine Georges Charpak
155 boulevard de l'Hôpital 75013 Paris France
www.cmbbe-symposium.com

AERO HANDLEBAR POSITIONS EFFECTS ON MUSCLE ACTIVITY, KINEMATICS OF THE LOWER LIMB AND OXYGEN CONSUMPTION

Mojtaba Ghasemi (1), Daniel Curnier (2, 3), Maxime Caru (1,2,3), Benjamin Pageaux (3), Jean-Yves Trépanier (1), Delphine Périé (1)

1. Department of Mechanical Engineering, Polytechnique Montreal, Canada; 2. Sainte-Justine University Health Center, Research Center, Canada; 3. School of Kinesiology and Physical Activity Sciences, Faculty of Medicine, University of Montreal, Canada

1. Introduction

Cyclists adopt a time trial position to optimize their aerodynamic resistance position, while simultaneously keeping their physiological responses unimpaired [1]. This study investigates the effects of altering aero handlebar positions on muscle activity, kinematics of the lower limb and oxygen consumption

2. Materials and Methods

Seven male competitive but non-elite cyclists or triathletes volunteered in this study. They underwent a maximal cardiopulmonary exercise test to assess their peak oxygen consumption (V̇O2peak: 61.4 ± 11.3 mL.kg -1.min-1). Six aero handlebar positions (handlebar at the preferred time trial position (TTP), TTP-30º up, TTP-30º and 5cm up, TTP-5cm down, TTP-5cm up and TTP-5cm forward) were randomized and tested during 6-min submaximal constant load exercise tests at a power output corresponding to 75% of gas exchange threshold. The kinematic variables, surface EMG and oxygen consumption were continuously collected during each session.

3. Results

The data showed a significant increase (p=0.004) in gluteus maximus and a decrease (p=0.012) in vastus lateralis activity level in TTP-5cm down, compared to other positions. The peak of ankle angles of TTP-5cm up and preferred TTP were higher (p=0.016 and p=0.017), compared to TTP 5cm down. The peak of knee angles of TTP-5cm up were higher (p=0.047), compared to TTP 5cm down, whereas the peak value of the hip angle of TTP-5cm down was higher (p=0.018) than TTP-5cm up. No differences were observed between handlebar positions and oxygen consumption (p=0.221).

		TTP 30° up	TTP 30° and 5cm up	TTP 5cm down	TTP 5cm up	Preferred TTP	TTP 5cm forward
Sagittal torso angle (°)		23.0 ± 2.1	27.3 ± 1.0	22.0 ± 2.8	31.0 ± 4.6	25.5 ± 2.1	23.0 ± 4.2
Shoulder angle (°)		71.5 ± 9.2	78.0 ± 2.9	84.0 ± 8.5	82.5 ± 10.4	83.5 ± 5.0	92.0 ± 12.0
Elbow angle (°)		73.0 ± 4.2	81.5 ± 1.0	110.0 ± 4.8	121.0 ± 5.2	118.0 ± 3.7	124.0 ±3.4
Peak angle (°)	Ankle	30.3 ± 14.8	34.1 ± 7.3	28.4 ± 6.3	39.6 ± 2.6*	35.5 ± 4.9*	30.4 ± 3.3
	Knee	98.3 ± 8.3	95.6 ± 20.6	92.8 ± 11.6	104.2 ± 4.8*	103.7 ± 7.2	103.5 ± 6.2
	Hip	101.8 ± 26.2*	96.1 ± 28.1	115.6 ± 31	84.5 ± 27.8*	97± 8.7	104.8 ± 18.9*
Range of motion (°)	Ankle	14.8 ± 5.3*	13.6 ± 10.9	16.1 ± 5	12.0 ± 21.5*	13.0 ± 9.1	14.4 ± 8.3
	Knee	71.4 ± 4.7	73.5 ± 16.7	74.1 ± 17.8	72.6 ± 5.7	70.0 ± 4.0	69.7 ± 3.4
	Hip	40.9 ± 12.4	41.4 ± 12.3	35.9 ± 18.1	36.8 ± 15.2	48.6 ± 8.6	37.2 ± 7.7
Peak angular velocity (deg/s)	Ankle	73.3 ± 35.9	108.2 ± 85.4	62.9 ± 26.9	120.9 ± 46.8*	100.0 ± 58.2	72.9 ± 29.4*
	Knee	315.7 ± 23.2	294.5 ± 65.6	287.9 ± 62.7	328.5 ± 38.2	306.0 ± 12.6	326.9 ± 30.8
	Hip	221.4 ± 86.4	190.0 ± 27.9	235.9 ± 92.7	176.0 ± 70.7*	190.0 ± 53.3	212.2 ± 39.1*

Table 1: Comparison of joint kinematics across positions using the peak values of angles and angular velocities and the range of motion for each lower joint.

4. Discussion and Conclusions

This study provides a practical understanding to researchers and coaches to optimize handlebar position. Altering aero handlebar positions affect the lower limb joint kinematics and muscle activity during submaximal exercise, without marked changes in participants' oxygen consumption. The handlebar position with the lowest height resulted in more GMax activity and hip extension angle. Thus, lowering the handlebar down in TTP-5cm modified EMG activity and timing, while improving biomechanical cycling performance. Our study reinforces that handlebar position alteration may be a critical adjustment when fitting a bicycle and allows cyclists to find a TTP that is aerodynamically optimized.

5. References

1. Fintelman, D.M., Sterling, M., Hemida, H., Li, F.X., 2014. Optimal cycling time trial position models: aerodynamics versus power output and metabolic energy. J. Biomech. 47, 1894-1898

Acknowledgements:
We thank all participants for devoting their time and energy to our study

CMBBE2023
18th International Symposium on Computer Methods in Biomechanics and Biomedical Engineering
3 - 5 May 2023, Paris, France
Arts et Métiers Institute of Technology
Institut de Biomécanique Humaine Georges Charpak
155 boulevard de l'Hôpital 75013 Paris France
www.cmbbe-symposium.com

MODELLING GLENOHUMERAL LIGAMENT STRAIN PATTERNS IN OVERHAND AND UNDERHAND PITCHING

Andrew Kraszewski, PhD

Hospital for Special Surgery, United States of America

email: kraszewskia@hss.edu; phone: +1 212-606-1727

1. Introduction

The underhand softball and overhand baseball pitch challenge the passive glenohumeral stabilizers, but ligament injury is more common in males and associated with fatigue. The objective was to explore baseline strain patterns in high school athletes during fastball pitches.

2. Materials and Methods

3D scapular and humeral bony morphology of a cadaveric shoulder was reconstructed from CT; ligament origin and insertion points and humeral head radius were extracted. A finite strand mesh was created in MATLAB to represent the glenohumeral ligament complex tissue. Each strand had linear stiffness properties taken from Bigliani et al [1]. Glenohumeral rotational kinematics from 5 female and 5 male pitchers were inputs to mesh simulations with fixed translation.

Optimization minimized total mesh strain energy at each pitch frame (Fig. 1). Average strain in the superior, anterior, inferior, and posterior capsule mesh regions was calculated.

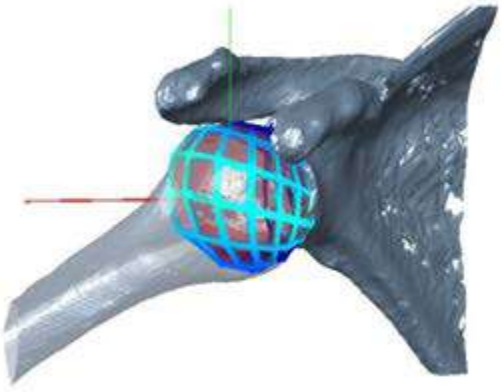

Figure 1: Mesh simulation of the overhand pitch at maximum humeral external rotation during the late pitching phase. The anterior capsule region (lightly shaded mesh) is under the highest strain.

3. Results

Underhand strain patterns (Fig. 2) were different from overhand, with early phase peaks in superior ligaments and late phase peaks in anterior and inferior ligaments. Overhand anterior strain peaked during the late phase.

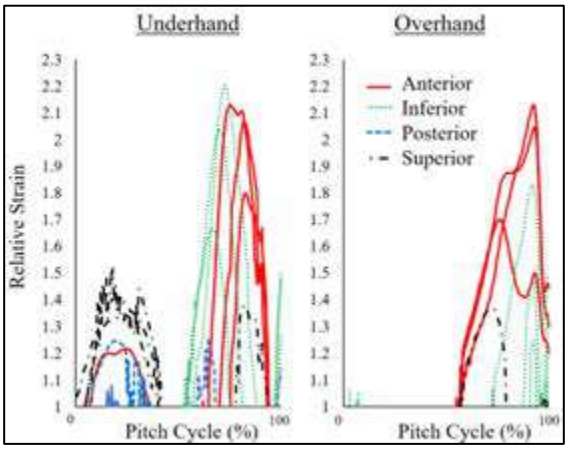

Figure 2: Average strain patterns across the pitching cycling for underhand and overhand throws.

4. Discussion and Conclusions

In the late pitching phase, strain magnitudes were similar between overhand and underhand throws. But it is now known how these patterns change after many throws when the athlete fatigues.

This project is ongoing; future work will explore additional: athlete's kinematics both before and after many throws, specimen geometries, and nonlinear constitutive models.

5. References

1. Bigliani et al. J Orthop Res. 1992; 10(2): p. 187-97.

Acknowledgements:
The author would like to thank Russell Warren MD and Andreas Kontaxis PhD.

CMBBE2023
18th International Symposium on Computer Methods in Biomechanics and Biomedical Engineering
3 - 5 May 2023, Paris, France
Arts et Métiers Institute of Technology
Institut de Biomécanique Humaine Georges Charpak
155 boulevard de l'Hôpital 75013 Paris France
www.cmbbe-symposium.com

NUMERICAL ANALYSES FOR EVALUATING STRAIN LOCALIZATION IN THE BRAIN CAUSED BY EXTERNAL IMPACT

Motoharu Terai (1), Atsushi Sakuma (2), Yuelin Zhang (3)

1. Graduate School, Kyoto Institute of Technology, Japan;
2. Kyoto Institute of Technology, Japan; 3. Sophia University, Japan

1. Introduction

The onset-risk prediction of concussion has been studied by a finite element method (FEM) [1]. In this paper, the computational simulation of FEM is also used to evaluate the process of brain injury due to head collision for the purpose of reducing brain injury in contact sports like American football. Here, the head is modelled as a 1/4 sphere model and a cubic with isotropic material for the simplification of its collision problem. In this discussion, the transient deformation due to the head collision is validated by changing the elastic modulus of impactor cubic, and its results are compared with the computed results by modal analysis for studying the mechanics of the onset-risk.

2. Modelling and Simulation

As a case of concussion, there is a collision between the heads in tackles of American football, as shown in Fig.1.



Figure 1: Modelling of collision problem in American football.

In the numerical simulation, the models of the head sphere and the impact cubic are simplified to 1/4 objects as shown in Fig.2(a) due to their symmetries. This modelling can compute the results shown in Fig. 2(b). Here, the stress wave propagating in the centre and the complex pressure distribution generated near the skull in the head part are confirmed in the results.

As for the results of modal analysis using same head model, it is confirmed that qualitative evaluation of complex distributions in soft brain part is possible as shown in Fig.3.

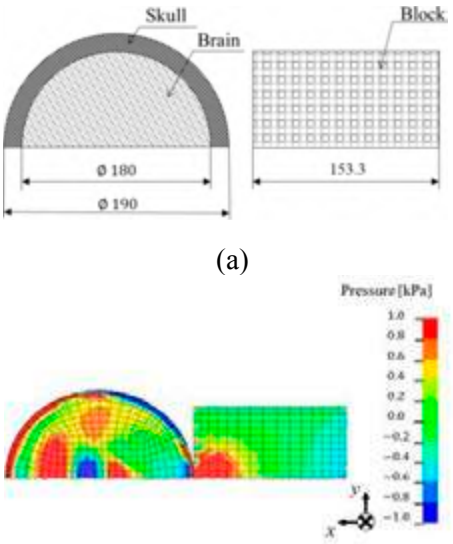

Figure 2: Condition of numerical analysis (a) and a computed result (b).

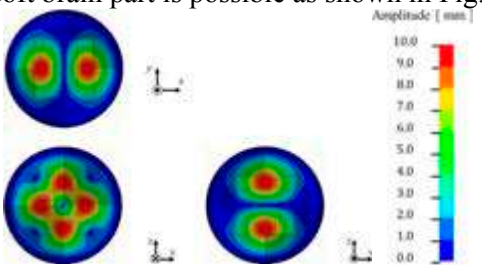

Figure 3: A result of modal analysis for head part.

3. Discussion and Conclusions

It is shown that the deformation problem of concussion in the low-elasticity region of brain elasticity, which causes many difficulties in transient analysis, can be discussed by fundamental modal analysis.

4. References

1. Aomura S, Zhang Y, Nakadate H, Koyama T, Nishimura A., J. Biomechanical Sci. and Eng., 11(4):16-00393 (2016)

CMBBE2023
18th International Symposium on Computer Methods in Biomechanics and Biomedical Engineering
3 - 5 May 2023, Paris, France
Arts et Métiers Institute of Technology
Institut de Biomécanique Humaine Georges Charpak
155 boulevard de l'Hôpital 75013 Paris France
www.cmbbe-symposium.com

INFLUENCE OF HEAD-FLOOR COMBINED STIFFNESS IN STAIR FALL HEAD IMPACT: A MULTI-BODY DYNAMICS STUDY

Sushil Kumar (1), Anoop Chawla (2), Kaushik Mukherjee (2)

1. *Transportation research and injury prevention center, Indian Institute of Technology Delhi, New Delhi, India.*
2. *Department of mechanical engineering Indian Institute of Technology Delhi, New Delhi, India.*

1. Introduction

Fall-based head injuries are the second leading cause of disability [1]. Although multiple studies of the head impact on various hard and soft surfaces are available [2], there is a scarcity of studies to compare the effect of different thicknesses of Softlayer on the concrete surface in head impact. In this multibody dynamics study, we investigated the influence of the combined stiffness of a soft layer and the concrete floor on a stair fall-based head impact.

2. Materials and Methods

MADYMO 50th percentile Hybrid-III male pedestrian model was used for simulations. The initial patient posture mimicked a condition wherein the right leg was on the fourth step of the stair, and the left leg was aerial. Varying backward inclinations (0^0, 10^0, 20^0, 30^0, and 38^0 CW) of the upper torso were modeled [Fig.1(a-b)]. Force penetration curves of the MADYMO dummy head model were changed according to the head response curve [3].

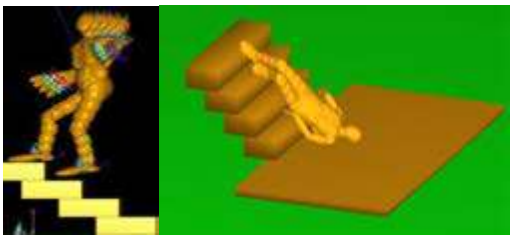

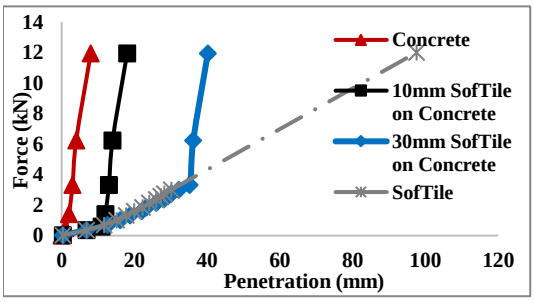

Figure 1. MADYMO simulation (a) initial posture (b) just before impact on the floor. (c) Combined force penetration characteristics of various floors.

Floor Type	Resultant Liner acceleration at head (CG)	Peak Head impact forces
Concrete	189±8.5g	13.26±0.06kN
10mm SofTile on Concrete	147±2g	12.55±0.255kN
30mm SofTile on Concrete	98±2.5g	10.61±0.12kN
SofTile	75±3.5g	5.25±0.05kN

Four flooring conditions (concrete, 10mm SofTile with concrete, 30mm SofTile with concrete, and only SofTile) representing varying floor stiffnesses [4] were considered [Fig. 1(c)]. Combined contact interaction (μ=0.55) was assigned between the head and the ground. 1000Hz channel frequency class filter was used to get the resultant linear acceleration of the Head CG.

3. Results

The floor stiffness largely influenced the immediate post-impact resultant linear acceleration of the hybrid-III dummy head. For varying upper torso inclination, the impact on concrete caused a high (189±8.5g) resultant linear acceleration of head CG. Consequently, the peak head impact force was also observed to be the highest (13.26±0.06kN). Adding a soft cushioning layer reduced the resultant linear acceleration of head CG and peak head impact force (Table 1).

4. Discussion and Conclusions

Our results corroborate well with previous studies wherein soft flooring have been shown to reduce the impact forces on head form and lower and upper limbs [2,4,5]. This study shows that low-stiffness floors can attenuate up to 60% of peak head impact forces.

5. References

1. WHO 2018 online:http://www.who.int/news-room/(assessed on date 10 November 2022).
2. Alexander D et al., 2011 Med Eng Phys 11.012
3. Yoganandan et al., 1995. J N Trauma 659–668.
4. Laing et al.,2009.AccidAnal Prev.2009.03.001.
5. Robinovitch et al., 1998 jorthop Res 309-13.

CMBBE2023
18th International Symposium on Computer Methods in Biomechanics and Biomedical Engineering
3 - 5 May 2023, Paris, France



Arts et Métiers Institute of Technology
Institut de Biomécanique Humaine Georges Charpak
155 boulevard de l'Hôpital 75013 Paris France
www.cmbbe-symposium.com

FREE MOMENT VARIABILITY FOR MAXIMUM VERTICAL JUMP FALLING RISK ASSESSEMENT

Carlos Rodrigues (1,2), Miguel Correia (1,2), João Abrantes (3)
Marco Benedetti (4), Jurandir Nadal (5)

1. FEUP, Portugal; 2. INESC TEC, Portugal; 3. MovLab - ULHT, Portugal
4. PPGEE - UFPE, Brazil; PEB - COPPE/UFRJ

1. Introduction

Maximum vertical jump (MVJ) is a common sport movement with long countermovement (CM) on countermovement jump (CMJ) and short CM assessed on drop jump (DJ) for powerful action in relation to squat jump (SJ) without CM [1]. Impulse phase plays on MVJ determinant role for higher vertical jump height with the center of pressure (COP) excursion studied for stability analysis in relation to different MVJ performance [2]. Complementarily, free moment has been pointed as an adequate measure for estimation of whole-body imbalance and falling risk on gait [3], with an open issue on free moment ability for MVJ impulse stability assessment at transversal plane and risk of falling.

2. Materials and Methods

Free moment variability was assessed trough vertical moment $\widetilde{M}_z = M_z/(W_i \times h_i)$ during impulse phase on different MVJ after normalization to subject weight W_i and height h_i by the $\widetilde{c_v}$ modified coefficient of variation. Data sample is composed by a group of six healthy students of sports degree S_k, ages (21.5 ± 1.4) years, (76.7 ± 9.3) kg mass and (1.79 ± 0.06) m height. Each subject performed after warm-up a total on nine MVJ, this being three SJ, CMJ and DJ. Best SJ, CMJ and DJ repetition was selected for each subject based on higher flight time. Vertical movement $\widetilde{M}_z$ variability was computed for each MVJ trial after normalization using Eq. 1 with $\tilde{\mu} = \frac{1}{n}\sum_{k=1}^{n}\left|\widetilde{M}_z^k\right|$ its mean of absolute value and σ its standard deviation during impulse phase, $k = 1 \ldots n$.

$$\widetilde{c_v} = \sigma/\tilde{\mu} \qquad (1)$$

Average $\widetilde{M}_z$ variability was compared between CMJ, DJ and SJ as well as between S_k subjects.

3. Results

Grouped results of $\widetilde{M}_z$ free moment variability assessed trough $\widetilde{c_v}$ modified coefficient of variation (Fig. 1) presented higher dispersion at DJ than SJ, both higher than CMJ as well as higher $\widetilde{c_v}$ mean at SJ than DJ and CMJ.

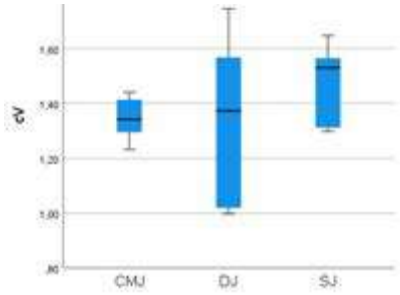

Figure 1: $\widetilde{c_v}$ boxplot of free moment $\widetilde{M}_z$.

Subject specific analysis of $\widetilde{M}_z$ free moment presented two distinct clusters, with S1, S2, S3 group G1 higher $\widetilde{c_v}$ at DJ than SJ, CMJ and S4, S5, S6 group G2 higher $\widetilde{c_v}$ at SJ than CMJ, DJ.

$\widetilde{c_v}$	CMJ	DJ	SJ
S1	1.293	1.475	1.296
S2	1.229	1.567	1.525
S3	1.348	1.746	1.311
S4	1.440	1.268	1.647
S5	1.412	0.998	1.565
S6	1.332	1.019	1.535

Table 1: Subject specific $\widetilde{c_v}$ of free moment $\widetilde{M}_z$.

4. Discussion and Conclusions

Higher free moment variability point to larger instability and risk of fall at SJ, DJ than CMJ.

5. References

1. Knudson D, Fundamentals of Biomechanics: Springer; 2007.
2. Rodrigues C et al., IEEE Eng in Med & Biol Soc (EMBC):4808-4811 (2021).
3. Daniel P, Stan G., Proc. Rom. Acad., Series B. 15(3):241-249 (2013).

CMBBE2023
18th International Symposium on Computer Methods in Biomechanics and Biomedical Engineering
3 - 5 May 2023, Paris, France



Arts et Métiers Institute of Technology
Institut de Biomécanique Humaine Georges Charpak
155 boulevard de l'Hôpital 75013 Paris France
www.cmbbe-symposium.com

THE USE OF MULTICHANNEL ELECTROMYOGRAPHY TO ASSESS MUSCLE ACTIVITY IN ERGONOMIC PUSHING TASKS

Usha Kuruganti, Jacqueline Toner and Victoria Chester

Faculty of Kinesiology, University of New Brunswick, Canada

1. Introduction

Surface electromyography (sEMG) is an important tool to evaluate ergonomic risks during work tasks, however there several factors limiting interpretation of the data including electrode position, subcutaneous tissue thickness, and recruitment strategies [1]. Multichannel or high-density EMG (HDEMG) overcomes previous limitations through the use of two-dimensional arrays of electrodes. HDEMG spatial parameters can then be used to assess muscle behaviour. While this technique shows promise for ergonomic applications, those spatial variables which provide the most useful information to understand work-related risks are yet to be determined. The purpose of this study was to examine HDEMG spatial parameters during an industrial pushing task to determine which spatial parameters are of relevance for ergonomic assessment.

2. Materials and Methods

Twenty men and women (mean age = 24.3 ± 4.3 years old) pushed an industrial platform cart with a load of 216 kg in a straight line over five meters. The cart was instrumented with six different handle designs: vertical (V), horizontal (H), and semi-pronated (S) at two different heights: shoulder (S) and hip (H). Two 32-channel electrode grids were placed over the left and right rectus abdominis, external obliques, and the erector spinae during 6 different pushes (each handle orientation and height). HDEMG maps representing the spatial distribution of intensities of active motor units over the surface of the muscle were developed:

$$\mathrm{HM_{ij}} = \mathrm{RMS(sEMG_{ij})} \qquad (1)$$

where HM is an activation map and each pixel in a map ($HM_{i,j}$) corresponds to an RMS value of a channel in an electrode array (position i,j). Spatial features of mean RMS, intensity, differential intensity and median frequency as well as entropy and coefficient of variation (features of muscle heterogeneity) were calculated and compared across handle designs.

3. Results

Significant differences were noted in mean RMS, intensity, differential intensity and median frequency in trunk muscles across different handle design. Shoulder height designs demonstrated significantly increased mean RMS values ($p<0.05$) compared to hip height designs. Significantly higher mean RMS values were observed in the rectus abdominis ($p=0.02$) and obliques ($p=0.02$) for shoulder height designs compared to the hip height design while using a similar handle orientation. Shoulder height designs also demonstrated significantly lower intensity (rectus) and MDF (obliques) values compared to hip height designs using similar handle orientation ($p=0.015$; $p=0.027$). Significant differences noted in differential intensity were dependant on both orientation and height. Muscle heterogeneity did not show any significant differences due to handle design.

4. Discussion and Conclusions

This work suggests that HDEMG and spatial parameters can be used successfully for ergonomic studies, however the choice of parameter is important. Future studies investigating machine learning algorithms may help to elucidate which spatial variables are most relevant for work related tasks.

5. References

1. Gazzoni M. Hum Fac & Erg in Man. 2010; 20(4):255-271 (2010).

Acknowledgements:
The authors would like to thank the New Brunswick Innovation Foundation (NBIF) and OT Biolelectronnica for providing financial support to this project.

CMBBE2023
18th International Symposium on Computer Methods in Biomechanics and Biomedical Engineering
3 - 5 May 2023, Paris, France
Arts et Métiers Institute of Technology
Institut de Biomécanique Humaine Georges Charpak
155 boulevard de l'Hôpital 75013 Paris France
www.cmbbe-symposium.com

INVESTIGATING JERSEY FINGER INJURY LOAD CASES USING A FINITE ELEMENT NEUROMUSCULAR HUMAN BODY MODEL

Lennart V. Nölle (1), Eduardo Herrera Alfaro (1), Oleksandr V. Martynenko (1), Syn Schmitt (1,2)

1. *Institute for Modelling and Simulation of Biomechanical Systems, University of Stuttgart, Germany*
2. Stuttgart Center for Simulation Science, University of Stuttgart, Germany

1. Introduction

A common hand injury in football, rugby and basketball is the so-called Jersey Finger injury, in which an eccentric overextension of the distal interphalangeal (DIP) joint leads to an avulsion of the connected *musculus flexor digitorum profundus* (FDP) tendon [1]. The goal of this study is to show how a finite element (FE) neuromuscular human body model (NHBM) can be modified to computationally assess tendon strains during general Jersey Finger injury load cases.

2. Materials and Methods

First, a Jersey Finger injury criterion covering the injury mechanisms of tendinopathy and avulsion was defined. Next, the right hand of the THUMS AM50 occupant model of academic version 3.0 [2] was modified to increase finger mobility. The model was then expanded by introducing eight Hill-type muscles to represent the *flexor digitorum superficialis* (FDS) and FDP muscles. Both tendon material parameters of the muscles and their moment arms were optimized to fit experimental data [3,4]. The tested Jersey Finger loading scenario was characterized by simulating the gripping of a rod which was then retracted with a velocity calculated from the sprinting acceleration of college football players [5], forcing the hand open during eccentric muscle contraction.

3. Results

The achieved moment arm curves are in good agreement with those reported in the literature [4] (Fig. 1). The results of the Jersey Finger injury assessment indicate that the strain put on the FDS and FDP tendons is not sufficient to cause tendinopathy of any kind, while the tendon forces where large enough to suggest the risk of tendon avulsion in singular digits.

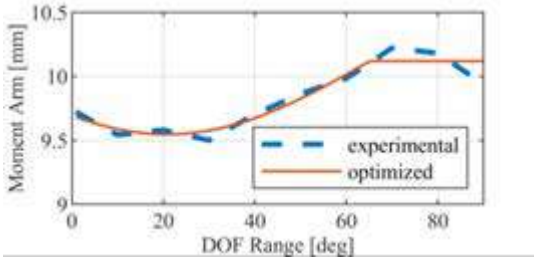

Figure 1: Moment arm of the middle finger FDP spanning the metacarpophalangeal joint.

4. Discussion and Conclusions

This study shows that given proper modification, FE-NHBMs can be used for the assessment of Jersey Finger injury severity. Further studies should focus on the experimental validation of the proposed tendinopathy and avulsion injury thresholds.

5. References

1. D. M. Avery, C. M. Rodner, C. M. Edgar, J., Orthop. Surg. Res.; 2016. 11, 99.
2. M. Iwamoto et al., in Proc. 6th European LS-DYNA Users' Conference; 2007. pp. 47–56.
3. J. V. Benedict, L. B. Walker, E. H. Harris, J. Biomech.; 1968. 1, 53–63.
4. M. T. Boots et al., bioRxiv; 2020.
5. W. F. Brechue, J. L. Mayhew, F. C. Piper, J. Strength Cond. Res.; 2010. 24, 1169–1178.

Acknowledgements:

This work was supported by the Deutsche Forschungsgemeinschaft (DFG, German Research Foundation) under Germany's Excellence Strategy - EXC 2075 - 390740016 (SimTech) and by the Federal Ministry for Economic Affairs and Climate Action of Germany (Bundesministerium für Wirtschaft und Klimaschutz) through the project "Artificial Intelligence for Real-Time Injury Prediction (ATTENTION)", grant number 19A21027D.



ANATOMICALLY-REALISTIC COMPUTATIONAL MODELING FOR TESTING THE EFFECTIVENESS OF PROTECTIVE PLATES

Maayan Lustig (1), Yoram Epstein (2), Amit Gefen (1)

1. Department of Biomedical Engineering, Faculty of Engineering, Tel Aviv University, Tel Aviv, Israel
2. Sackler Faculty of Medicine, Tel Aviv University, Tel Aviv, Israel

1. Introduction

A ballistic protective plate (BPP) is standard military equipment that reduces the risk of severe injuries in the torso area which are common in combat environments, being approximately 25-30% of all injuries [1]. Non-penetrating impacts of bullets or other ballistic threats such as blast explosions, shrapnel, or shrapnel shells with the BPP are accompanied by rapid and immediate deformations of the armor and underlying tissues. These are translated to mechanical energy absorbed in the tissues behind the armor, causing the injury known as 'behind armor blunt trauma' (BABT) [2]. That absorbed energy takes the form of pressure waves that propagate through the tissues, including deep tissues that are not in direct contact with the gear, resulting in rapid deformations, stretching and collapse of the tissues and associated cell and tissue death [3], [4]. To date, there is no effective and cost-effective procedure for rapid testing of BPP designs.

2. Materials and Methods

The objective of this study was to develop a novel, anatomically-accurate, finite element modeling framework as a decision-making tool to evaluate and rate the biomechanical efficacy of BPPs in protecting the torso from battlefield-acquired non-penetrating impacts. To simulate a blunt impact with a BPP, two types of BPPs (type 3 and type 4) and a 5.56 mm bullet were modeled based on their real dimensions, physical and mechanical characteristics.

3. Results

Be aware that the figures (Fig. 1) will both be available as a PDF file (colour pictures) and printed, in black and white, in the book of abstracts. So please make sure your pictures also look good in print.

4. Discussion and Conclusions

The results indicated that plate type 4 induces greater tissue strains and stresses post the ballistic impact; this is due to the fact that plate type 4 is larger, thicker and heavier than plate type 3, and therefore, its kinetic energy is higher and so is the shock wave which is transferred to the tissues behind plate type 4. These findings are nonintuitive as many stakeholders in the field believe that thicker and heavier BPPs protect the torso better than thinner, lighter plates. Our modelling provides a versatile, powerful testing framework for both industry and clients of BPPs, at the prototype design phase, or for quantitative standardized evaluations of candidate products in purchasing decisions and bids.

5. References

1. N. R. Koreerat and C. M. Koreerat, "Prevalence of Musculoskeletal Injuries in a Security Force Assistance Brigade Before, During, and After Deployment," Mil. Med., vol. 186, no. Supplement_1, pp. 704–708, Jan. 2021
2. D. Drobin et al., "Electroencephalogram, circulation, and lung function after high-velocity behind armor blunt trauma," J. Trauma - Inj. Infect. Crit. Care, vol. 63, no. 2, pp. 405–413, 2007
3. L. Cannon, "Behind Armour Blunt Trauma - an emerging problem," J. R. Army Med. Corps, vol. 147, no. 1, pp. 87–96, Feb. 2001
4. J. Van Bree and N. Van der Heiden, "Behind armour blunt trauma analysis of compression waves," in Personal Armour Systems Symposium 1998 (PASS98), 1998.

Acknowledgements:

The research is funded by a grant from the Israel Defense Forces Medical Corps (grant number: 4440991484), and by the Israel Ministry of Innovation, Science & Technology (doctoral scholarship awarded to Maayan Lustig).

CMBBE2023
18th International Symposium on Computer Methods in Biomechanics and Biomedical Engineering
3 - 5 May 2023, Paris, France



Arts et Métiers Institute of Technology
Institut de Biomécanique Humaine Georges Charpak
155 boulevard de l'Hôpital 75013 Paris France
www.cmbbe-symposium.com

CO-CONTRACTION CAUSES HIGHER JOINT LOADS IN PEOPLE WITH INCREASED NECK-SHAFT AND ANTEVERSION ANGLES

Hans Kainz (1), Basílio Gonçalves (1), Willi Koller (1), Gabriel Mindler (2), Andreas Kranzl (2)

1. Centre for Sport Science and University Sports, University of Vienna, Austria

2. Department of Pediatric Orthopaedics, Gait Analysis Lab, Orthopedic Hospital Speising, Austria

1. Introduction

Torsional deformities of lower limbs, e.g. increased anteversion angle (AVA), are common in people with and without neurological disorders. A high prevalence of hip and knee pain has been reported in children with torsional deformities [1]. Previous musculoskeletal simulation studies showed that increased AVA alters the moment arms of muscles and leads to increased joint contact forces (JCF), which can be compensated with an altered gait pattern [2-5]. However, it remains unclear how the altered moment arms influence muscle forces and the generated moments by each muscle and therefore alter JCF. Furthermore, it is unknown how the neck-shaft angle (NSA) influences and contributes to the altered muscle forces and JCF. The aim of our study was to comprehensively investigate the influence of femoral AVA and NSA on muscle forces during walking.

2. Materials and Methods

We created 25 musculoskeletal models with a variety of NSA (± 30° in 15° steps, absolute NSA between 93° and 153°) and AVA (± 30° in 15° steps, absolute AVA between − 12° and 48°). Each model was scaled to the anthropometry of our healthy participant. For each model we calculated joint angles, joint moments, muscles' moment arms, muscle forces, muscle moments, i.e. moment each muscle/muscle group generates, and JCF based on the motion capture data of our participant with a typical gait pattern using OpenSim. Co-contraction was quantified as the ratio between agonist and antagonist muscle moments [6].

3. Results

We found a significant increase in co-contraction in hip and knee joint spanning muscles with increasing AVA and NSA (Fig. 1). Increased hip flexor and extensor muscle moments explain the increase in hip JCF in models with increasing AVA. In models with increasing NSA, the majority of hip muscles' moment arms decreased and muscle forces increased, which explains the increased hip JCF despite similar agonist and antagonist muscle moments. Increased rectus femoris and gastrocnemius muscle forces were mainly responsible for the increased knee JCF in models with increasing AVA and NSA.

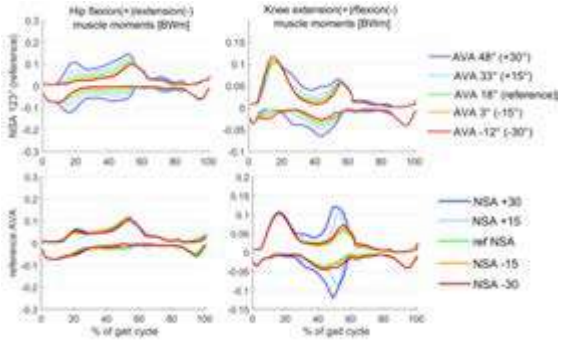

Fig. 1. Agonist and antagonist muscle moments for models with different AVA (top) and NSA (button).

4. Discussion and Conclusions

Increased hip and knee JCF in models with increased AVA and NSA were linked to changes in hip muscle moment arms and compensatory increases in hip and knee muscle forces. Decreased AVA and NSA had a minor impact on muscle moments and JCF. Our findings might help to explain several clinical observations, e.g. increased AVA is associated with hip osteoarthritis [7], increased NSA increases the risk of knee osteoarthritis [8], hip and knee pain in children with increased AVA [1].

5. References

[1] Mackay. *Gait & Posture*, 86, 144-49, 2021
[2] Arnold, *Dev.Med.Child Neurol.* 39,40–44, 1997
[3] Bosmans, *Gait & Posture*, 44, 61-67, 2016
[4] Kainz, *PLoS One* 15, e0235966, 2020
[5] Modenese, *Gait & Posture*, 88, 318–321, 2021
[6] Hoang, *J. Biomech.* 83, 134–142, 2019
[7] Parker, *Arthr.Sport.Med.Reh.* 3,e2047–58, 2021
[8] Coskun Benlidayi, *Surg Radiol Anat* 37, 369–376, 2015

CMBBE2023
18th International Symposium on Computer Methods in Biomechanics and Biomedical Engineering
3 - 5 May 2023, Paris, France
Arts et Métiers Institute of Technology
Institut de Biomécanique Humaine Georges Charpak
155 boulevard de l'Hôpital 75013 Paris France
www.cmbbe-symposium.com

LASER PHOTOTHERMAL THERAPY SIMULATION FOR DESIGNING BREAST TUMOR TREATMENT PROTOCOL

Edwin A Quinn, Manpreet Singh, Liang Zhu

University of Maryland Baltimore County, United States of America

1. Introduction

Recently, gold nanorods have been used to enhance laser absorption in tumors. Experimental studies have demonstrated that the absorption coefficient in nanorod-deposited tumors was almost twice of that in tumors without gold nanorods, leading to selective and enhanced laser energy absorption in those tumors [1]. In this study, we simulate laser absorption in a tumor embedded in a breast model to design heating treatment protocols.

2. Materials and Methods

Figure 1 shows a 10 mm dia. tumor embedded in a human breast model. An 800 nm laser is incident on the skin surface, with a spot size of 10 mm dia. and radiance of 24,000 W/m^2. The Pennes bioheat equation is used to simulate the transient tissue temperature field [2] as:

$$\rho c \frac{\partial T}{\partial t} = k_{tissue} \cdot \nabla^2 T + \omega \rho_b c_b (T_b - T) + Q_{met} + q'''_{Laser} \quad (1)$$

In Eq.1, the volumetric heat generation rate due to laser absorption in the tissue (q'''_{Laser}) is derived based on the modified Beer's law with an effective attenuation coefficient μ_{eff}. In healthy breast tissue μ_{eff} is 91 m^{-1}, while for the gold nanorod deposited tumor μ_{eff} increases to 180 m^{-1}. The boundary conditions include prescribed 37°C at the breast surfaces and cooling by cold water at the laser spot (T_∞=5°C and h=1000 W/m^{2}K). Simulations were carried out in COMSOL software.

3. Results

Figure 1 gives the temperature contours at the central slice of the simulation domain at various instants. The temperature distribution before the heating is almost uniform around 37°C. Once the laser treatment is initiated, one can see steady temperature elevations in the tumor region with the majority of laser absorption. Steady state temperature field is established after 200 s. T_{max} in the tumor (60°C) occurs at a deep tumor location, while T_{min} in the tumor is 47°C. Based on the location of $T_{min,}$ we estimate that it takes 916 s to cause irreversible thermal damage to the entire tumor. Collateral thermal damage along the laser path occurs, however, it is minimized via surface cooling and enhanced laser absorption in the tumor.

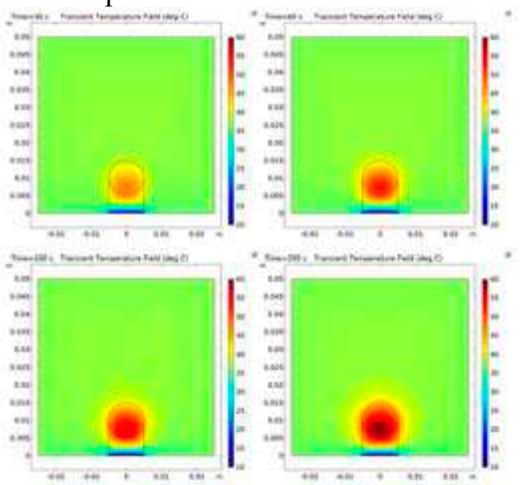

Figure 1. Schematic diagram of a spherical tumor embedded in a simplified geometry of a human breast model. Temperature fields are shown at 30 s, 60 s, 100 s, and 200 s.

4. Discussion and Conclusions

We demonstrated selective laser ablation in a gold nanorod-deposited breast tumor. A laser intensity of 24000 W/m^2 at the skin surface with a laser spot of 10 mm in diameter is needed to achieve a minimal temperature within the tumor [2] at 47°C. Results is used to design heating protocol to maximize thermal damage to tumors via minimizing thermal damage to healthy tissue along the laser path.

5. References

1. Manuchehrabadi N, Chen Y, Lebrun A, Ma R, Zhu L. J. Biomech. Eng. 135(12):121007(2013)
2. Manuchehrabadi N, Zhu L. International J. Hyperthermia 30(6):349-361(2014)

Acknowledgements:
The research was supported by NSF (Grant no: CBET-1765538).

CMBBE2023
18th International Symposium on Computer Methods in Biomechanics and Biomedical Engineering
3 - 5 May 2023, Paris, France
Arts et Métiers Institute of Technology
Institut de Biomécanique Humaine Georges Charpak
155 boulevard de l'Hôpital 75013 Paris France
www.cmbbe-symposium.com

HEMODYNAMICS OF CIRCLE OF WILLIS HAVING HYPOPLASTIC ANTERIOR COMMUNICATING ARTERY

Shine S R (1), Jayanand Sudhir Bhanu (2)

1. *Department of Aerospace Engineering, Indian Institute of Space Science and Technology, Thiruvananthapuram, India*
2. *Department of Nuerosurgery, Srree Chitra Tirunal Institute for Medical Sciences and Technology, Thiruvananthapuram, India*

1. Introduction

The major abnormal configurations of the circle of Willis (CoW) include fetal and fetal-type or hypoplastic arteries. Hypoplastic or absence of one of the pre-communicating segments of an anterior cerebral artery is an anatomic variation observed in the anterior part of the circle of Willis [1]. Lippert and Pabst [2] analyzed various anatomical cases and observed that 50% of the population might have a CoW with an absent or hypoplastic artery. In this study, we investigate the effect of a hypoplastic A segment of ACA on the hemodynamics of the entire CoW. Simulations are conducted by varying the degree of hypoplasticity.

2. Materials and Methods

A CFD model of the complete CoW with various hypoplastic ACA A1 segment levels is developed. An idealized geometry of CoW is generated by extracting the center lines from a patient-specific CT image. Pulsating, Laminar, incompressible, non-Newtonian blood flow is modeled using Navier–Stokes equations. The work highlights the flow, WSS features, and aneurysm initiation risk due to the hypoplastic segment.

3. Results and discussions

Flow rates through different cross-sections of ACoA-ACA junction for the various cases of hypoplasic A1 of ACA during early diastole are shown in Fig. 1. As constriction increases, there is no significant change in the mass flow rate through planes D and E. The blood flow is re-routed from the normal ACA A1 to the other side. Therefore the primary effect is the substantial increase in flow on one side of the ACoA complex and the severe flow diversions at the ACoA-ACA junction.

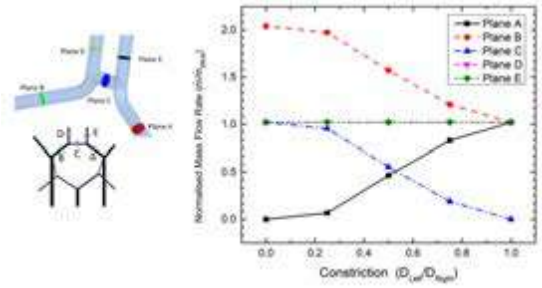

Figure 1. Variation of normalized mass flow rate in various segments with a hypoplastic A1 segment of ACA

Fig. 2 shows the various cases' peak WSS locations (ACA-ACoA junction and the ACA A1 initiation site). These locations are characterized by high curvature and bifurcation angles, and are the most vulnerable locations for aneurysm formation.

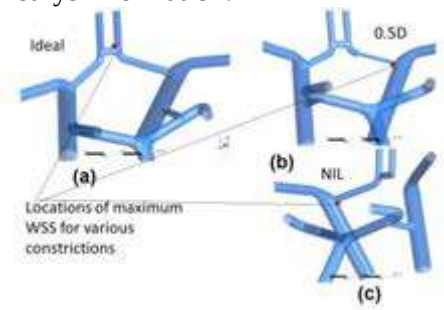

Figure 2. WSS contours at artery wall with changing diameters of A1 segment of left ACA at peak systole

4. Conclusions

This study provides a better understanding of cerebral hemodynamics with a hypoplastic A1 segment of ACA. Results indicate that the overall perfusion rate to the brain is maintained even when a hypoplastic A1 ACA exists.

5. References

1. Krabbe-Hartkamp, et al. Radiology, 207, no. 1 103-111 (1998).
2. Lippert, Herbert, and Reinhard Pabst. München: JF Bergmann Verlag, (1985).

CMBBE2023
18th International Symposium on Computer Methods in Biomechanics and Biomedical Engineering
3 - 5 May 2023, Paris, France
Arts et Métiers Institute of Technology
Institut de Biomécanique Humaine Georges Charpak
155 boulevard de l'Hôpital 75013 Paris France
www.cmbbe-symposium.com

FINITE ELEMENT MODEL OF THE HUMAN BREAST FOR LARGE DEFORMATIONS APPLICATIONS

Mariana Carvalho[1,2], Alessandro Arduino[3], Marco Parente[1,2], Renato Natal[1,2], João Ferreira[1]

1. Department of Mechanical Engineering, Faculty of Engineering, University of Porto, Portugal; 2. Institute of Science and Innovation in Mechanical and Industrial Engineering, Portugal; 3. Department of Civil, Environmental and Architectural Engineering, University of Padova, Italy

1. Introduction

Breast cancer is the most incident cancer among adult women [1]. X-ray mammography is the standard technique for its detection. During mammography, the breast is compressed between two paddles: craniocaudal (CC) or mediolateral oblique directions [2]. These provide a uniform compressed breast thickness (CBT) and improve differentiation between tumours and normal tissue [3]. This study developed an *in-silico* model of the human breast structure during mammography.

2. Materials and Methods

The breast model contains linear elastic ribs, pectoralis muscle and skin, and hyperelastic isotropic adipose and fibro-glandular tissues. The volume is characteristic of a very small breast (0.20-0.52 dm^3 [4]). Hexahedral elements (C3D8) are applied to enable mesh continuity, and the skin is meshed by shell elements (S4). The quasi-static finite element analysis of the CC compression is performed in Abaqus Explicit (Fig. 1). The breast model is placed between analytical rigid paddles with symmetric displacements Δz. CC breast compression is defined by a deformation (Δz = 50 mm, Δt = 7.5s), a clamping (Δz = 0, Δt = 12.8s) and a release phase (Δz = -50 mm, Δt = 3s) [4].

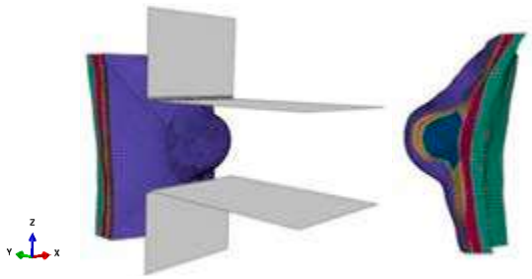

Figure 1: Quasi-static finite element analysis of the CC mammographic compression, with illustration of the different layers.

3. Results

The kinetic/internal energy ratio is below 5%, which validates the quasi-static assumption. A 50-mm CBT is obtained by a compression force of about 140 N (14.3 kgf). The maximum principal stress in the skin is higher at the contact area closer to the ribs and decreases towards the nipple (Fig. 2). The in-plane geometry is enlarged by paddles compression.

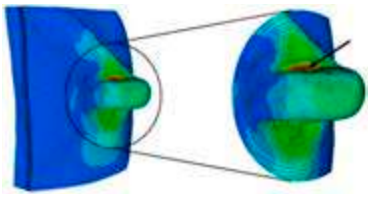

Figure 2: Breast deformation and maximum stress distribution (arrow points to the maximum value).

4. Discussion and Conclusions

An *in-silico* breast model is adapted to accommodate breast compression. The material models and properties employed enabled a realistic deformation, as the breast expanded in between paddles. Even though this work is not based on real set-ups, it approaches numerical [3] and clinical [4] results on the same CBT, force and volume. Future work will include viscous and damage effects and breast tumors to test the pathological condition.

5. Reference

1. Sung H et al. CA Cancer J Clin 2021;71:209-49.
2. Pianigiani S et al. Front Bioeng Biotechnol 2015;3.
3. Liu YL et al. Radiat Phys Chem 2017;140:295-9.
4. de Groot JE et al. BMC Womens Health 2015;15:26.

Acknowledgements:
The authors gratefully acknowledge the support from Portuguese Foundation of Science under research project PTDC/EME-APL/1342/2020 (CyclicCell).



LARGE-SCALE FINITE ELEMENT MODELING OF PRE-STRESS IN ARTICULAR CARTILAGE

Seyed Shayan Sajjadinia* (1), Bruno Carpentieri (1), Gerhard A. Holzapfel (2,3)

1. Faculty of Computer Science, Free University of Bozen-Bolzano, Italy; 2. Institute of Biomechanics, Graz University of Technology, Austria; 3. Department of Structural Engineering, Norwegian University of Science and Technology, Norway

*Corresponding author: e-mail: ssajjadinia@unibz.it

1. Introduction

Articular cartilage (AC) is largely modeled by finite element (FE) methods and multiphasic equations, e.g., [1]. Since the *in vivo* stress-free state of AC is usually unknown, a pre-stressing algorithm (PSA) is typically needed to determine this state by custom optimizers, which has been successfully implemented in small-scale models with simple geometries [2]. The main goal of this work is the extension to a large-scale AC model in a human tibiofemoral joint.

2. Materials and Methods

An FE model is extracted from the Open Knee Project [3] to be integrated into the multiphasic model and the PSA. Since most AC constitutive equations are depth dependent, the normalized depth (ND) of each point is approximated by the points on the surfaces. Then the fibrillar orientations are approximated by their corresponding split lines and NDs. The FE analysis of pre-stressing is performed using an accelerated PSA with a unified optimizer (comparing to our previous work that requires separate optimizers for geometrical and material parameters).

3. Results

The optimizer finds the pre-stressed state by forward and inverse FE analyses in around 3 hours (and 14 steps) with a regular computer. The recorded stresses (Fig. 1) are strongly dependent on the depth. To assess the validity of the results, the load-resistance of the AC constitutive components, e.g., the stress in the fibrils, is calculated and compared.

4. Discussion and Conclusions

While previous large-scale FE models of AC simplified the multiphase equations by ignoring the pre-stressing and osmotic pressure, this work could present an automatic framework with a pre-stressing optimizer for large-scale and multi-physics FE modeling of AC, which is also used to demonstrate the significant zone-dependent effect of pre-stress.

5. References

1. Sajjadinia SS et al., Proc. Inst. Mech. Eng. Part H J. Eng. Med; 233(9):871–882 (2019).
2. Sajjadinia SS et al., J. Mech. Behav. Biomed. Mater; 114: 104203 (2021).
3. Erdemir A, J. Knee Surg; 29(2):107–116 (2016).

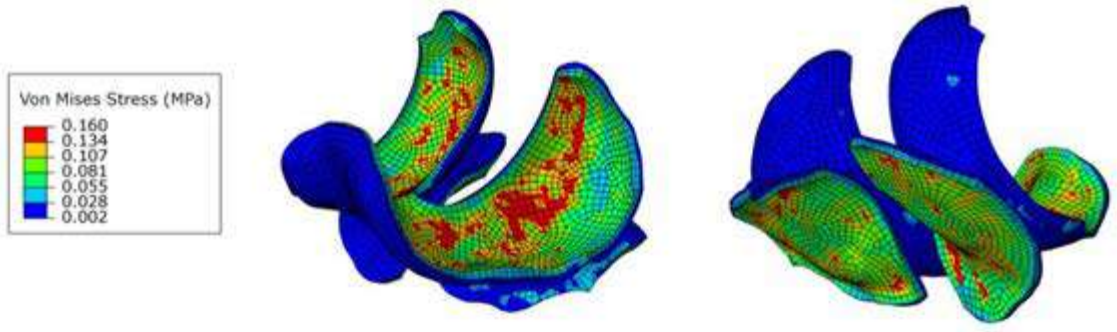

Figure 1. Von Mises stress contours (in MPa) after applying the pre-stress.



SIMULATING CARDIOVASCULAR DYNAMICS THROUGH DATA-DRIVEN REDUCED ORDER MODELS

Nicola Demo (1, 2), Michele Girfoglio (1), Gianluigi Rozza* (1, 2)

** Corresponding author: grozza@sissa.it,*

1. SISSA, International School for Advanced Studies, Mathematics Area, Mathlab, Trieste, Italy

2. FAST Computing srl, Trieste, Italy

1. Introduction

In recent years, the medical community has shown an increasing interest in developing numerical methods for simulating biomedical dynamics as a support for surgery or to predict the course of a disease. One of the main difficulties in this field is the accessibility of these simulators, in terms of memory and computational efficiency. To this aim, we focus our attention on the study of reduced order models (ROMs), which are specifically designed to reduce the computational cost of complex dynamics which usually emerge in biomedical applications. The study of cardiovascular flows is the main goal of our research.

2. Materials and Methods

The methodology is based on non-intrusive ROMs [1,2]. The goal of ROMs is the approximation of the solution to an unknown dynamic starting from a dataset of real data, denoted by *snapshots*, corresponding to a set of physical/geometrical parameters. Typically, such dynamics are described by incompressible Navier-Stokes equations.

The procedure is divided into two stages: the offline and online phase. During the offline phase we first collect the snapshots into a proper matrix S; then we apply the proper orthogonal decomposition to recover the reduced basis space and we define a map between the set of parameters and the modal coefficients space. This stage is usually very expensive, but only needs to be done once. It noteworthy to point out that the modal coefficients depend only on the parameter while the reduced basis space does not depend on it. Hence, this allows us to obtain a complete decoupling between the offline and online phase. The latter is reduced to the approximation of the solution as the linear combination between the modal coefficients corresponding to a new parameter and the reduced basis space.

3. Results

Several cardiovascular applications are analyzed, such as the simulation of blood flows in coronary/carotid arteries, left atrium and aorta. Data-driven techniques provide real-time evaluation for different parameter values. This allowed us to develop a computational interface, ATLAS [3], which is a ready-to-use tool based on ROMs, part of ARGOS.

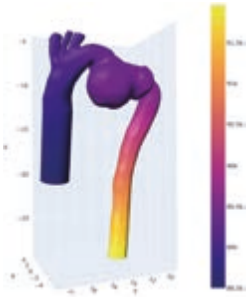

Figure 1: Pressure of thoracic aortic aneurism.

4. Discussion and Conclusions

The platform developed aims at spreading the use of ROMs in the medical community. The final goal is to build a tool that can be used in the medical routine as a decision support.

5. References

1. Hesthaven JS et al, Springer, 2016.
2. P. Benner et al, *De Gruyter*, Berlin, 2020.
3. ATLAS web page: https://argos.sissa.it/atlas

Acknowledgements:

The authors would like to acknowledge the European Research Council (Grant no: 681447, AROMA-CFD) for providing financial support to this project, as well as ARGOS PoC, as well as University of Pavia, Prof. Michele Conti and Prof. Ferdinando Auricchio, Comp. Mech and Adv. Materials group, and SISSA mathLab researchers Pierfrancesco Siena and Caterina Balzotti.



PREDICTION ACCURACY OF COLLATERAL LIGAMENT STRAINS OF HOLZPFEL-GASSER-OGDEN-BASED POST-TKA KNEE MODEL

Lucas Milakovic (1), Félix Dandois (1), Heleen Fehervary (2), Lennart Scheys (1,3)

1. Institute for Orthopaedic Research and Training, Department of Development and Regeneration, KU Leuven, Belgium

2. Biomechanics Section, Mechanical Engineering Department, KU Leuven, Leuven, Belgium

3. Division of Orthopaedics, University Hospitals Leuven, Leuven, Belgium

1. Introduction

Medial and Lateral Collateral ligaments (MCL/LCL) are key contributors to medial and lateral knee stability a fortiori after a Total Knee Arthroplasty(TKA) has been performed. Improved insight in ligament properties thus has the potential to further enhance TKA outcome. However, most models for pre-operative TKA planning rely on non-linear spring formulations, such as Blankevoort formulation[1]. Alternatively, Holzpfel-Gasser-Ogden(HGO) formulation[2], is increasingly being used as a continuum formulation[3,4]. The study objective is the accuracy assessment of knee collateral ligament strains using a subject-specific HGO formulation defined through a dynamic cosimulation workflow[5].

2. Materials and Methods

Two cadaveric post-TKA knees with posterior stabilized implants were subjected to dynamometer-controlled varus/valgus stress and bone-pin based kinematic tracking[6]. Digital Image Correlation(DIC) was used to measure Medial and Lateral Collateral Ligaments (MCL/LCE) ground-truth strains. Bones and implants were reconstructed from CT-scans and modelled as rigid bodies in multibody dynamics simulation software (MSC Adams, MSC Software, USA). 3D morphology of both MCL and LCL was based on MRI-scans and used for defining HGO-based finite element models in Abaqus (Simulia, USA). Next, HGO and Blankevoort parameters optimization were performed using gradient descent approach by minimizing the Root Mean Square Error(RMSE) between the experimental and simulation-based kinematics in CasADi[7], a toolbox available in MATLAB (The MathWorks Inc., Natick, MA, USA).

3. Results

Mean RMSE	Principal strains HGO	Engineering strains Blankevoort
Valgus loading(MCL)	0.65 ± 0.18	1.43 ± 0.34
Varus loading (LCL)	1.285 ± 0.56	0.89 ± 0.47

Table 1: Average of strains RMSE among specimens. Ground-truth strains were collected using DIC.

4. Discussion and Conclusions

On average, HGO-based models have better strains accuracy than Blankevoort-based models. Interestingly, the implemented kinematics-based HGO parameter optimization was faster compared to the literature (150h/subject vs 600h/subject[3]). In the future, a strain-based optimization will be implemented and integrated in a non-invasive 3D ultrasound-based platform for the evaluation of soft-tissue balancing in joint replacement surgery.

5. References

1. Blankevoort *et al*. *J Biomech*, *29*(7), 955–961, 1996
2. Gasser *et al*. *Interface Focus*, *3*(6), 15–35, 2006
3. Beidokhti *et al*. *J Biomech*, *65*, 1–11, 2017
4. Sadeqi *et al*. *Appl Math*, *12*(12), 1166–1188, 2021
5. Müller *et al*. *Comput Methods Biomech Biomed. Engin.*, *23*(11), 718–733, 2020
6. Dandois *et al*. *Sensors*, *21*(5), 1–14, 2021
7. Andersson *et al*. *Math Program Comput*, *11*(1), 1–36, 2019.

Acknowledgements:

The authors would like to thank the KU Leuven Interdisciplinary Network (ID-N) for providing financial support to this project.

CMBBE2023
18th International Symposium on Computer Methods in Biomechanics and Biomedical Engineering
3 - 5 May 2023, Paris, France
Arts et Métiers Institute of Technology
Institut de Biomécanique Humaine Georges Charpak
155 boulevard de l'Hôpital 75013 Paris France
www.cmbbe-symposium.com

OPEN SOURCE HEAD MODEL FOR SKELETAL INJURY ANALYSIS: DEVELOPMENT AND VALIDATION CATALOG

Jobin John (1), Yash Poojary (1) Jia Cheng Xu (2), Robert Thomson (1)

1. Chalmers University, Sweden; 2. VTI, Sweden

1. Introduction

Finite element (FE) models of head are used to analyze and predict head injuries, commonly in road safety and sports injuries. The emphasis in this study has been traumatic brain injury with attention to skull fracture. This presentation intends to report the development of an open source head FE model with the objective to predict skull injuries.

2. Materials and Methods

The FE model was developed to represent an average female of height 1.62 m and mass 63 kg [1]. Cranium and scalp geometry were based on a statistical shape model [2]. The trabecular bone is modeled as hexahedral solid elements and the cortical bone as quadrilateral shell elements, with variable nodal thickness for the different regions of the cranium. Bone material models were based on component tests of cortical and trabecular bone [3,4]. Soft tissues were defined as hexahedral solid adipose layers and quadrilateral shell skin layer. As an initial validation, the model responses were evaluated in impacts to the frontal and temporoparietal regions (Table 1).

Table 1: Validation simulations

Experiment	Impact type/location
Delye 2007	Pendulum impact on frontal
Yoganandan 1995	Blunt impact on frontal
Raymond 2009	Blunt impact on parietal
Yoganandan 2004	Temporoparietal impact on drop



Figure 1: The skeletal mesh, with the surrounding soft tissues shown in transparent shading.

3. Results

The head FE model is shown in Fig 1. Fig 2 shows component test response in tensile loading. The simulation setups will be available under free and open source licenses on OpenVT (https://openvt.eu/fem/viva/vivaplus).

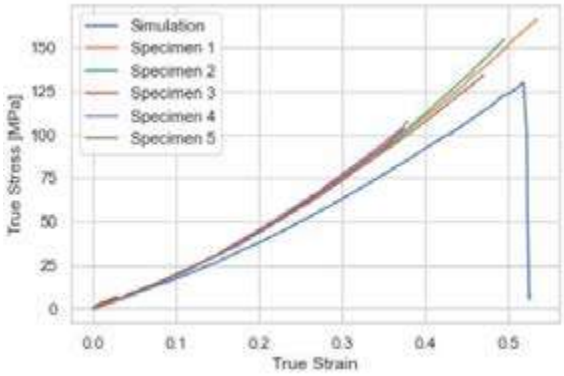

Figure 2: Tensile stress-strain response compared to experiment at a strain rate of 32/s [3]

4. Discussion and Conclusions

The head model is integrated with VIVA+ models for road user injury evaluations. The models and validations are released openly on a collaborative repository to foster an Open Science community-based development and evaluation. Such an approach can contribute to various facets of in-silico model credibility in product development, virtual testing, and translational biomechanics [5].

5. References

1. John J, et al. *Frontiers in Bioengineering and Biotechnology* 2022; **10**: 918904.
2. Wei A, adult populations. *Computer Methods and Programs in Biomedicine* 2022; **220**: 106805.
3. Wood JL. *Journal of Biomech* 1971; **4**: 1–12.
4. Boruah S, et al. *IRCOBI Conference Proceedings*. 2013: 497–508.
5. Erdemir A, et al. *Journal of Translational Medicine* 2020; **18**: 369.

Acknowledgements:
The authors would like to acknowledge project funding from VINNOVA (2018-02879)



ULTRASOUND-BASED MODELING OF ABDOMINAL AORTIC ANEURYSMS: MODEL COMPLEXITY AND PERSONALIZATION

Judith Fonken (1,2), Eline van Engelen (1), Esther Maas (1,2), Arjet Nievergeld (1,2), Marc van Sambeek (1,2), Frans van de Vosse (1), Richard Lopata (1)

1. Eindhoven University of Technology, Netherlands; 2. Catharina Hospital Eindhoven, Netherlands

1. Introduction

Insight in abdominal aortic aneurysm (AAA) development, growth and rupture risk requires a large, longitudinal study on mechanical properties of AAAs. For patient-specific risk assessment and analysis of the mechanical state, fluid-structure interaction (FSI) models are considered, which require the AAA geometry and its dynamics. Time-resolved 3-dimensional ultrasound (3D+t US) is the preferred image modality to extract the patient-specific geometry, since it is safe, fast, affordable and provides functional information such as wall motion and blood velocity. A previous study has shown the feasibility of 3D+t US-based FSI simulations [1]. In this study, the complexity of the US-based FSI framework was increased and more PS information was included (Figure 1), to better approach the in-vivo situation.

2. Materials and Methods

Due to the limited field-of-view of 3D+t US, the aorto-iliac bifurcation is often not included in the US acquisition. Due to this limitation, a single outlet AAA geometry was used in our previous study. However, the bifurcation does influence the hemodynamics in the aneurysm region. In this study, the feasibility of replacing the PS bifurcation (obtained with CT) by a parametric one was investigated.

The framework was further personalized by including PS flow parameters derived from US Doppler acquisitions. These flow parameters include the flow pulse, velocity profile over the vessel cross-section, inlet radius and distance. Finally, the AAA geometry was embedded in a surrounding soft tissue and spine was included at the posterior side modelled by a stiff rod.

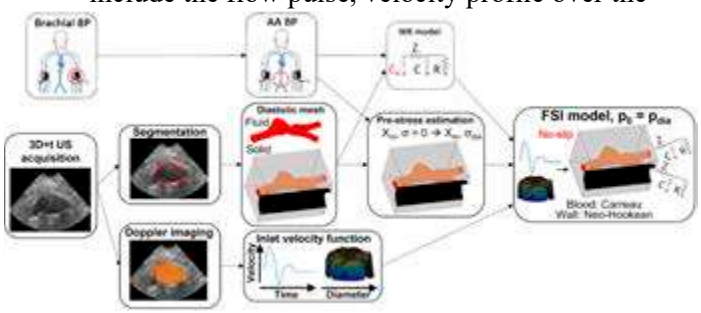

Figure 1: FSI framework including surrounding tissue and patient-specific blood pressure (BP), AAA geometry and velocity profiles.

3. Results

Replacing the PS bifurcation with a parametric bifurcation yields median differences in AAA hemodynamics below 1%. Simulations employing PS flow parameters yielded mean differences of 168% (TAWSS), 40% (OSI) and 7% (wall stress). The addition of surrounding tissue, including the spine, resulted in a decrease (mean: 34%) in displacement, especially at the posterior wall, and a homogenization and slight decrease (mean: 14%) in wall stress, similar to [2].

4. Discussion and Conclusions

This study showed the feasibility of adding a parametric bifurcation and the importance of including surrounding tissue and PS flow parameters. As expected, the surrounding tissue mainly influenced the AAA wall mechanics, whereas the PS flow parameters mainly influenced the AAA hemodynamics.

In future studies, the obtained framework will be further personalized using 4D US speckle tracking for wall motion, and validated with the use of 4D flow MRI. The envisioned framework for realistic and personalized 3D+t US-based FSI simulations paves the way for longitudinal studies on AAA development, growth, and rupture risk.

5. References

1. Fonken et al., Front. Physiol., 1255, 2021.
2. Petterson et al. J. Biomech., 126-133, 2019.

Acknowledgements:

This work was supported by the Dutch Research Council (NWO) and received funding from the NWO talent program VIDI. This work was carried with the support of SURF Cooperative.



ON THE ASSUMPTION OF RIGID WALLS IN ATRIAL FIBRILLATION PATIENTS; IMPLICATIONS FOR PREDICTION OF HEMODYNAMICS AND THROMBOEMBOLIC INDICATORS

Henrik A. Kjeldsberg, Joakim Sundnes, Kristian Valen-Sendstad

Simula Research Laboratory, Norway

1. Introduction

In recent years, there has been a growing interest in patient-specific computational fluid dynamics (CFD) in the left atrium (LA) to mechanistically understand thrombus formation in patients with atrial fibrillation (AF). Although several studies report predictors of flow stagnation and thromboembolism [1,2,3], the fluid mechanical aspect of the problem is rarely reported, resulting in subjective and possibly unphysiological modelling of LA hemodynamics. The present study will investigate CFD simulations from a fluid mechanical perspective to better understand the numerical conditions required to accurately represent flow inside the LA.

2. Materials and Methods

We analysed 4D-CT acquisitions of an AF patient using the open-source CFD solver *OasisMove* [4]. For sensitivity analysis we investigated a rigid model, with no-slip conditions, in comparison to a dynamic model, where the boundary movement was registered from the CT images. For the simulations, we considered blood to be a Newtonian fluid, applied a Womersley velocity profile at the pulmonary veins, where the flow rates were based on LA and left ventricular volume, and ran the simulations for five cardiac cycles with a time step of 0.2ms. The final computational model consisted of 3M cells and included boundary layers to more accurately capture hemodynamics and relative residence time (RRT). For analysis, we performed spatial, temporal and cycle convergence tests, and their effect on the volume-averaged kinetic energy, dissipation and turbulence intensity.

3. Results

Spatial convergence results showed that finer grids resulted in increased turbulence intensity, and RRT increased by a factor of 25%. The temporal convergence study revealed that both fluid mechanical and hemodynamic metrics converged for simulations of >5000 time steps per cycle. The cycle convergence revealed that a pseudo-periodic velocity field was reached after 5 cycles. The high-resolution moving domain simulations revealed areas of high turbulence intensity and showed a 10-fold reduction in common indices used for thromboembolic prediction.

4. Discussion and Conclusions

We have shown the numerical requirements to adequately capture LA hemodynamics, but also revealed turbulent-like flow inside the chamber. This observation may indicate that the common assumption that blood flow can be modelled as laminar is misleading and does not represent the physiology, although we have only shown this for one model. Furthermore, we have shown that dynamic and static models give markedly different results in terms of hemodynamic predictors of thromboembolism.

5. References

1. Fanni, B.M., et al., Applied Sciences, 10(4), p.1448 (2020).
2. Sanatkhani, S. et al., Frontiers in Physiology, p.512 (2021).
3. Corti, M. et al., Computers in Biology and Medicine, 150, p.106143 (2022).
4. Kjeldsberg H, GitHub; https://github.com/KVSlab/OasisMove/ (2022).

Acknowledgements:

The authors would like to thank J. Mill, C. Lucas, Prof. O. Camara, and MD D. Medel for contribution to data acquisition and processing. The authors would also like to thank the European Union's Horizon 2020 research and innovation programme under grant No. 643271 and No. 101016496 for providing financial support to this project.

CMBBE2023
18th International Symposium on Computer Methods in Biomechanics and Biomedical Engineering
3 - 5 May 2023, Paris, France



Arts et Métiers Institute of Technology
Institut de Biomécanique Humaine Georges Charpak
155 boulevard de l'Hôpital 75013 Paris France
www.cmbbe-symposium.com

EFFECT OF THE THICKNESS OF PEG HYDROGEL PATCH ON THE DIFFUSION OF WOUND ANTIMICROBIALS

Pooja Vardhini Natesan and Ramakrishnan Swaminathan

Department of Applied Mechanics, Indian Institute of Technology Madras, Chennai, India

1. Introduction

The occurrence of infections plays a vital role in the transition of wounds from acute to chronic non-healing state [1]. The evolution of drug resistant microbes necessitates the development of novel treatment strategies. Topical application of antimicrobial formulations through hydrogel wound dressings offers beneficial therapeutic outcomes [2]. In this study, a computational model based on the free volume theory (FVT) has been applied to predict the diffusion of the natural and synthetic wound antimicrobials for varied thicknesses of the Polyethylene Glycol (PEG) hydrogel patch.

2. Materials and Methods

PEG hydrogel having a molecular weight of 20,000 g/mol is assumed to be in the form of a cylindrical patch of thickness L which is varied from 1 mm to 5 mm. FVT has been utilized to estimate the diffusivity (D) of two plant metabolites with inherent antimicrobial activity namely, Cinnamaldehyde and Curcumin and two synthetic antimicrobial drugs namely, Amphotericin B and Vancomycin as per Eq. 1:

$$\frac{D}{D_o} = \left(1 - \frac{r_s}{\xi}\right) \exp\left(-Y\left(\frac{v_{2,s}}{1 - v_{2,s}}\right)\right) \quad (1)$$

Here, r_s and D_0 denote the hydrodynamic radius and diffusivity of the compound in water respectively. ξ and $\nu_{2,s}$ represent the mesh size and polymer volume fraction of the hydrogel respectively. According to FVT, Y refers to the ratio between the critical volume for diffusion and the available free volume and is usually approximated as 1 [3]. The cumulative drug release fraction can be calculated using Eq. 2:

$$\frac{M_t}{M_\infty} = 1 - \sum_{n=0}^{\infty} \frac{8}{(2n+1)^2 \pi^2} \exp\left(\frac{-D(2n+1)^2 \pi^2 t}{L^2}\right) \quad (2)$$

The diffusion time of the antimicrobial agents is determined when M_t/M_∞ is 1. Furthermore, an empirical exponential relation between the diffusion time and hydrogel patch thickness L has been established.

3. Results

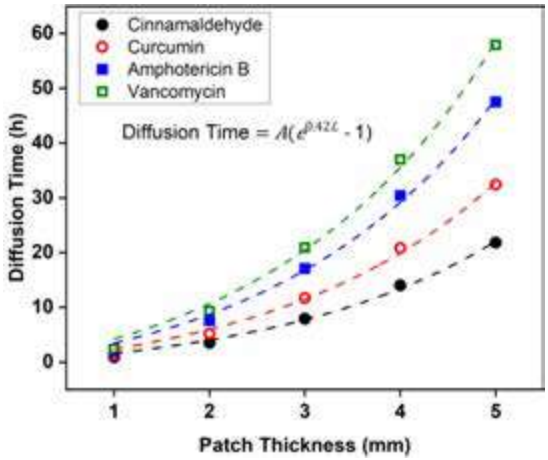

Figure 1: Variation of diffusion time of antimicrobial agents with thickness of hydrogel patch (Dashed line: Fitted function)

4. Discussion and Conclusions

Fig. 1 shows that an increment in L results in extended diffusion time. The relation is observed to be exponential in nature, with an order of 0.42 mm^{-1} for all the compounds (R^2 = 0.99). However, the value of A is observed to be linearly varying with the solute molecular weight, the values being 3.05 and 7.98 for Cinnamaldehyde and Vancomycin respectively. Hence, the present study will be clinically useful for designing the hydrogel wound dressings from simple empirical relations.

5. References

1. Kopecki Z. Biosci Rep; 41(2):BSR20203404 (2021).
2. Thapa RK et al., Eur J Pharm Sci; 166:105990 (2021).
3. Lin CC, Metters AT. Adv Drug Del Rev; 58(12-13):1379-1408 (2006).

Acknowledgements

Pooja Vardhini Natesan would like to thank the Government of India for providing the Prime Minister's Research Fellowship to carry out this study.



MODELLING THE PLACENTA VASCULATURE FOR CLINICAL DECISION SUPPORT

Pascalle Wijnjes (1,2,3), Beatrijs van der Hout-van der Jagt (2,3,4), Wouter Huberts (1,3,5), Frans van de Vosse (1,3)

1. Dept. of Biomedical Engineering, Eindhoven University of Technology, The Netherlands, 2. Máxima Medical Center, The Netherlands, 3. Eindhoven MedTech Innovation Center, The Netherlands, 4. Dept. of Electrical Engineering, Eindhoven University of Technology, The Netherlands, 5. Dept. of BioMedical Engineering, Maastricht University, The Netherlands

1. Introduction

Approximately 10% of all pregnancies are affected by hypertensive disorders, with 3% being affected by the more severe condition of pre-eclampsia [1]. Studies show that multiple pregnancy complications are caused by abnormal placentation leading to placental dysfunction and severe complications [2]. Therefore, it is important to look at the placenta vasculature in more detail. In this study, we will investigate if it is possible to gain more insights into the placenta physiology, i.e. its functioning and remodelling, by creating a hemodynamic vasculature model of the placenta. This new knowledge could be used in (hybrid) prediction models for pregnancy complications like pre-eclampsia.

2. Materials and Methods

A space-filling algorithm [3,4] is applied to the placental geometry, for which the feto-placental vessels grow within the functional units (cotyledons). The model is assembled by assumptions made in the mathematical model based on literature and clinical knowledge.

For cardiovascular simulations, a combination of a 1D pulse wave propagation model and 0D windkessel models, representing the placental arterial system and the venous system respectively, can be applied on the vessel structure.

3. Results

The resulting modelled placenta (see Fig. 1) realistically mimics the placental vasculature on visual inspection. Next to the normal points of insertion (central and marginal), our model was also able to accurately construct the vasculature of abnormal connections (e.g. velamentous insertions) of the umbilical cord to the placenta.

4. Discussion and Conclusions

The model visually represents a healthy placenta and can be used to evaluate the hemodynamic functioning of a placenta for clinical scenarios.

Ultimately, the goal is that this model and its simulations will in the future be able to support clinical decision-making and give a basis for new prediction models for pregnancy complications.

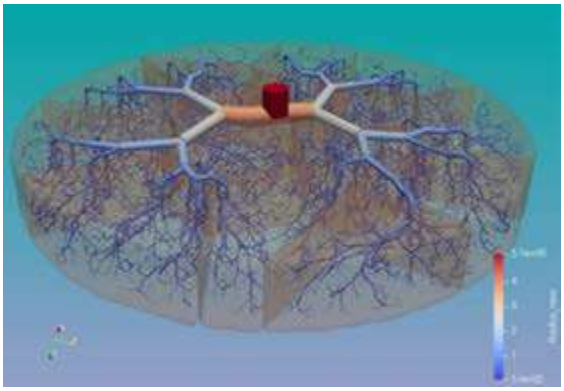

Figure 1: Feto-placental vasculature. The colour scale shows the decline in diameter, where red is the greatest diameter and dark blue the smallest. On top, the umbilical arteries are entering the placental surface on which the branching starts.

5. References

1. Hutcheon J A et al., Best Pract Res Cl Ob, 25(4): 391-403 (2011)
2. Schiffer et al., Eur. J. Obstet. Gynecol. Reprod. Biol., 262: 45-56 (2021)
3. Clark et al. Interface Focus, 5(2) (2015)
4. Tawhai et al., Ann Biomed Eng, 28(7): 793-802 (2000)

Acknowledgements:

We acknowledge the Eindhoven MedTech Innovation Center (e/MTIC, Grant PICASSO) for funding.



SENSITIVITY ANALYSIS OF MENISCAL TISSUE MATERIAL PARAMETERS TO ITS KINEMATICS AND CONTACT MECHANICS

Sherif Zantiba, Nagitha Wijayathunga, Marlene Mengoni, Ruth Wilcox

1. University of Leeds, Institute of Medical and Biological Engineering, School of Mechanical Engineering, Leeds, United Kingdom

1. Introduction

The meniscus is known for its load bearing, stability, and congruency function within the knee joint [1], however efforts to quantify the meniscal tissue material parameters has proven difficult due to interactions that cannot be replicated ex-vivo. Inverse finite element (FE) analysis provides a means by which these parameters can be quantified non-destructively [2]. To inform such analysis, the aim of this study was to examine the sensitivity of meniscal kinematics and contact pressures to changes in meniscal tissue material parameters.

2. Materials and Methods

An image based FE model, developed and validated for the static contact mechanics of the knee joint in full extension was used [3]. The model comprised the femur, tibia, tibiofemoral articular cartilage and the lateral and medial menisci. Following initial sensitivity tests with an orthotropic material model, the meniscus was modelled as a transverse isotropic linear elastic material, resulting in five parameters (E_{plane}, E_{fibre}, $v_{plane\text{-}plane}$, $v_{fibre\text{-}plane}$ and $G_{fibre\text{-}fibre}$). The One-at-a-time sensitivity analysis method was used where E***** and G***** variables were doubled and the Poisson's ratio halved. Three flexion cases (0°, 30° and 45°) were investigated, and in each case four load steps in increments of 750N, applied vertically via the centre of rotation of the femur. Contact pressure and meniscal kinematics, defined as nodal displacements along the periphery of the menisci, were measured (Figure 1).

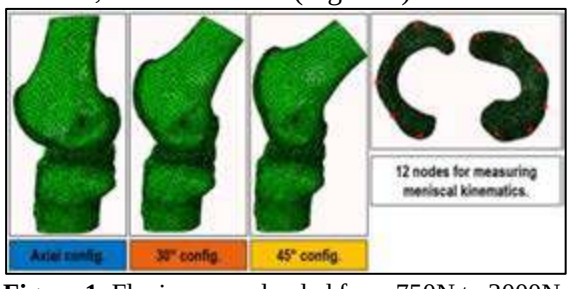

Figure 1: Flexion cases loaded from 750N to 3000N in four steps and meniscal kinematics definition.

3. Results

The meniscal kinematics showed an average displacement of 7% from the baseline for E_{fibre} test cases (Figure 2). E_{plane} and E_{fibre} had similar effects on contact pressure (~18%) while $G_{fibre\text{-}fibre}$ resulted in a change of ~10% (Figure 3).

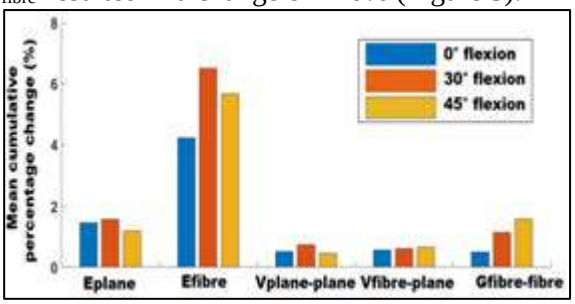

Figure 2: Mean cumulative change of kinematics with changes in tissue parameters at 750N.

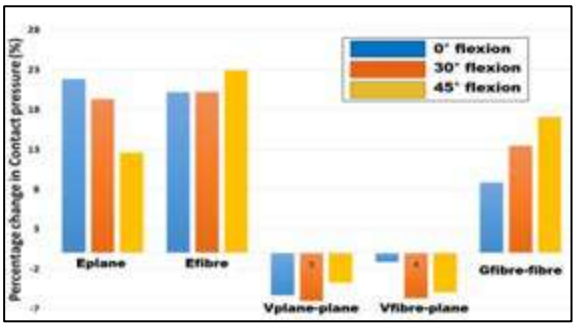

Figure 3: Change in mean contact pressure with changes in meniscal tissue parameters at 750N.

4. Discussion and Conclusions

The elastic and shear parameters of the meniscus appear to dominate the contact mechanics, whereas E_{fibre} is important for the kinematics. This knowledge will inform the measurements needed and parameters that can be optimised in future inverse FE studies.

5. References

[1] Fox et al, Sports Health 2012; [2] Freutal et al, J. Biomechanics 2015; [3] Day et al, CMBBE, 2021.

Acknowledgements:

Funded by the EPSRC through EP/P001076/1 and EP/T517860/1.



"ULTRASOUND-BASED AUTOMATIC 3D MODULOGRAPHY FOR ATHEROSCLEROTIC CAROTID ARTERY PLAQUES

Koen Franse (1), Jan-Willem Muller (2), Marc van Sambeek (1,2), Richard Lopata (1)

1. Photoacoustics & Ultrasound Laboratory Eindhoven (PULS/e), Eindhoven University of Technology, the Netherlands; 2. Department of Surgery, Catharina Hospital Eindhoven, the Netherlands

1. Introduction

Currently invasive surgery on atherosclerotic plaques in the carotid artery is performed in case of stenosis >70% [1]. However, retrospective studies show that this intervention is only needed in one out of six patients. Mechanical modelling of the arterial wall with patient-specific local material parameters can improve clinical decision making by characterizing the plaque's morphology and prevent rupture. This study presents a 3D inverse finite element (FE) algorithm that can locally reconstruct the heterogeneous characterization of the arterial plaque based on non-invasive ultrasound (US).

2. Materials and Methods

The input for the inverse FE algorithm is strain data, which can be obtained by performing strain imaging on US data. In this study, cross-sectional 2D three-angle plane wave US acquisitions are simulated using the k-wave toolbox [2]. The simulations are based on 3D FE models. One geometry is used to create a polyvinyl-alcohol (PVA) phantom, on which US scanning is performed with the same protocol as for the simulations.

The inverse FE workflow initiates with a homogeneous plaque model. The ratio between the FE stress and the input strain is used to compute the apparent Young's modulus (AYM) locally [3]. This parameter is further optimized to minimize the error between the input strain and the iteratively computed FE strain.

The algorithm is tested on two geometries – one with only a lipid pool in the plaque, and one that also includes calcifications. The resulting material parameters are compared with those in the ground-truth FE model for three cases: the inverse reconstruction based on FE strain input data, US simulations and US scan strain imaging data.

3. Results

Using FE strain data as an input, the 3D inverse algorithm demonstrates the ability to reconstruct the 3D geometry of the plaque, including local details as the lipid pool and small calcifications. The estimation of the Young's modulus is too high for softer materials such as lipid, and too low for stiffer materials such as calcifications. However, the magnitude difference with the other arterial tissue is clearly visible.

On the other hand, when using the strain imaging data from either the US simulation or US scan as input, the algorithm is not able to reconstruct local plaque details correctly.

4. Discussion and Conclusions

The results based on FE strain data input prove that the 3D inverse algorithm is capable of reconstructing local material parameters in an artery plaque without prior segmentation. However, the poor performance of the US strain-based reconstruction is due mainly to the lack of precision and resolution in the lateral US data. Further research will be aimed at improving this by using more compounded plane wave angles and FE-based regularization methods.

5. References

1. Bonati L et al, European Stroke Journal; 6(2):I-XLVII (2021)
2. Treeby B and Cox B, J. Biomed. Opt. 15(2):021314 (2010)
3. Porée J et al., IEEE Trans on US, FE and FC; 64(12):1805-1817 (2017)

Acknowledgements:

The authors would like to thank the Dutch Research Council (Perspectief program ULTRA-X-TREME, project DiagnostiX - Grant no: P17-32) for providing financial support to this project.



MATERIAL PROPERTIES IDENTIFICATION OF PORCINE PERINEAL TISSUES

T. KADIAKHE[a], M. LALLEMANT[a,b], J. CHAMBERT[a], A. LEJEUNE[a], N. MOTTET[b], E. JACQUET[a]

a. UBFC, Institut FEMTO-ST, Département Mécanique Appliquée, Besançon, France
b. Service de gynécologie obstétrique, CHU Jean Minjoz, Besançon, France

1. Introduction

The female perineum is a multilayer structure located under the pelvic floor. It contributes to the mechanical integrity of the pelvis and deforms largely during childbirth, deformation that often causes more or less severe tears. The objective of the present work is to investigate the mechanical properties of the perineal tissues.

2. Materials and Methods

Because of the difficulty in acquiring human tissues, we selected the sow as it presents anatomical similarities with humans. Two samples were taken from each layer of the perineum: skin, vaginal mucosa, anal mucosa, external anal sphincter (only one sample) and internal anal sphincter.

The samples (10 for the external anal sphincter and 20 for the remaining tissues) were tested in quasi-static uniaxial tension using the testing machine Mach-1 (Biomomentum Inc, Canada). The tests were done in the general fiber direction until failure at 0.1 $mm.s^{-1}$ and 1 $mm.s^{-1}$ at a constant temperature of 21°C.

Soft biological tissues exhibit non-linear hyperelastic behaviour [1]. Many hyperelastic models were proposed in the literature. Because of a lack of studies on porcine perineal tissues, we will try to identify their material properties with different behaviour laws similarly as in [1]: Yeoh, Mooney-Rivlin, Ogden, Humphrey, Veronda-Westmann, Martins.

The material parameters were identified by inverse method. For each sample, we obtained the Pearson correlation coefficient and the p-value with the null hypothesis that there was no correlation between the experimental and numerical stresses.

3. Results

The results show high correlation coefficients between the numerical and experimental curves confirmed by p-values less than 0.05. The mean correlation coefficient for all models is greater than 0.99 for each tissue. As shown in Fig. 1, the mechanical behaviour is different from one tissue to another which is normal due to the structural differences between the different tissues (some more fibrous than others).

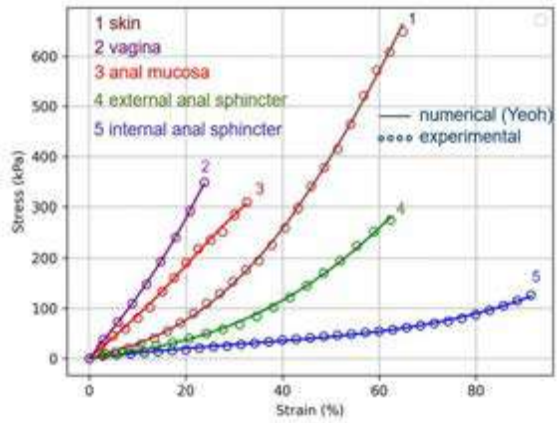

Figure 1: Stress-strain curves for different soft tissues from one sow perineum at 0.1 $mm.s^{-1}$

4. Discussion and Conclusions

In this work, we managed to implement a dissection methodology for perineal tissues and characterize their material properties. Amongst the chosen constitutive laws, the best fit was obtained with Yeoh model except for the external anal sphincter for which Martins model fits better. We also observe a high variability in the response of the tissues depending on the sow.

5. References

1. Martins PALS, Natal Jorge RM, Ferreira AJM, Strain; 42(3):135-147 (2006).



LOCAL MECHANICAL PROPERTIES IN BONE ALLOGRAFTS CORRELATE WITH ELLIPSOID FACTOR

Zhuang Xiong (1), Léa Rouquier (1), Esther Potier (1), Manon Bachy-Razzouk (1,2), Xingrong Huang (3), Morad Bensidhoum (1), Thierry Hoc(1,4)

1. Université Paris Cité, CNRS, INSERM, ENVA, B3OA, France; 2. APHP, France; 3. Beihang University, China; 4. Ecole Centrale Lyon, France

1. Introduction

Bone allografts are wildly used to repair bone defects. In addition, allograft micro-structure is able to provide mechanical stimulus to cells at local scale, which is a key factor in the osteogenesis process [1]. This local mechanical environment remains unknown while it could be useful to identify the optimal macroscopic mechanical conditions for osteogenesis in *in vitro* experiments. Numerous morphological parameters have been used to characterize the complex micro-structure of allografts [2], including the Bone Volume Fraction (BV/TV), the Structure Model Index (SMI) and more recently the Ellipsoid Factor (EF).

In the present study we investigated the relationship between local mechanical parameters derived from the finite element modelling and three morphological parameters mentioned above obtained from micro-CT images of human bone allografts.

2. Materials and Methods

29 bone allografts were obtained from a commercialized bone bank that collects trabecular bone from femoral heads of human donors. A cylindrical trabecular bone sample was harvested for all the allografts with a radius of 3.5 mm and an height of 8 mm. Micro-CT images were acquired with a precision of 7.9 µm. Isotropic elastic behaviour with Young's modulus of 15 GPa and Poisson's ratio of 0.3 was employed to conduct finite element uniaxial compression tests at 0.2% macroscopic strain, which was considered as a physiological mechanical condition [3].

3. Results

Analysis of the three architectural parameters BV/TV, SMI and EF showed that only the EF was substantially linearly correlated (Pearson correlation coefficient r greater or equal to 0.7) with uniaxial strain, uniaxial stress and strain energy density. A higher value of EF led to a higher local level of strain, stress and strain energy density. For the other two microarchitectural parameters evaluated in this study, the linear relationship with the local mechanical parameters gave very low Pearson correlation coefficient ($r < 0.6$).

4. Discussion and Conclusions

A weak correlation of local mechanical properties with BV/TV was expected as it measures the bone volume, which is usually associated with macroscopic mechanical properties [4]. In contrast, SMI and EF take into account the distribution of plates and rods within the allografts micro-structure. However, the calculation of SMI is controversial due to the negative contribution that comes from the conceptual mathematic formulation [5], which was frequently observed in the analysis results of this study. The results of the present study illustrate that EF can predict local strain, stress and energy level better than BV/TV and SMI. Hence EF should be used in tissue engineering as a predictor of the cellular mechanical environment.

5. References

1. Zhu et al., Bioactive Materials; 6, 4110 (2021).
2. Odgaard A. Bone; 20, 315–328 (1997).
3. Ehrlich P, Lanyon L. Osteoporosis Int ;13(9): 688-700 (2002).
4. Nazatian A et al., Calcif Tissue Int;83, 368 (2008).
5. Salmon P.L et al., Frontiers in Endocrinology; 6, (2015).

Acknowledgements:

The authors would like to thank ANR 2021_CE19_Smart Bone organoid and CSC for their financial support.



IDENTIFICATION OF MECHANICAL PROPERTIES OF HUMAN ABDOMINAL WALL BASED ON IN VIVO MEASUREMENTS

Katarzyna Szepietowska (1), Mateusz Troka (1), Izabela Lubowiecka (1)

1. Department of Structural Mechanics, Faculty of Civil and Environmental Engineering, Gdańsk University of Technology, Poland

1. Introduction

This abstract concerns mechanical properties of living human abdominal wall. Understanding the abdominal wall mechanics is believed to be needed to improve efficiency of hernia repairs. Majority of works on mechanics of abdominal tissue are based on *ex vivo* tests [1]. Although abdominal wall material parameters have been identified *in vivo* in humans [2], and rabbits [3], there is still need to identify properties in different areas of human living abdominal wall. In the current work, we present *in vivo* identification of abdominal wall mechanical properties by inverse methods [4] using digital image correlation (DIC) data collected during peritoneal dialysis.

2. Materials and Methods

DIC system has been used for non-invasive measurement of deformation of external surface in abdominal wall of patients undergoing standard peritoneal dialysis. Intraabdominal pressure can be measured at final stage of introduction of dialysis fluid. Therefore information on both deformation (Fig.1) and loading can be obtained [5]. That serves as an input data for an inverse analysis in order to identify properties of living human abdominal wall. Abdominal wall is treated as a shell without distinction of multi-layers of abdominal wall. In this work only passive behaviour of abdominal wall is taken into account.

3. Results

Preliminary results are obtained by procedure of identification the hyperelastic material model parameters that has been found as important with use by global sensitivity analysis [6].

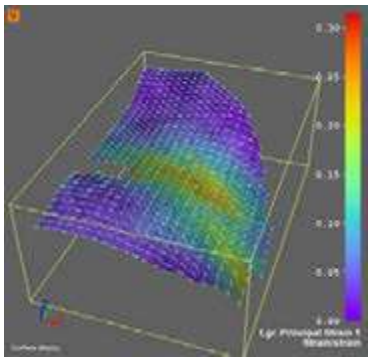

Figure 1: Principal strain and direction on surface of abdominal wall at the end of peritoneal dialysis procedure.

4. Discussion and Conclusions

In vivo identification of human abdominal wall material model parameters based on full-field measurement and knowledge on intraabdominal wall pressure during peritoneal dialysis is proposed. Obtained properties will be used next in modelling of abdominal wall – surgical mesh system. Such model can be employed to optimise choice of surgical mesh.

5. References

1. Deeken CR, Lake SP., J Mech Behav Biomed Mater; 74:411-427 (2017).
2. Song C et al., J Biomech; 39(3) :587-591 (2006).
3. Simón-Allué R et al., J Mech Behav Biomed Mater; 66: 127-137. (2017).
4. Avril S et al., Experimental Mechanics; 48: 381-402. (2008).
5. Lubowiecka I et al., J Mech Behav Biomed Mater . 125: 104902. (2022).
6. Szepietowska et al., CMBBE 2019, Springer (2019)

The authors would like to thank the National Science Centre, Poland (Grant no: UMO-2017/27/B/ST8/02518) for providing financial support to this project. Computations were performed partially in TASK Computer Science Centre, Gdańsk, Poland.



COMPARISON OF TWO MACHINE-LEARNING METHODS TO PREDICT INTERVERTEBRAL DISC PROPERTIES

Emily Kelly (1), Akbar A. Javadi (1), Tim Holsgrove (1), Michael Ward (2), David Williams (3), Dionne Shillabeer (3), Cathy Holt (3), Judith Meakin (2)

1. *Department of Engineering, University of Exeter, UK; 2. Department of Physics and Astronomy, University of Exeter, UK. 3. School of Engineering, Cardiff University, UK*

Corresponding author: Emily Kelly, e.kelly2@exeter.ac.uk

1. Introduction

Evolutionary polynomial regression (EPR) uses a genetic algorithm and least square regression to learn complex relationships in the form of clear transparent mathematical equations [1, 2], providing benefits over black-box artificial neural networks (ANN). EPR may help define intervertebral disc (IVD) material properties for FE modelling, which have been approximated in different ways, often generically. Improved subject-specific IVD representation would aid understanding of spinal loading. This study aimed to compare the accuracy of EPR with ANN in predicting IVD material properties.

2. Materials and Methods

This study used previously collected 6-axis in vitro data of six porcine IVD specimens [3]. The data contained applied translations/rotations, with corresponding forces/moments: FX (anteroposterior shear), FY (lateral shear), FZ (compression), MX (lateral bending), MY (flexion/extension), and MZ (axial rotation). EPR (EPR-MOGA-XL, v1.0 [1, 2]) and ANN (MATLAB, R2022a) were used to predict each specimen-specific force/moment output from all translation and rotation inputs, allowing coupled motions. Both methods used a 60/40% ratio for training/test data, and software parameters were optimised.

3. Results

The R^2 and normalised mean square error (NMSE) of both methods were compared for each axis (Table 1). Most models had R^2 values above 0.85, across all specimens and axes. Differences between the methods were limited in most axes, though ANN tended to perform better than EPR. The greatest differences were in compression (FZ), ranging from 0.024 to 0.071 for R^2 and 3.54 to 10.72 for NMSE. The other axes had smaller differences, at -0.003 to 0.016 for R^2, and -0.002 to 0.076 for NMSE.

Table 1: EPR and ANN test data results for each force/moment axis (medians across 6 specimens)

	R^2		NMSE	
	EPR	**ANN**	**EPR**	**ANN**
FX	0.992	0.993	0.178	0.151
FY	0.986	0.987	0.214	0.198
FZ	0.887	0.924	16.85	10.46
MX	0.898	0.910	0.115	0.110
MY	0.917	0.920	0.087	0.083
MZ	0.964	0.962	0.032	0.031

4. Discussion and Conclusions

Both ANN and EPR methods predicted IVD properties with a high degree of accuracy. The lower accuracy in some axes (e.g. FZ) may be due to IVD creep, which was unaccounted for. Although the ANN models were usually more accurate, the differences were often small. In the future, the biomechanical relevance of these differences could be assessed through FE analysis, incorporating the generated material models. Such use of the models could improve IVD representation, and knowledge of specimen-specific spinal loading.

5. References

1. Giustolisi O, Savic DA. J. Hydroinformatics. 2006; 8(3): 207-222.
2. Giustolisi O, Savic DA. J. Hydroinformatics. 2009; 11(3): 225-236.
3. Holsgrove TP et al., Spine J. 2015; 15(1): 176-184

Acknowledgements:
The authors would like to thank the EPSRC (EP/V036602/1) for providing financial support to this project.

CMBBE2023
18th International Symposium on Computer Methods in Biomechanics and Biomedical Engineering
3 - 5 May 2023, Paris, France



Arts et Métiers Institute of Technology
Institut de Biomécanique Humaine Georges Charpak
155 boulevard de l'Hôpital 75013 Paris France
www.cmbbe-symposium.com

A MACHINE LEARNING APPROACH TO PREDICT CARDIOVASCULAR COLLAPSE IN HEMORRHAGE PATIENTS

Matthew Bernstein (1), Aaron Bray (1), and Rachel B. Clipp (1)

1. Kitware,Inc., United States

1. Introduction

The Pulse Physiology Engine [1] is an open source computational model of the human body. Pulse uses lumped-parameter models for fast simulation (~10x real-time). However, its use as a diagnostic tool is limited by execution time, particularly for long running patient predictions. Therefore, a deep learning-based surrogate model was developed for specialized long time series forecasting. Acute hemorrhage was the initial use case, chosen for its clear start time, relative independence of patient history, and binary outcome (survive or not). The goals were vital sign forecasting and prediction of cardiovascular collapse (CVC).

2. Materials and Methods

The use of simulated or synthetic data bypasses the missingness problems inherent with patient data and addresses a limitation for current deep learning approaches. Eleven vital signs were predicted, including heart rate, cardiac output, and mean arterial pressure (MAP). 217 simulated patients with varying hemorrhage severities were generated using the Pulse models. Vital sign data (vitals) was output every 2 seconds (s). A Temporal Fusion Transformer (TFT) [2] was chosen due to its handling of static, time-varying known, and time-varying unknown covariates; however, a recurrent neural network (RNN) was also tested. Training was executed using a fixed period of observed vitals between 0 and 20 minutes (min) after hemorrhage onset, with the model asked to forecast until a cutoff of 120 min. The model is also given static covariates, such as patient height, weight, and age. CVC was defined as a MAP < 40 mmHg. Thirteen of the 42 patients experienced a CVC in the observation period and were excluded.

3. Results

The 11 vitals were forecasted within 10% error. The forecast captures the dynamics of hemorrhage, Fig. 1. The mean absolute percentage errors were 0.031 and 0.154 across all vitals/patients for the TFT and RNN, respectively. CVC was predicted with 76% accuracy and with good temporal accuracy, a mean and standard deviation of 25.3s and 107.1s within the 100 min prediction period.

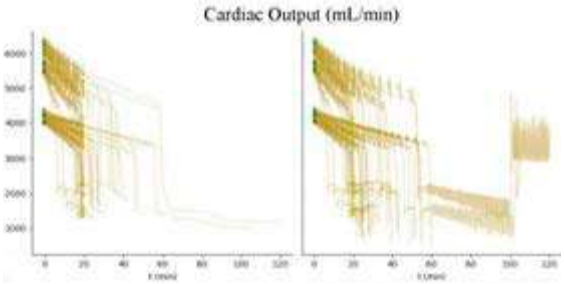

Figure 1: Predicted (left) and true (right) cardiac output of 42 test set patients. Dashed lines are the prediction period.

4. Discussion and Conclusions

This work demonstrates that a surrogate transformer model was able to forecast simulated vitals into the future, and that this forecast contains richer information than the simplified task of binary classification of an event of interest.

5. References

1. Bray, Aaron, et al. SN Comprehensive Clinical Medicine 1.5 (2019): 362-377.
2. Lim, Bryan, et al. International Journal of Forecasting 37.4 (2021): 1748-1764.

Acknowledgements:
The authors would like to thank the NIH (grant R44DE027574) and DoD (W81XWH2010471) for providing financial support to this project.

CMBBE2023
18th International Symposium on Computer Methods in Biomechanics and Biomedical Engineering
3 - 5 May 2023, Paris, France



Arts et Métiers Institute of Technology
Institut de Biomécanique Humaine Georges Charpak
155 boulevard de l'Hôpital 75013 Paris France
www.cmbbe-symposium.com

PREDICTING GREYHOUND SPEED IN THE RACE BY CREATING A HISTORICAL DATA PLANE OF RACE DATA

Md Imam Hossain (1), David Eager (1)

1. University of Technology Sydney, Australia

1. Introduction

Consideration of racing greyhound speed at the oval track is important for designing and maintaining a track that is safe and also for cambers that meet the safety rules. This research attempts to provide an explanation that can be used to efficiently build a data structure from the available greyhound race data to predict greyhound speed in different conditions such as track shapes and race start locations with respect to the track.

2. Data encapsulation and predicting

The data from the variables affecting greyhound speed were used for encapsulating the information into a data structure used for predicting greyhound speed. From the available data, greyhound run distance (X-axis) and the corresponding track curvature (Y-axis) and greyhound acceleration data (Z-axis) were encapsulated into a three-dimensional data structure like shown in Fig. 1, where it can be said that greyhound speed is a function of dimensional axis values shown in Eq. 1.

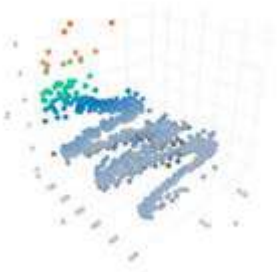

Figure 1: Three-dimensional data structure encapsulating data points information for greyhound speed.

$$speed_i = f(X_i, Y_i, Z_i) \quad (1)$$

Finally, the data structure was used for searching and predicting new data points by matching greyhound run distance and track curvature data points for a race start location and track shape. By using Eq. 2 greyhound speed profile was predicted as shown in Fig. 2. In Eq.2 the acceleration was extracted from the data structure where i-1 denotes the previous instantaneous speed and C is a constant that depends on the initial conditions of the predicting variable.

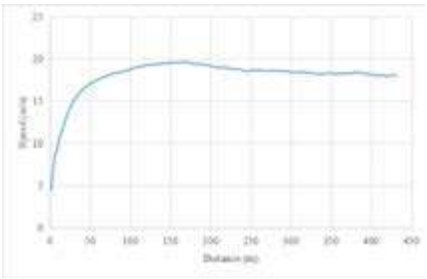

Figure 2: A greyhound speed profile prediction from historical greyhound data analysis.

$$speed_i = (speed_{i-1} + acceleration_i * stride\ duration_i) * C \quad (2)$$

3. Results and Discussion

The predicted greyhound speed profile showed a high degree of features and accuracy as found in a measured speed profile. It was noted that the accuracy of the prediction can be increased by incorporating more dimensions into the data searching algorithm.

4. Conclusions

This research presented greyhound speed data prediction by formulating a data structure that can be used for efficiently searching new data points for various track and racing start conditions.

Acknowledgements:
The authors would like to thank and acknowledge the support of Greyhound Racing Victoria for providing access to race data.

CMBBE2023
18th International Symposium on Computer Methods in Biomechanics and Biomedical Engineering
3 - 5 May 2023, Paris, France
Arts et Métiers Institute of Technology
Institut de Biomécanique Humaine Georges Charpak
155 boulevard de l'Hôpital 75013 Paris France
www.cmbbe-symposium.com

MECHANICAL PERFORMANCE OF HUMAN ABDOMINAL WALL BASED ON IN VIVO TESTING AND ANN ANALYSIS

Izabela Lubowiecka* (1), Katarzyna Szepietowska(1), Mateusz Troka (1), Michał Chmielewski (2), Monika Lichodziejewska-Niemierko (2)

1. Department of Structural Mechanics, Faculty of Civil and Environmental Engineering, Gdańsk University of Technology, Poland

2. Department of Nephrology, Transplantology and Internal Medicine, Medical University of Gdańsk, Poland

*Corresponding author: lubow@pg.edu.pl

1. Introduction

The main objective of this study is to find regions of human abdominal wall that would behave similarly under intraabdominal pressure load. The motivation was mechanical compatibility of the abdominal wall and surgical meshes used for ventral hernia repair [1], which is the key concept in their proper design.

2. Materials and Methods

The presented research is based on *in vivo* experiment and data analysis. Digital Image Correlation system (DIC) was used to the full-field measurement of deformation of the abdominal wall surface during changes in the intraabdominal pressure of a patient undergoing a peritoneal dialysis.

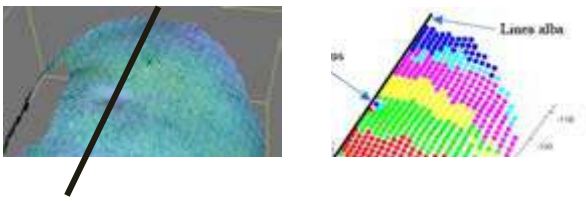

a) b)

Figure 1: Human abdominal wall: a) principal strains and directions, subject during inhalation (drained abdominal cavity); b) clusters of data points mapped on a half of the abdominal wall geometry. The geometry of abdomen presented in [mm].

The experimentally achieved data was used to study principal strains and directions (Fig. 1a) of the tested area and their evolution depending on the load. Four conditions of the abdominal cavity were considered: filled with dialysis liquid and drained; both during inhalation and exhalation. A specific Artificial Neural Networks called Self-Organising Maps (SOM) [2] were applied to the data where the complex data representing all patient conditions can be analysed simultaneously.

3. Results

The obtained data were clustered using SOM into regions with similar features. Figure 1b shows the clusters mapped on the abdominal wall. These are groups of data points on the abdominal wall that reveal similar mechanical behaviour under pressure.

4. Discussion and Conclusions

The analysis shows that not only principal strains values evolve with the changing load, but also principal strain directions change. The use of SOM in identifying regions of similar mechanical behaviour under pressure may be helpful in the identification of mechanical properties of abdominal wall, which is a complex structure. All this can support better understanding of the mechanics of abdominal wall of living humans.

5. References

1. Maurer M. et al., J. Mech. Behav. Biomed. Mater., 40:42–58 (2014).
2. Kohonen T., Springer Berlin Heidelberg, 1997.

Acknowledgements:
This work was supported by the National Science Centre (Poland)
[grant No. UMO-2017/27/B/ST8/02518].
Calculations were carried out at the Academic Computer Centre in Gdańsk.



FEATURE SELECTION APPLIED TO MICROBIOME FOR DRUG DISCOVERY

David Rojas-Velazquez (1,2), Sarah Kidwai (1), Lara Cerezin(1), Luciënne de Vries(1), Kosta Besermenji(1), Paula Perez-Pardo(1), Alejandro Lopez-Rincon (1,2)

1. Utrecht University, Pharmacology, Netherlands; 2. Julius Center UMC Utrecht, Netherlands

1. Introduction

Inflammatory bowel disease (IBD) is a term that describes conditions characterized by chronic inflammation of the gastrointestinal (GI) tract caused by various factors: abnormal gut microbiota, immune response dysregulation, environmental changes and gene variants. There are two types of IBD: Crohn's disease (CD) and ulcerative colitis (UC). Currently, there is no treatment for IBD, but it can be managed by using aminosalicylates, immunosuppressants or biologics[1].

2. Materials and Methods

The data used is from *Alam et al* [1], where fecal samples were collected from 30 individuals (20 IBD and 10 healthy volunteers) with 16S rRNA taxonomic profiling. Raw data was analysed using the DADA2 pipeline [2] and the Recursive Ensemble Feature Selection (REFS), and we compared with the original results. REFS is a method to discover biomarkers, the ensemble for the feature selection phase is composed by 8 classifiers from the sci-kit learn toolbox [3]: Stochastic Gradient Descent, Support Vector Machine classifier, gradient boosting, random forest, logistic regression, passive aggressive classifier, ridge classifier and bagging [4,5]. Once the features were selected, are validated using 5 different classifiers from the sci-kit learn toolbox [3] not part from the ensemble.

3. Results

REFS selected 5 sequences (features) from the original 3226, with an AUC of 0.92, considered as excellent in medical diagnostics [6]. The resulting taxa are 5 out 3 at genus level: *Lactobacillus* (F1), *UCG-002* (F2) and *Fusicatenibacter* (F5), and 2 *Lachnospirales* that will require more study in tools such as BLAST[2].

4. Discussion and Conclusions

As shown inFigure 2, the use of ML with REFS give us better results and closer to reality. E.g. the first feature selected was genus lactobacillus

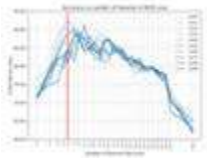

Figure 1: 10 runs of the REFS algorithm, with best answer at 5 taxa (vertical red line).

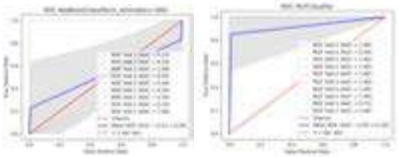

Figure 2: ROC Comparison between the original results from [1] (left) and the results using REFS (right).

and it was shown to be underexpressed in IBD patients. Lactobacillus is a component of lactic acid bacteria, a bacteria group described by the formation of lactic acid as a main end product of carbohydrate metabolism [7]. Lactobacilli are a major part of the commensal microbial flora of small and large intestine in humans and animals, and are often used as probiotics [8]. An overview in [9] described the use of VSL #3 which consists of 8 bacterial strains, 4 of those are Lactobacillus strains. It has been shown that VSL #3 was able to induce a significant increase in protective bacterial strains and can induce remission in patients with mild to moderate UC [9], this could be a first step towards a treatment.

5. References

1. Alam MT et al., Gut pathogens. 2020;12(1):1-8 (2020).
2. Callahan B et al., Nature methods. 2016;13(7):581-583 (2016).
3. Pedregosa F et al., The Journal of machine Learning research. 2011;12:2825-2830 (2011).
4. Lopez-Rincon A et al., BMC bioinformatics. 2019;20(1):1-17 (2019).
5. Lopez-Rincon A et al., BMC bioinformatics. 2020;12(7):785 (2020).
6. Šimundić AM, ejifcc. 2009;19(4):203 (2009).
7. Tannock GW, Applied and Environmental Microbiology. 2004;70(6):3189–94 (2004).
8. Christensen HR, The Journal of Immunology. 2002;168(1):171–8 (2002).
9. Cheng FS, World Journal of Clinical Cases. 2020; 8(8):1361–84 (2020).

[1] https://www.nhs.uk/conditions/inflammatory-bowel-disease/

[2] https://blast.ncbi.nlm.nih.gov/Blast.cgi



GENERATION OF ANTHROPOMORPHIC GRASP HYPOTHESES FOR GRASPING SIMULATION

Immaculada Llop-Harillo*, Néstor J. Jarque-Bou, Antonio Pérez-González, Jose L. Iserte, Javier Andrés-Esperanza

Universitat Jaume I (UJI), Spain

**Department of Mechanical Engineering and Construction, Universitat Jaume I, 12071 Castellon, Spain*

1. Introduction

In the last years, the design of anthropomorphic hands has been rising. However, a parallel development of objective methods is needed to assess the performance of different hand designs. Experimental approaches are costly, time consuming, and inconvenient in early design stages. Alternatively, grasping simulation could be a useful tool for the assessment of artificial hand designs, of both prosthetic and robotic hands, in order to optimize their functionality. One of the most common method used in grasping simulation in virtual environments, as OpenRAVE, for generating grasp hypotheses (GHs) is the brute-force approach. This method has the advantage of being general and applicable to any hand or object, but it requires a long time to compute a significant sample. This is due to the fact that some of the GHs generated are redundant for symmetrical objects. Besides, most of the final grasps obtained are not realistic for activities of daily living. Therefore, the objective of this work is to develop a methodology to obtain the optimal orientation and position of the artificial hand with respect to the object to be grasped according to human experience. The use of human oriented approaches could solve some of the aforementioned limitations. Additionally, the definition of a metric for benchmarking anthropomorphic hands through grasping simulations based on experimental benchmarks, as the Anthropomorphic Hand Assessment Protocol (AHAP) [1] and adapted to a simulation environment [2] is crucial for the improvement of the anthropomorphism of artificial hands. With this work, we aim to improve the generation of the GHs in grasping simulation through experimental tests with the human hand performing the AHAP.

2. Materials and Methods

The experimental grasping test was performed on ten right-handed healthy subjects and the 26 objects of the AHAP [1], using an electromagnetic tracking system (Viper) that records the position and orientation of the sensors (in the hand of the subject and in each object) with respect to a static receptor.

Based on the data obtained in the experimental tests, the optimal orientation and position of the hand with respect to the object to be grasped was analysed using Matlab. Finally, the anthropomorphic GHs with the prosthetic hand, IMMA hand, and each object of the AHAP, were computed using this data in the OpenRAVE simulation environment.

3. Results

With the method proposed in this work, a database of optimal position and orientation for the grasping simulation of the grasps performed in an experimental benchmark (AHAP) has been obtained.

4. Discussion and Conclusions

With this database, the simulation benchmark with an anthropomorphic grasp approach proposed in [2] has been improved and completed with all the grasp types and objects of the AHAP.

5. References

1. Llop-Harillo et al, Rob Auton Syst; 121:1-12, (2019).
2. Llop-Harillo et al, J Comput Des Eng; 9(2):330-342, (2022).

Acknowledgements:

This publication is part of the R+D project PID2020-118021RB-100, funded by MICIN/AEI/ 10.13039/501100011033.

CMBBE2023
18th International Symposium on Computer Methods in Biomechanics and Biomedical Engineering
3 - 5 May 2023, Paris, France
Arts et Métiers Institute of Technology
Institut de Biomécanique Humaine Georges Charpak
155 boulevard de l'Hôpital 75013 Paris France
www.cmbbe-symposium.com

COMPUTATIONAL EVALUATION OF EXOSKELETON CONTROLLERS WITH A SCALABLE BIOMECHATRONICS MODEL

Ali Nasr, John McPhee

Systems Design Engineering, University of Waterloo, Canada

1. Introduction

Power assistive, haptic, and neuromuscular rehabilitation may use wearable robots or exoskeletons. The control units of exoskeletons must concurrently govern the dynamics of the wearable robot and the user's musculoskeletal biomechanics, as well as human adaptation to the robot [1,2]. Before experimental implementation, computational assessment of human-robot interactions and adaptations is the goal of this paper.

2. Model and Simulation

As shown in Fig. 1, the human-robot consists of 6 sub-models: I) the human central nervous system, which coordinates motion by prediction and error correction, was modeled with nonlinear model predictive controllers (CNS-NMPC) to coordinate the human body with respect to constraints and according to minimization of a cost function [1]. II) the muscles or the biomechanical joint torque modeled with muscle torque generators [3] and includes five sub-functions: (1) passive torque, (2) peak joint isometric strength, (3) active-torque-angle scaling, (4) active-torque-angular-velocity scaling, and (5) excitation-to-activation signal functions. These functions are scalable with sex, age, body mass, height, dominant side, and physical activity. III) the skeletal system was created with respect to the body segment inertial parameters and degrees of freedom according to the International Society of Biomechanics standard. IV) the interaction, compliance, and connection model relate the human body to the robotic structure system. Here, we modeled a kinematical human-robot connection. V) the robot actuator and passive mechanism systems were modeled according to experimental identification and added to the robot structure [2]. VI) the robot's actuators were controlled with a hierarchical control scheme that comprises high-level (estimates future human intent), mid-level (defines the commanded assisted torque), and low-level (decreasing the actuator error) controllers [1].

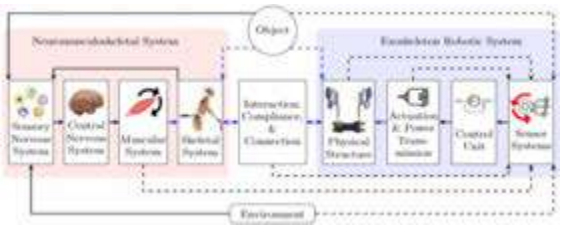

Figure 1: The human-robot-environment structure.

3. Results

The model was used to design, test, and tune the exoskeleton's controller, which performs safely and well in experiments, as well as reduces human fatigue. While the human has not adapted to the robot or when the hierarchical controller has a significant delay (for fast motion), the robot is not cooperating (resisting instead of assisting), and uncomfortable human-robot interactions occur.

4. Discussion and Conclusions

Using the multibody dynamic model helped to test and tune the hierarchical controller. By changing the weight of the CNS-NMPC cost function and using the human-robot interaction force/torque as un/measured disturbances, the human adaptation to the robot was assessed.

5. References

1. Nasr A et al., Robotics. 11(1):20 (2022).
2. Nasr A et al., Multibody System Dynamics. In press (2022).
3. Inkol KA et al., Multibody System Dynamics. 50(4), 435-452 (2020).

Acknowledgements:
This research is supported by funding from the Canada Research Chairs Program and the Natural Sciences and Engineering Research Council of Canada.



DIGITAL TWINS FOR DECISION SUPPORT IN FONTAN-PALLIATED PATIENTS

Jan Brüning (1,2), Pavlo Yevtushenko (1), Marie Schafstedde (1,2)

1. Institute of Computer-assisted Cardiovascular Medicine; Charité – Universitätsmedizin Berlin; Germany 2. DZHK (German Center for Cardiovascular Research), Partner Site Berlin

1. Introduction

There are several congenital heart defects that result in a shunt between the left and the right ventricle and thus in univentricular physiology. Ideally, biventricular repair via cardiac surgery or interventional approaches is feasible. However, this goal cannot be achieved for all patients depending, among others, on the patient-specific anatomy and the complexity of the congenital heart defect. For those patients, univentricular palliation via several staged cardiac surgeries must be performed. After the final surgery, the Fontan procedure, the superior and inferior vena cava are connected to the pulmonary artery, facilitating the so-called total cavopulmonary connection (TCPC).

The morphology and hemodynamics within the TCPC are subject to severe patient-specific heterogeneity. Furthermore, some patients require recurrent surgical and interventional treatments, further adding to the already heterogeneous patient-population. Due to this heterogeneity in both anatomy and function generalized treatment strategies are often not feasible. Image-based diagnosis, for example via CT or MRT can also be severely constrained due to the patient-specific treatment history, e.g., by implantation of metallic stents.

In this project, we aim to evaluate the potential of digital twins for identification of personalized strategies for diagnosis as well as for treatment-planning for Fontan-palliated patients.

2. Materials and Methods

For generation of the digital twins, a three-dimensional, anatomical representation of the TCPC has to be reconstructed from different imaging sources, as for example MRI, CT and angiography. By simulation of the patient-specific blood flow within the TCPC via computational fluid dynamics, these purely anatomical models can be enhanced by functional information. This approach allows to assess the entire patient-specific hemodynamics, including parameters such as pressure gradients, the power loss, or the distribution of hepatic blood towards the pulmonary arteries.

To assess the viability and outcome of different treatment strategies, these digital twins can be altered virtually, to mimic the respective surgical or interventional procedure, such as implantation of covered stents or vascular grafts. Thus, the immediate functional outcome of different treatment strategies can be assessed and compared against other treatment options, allowing to identify the optimal treatment for a given patient.

3. Results and Discussion

The project is currently ongoing and only preliminary results are available yet. The anatomical models alone, especially when superimposed to image data, provide additional information for treatment planning, as the entire complex anatomy can be visualized, and constraints imposed by surrounding tissue can be assessed. The outcome prediction of different treatment strategies holds the promise to provide additional objective information, allowing to better stratify treatment risks and potential outcomes on a patient-specific level. Thus, digital twins are a promising approach to overcome the obstacles imposed by the heterogeneity found in patients with univentricular palliation.

Acknowledgements:

This work is funded by the Supported by the DZHK (German Centre for Cardiovascular Research).



ARTERY WALL THICKNESS EFFECT ON VISCOELASTIC WALL MOTION USING A STANDARD LINEAR MODEL

Duc Manh Dinh and Kyehan Rhee

Department of Mechanical Engineering, Myongji University, Republic of Korea

1. Introduction

As atherosclerosis progressed, artery wall deterioration and tissue constituent change affect arterial wall's physical properties. Assessment of arterial wall viscoelasticity has been performed using the pressure and diameter (P-D)) relationship in carotid arteries because non-invasive clinical measurement of artery wall motion is easily available using ultrasound images. This study aims to show the effect of wall thickness on the radial wall motion of a viscoelastic carotid artery model using a finite element method.

2. Materials and Methods

The artery was modelled as a thin wall tube, and the standard linear model (SLM) was implemented to consider the viscoelastic wall response to the pulsating intramural pressure. The effect of intima-media thickness (IMT) on arterial wall motion was simulated using commercial software (Ansys Workbench, ANSYS, Inc., Canonsburg, PA). A carotid artery was modelled as a 100 mm long cylinder with a 3 mm inner radius. The wall thickness was varied from 0.5 to 1.5 mm to simulate different IMTs. The artery wall was assumed to be isotropic elastic with a Poisson ratio of 0.49. Pressure was estimated from the brachial pressure waveform in the pulse wave velocity test data and the diameter waveform was measured from B-mode ultrasound images [1]. Both ends of a cylindrical tube were fixed in all directions, and the estimated carotid pressure waveform was applied to the inner wall of the cylinder. The viscoelastic parameters (E_0=400kPa, α=0.5, τ_ε=0.02s) were applied to simulate the measured diameter waveform of a patient.

3. Results

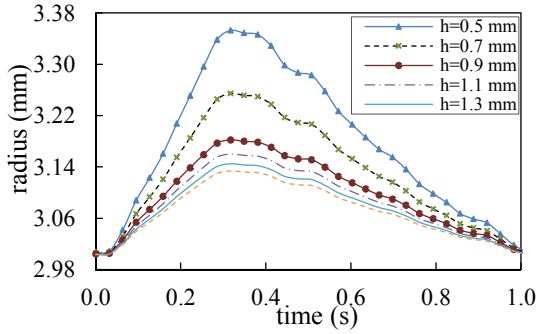

Figure 1: Radius waveforms for different IMTs

The amplitude of the radius waveforms decreased as the IMT increased, but the phase lags between the pressure and the radius waveforms were not changed noticeably (Fig.1). The amplitudes of radius waveform decreased from 0.35 mm to 0.13 mm as the IMT increased from 0.5 mm to 1.5 mm. The energy dissipation ratio (EDR), which was defined as the hysteresis loop area of the P-D curve during a cardiac cycle divided by the area under the systolic loading curve of the loop, was computed to quantify wall viscosity. EDR decreased from 3.41% to 3.11 % as the IMT increased from 0.5 mm to 1.5 mm.

4. Discussion and Conclusions

IMT thickening caused a decrease in radial wall motion as expected in the theory of a thin tube cylinder whereas it did not affect the viscous response of the arterial wall (phase delay and EDR). IMT may not be considered to assess arterial wall viscosity using a P-D curve because the viscous effect of the arterial wall was not noticeable for the pressure and wall motion of a human carotid artery model.

5. References

1. Shin J et al. Med Eng Phy.108:103886 (2022).

Acknowledgements:
This work was supported by the Research Fund NRF-2020R1A2C1004354.



PARAMETRISATION-BASED QUANTIFICATION OF AAA EVOLUTION

Ludovica Saccaro (1), Gwladys Ravon (1), Florian Bernard (2), Angelo Iollo (1,3)

1. INRIA – Bordeaux Sud-Ouest, MEMPHIS, 33405, Talence, France; 2. NUREA, 33000 Bordeaux, France; 3. IMB, UMR 5251, Université de Bordeaux, Talence, France;

1. Introduction

An abdominal aortic aneurysm (AAA) is an abnormal dilatation of the aorta between the renal and iliac arteries, that leads to rupture and death if left without treatment. In particular post-operative surveillance helps prevent the arise of complications, or of further degradation of the aortic wall [2]. Registration consists in the comparison of two aneurysms, before and after treatment, to qualitatively and quantitatively assess the progression of the disease. In this work we propose a patient-specific, automated pipeline that starts with CT scans as input, gives a suitable parametrisation of the aneurysm geometry, and then exploits such framewortk to perform registration, by computating a displacement map of the aortic wall. Initial dataset is provided by NUREA (https://www.nurea-soft.com).

2. Parametrisation

Given the initial 3D reconstruction of an aneurysm, a suitable parametrisation is individuated. The aneurysm is described thought its *centreline* $\mathbf{P} = [p_1, p_2, \ldots, p_S]$ that runs in the centre of the vessel. The wall is described cutting the reconstruction on the planes perpendicular to each point p_s, thus individuating a *section* on the wall. Each section is approximated with a Fourier series, (**Figure 1**):

$$R(\theta) = a_0 + \sum_{j=1}^{N} a_j \cos(j\,\theta) + b_j \sin(j\,\theta).$$

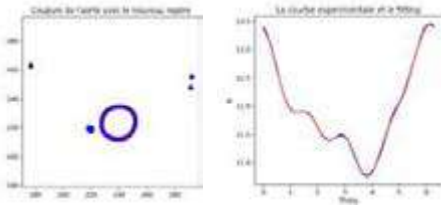

Figure 1: Left: Approximated section of aneurysm, with spurious vases. Right: Original profile in blue, Fourier approximation of profile in red.



Figure 2: Example of parametrised aneurysm; centreline in red, aortic wall in black. In grey in the initial 3D reconstruction.

The same number of sections S is used through all the dataset, so that all aneurysms are now easily comparable (**Figure 2**).

3. Registration

As preliminary step we align with a rigid roto-translation the two aneurysms, using the renal arteries as point of reference [1]. We proceed comparing the s-th section of the aneurysm before surgery with the s-th section of the aneurysm after surgery. We compute the vector difference of the two profiles and thus construct the displacement map for the wall (**Figure 3**).

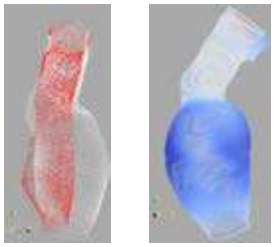

Figure 3: Left: Example of two aneurysms, pre-surgery in white and post-surgery in red. Right: displacement map.

4. Results and Conclusions

Parametrisation-based registration is an efficient approach, completely automatic, that provides patient-specific, quantitatively results of the aneurysm evolution.

5. References

1. Ravon G et al., https://hal.inria.fr/hal-03600571/file/main.pdf (2022).
2. Stather et al. Journal of British Surgery **100**(7) (2013).

Acknowledgements:

The study is part of the European project ARIA. (https://cordis.europa.eu/project/id/872442) NUREA has provided the dataset for this study and medical consultation to discuss the results.

CMBBE2023
18th International Symposium on Computer Methods in Biomechanics and Biomedical Engineering
3 - 5 May 2023, Paris, France
Arts et Métiers Institute of Technology
Institut de Biomécanique Humaine Georges Charpak
155 boulevard de l'Hôpital 75013 Paris France
www.cmbbe-symposium.com

PASSIVE LEFT VENTRICLE TISSUE BIAXIAL CHARACTERIZATION

Mogane Evin (1), Siyu Lin (2), Wei Wei (1), Alain Lalande (2)

1. Laboratoire de Biomécanique Appliquée, Université Gustave Eiffel, Aix-Marseille Université, France; 2. Université de Bourgogne, France;

1. Introduction

Myocardium modelling has been largely reported using uniaxial and biaxial testing [1]. Performing equi-biaxial traction test to rupture enables threshold identification for further testing at different strain rates.

2. Materials and Methods

Two Landrace swine hearts were extracted and frozen at -20°C before dissection of the myocardium. Four $15 \times 15 mm^2$ samples per heart were harvested at the medial, lateral (right and left) and apex part of the septum and cut to ensure similar thickness between samples. Thickness measurements were performed in 5 locations of the sample and averaged to provided Mean± standard deviation.

Biaxial traction tests were performed on a LM1, TA Instruments system (ElectroForce® System Group, USA). They consisted of 10 pre-conditioning cycles (sinus, 2.96%, 1Hz) after a preloading of 0.1 N and traction test with an identic condition on both axis until rupture at a strain rate of 2%/s (0.24 mm/s with 12 mm experimental length).

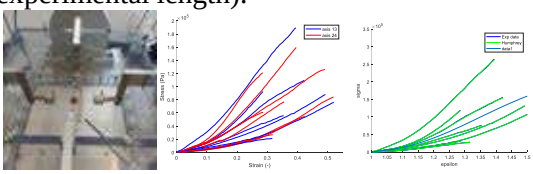

Figure 1: Equi-biaxial test system (left); engineering strain-stress curves for biaxial test of the 8 samples (middle) and average fitted Humphrey model (right).

Bi-linear regressions were performed on the tested samples using iterative search for maximal r^2 sum of both parts. Rupture test and Humphrey based model is described using strain energy function as follow:

$$\psi = c_1(\alpha - 1)^2 + c_2(\alpha - 1)^3 + c_3(I_1 - 3) + c_4(I_1 - 3)(\alpha - 1) + c_5 (I_1 - 3)^2 \quad (1)$$

Constitutive model parameters were identified using lsqcurvefit Matlab 2020b (MathWorks, Natwiks, USA) and assessed using r^2 and root mean square error (RMSE).

Humphrey	n=8
c1	-2965649±9402626
c2	-182453±481137
c3	904278±2717496
c4	1489296±4158196
c5	74307±103892

Table 1: Humphrey model parameters c_i (crn.m-2).

3. Results

Thickness measurements of the sample resulted in 3.12±0.68 mm at the medial location, 3.46±0.7 mm in lateral part and 2.36±0.95 mm in Apex. Elastic part of the bi-linear regressions showed higher elastic modulus found in apex (438.1±199.8 MPa) compared to medial and lateral parts (322.7±167.2 and 222.4±104.3 MPa). Maximum stress was found to be lower in lateral parts with 33.496±19.169 MPa (vs 125±58.1 and 90.5±3.13 MPa in respectively in apex and medial parts). Constitutive models identified for each of the experimental tests resulted in a r^2=0.99 and RMSE of 413±234. Averaged pmodel well depicted experimental data (Fig1).

4. Discussion and Conclusions

While reported results were limited in term of sample number, sample thickness reduction and variability in term of identified parameters was high, threshold for further biaxial testing at this 2% strain rate has been identified. Using average parameter for Humphrey modelling appears to be appropriate for model passive ventricle myocardium.

5. References

[1] R. Avazmohammadi, J. S. Soares, D. S. Li, S. S. Raut, R. C. Gorman, et M. S. Sacks, « A Contemporary Look at Biomechanical Models of Myocardium », *Annu Rev Biomed Eng*, vol. 21, p. 417-442, juin 2019, doi: 10.1146/annurev-bioeng-062117-121129.



IMPACT OF PATIENT-SPECIFIC OCCLUDER CONFIGURATION IN DEVICE-RELATED THROMBUS: AN IN-SILICO ANALYSIS

Carlos Albors[1], Jordi Mill[1], Andy L. Olivares[1], Xavier Iriart[2], Hubert Cochet[2], Oscar Camara[1]

[1] Sensing in Physiology and Biomedicine (PhySense), Universitat Pompeu Fabra, 08018 Barcelona, Spain
[2] Hôspital Haut-Lévêque, Bordeaux, France

1. Introduction

Device-related thrombosis (DRT) has emerged as a worrisome complication following a left atrial appendage occlusion (LAAO), the alternative procedure to life-long anticoagulants. Optimal LAAO configuration (i.e., type, size, location) for each LAA geometry remains unclear. To further understand the pathophysiological mechanisms underlying DRT, in-silico models can help to describe the complex LA/LAA hemodynamics, being useful in the device size and landing zone selection. In this study, a computational fluid dynamics (CFD) analysis of patient-specific geometries mimicking real device deployment after LAAO was performed with different types of occluders. A better device setting to prevent DRT was also suggested.

2. Materials and Methods

Two patient-specific LA geometries were studied by implanting computer-aided design (CAD) models of the Amplatzer Amulet (St.Jude Medical-Abbott, United States) and Watchman FLX (Boston Scientific, United States) occluders in two different positions: the real device deployment extracted from the post-occlusion CT scan and the optimized one covering the pulmonary vein ridge (PR), a potential independent DRT risk factor [1]. Fluid flow simulations combined with a platelet adhesion model were carried out within the CFD solver Ansys Fluent 2019 R3 (Ansys Inc., USA). A generic pressure measurement of an atrial fibrillation patient in the pulmonary veins, a velocity curve extracted from Doppler echo in the mitral valve, and a spring-based dynamic mesh approach describing a longitudinal excursion of the mitral valve annulus, were defined in the model as boundary conditions. Two cardiac beats were simulated.
Average velocities, swirling flow patterns, the endothelial cell activation potential (ECAP) thrombogenic index, and the number of wall adhered platelet were the main indices assessed near of device surface.

3. Results

Significant differences in platelet accumulation with a PR uncovered were observed in both devices, with the Watchman FLX having a larger density on its surface. Only in the Amplatzer Amulet, streamlines revealed low flow velocities with swirling patterns in the LAAO device deployment during the whole cycle. No complex patterns with high average velocities were obtained in the optimized position.

4. Discussion and Conclusions

Pulmonary ridge coverage seems a potential independent factor for DRT prevention. Further research would be needed to validate this assumption in a larger cohort.

5. References

1. Mill, J., et al.: Impact of flow dynamics on device-related thrombosis after left atrial appendage occlusion. Canadian Journal of Cardiology 36 (2020).

Acknowledgments:

This project has received funding from the European Union's Horizon 2020 research and innovation programme under grant agreement No 101016496 (SimCardioTest).

CMBBE2023
18th International Symposium on Computer Methods in Biomechanics and Biomedical Engineering
3 - 5 May 2023, Paris, France



Arts et Métiers Institute of Technology
Institut de Biomécanique Humaine Georges Charpak
155 boulevard de l'Hôpital 75013 Paris France
www.cmbbe-symposium.com

SYMMETRY-CONSTRAINED COMPACT TENSION TEST TO INVESTIGATE THE FRACTURE PROPERTIES OF VASCULAR TISSUE

Marta Alloisio[1], Marina Chatziefraimidou[1], T.Christian Gasser[1,2]

1. Department of Engineering Mechanics, KTH Royal Institute of Technology, Sweden
2. Faculty of Health Sciences, University of Southern Denmark, Odense, Denmark

1. Introduction

Regardless failure plays a critical role in progression of vascular diseases [1], little is known concerning failure mechanisms at different length-scales. In-vitro experimental methods to acquire failure properties are limited. We, therefore, propose the symmetry-constrained Compact Tension (symconCT) test, a novel experimental method to study the failure of vascular tissue.

2. Materials and Methods

The symconCT test further develops the classical CT test by pre-straining the tissue and enforcing the fracture (starting from a pre-notch) to stay in the middle of the specimen. An elastic beam connects the two grips, which in turn promotes a symmetric deformation of the specimen. The test has been performed at physiological conditions using a uniaxial tensile machine (ADMET eXpert 4000 Universal Testing System) at a clamp displacement rate of 3 *mm/min*. During the test, Digital Image Correlation (DIC) provides full-filed strain measurements, taken at the intimal surface of the vessel wall, see Figure 1. In total 23 specimens (30*x*35 mm^2) with a 10 *mm* pre-notch perpendicular to the loading direction have been tested. The specimens ware taken from normal porcine aortas and the adventitia was removed prior to testing.

A 2D Finite Element (FE) model, incorporating a viscoelastic Yeoh model and a cohesive description of the fracture, was used to explore the experimental findings.

3. Results

Given loading along the axial tissue direction, the fracture propagated in the circumferential direction, almost exactly perpendicular to the loading, see Figure 1.A. In contrary, circumferential load resulted in a zig-zagging failure pattern, still staying within the centre of the specimen, see Figure 1.B. Vascular tissue withstood a maximum force of 3.89 ± 0.34 N when loaded in axial direction, which was significantly (t-test, $p = 1.31e^{-6}$) lower than 5.76 ± 0.24 N under circumferential load.

The external work of the experiment was normalized by the initial specimen thickness and length of the fracture path. Whilst the average value of the normalized work differed (axial loading: 1.07 ± 0.15 kJ/m^2; circumferential loading: 1.54 ± 0.55 kJ/m^2), this difference was not significant (Wilcoxon rank sum test, $p = 5.59e^{-2}$).

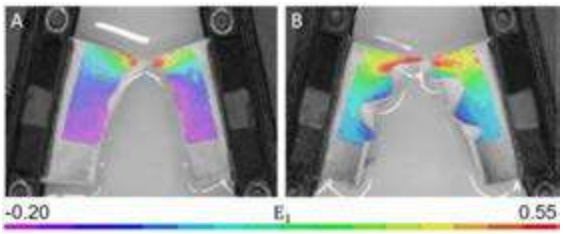

Figure 1: DIC-based maximum principal strain E_1 field of symconCT rupture tests under axial loading (A), and under circumferential loading (B) of healthy porcine aortic media.

4. Discussion and Conclusions

The symconCT was able to reproduce stable crack propagation in vascular tissue at low strain rates. The acquired force-displacement experimental data and DIC measurements allowed for the calibration of our FE model and in-depth exploration of the deformation during tissue fracture.

References

1. L. Aslanidou et al., Biomech. Model. Mechanobiol. 19, 2020

CMBBE2023
18th International Symposium on Computer Methods in Biomechanics and Biomedical Engineering
3 - 5 May 2023, Paris, France



Arts et Métiers Institute of Technology
Institut de Biomécanique Humaine Georges Charpak
155 boulevard de l'Hôpital 75013 Paris France
www.cmbbe-symposium.com

SUBJECT-SPECIFIC SPINE MODELLING USING A BAYESIAN COHERENT POINT DRIFT ALGORITHM

Joeri Kok* (1), Bert van Rietbergen (1), Yulia Shcherbakova (2), Tom Schlösser (2), Peter Seevinck (2), René Castelein (2), Keita Ito (1,2)

1. Eindhoven University of Technology, Netherlands; 2. University Medical Center Utrecht, Netherlands

**Corresponding author: j.kok@tue.nl*

1. Introduction

Finite element (FE) models of the spine are widely used for research. Meshing the subject-specific thoracolumbar spine is a labour-intensive process and accuracy can vary depending on the user. Mesh morphing can be used to adjust a pre-existing template to a subject-specific geometry. Bayesian coherent point drift (BCPD) is an affine registration method that can account for large local deformations [1]. The aim of this study was to develop a method for the morphing of a thoracolumbar spine template to subject-specific segmentations based on BCPD.

2. Materials and Methods

Magnetic resonance images of two adult subjects, one with a healthy spine and one with scoliosis (Cobb angle ~30°), were obtained. Synthetic CT scans were generated from the images (BoneMRI V1.5, MRIguidance). The intervertebral discs (IVDs) and vertebrae were automatically segmented from these scans (Fig. 1A). A template mesh (GHBMC F05-P, Elemance, LLC) was morphed to fit the segmentations using a BCPD algorithm (Fig. 1B). All vertebrae and discs that were part of the segmentations were selected from the template. The template was aligned using rigid registration. The IVDs and vertebrae were morphed to their respective segmentations. Finally, the complete structure was morphed to the already morphed IVDs and vertebrae to ensure a good connection between the parts.

3. Results

Individual vertebrae and IVDs were successfully morphed to the segmentations for both subjects. 94% of the complete morphed healthy and scoliotic spine, were within 2 mm of the segmentations (Fig. 1C). Regions where this distance was larger than 3 mm occurred in the spinous and transverse processes, often as a result of incorrect or incomplete segmentations.

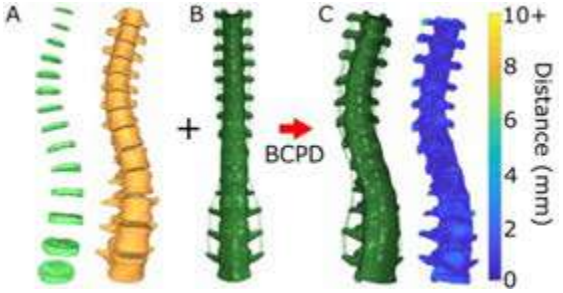

Figure 1: A) Subject-specific segmentations of IVDs and vertebrae. B) Template spine mesh. C) A template mesh morphed to the segmentations with a measure of the shortest distance between the mesh and the surface of the segmentation.

4. Discussion and Conclusions

An automated workflow for spine modelling from MR images has been developed. The deformation of the template mesh using BCPD is dependent on the settings (e.g., smoothing of the deformation vector, number of outliers, expected deformation). This allows for large deformations of complex structures while maintaining a good mesh. The deformation of the complete spine can be optimized by using different settings for the individual parts of the spine.

5. References

1. Hirose O, IEEE Trans. Pattern Anal. Mach. Intell.; 43(8):2858-2865

Acknowledgements:

The authors would like to thank the European Research Council (Grant no: 101020004) for providing financial support for this project.

CMBBE2023
18th International Symposium on Computer Methods in Biomechanics and Biomedical Engineering
3 - 5 May 2023, Paris, France



Arts et Métiers Institute of Technology
Institut de Biomécanique Humaine Georges Charpak
155 boulevard de l'Hôpital 75013 Paris France
www.cmbbe-symposium.com

A COMPUTATIONAL FRAMEWORK TO STUDY THE EFFECTS OF SPINAL CORD STIMULATION (SCS)

Tom Le Tutour (1,2,3), Karim El Houari (2), Sophie Collin (2), Jonathan Dany (1), Mohamed Et Talby (1), Laëtitia Caillé (3), Wenfeng Ye (2), Maxime Billot (1), Manuel Roulaud (1), Michel Rochette (2), Arnaud Germaneau (3), Philippe Rigoard (1,3)

1. PRISMATICS Lab (Predictive Research in Spine/Neuromodulation Management and Thoracic Innovation/ Cardiac Surgery), Poitiers University Hospital, Poitiers, France

2. Ansys France, Villeurbanne, France

3. Institut Pprime UPR 3346, CNRS – Université de Poitiers – ISAE-ENSMA, Poitiers, France

1. Introduction

10-50% of patients experience persistent leg or back pain after spine surgery [1] which can be treated with Spinal Cord Stimulation (SCS). SCS consists in implanting a lead array in the epidural space, targeting nerve fibers of the spinal cord to activate the inhibitory circuitry of pain [2]. Many parameters can be tuned in SCS, including lead shape, electrode programming, and stimulation frequency. These parameters are still chosen empirically, highlighting the need for accessible computational models. The goal of the present study is to develop such models based on literature [3,4].

2. Materials and Methods

To accurately model the effects of spinal cord stimulation, 3 steps are of importance. (Fig. 1).



Figure 1: An illustration of the steps needed to model SCS.

First, we built a detailed geometry representing the spinal cord using morphometric measurements. Then, we computed the steady-state electric field generated by stimulation using Ansys MAPDL, using the finite-element method which solves the system Eq. 1, 2:

$$-\nabla \cdot ([\sigma]\nabla V) = 0 \quad (1)$$

$$V_{electrode} = V_{imposed} \quad (2)$$

where σ is the electric conductivity, V is the electric potential, $V_{electrode}$ is the electric potential prescribed to $V_{imposed}$. Finally, we assessed the effects of this field on electrical nerve fibers models. The electric potential is then used as input to nerve fiber models such as the McNeal fiber model [5].

3. Results

We successfully implemented a workflow that can simulate the physics behind spinal cord stimulation. Lower stimulation threshold for fibers with higher diameter, and increased selectivity of dorsal root (DR) fibers over dorsal column (DC) fibers during monopolar stimulation were observed, which seems in accordance with the literature [3,4].

4. Discussion and Conclusions

The perspective of this work is to use these methods to help clinicians during the pre-operative planning phase to determine which stimulation parameters would fit a patient best.

5. References

1. Chan C, Peng P. *Pain Med*. 2011;12(4):577-606
2. Melzack R, Wall PD. *Science*. 1965; 150(3699): 971-979.
3. Holsheimer J et al. *Med Biol Eng Comput*. 1995; 33(5):676-682.
4. Dura JL et al. *Neuromodulation Technol Neural Interface*. 2019;22(3):269-279.
5. McNeal DR. *IEEE Trans Biomed Eng*. 1976; BME-23(4):329-337.

Acknowledgements:

The authors would like to thank the Association Nationale Recherche Technologie (ANRT) for providing financial support to this project. (CIFRE: 2021-1405)

CMBBE2023
18th International Symposium on Computer Methods in Biomechanics and Biomedical Engineering
3 - 5 May 2023, Paris, France
Arts et Métiers Institute of Technology
Institut de Biomécanique Humaine Georges Charpak
155 boulevard de l'Hôpital 75013 Paris France
www.cmbbe-symposium.com

THE EFFECT OF SPINAL FUSION SURGERY ON GAIT IN ADOLESCENT IDIOPATHIC SCOLIOSIS PATIENTS

Rounak Bhattacharya (1), Bhavuk Garg (2), Manish Gupta (2), Rajesh Malhotra (2), Anoop Chawla (3), Kaushik Mukherjee (3)

1. School of Interdisciplinary Research, Indian Institute of Technology Delhi, New Delhi, India
2. Department of Orthopaedics, All India Institute of Medical Sciences, New Delhi, India
3. Department of Mechanical Engineering, Indian Institute of Technology Delhi, New Delhi, India

1. Introduction

Adolescent Idiopathic Scoliosis (AIS) is a complex structural deformity of the spine whose aetiology and pathomechanics are poorly understood [1]. Rapid progression of spinal curve often requires surgical intervention. AIS is also associated with abnormal gait patterns [2]. However, the influence of AIS and subsequent spinal fusion on kinematic and kinetic gait variables is still unclear. Therefore, this study aimed to compare the gait parameters of AIS patients during the preoperative and post-operative conditions.

2. Materials and Methods

Five AIS patients and three age-matched healthy controls were included in the study following approval of the institutional ethics committee. The gait data were captured using 12 BTS SMART DX-7000 cameras (BTS Bioengineering) and eight force plates (AMTI, Watertown, MA, USA). A generic musculoskeletal model (gait2392 OpenSim) [3] was scaled to match the subject's anthropometry. Joint moments were calculated using the inverse dynamics approach and statistically compared across different groups.

3. Results

The AIS patients showed altered lower extremity joint kinetics compared to the control group [Fig. 1]. Preoperatively, the hip and knee flexion moments were significantly lower in the AIS patients compared to the healthy subjects during the early stance phase. Postoperatively, the hip and knee flexion moments significantly increased during the stance phase. Moreover, differences were observed in the ankle dorsiflexion moment between the AIS patients and healthy subjects in both the pre and post-operative conditions.

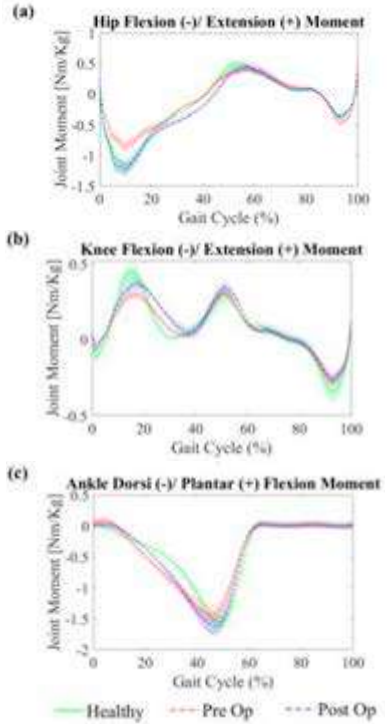

Figure 1: Comparison of (a) hip (b) knee (c) ankle joint kinetics of AIS patients and healthy population.

4. Discussion and Conclusions

The correction of the scoliotic deformity with spinal fusion surgery resulted in a positive change in the lower extremity joint moments. Future studies would investigate the influence of the surgical technique and instrumentation configuration on gait variables in AIS patients.

5. References

1. Cheng *et al.*, Nat. Rev. Dis. Primers; 1.1:1-21 (2015).
2. Daryabor *et al.*, Ann. Phys. Rehabil.; 60.2: 107-116 (2017).
3. Delp *et al.*, IEEE Trans. Biomed. Eng.; 54.11: 1940-1950 (2015).

CMBBE2023
18th International Symposium on Computer Methods in Biomechanics and Biomedical Engineering
3 - 5 May 2023, Paris, France
Arts et Métiers Institute of Technology
Institut de Biomécanique Humaine Georges Charpak
155 boulevard de l'Hôpital 75013 Paris France
www.cmbbe-symposium.com

BIOMECHANICAL ANALYSIS OF UNILATERAL PEDICLE SCREW FIXATION OF LUMBAR SPINE

Kuo-Chih Su (1), Yu-Chun Yen (1), Cheng-Hung Lee (1)

1. Taichung Veterans General Hospital, Taiwan

1. Introduction

The use of traditional lumbar screw fixation is a common surgical method for the spine and lumbar spine. However, clinically, unilateral fixation with pedicle screw is also used, the biomechanical effect of unilateral pedicle screw fixation is unclear. Therefore, this study mainly used finite element analysis to evaluate the biomechanical effects of unilateral pedicle screw fixation.

2. Materials and Methods

The finite element analysis computer model is lumbar spine in study, and cage and pedicle screw are implanted between the lumbar L3 and L4 (Fig. 1). The group 1 is the traditional pedicle screw fixation. The group 2 is the unilateral pedicle screw fixation. This study used the finite element analysis software ANSYS Workbench for analysis. Fig. 2 shows the load conditions (flexion, extension, lateral bending, and axial rotation) in this study [1].

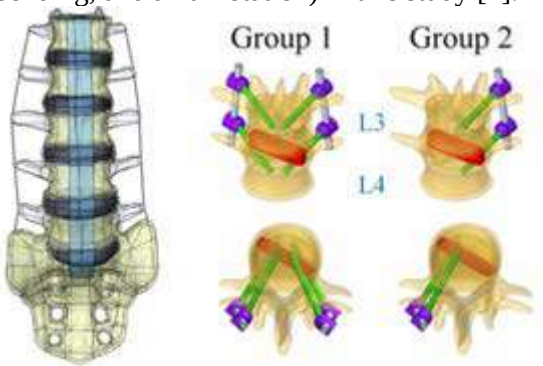

Figure 1: The finite element analysis model of this study.



Figure 2: Load conditions in this study.

The main observation indicators are total deformation of the lumbar spine, the peak von Mises stress on the lower endplate of L2 and the upper endplate of L5.

3. Results

Fig.3 shows the total deformation of the lumbar spine.

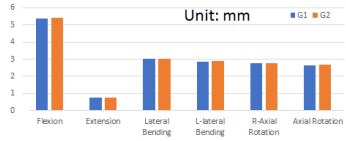

Figure 3: The total deformation on the spine

Fig. 4 and Fig.5 show the peak von Mises stress on the lower endplate of L2 and the upper endplate of L5.

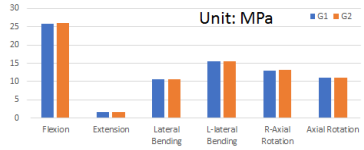

Figure 4: The peak von Mises stress on the lower endplate of L2

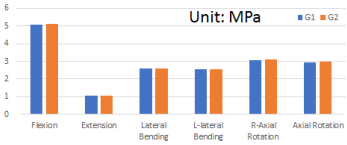

Figure 5: The peak von Mises stress on the upper endplate of L5.

4. Discussion and Conclusions

The result shows that when using traditional or unilateral pedicle screw fixation, the total deformation and the stress value on the adjacent endplate are not much different.

5. References

1. Su KC et al., Appl. Sci. 2021, 11(22):10583 (2021).

Acknowledgements:

We would like to thank the National Science and Technology Council of Taiwan (110-2221-E-075A-001, 111-2221-E-075A-002 and 111-2314-B-075A-005-1)

CMBBE2023
18th International Symposium on Computer Methods in Biomechanics and Biomedical Engineering
3 - 5 May 2023, Paris, France
Arts et Métiers Institute of Technology
Institut de Biomécanique Humaine Georges Charpak
155 boulevard de l'Hôpital 75013 Paris France
www.cmbbe-symposium.com

EVALUATION OF BIOMECHANICAL CHARACTERISTIC CHANGES OF SPINE ACCORDING TO L4-5 LORDOSIS ANGLES IN PLIF

Jun-Sung Park (1), Chanhee Song (1), Tae Sik Goh (2), Jung Sub Lee (2), Chiseung Lee (1)

1. Pusan National University, South Korea;
2. Pusan National University Hospital, South Korea

1. Introduction

Posterior lumbar interbody fusion (PLIF) is a treatment for degenerative spinal disease. Through posterior lumbar interbody fusion, it repairs the unstable lumbar spine and corrects lumbar lordosis. However, a large load on adjacent segments is applied after surgery, resulting in specific complications such as adjacent segment degeneration [1].

2. Materials and Methods

Lumbar spine segments were modeled from L3 to S1. Additionally, detailed modeling of intervertebral discs, ligaments (ALL, PLL, ITL, FJL, SSL, ISL, and LF), and implants were performed. In addition, surgical segmentation of the lumbar spine was assumed to be L4-L5. And three types of finite element models with lordosis angles between fusion segments of 0, 5, and 10(degrees) were constructed. A simulation of flexion, extension, axial rotation, and lateral flexion corresponding to spine motion was performed [2]. A 7.5 Nm of loading condition was applied to the top surface of L3. And the bottom surface of the sacrum was fixed to the boundary condition.



Figure 1: Finite element models of L3-S1 with different lordosis angle between PLIF segment.

3. Results

After finite element analysis, the range of motion at the adjacent segment to PLIF, and the maximum equivalent stress of the intervertebral disc, endplate, and PLIF cage were compared and analysed. When lordosis angles between fusion segments were 5 degrees, it was confirmed that the range of motion was larger than other models, and the maximum equivalent stress of the intervertebral disc, endplate, and PLIF cage was relatively low.

4. Discussion and Conclusions

In this study, we evaluated the mechanical characteristics of adjacent segments according to the lordosis angle between the fusion segments after PLIF. And if the load on adjacent segments is reduced through the lordosis angle between fused segments, it is thought that adjacent segment disease can be prevented.

5. References

1. Bastian, Leonard et al. European Spine Journal; 10.4:295-300 (2001).
2. Huang et al. PloS one. 2016;11.11:e0166452 (2016).

Acknowledgements:

This work was supported by the National Rese arch Foundation of Korea (NRF) grant funded by the Korea Government (MSIT) (No. NRF-2 022R1F1A1066509; No. NRF-2021R1A2C101 3867; No. NRF-2021R1F1A1064056; No. NR F-2021R1A2B5B01087440).

CMBBE2023
18th International Symposium on Computer Methods in Biomechanics and Biomedical Engineering
3 - 5 May 2023, Paris, France
Arts et Métiers Institute of Technology
Institut de Biomécanique Humaine Georges Charpak
155 boulevard de l'Hôpital 75013 Paris France
www.cmbbe-symposium.com

THE AGEING SPINAL LUMBAR LORDOSIS - EFFECTS ON THE INTERVERTEBRAL DISCS

Sabine Bauer (1), Ivanna Kramer (2)

1. Institute for Computational Visualistics, University of Koblenz, Koblenz, Germany; 2. Institute of Medical Technology and Information Processing, University of Koblenz, Germany

1. Introduction

The alignment of a lumbar spine is usually characterized by lordosis in the sagittal plane. Studies have shown that the lumbar alignment differs from person to person [1]. Until now, just a little is known about how spinopelvic alignment affects the spinal load distribution in general [2]. The effects of the aging lumbar spine and the associated change in the lumbar alignment on the load situation of the spinal structures are almost unknown. Therefore, we developed biomechanical simulation models with age-adjusted lumbar spine curvatures to predict the effects of an aging spine on the intervertebral discs and facet joints.

2. Materials and Methods

Four simulation models were created representing the lumbar spine alignment of the age groups of 40-49-year-old, 50-59-year-old, 60-69-year-old, and over 70 -year-old. The orientation of the vertebrae were taken from [3]. In all models, the structures' biomechanical properties are considered. The upright standing is chosen as the simulation case.

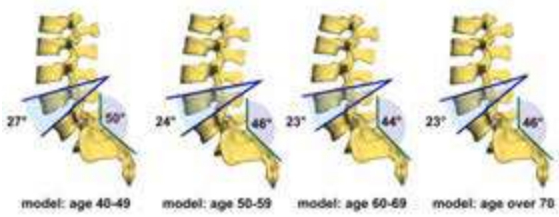

Figure 1: Illustration of the age-dependent vertebral alignments and sacral inclination, shown using the functional unit L5-L4 as an example.

3. Results

The simulation showed that the load was redistributed from the intervertebral discs to the facet joints in the older age groups. In particular, there was a significant increase in facet joint loading in the age group over 70 years (see Figure 2).

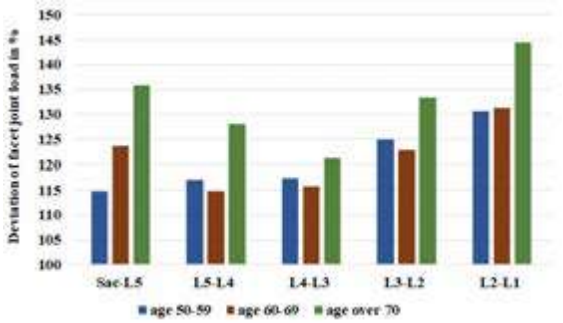

Figure 2: Percentage increase in facet joint loading compared to the loading situation in a 40-49 year old age group.

4. Discussion and Conclusions

The aim of this study is to use the predictive load analyses to derive preventive measures, e.g. to slow down degenerative processes or, in the best case, to avoid them. These findings can also contribute to optimized treatment and rehabilitation of diseases.

In the current model, only the spine's alignment was adapted to the age. However, the aging processes that may occur in the spinal structures, such as in the intervertebral discs or facet joints, are not considered. As a next step, the presented models will be expanded by including further age-specific parameters.

5. References

1. Legaye J. The femoro-sacral posterior angle: an anatomical sagittal pelvic parameter usable with dome-shaped sacrum. Eur Spine J. 2007;16(2): 219-25.
2. Bassani, T, Casaroli, G, Galbusera, F. Dependence of lumbar loads on spinopelvic sagittal alignment: An evaluation based on musculoskeletal modeling. 2019;14(3).
3. Gelb, D. et al. An Analysis of Sagittal Spinal Alignment in 100 Asymptomatic Middle and Older Aged Volunteers. Spine 20(12):1351-1358, June 1995.



Validation of a Lumbar Functional Spine Unit FEM Model

Subin P George (1), Saravana Kumar G (2), Venkatesh K (3)

1. Department of Engineering Design, Indian Institute of Technology Madras, Chennai, India

2. Department of Engineering Design, Indian Institute of Technology Madras, Chennai, India

3. Spinal Disorders and Surgery Unit, Christian Medical College, Vellore, India

1. Introduction

A lumbar functional spine unit (FSU) is the basic motion unit in the whole spine that imparts motion to it. Finite Element Models (FEM) are used to predict the biomechanics of spine when subjected to instrumentations[1]. Here a simplistic FEM of L1L2 spine is constructed in ANSA BETA CAE™ from open-source mesh models and then validated with physiological moment loadings. The purpose of development of this model is to make it amenable for easy morphological operations corresponding to different anthropometric features.

2. Materials and Methods

A lumbar FSU is prepared from a female spine model and meshed with the hexahedral element. Hexahedral and quadrilateral elements were used to define the solid and shell elements for the hard and soft tissue modeling (Fig .1). Non-linear material models were used for the material properties of the soft tissues that deformed in the articulations. The mesh quality of the developed model was ensured for: aspect ratio < 5 [shell], <8 [solid]; skewness < 50; Jacobian < 0.5. The element type and material properties for each component were taken from the literature [2]. The bottom plate of L1 was fixed and the top plate was given moment loading in the sagittal direction.

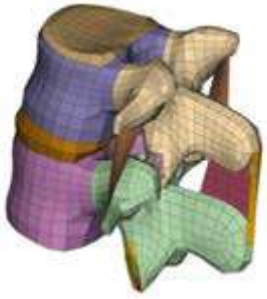

Figure 1 L1L2 FSU model

3. Results

Kinematic output profiles of flexion & extension, Bending & Axial Rotations were generated for the Lumbar FSU for 10 Nm loading (Flexion Extension shown in Fig 2). The results are well agreeing with that of Simulation and Experimental results[2].

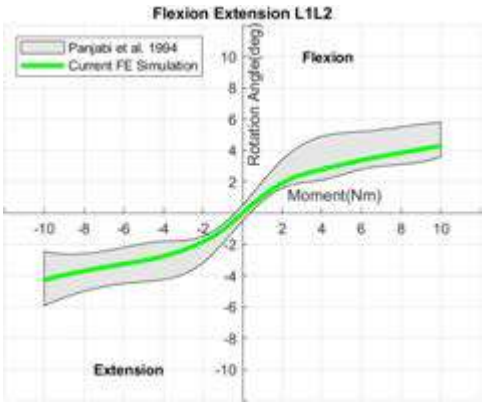

Figure 2 Flexion Extension curves for L1L2 FSU

4. Discussion and Conclusions

Geometric, material and contact non linearities were captured in the developed L1L2 FE model. The initial displacement was high till 2 NM after which it reduce and this is well correlated to the actual response [2]. The non linearity of the facet joints were also captured with a peak contact force of 30 N [3]

5. References

[1] J. D. John, G. S. Kumar, N. Yoganandan, and V. Rajshekhar, "Influence of cervical spine sagittal alignment on range of motion after corpectomy: a finite element study," *Acta Neurochir. (Wien).*, 163(1)251–257 (2021)

[2] S. Umale, N. Yoganandan, and S. N. Kurpad, "Development and validation of osteoligamentous lumbar spine under complex loading conditions: A step towards patient-specific modeling," *J. Mech. Behav. Biomed. Mater.*,110, May, 103898, (2020)

[3] M. Dreischarf *et al.*, "Comparison of eight published static finite element models of the intact lumbar spine: Predictive power of models improves when combined together," *J. Biomech.*, 47(8),1757–1766(2014)

Acknowledgements:
Nil



REVIEWING THEORETICAL AND EXPERIMENTAL METHODS FOR TIME-DELAY ESTIMATION IN BIOMECHANICAL STABILITY

Blandeau Mathias (1), Shokouhyan Seyed Mohammadreza (1), Wallard Laura (1), Barbier Franck (1)

1 : Laboratoire d'Automatique, de Mécanique et d'Informatique industrielles et Humaines (LAMIH UMR CNRS 8201), Université Polytechnique Hauts-De-France, Valenciennes France

1. Introduction

Postural stability, following a pathology or an accident (e.g. spinal cord injury), is one fundamental objective of rehabilitation [1] thus being the subject of numerous modeling and simulation works [2]. Inherent delays and latencies of the nervous system increase the difficulty of stabilizing these models and must therefore be known precisely. Current research papers show great heterogeneity in estimation methods of those delays. This is why a literature review was conducted to better characterize and categorize these methods.

2. Materials and Methods

Following PRISMA recommendations [3], we searched 5 databases (EMBASE, PubMed, Scopus, IEEE and Web of Science) according to a combination of keywords related to latency, biomechanical models, postural control and integration sensory. After duplicate removal and selection was performed on title and abstract, then on full articles. The selected articles were then screened for the type of time delay estimated and the method used to do so.

3. Results

The keyword combination yielded 10915 articles from which 4795 duplicates were removed. Then a title and abstract selection further refined to 59 articles from which 46 articles were kept after full article reading. The vast majority of movements studied concern standing (n=22) or seated (n=20) stability. More than 70% of articles are solely focused on healthy subjects. On the 34 articles using external perturbation for challenging subjects' stability, 24 used unexpected perturbation. All found articles are based on experimental data and half add a theoretical simulation step based on mostly linear models (n=20). In 60% of the articles, the nature of the estimated delay is not clearly defined.

4. Discussion and Conclusions

This review of the literature highlights the lack of homogeneity of scientific work on the estimation of latencies of the nervous system. The biomechanical delay can be separated in three main parts being onset (sensory or muscular), transport and processing [4]. Moreover, the nervous system will react differently to a variability of simulation; whether it is known or not, external (push on the back) or internal (sensory alteration). Hence it is unfortunate to witness so little article explaining the physiological nature of the estimated delay in their works. The use of very different simulated models or the estimation based on experimental data with various methods prevents the good comparison of the estimated results. This field of research would benefit from standardizing its approach in order to improve knowledge and understanding of the underlying phenomena.

5. References

1 D. Gagnon, C. Duclos, P. Desjardins, S. Nadeau, and M. Danakas, J. Biomech., vol. 45, no 8, p. 1554-1558, (2012)
2 M. Blandeau, V. Estrada-Manzo, T. M. Guerra, P. Pudlo, and F. Gabrielli, Eng. Appl. Artif. Intell., vol. 67, p. 381-389, (2018)
3 A. C. Tricco et al., Ann. Intern. Med., vol. 169, no 7, p. 467-473, (2018)
4 A. Vette, K. Masani, J.Y. Kim, M.R. Popovic, Neuromodulation, vol 12, no 1, p 22-32, (2009)

Acknowledgements:

This work is supported by the French Ministry of Higher Education and Research, the National Center for Scientific Research (CNRS)

CMBBE2023
18th International Symposium on Computer Methods in Biomechanics and Biomedical Engineering
3 - 5 May 2023, Paris, France
Arts et Métiers Institute of Technology
Institut de Biomécanique Humaine Georges Charpak
155 boulevard de l'Hôpital 75013 Paris France
www.cmbbe-symposium.com

BIOPHYSICAL HILL-TYPE MODEL OF THE MUSCLE SPINDLE

Pablo FS Chacon (1), Maria Hammer (1,2), Isabell Wochner (1,2), Syn Schmitt (1,2)

1. Institute for Modeling and Simulation of Biomechanical Systems, University of Stuttgart, Germany;
2. Stuttgart Center for Simulation Science, University of Stuttgart, Germany

Correspondence: Pablo FS Chacon, pablo.chacon@imsb.uni-stuttgart.de

1. Introduction

The muscle spindle is considered the main proprioceptor, playing the major role in the sensation of limb position and movement. Even though models of such proprioceptor exist for several years, the gold standard for motor control in biomechanics are still sensors build of homogenized spindle output models. This work establishes a biophysical model of muscle spindle considering the individual characteristics of involved tissue compartments. We hypothesize that each intrafusal fibre of a muscle spindle can be represented by a Hill-type model [1], commonly used for muscles, to predict Ia and II afferent signals.

2. Materials and Methods

The starting point was to convert the established spindle model [2] to a pure Hill-type based model by removing the mass element. In a next step, we replaced the [2] intrafusal fibre model by the Hill-type muscle from [1], creating a new spindle model. A damping element parallel to the contractile element was added in the original [1] muscle model to construct the polar region of the spindle.

3. Results

After initial parameter adaptations in our Hill-type muscle spindle model, the resulting afferent firing rates were consistent with experimental data [3,4] when optimized for individual stretch scenarios (Fig. 1).

4. Discussion and Conclusions

The concept of representing intrafusal fibres using a Hill-type model was investigated before in [2]. However, our work presents a pure Hill-type model, without any mass element, as muscle spindle intrafusal fibres. It also includes non-linear force-length and force-velocity characteristics. Thereby, the current work represents a more biophysical model that accounts for real sarcomere force-length and force-velocity aspects.

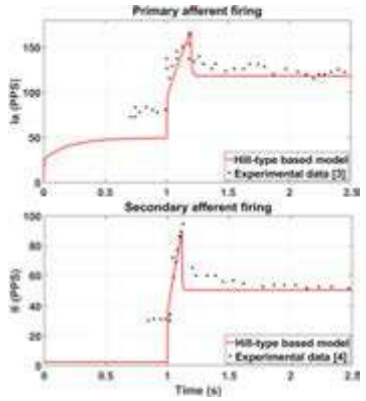

Figure 1: Exemplary comparison of experimentally measured [3,4] and predicted firing rates with our new Hill-type representation of intrafusal fibres.

5. References

1. Haeufle, D et al., Hill-type muscle model with serial damping and eccentric force–velocity relation. *Journal of Biomechanics* (2014).
2. Mileusnic, MP et al., Mathematical models of proprioceptors. I. control and transduction in the muscle spindle. *Journal of Neurophysiology* (2006).
3. Crowe, A et al., The effects of stimulation of static and dynamic fusimotor fibres on the response to stretching of the primary endings of muscle spindles. *The Journal of Physiology* (1964).
4. Matthews, PBC. The response of de-efferented muscle spindle receptors to stretching at different velocities. *Journal of Physiology* (1963).

Acknowledgements:
The authors thank the International Max Planck Research School for Intelligent Systems for supporting us. This work was supported by the Deutsche Forschungsgemeinschaft under Germany's Excellence Strategy - EXC 2075 - 390740016 (SimTech).

CMBBE2023
18th International Symposium on Computer Methods in Biomechanics and Biomedical Engineering
3 - 5 May 2023, Paris, France



Arts et Métiers Institute of Technology
Institut de Biomécanique Humaine Georges Charpak
155 boulevard de l'Hôpital 75013 Paris France
www.cmbbe-symposium.com

CLASSIFICATION OF YOUNG AND OLDER ADULT GAIT USING SINGLE AND MULTISEGMENT FOOT KINEMATIC FEATURES

Victoria Chester (1), Karansinh Padhiar (1), Nayeli Munoz (1), Abirath Raju (1), Deepakraja Rajendran (1), Usha Kuruganti (1), Ashirbad Pradhan (2)

1. Kinesiology, University of New Brunswick, Canada; 2. Engineering, University of Waterloo, Canada

1. Introduction

Currently, age-related changes in foot mechanics are poorly understood. A greater understanding of the natural changes in foot motion is needed to improve our understanding of aging and pathological foot conditions. Existing studies have mainly used single segment foot (SSF) data, while only a few studies have examined more complex multisegment foot (MSF) kinematics [1]. Using these data, machine learning analysis can be used to classify gait patterns of older and younger adults accurately, and also identify the most contributing features. The purpose of this study was to investigate the classification of young vs older adult gait patterns using foot kinematic data (SSF, MSF and planar angles).

2. Materials and Methods

Twenty young participants (10 male, 10 female, mean age 23.75±3.38 years old, mean height 1.71±0.12 m, mean weight 68.26±15.46 kg) and twenty older adults (10 male, 10 female, mean age 72.7±5.56 years old, mean height 1.67±0.09 m, mean weight 80.92±14.13 kg) participated in the study. A 12-camera Vicon T160 motion capture system (Oxford Metrics Group Ltd., UK), sampling at 100 Hz, was used to track 32 reflective markers using a modified version of a 5-segment MSF model used [2]. The MSF features were extracted from the angles between the shank (Sha), calcaneus (Cal), midfoot (Mid), and forefoot (Met) rigid segments, whereas, the SSF features were extracted from the angles between the rigid shank and foot segments. These features included max/min angular values and their timing at key gait events. The MSF, SSF, and planar features, individually and combined, served as input to a support vector machine (SVM) classifier with a radial basis function (RBF) kernel. A wrapper-based sequential forward feature selection algorithm was used for selecting the feature subset that contributed the most to accurate classification of young and older gait patterns.

3. Results

Using a SVM with RBF, the SSF segment demonstrated a classification accuracy of 87.5% (Table 1). Similar results were found for the planar angles. The individual MSF segments gave an average classification accuracy of 87.9%. However, combining all 4 MSF segments improved the accuracy score to 97.2% using 52 features (out of 96). The combination of MSF and SSF resulted in no further increase in classification accuracy with 28 features (out of 120). From among the features, those extracted from the Cal-Mid angles had the highest contribution to the classification.

Table 1: Classification performance evaluation

Segment	Angle	#Features	Accuracy	Precision	Recall	F1
SSF	Sha-Foot	7	87.5	88.6	86.1	87.3
MSF	Cal-Met	8	87.5	88.6	86.1	87.3
	Cal-Mid	14	93.1	91.9	94.4	93.2
	Mid-Met	15	83.3	83.3	83.3	83.3
	Sha-Cal	19	87.5	93.5	80.6	86.6
Cal-Mid + Mid-Met		33	97.2	97.2	97.2	97.2
Cal-Met + Mid-Met + Sha-Cal		14	97.2	100	94.4	97.1
MSF (all combined)		52	97.2	100	94.4	97.1
SSF + MSF		28	97.2	100	94.4	97.1
Planar		16	87.5	91.7	83.3	87.0

4. Discussion and Conclusions

The results suggest that MSF data provides more accurate classification of young vs older gait than SSF alone. Combining SSF and MSF contributed to classification by reducing the number of features considered. Individually, Cal-Mid angles had the highest contribution to the classification. Further research is needed to identify age-related changes in foot/ankle function using SSF and MSF angles.

5. References

1. Buldt et al. (2018). Gait Posture, vol.52, p.56-67.
2. Leardini et al. (2007). Gait Posture, 25, p.453-62.



EMOTIONAL CHALLENGE AS AN EFFECTOR OF THE HUMAN GAIT CYCLE: A MULTI-SIGNAL STUDY

Herbert F. Jelinek [1,2,3], Mary K. Catacutan[1], Deema K. Islayem[1], Sona M. Al Younis[1], Fatima Y. Alshamsi[1], Kinda Khalaf [1,2*]

1. Department of Biomedical Engineering, Khalifa University of Science and Technology, Abu Dhabi, United Arab Emirates; 2. Health Engineering Innovation Center, Khalifa University of Science and Technology, Abu Dhabi, United Arab Emirates; 3. Biotechnology Center, Khalifa University of Science and Technology, Abu Dhabi, United Arab Emirates

1. Introduction

The emotional state of patients has a direct impact on the outcomes of a treatment plan. During rehabilitation, postoperative and post-injury patients often experience depression and anxiety [1]. A negative emotional status often inhibits rehabilitation outcomes, as patients are less likely to adhere to regimens, hence hindering optimal recovery [2]. Few studies have focused on the effect of emotions on balance and gait metrics, such as ground reaction force (GRF) and center of pressure (COP) [3]. In neurorehabilitation, patients must be motivated to progress or recover while using supportive devices. Only one reported study recorded electroencephalography (EEG) and HRV to recognize emotions [4]. There is a lack of studies exploring biomarkers for emotional state classification from biosignals and their correlation to gait and balance parameters that can play a role in posture and gait rehabilitation settings.

2. Materials and Methods

Twenty one healthy subjects were recruited to complete 5 gait cycles performed over multiple in-ground force plates. Pulse rate and force plate data were collected whilst participants were exposed to video clips validated to evoke three mild emotions (neutral, sad, and happy) during walking. The signals were analyzed using time and frequency domain analyses. Statistical analysis included Kruskal Wallis nonparametric and Mann-Whitney *post hoc* tests, and statistically significance was set at $p \leq 0.05$.

3. Results

The time domain feature, PNN50 was found to identify significant differences between a neutral video and happy ($p=0.008$) and sad ($p=0.023$) video representations. The average GRF along the x-axis showed significant changes across emotions ($p=0.0033$), specifically between happy and sad ($p=0.0022$) and happy and neutral ($p=0.014$) states. Similarly, the COP along the x-axis was significantly different between the happy and sad emotional states ($p=0.048$).

4. Discussion and Conclusions

Our findings suggest that gait rehabilitation exercises should include information on the emotional state of the patient, in conjunction with gait parameters, to optimize treatment outcomes. Future work will investigate the effect of emotional states in diverse gait and balance rehabilitation settings using multiple biomechanical measures in order to adapt treatment plans accordingly.

5. References

1. M. Arvinen-Barrow, W. V. Massey, and B. Hemmings, "Role of Sport Medicine Professionals in Addressing Psychosocial Aspects of SportInjury Rehabilitation: Professional Athletes' Views," *Journal of Athletic Training*, vol. 49, pp. 764–772, 12 2014.
2. S. C. M. te Wierike, A. van der Sluis, I. van den Akker-Scheek, M. T. Elferink-Gemser, and C. Visscher, "Psychosocial factors influencing the recovery of athletes with anterior cruciate ligament injury: A systematic review," *Scandinavian Journal of Medicine & Science in Sports*, pp. n/a– n/a, 12 2012.
3. K. L. Schmidt, Z. Ambadar, J. F. Cohn, and L. I. Reed, "Movement Differences between Deliberate and Spontaneous Facial Expressions: Zygomaticus Major Action in Smiling," *Journal of Nonverbal Behavior*, vol. 30, pp. 37–52, 3 2006.
4. E. Tanaka, J.-R. Zhuang, B.-R. Yang, G.-Y. Wu, H. H. Lee, and L. Yuge, "A Walking Assistive Device of the Ankle Joint Motion and the Control Method According to the Emotion Condition," in *2020 IEEE/SICE International Symposium on System Integration (SII)*, pp. 623–627, IEEE, 1 2020.

Acknowledgements:

The authors would like to thank all of the individuals who participated in this experiment for their cooperation during the EEG recording.

CMBBE2023
18th International Symposium on Computer Methods in Biomechanics and Biomedical Engineering
3 - 5 May 2023, Paris, France



Arts et Métiers Institute of Technology
Institut de Biomécanique Humaine Georges Charpak
155 boulevard de l'Hôpital 75013 Paris France
www.cmbbe-symposium.com

EXPLOITING OPEN SYSTEM PERIDYNAMICS FOR NONLOCAL BONE REMODELLING

Emely Schaller (1), Ali Javili (2), Paul Steinmann (1)

1. Institute of Applied Mechanics, Friedrich-Alexander-Universität Erlangen-Nürnberg, Germany
2. Department of Mechanical Engineering, Bilkent University, Turkey

1. Introduction

Peridynamics is a nonlocal continuum theory, where every continuum point is influenced by its finite-sized neighbourhood. In contrast to classical continuum mechanics, the governing equations are obtained by integro-differential terms instead of divergence terms, allowing to easily model discontinuities. For this reason, it is widely used in fracture mechanics and related fields. However, its application has extended significantly in recent years to capture nonlocal material behaviour, even in fields unrelated to fracture mechanics. Our aim is to exploit the peridynamic theory for biomechanical processes, in particular for the complex process of bone remodelling.

2. Materials and Methods

Bone remodelling describes the ability of bone tissue to adapt its external and mainly internal structure to external biological and mechanical stimuli. To model and investigate the influence of external mechanical loading on the bone density evolution with a peridynamic approach, we propose in [1], for the first time, a thermodynamically consistent formulation for open system (continuum-kinematics-inspired) peridynamics by exploiting the local evolution equations of Kuhl and Steinmann [2]. In open systems, mass can no longer be considered a conservative property as in closed systems, which is why the balance of mass in [1] is governed by a mass source.

In our peridynamic formulation for nonlocal bone remodelling [1,3], we maintain the mass source function of [2] that gets its nonlocal characteristic from the peridynamic energy density. To justify our formulation for nonlocal bone remodelling and to demonstrate the influence of nonlocality, we employ our peridynamic model for a unit square and a proximal femur example [3]. We compare our peridynamic simulations with local finite element simulations to verify convergence with diminishing neighbourhood size.

3. Results

The results of our peridynamic simulations highlight the influence of nonlocality by increasing the neighbourhood size and show a good agreement with the local finite element simulations, when a small neighbourhood is used compared to the domain size.

4. Conclusions

We propose in [1] a thermodynamically consistent framework for open system peridynamics that can be used to study and better understand biomechanical and chemomechanical processes. In [3], we show that our peridynamic model for open systems can be used to model and investigate nonlocal material behaviour during the complex bone remodelling process, where the bone density changes in time due to a nonlocal mass source.

5. References

1. Schaller E, Javili A, Steinmann P. Open system peridynamics. *Continuum Mech. Thermodyn*; **34**: 1125–1141 (2022). https://doi.org/10.1007/s00161-022-01105-8
2. Kuhl E and Steinmann P. Theory and numerics of geometrically non-linear open system mechanics. *Int. J. Numer. Meth. Engng*; **58**: 1593-1615 (2003). https://doi.org/10.1002/nme.827
3. Schaller E et al. A peridynamic formulation for nonlocal bone remodelling. *Comput. Methods Biomech. Biomed. Engin.* (2022). https://doi.org/10.1080/10255842.2022.2039641

CMBBE2023
18th International Symposium on Computer Methods in Biomechanics and Biomedical Engineering
3 - 5 May 2023, Paris, France
Arts et Métiers Institute of Technology
Institut de Biomécanique Humaine Georges Charpak
155 boulevard de l'Hôpital 75013 Paris France
www.cmbbe-symposium.com

A COMPARISON OF INJURY RISK BETWEEN 44 MM AND 58 MM CLAY-DISPLACEMENT FOR BEHIND ARMOR BLUNT TRAUMA

Lance Frazer (1), Vivek Kote (1), Matt Davis (2), Dale Bass (3), Tim Bentley (4), Daniel P. Nicolella (1)

1. Southwest Research Institute, USA; 2. Elemance LLC, USA; 3. Duke University, USA; 4. Office of Naval Research, USA

1. Introduction

Body armor has historically been assessed by measuring the permanent deformation in a block of Roma Plastilina no. 1 clay with the armor mounted in front of it. However, this standard poorly correlates to specific behind armor blunt trauma (BABT) injuries in humans [1]. FE models may provide a better alternative. In this study, the I-PREDICT Human Body Model (HBM) was used to predict BABT injury given a liver impact.

2. Materials and Methods

An indentor has been developed to simulate the backface deformation in a BABT event [2]. Clay indentation tests were performed by propelling the indentor with high-pressure helium gas using NIJ 0101.06 standards for Roma Plastilina no. 1 clay preparation and ballistic testing. The kinetic energy of each shot was calculated using the velocity obtained from high-speed camera images and the mass of the indentor. Kinetic energies that resulted in 44 mm and 58 mm of permanent clay deformation were used as liver impact boundary conditions to the I-PREDICT HBM.

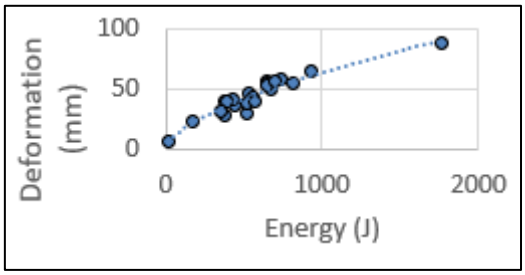

Figure 1: Deformation vs. Energy for the experimental clay indentation impacts.

The analysis was performed probabilistically with material parameters for anatomical tissues prescribed as random variables according to reported uncertainty and variability. Military functional incapacitation scores (MFIS) were calculated using published injury criteria and MFIS correlates for the liver and ribs.

3. Results

Both 44 mm and 58 mm clay-displacement-equivalent impacts resulted in significant injury with a 44 mm displacement predicted to cause *at least* an MFIS 2 injury in the ribs with 50% probability and an MFIS 4 injury in the liver with 80% probability (Figure 2).

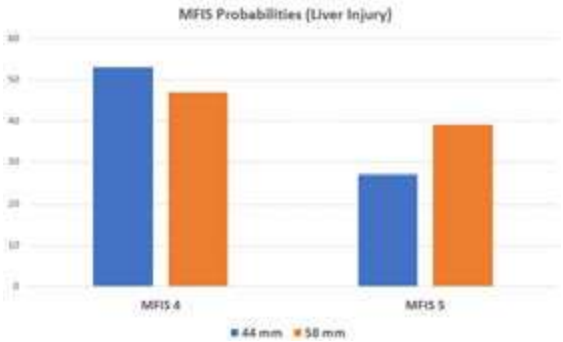

Figure 2: Deformation vs. Energy for the experimental clay indentation impacts.

4. Discussion and Conclusions

The current 44 mm (and proposed 58 mm) clay displacement standard may not be a suitable standard for assessing body armor. Validated FE models provide an alternative means for testing.

5. References

1. U.S DoJ. NIJ Standard-0101.06 (2008).
2. Op 't Eynde J. PLoS One. 2020;7(9):e44281 (2020).

Acknowledgements:

The authors would like to thank the Office of Naval Research for providing financial support to this project.

CMBBE2023
18th International Symposium on Computer Methods in Biomechanics and Biomedical Engineering
3 - 5 May 2023, Paris, France



Arts et Métiers Institute of Technology
Institut de Biomécanique Humaine Georges Charpak
155 boulevard de l'Hôpital 75013 Paris France
www.cmbbe-symposium.com

EXPERIMENT AND SIMULATION STUDY OF THE ENERGY ABSORBTION IN BIOMIMETIC SCAFFOLD LATTICES

Mahtab Vafaeefar (1), Kevin M. Moerman (2), Ted J. Vaughan (1)

1. Biomedical Engineering, University of Galway, Ireland; 2. Mechanical Engineering, University of Galway, Ireland

1. Introduction

Architecture materials have been recently attracting attention due to their high stiffness-to-density ratio, tailored bio/mechanical properties, and high energy absorption [1,2]. In this work, the effect of structure and volume fraction, as morphological factors, on the energy absorption of two lattices as biomimetic scaffolds is studied through experimental and numerical approaches.

2. Materials and Methods

The ABAQUS/Explicit finite element software was used to simulate the compression behaviour and energy absorption characteristics for the gyroid and dual-lattice structures. Models were meshed using linear tetrahedral (C3D4) elements and the material properties was according to Table 1. Stress-strain responses and energy absorption characteristics of the same volume fraction of each structure was analysed under large compression deformations (up to 85%). The energy absorption per unit volume, W, for a lattice structure under compression with the strain up to ε, is calculated by Eq. 1 [3].

$$W = \int_0^{\varepsilon} \sigma(\varepsilon) d\varepsilon \qquad (1)$$

Experimental tests were conducted to verify and validate the explicit FEA results. In the experiment phase, samples were manufactured using a FormLab3 elastic resin printer (SLA technology), then washed and cured to achieve the maximum material properties. Samples were testing under uniaxial compressed using a Zwick mechanical tester (Zwick Roell, GmbH & Co., Germany) as shown in Fig. 1.

Table 1: Fitted material properties of E 50A resin from the standard tensile test (ASTM D638).

Physical and mechanical properties			
	Elastic Material		
Material	E	ν	Density
Elastic 50A	2.4 (Mpa)	0.45	1.20 g/cm^3

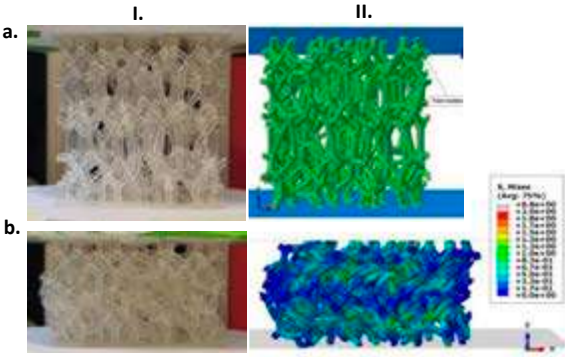

Figure 1: 3D-printed dual-lattice sample (I), and its FEA model (II), in their initial state (a) and 50% deformation (b).

3. Results

Our simulation results show good agreement with the experimental data. Based on the stress strain results in Fig. 2, the dual-lattice structure showed an initial linear region, followed by a buckling, then plateau region as components began to touch each other and finally followed by densification region. On the other hand, the gyroid structure showed more linear behaviour. Based on the explicit models, the dual-lattice structure has higher energy absorption per unit volume.

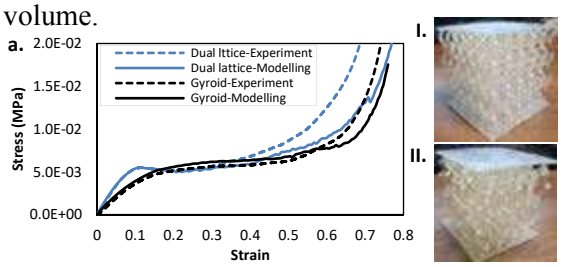

Figure 2: Stress strain (a) results for the gyroid (I) and dual-lattice (II) structures, volume fraction of 10%.

4. Discussion and Conclusions

These structures can be used to study the influence of morphological factors, specifically volume fraction on energy absorption characteristics, as biomimetic scaffolds.

5. References

1. Rahman, H., et al., Materials; 14:1366 (2021).
2. Zhang, C., et al., Crystals; 12:408 (2022).
3. Habib, F.N, et al., Materials and Design; 155:86-98 (2018).

Acknowledgements:
Funding provided by the European Research Council under GA No. 804108.



NEGATIVE EFFECTS ON PEDIATRIC HEARING DUE TO TYMPANOSTOMY TUBES

Razvan Rusovici (1), Manuel Bucheli (2)

1. Florida Institute of Technology, USA; 2. Florida Institute of Technology, USA;

1. Introduction

Recurrent ear infections in the middle ear (otitis media) are commonly treated using either medical or surgical therapies. Surgical therapy often comes in the form of tympanostomy, which is the placement of a tube through an incision in the tympanic membrane (TM), which helps pus drainage from the middle ear to the external ear canal. This treatment relieves middle ear pressure and infectious bacterial presence but creates a series of negative effects, some of which are studied in the current research. The loss of stiffness, due to the surgical incision, coupled with the extra tube mass leads to a significant change in natural frequencies of the membrane and hence in the transmissibility of the incoming sound.

2. Materials and Methods

The research employed structural and acoustic finite element models (FEM) calibrated on existing literature. Structural modal analysis was performed first and showed significant changes in TM natural frequencies. Then, acoustic-structural coupled models (Figure 1) were used to obtain harmonic responses of the healthy vs. tympanostomy TM to an input 80 dB SPL sound.

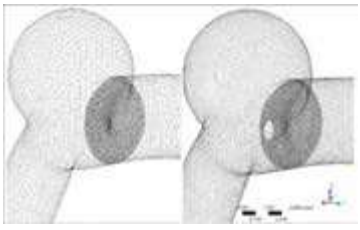

Figure 1: FEM mesh for coupled acoustic-structural studies

The models employed a simplified model of the TM and middle ear by imparting a prestrain to the TM without modelling the ossicles involved in sound transmission [1]. The tubes were modelled as distributed masses around the circular incision. Material properties were gathered from literature [1].

3. Results

Figure 2 shows the shift in the first two natural frequency of the TM due to tube placement.

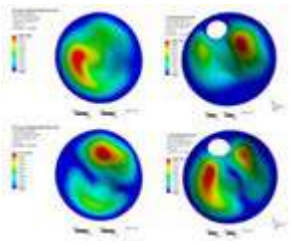

Figure 2: Change in first two natural frequencies of the TM (right column shows TM with tubes)

Figure 3 shows the results of a harmonic analysis on a surgically treated vs normal paediatric TM showing changes in peak frequency and transmitted sound levels caused by an incoming 80dB SP input.

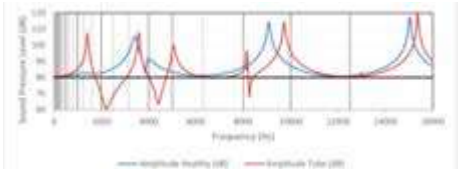

Figure 3: Change in transmitted SPL levels between healthy and treated TM

4. Discussion and Conclusions

The research performed shows that hearing is impaired in pediatric patients due to lower TM response to external sound excitation and the corresponding frequency shift of TM natural frequencies from the consonant hearing range (approximately 2-4 kHz) to lower frequency ranges.

5. References

1. Aernouts J et al.. Hear Res. 290(1–2):45–54. doi:10.1016/j.heares.2012.05.001. (2012).

CMBBE2023
18th International Symposium on Computer Methods in Biomechanics and Biomedical Engineering
3 - 5 May 2023, Paris, France
Arts et Métiers Institute of Technology
Institut de Biomécanique Humaine Georges Charpak
155 boulevard de l'Hôpital 75013 Paris France
www.cmbbe-symposium.com

THE EFFECT OF CORTEX THICKNESS ON HUMERUS BIOMECHANICS: A FINITE ELEMENT ANALYSIS

Hassan Sarailoo (1), Habiba Bougherara (1)

1. Department of Mechanical and Industrial Engineering, Toronto Metropolitan University, Canada

1. Introduction

In adults, proximal humerus fractures are the third most common osteoporotic fractures after the femur and the distal radius [1]. However, there is still a lack of research on the effects of cortical wall thickness on the biomechanics of the humerus bone. Therefore, the present study intends to analyse the biomechanical behaviour of the humerus under transverse loading, considering the effect of mesh quality on the obtained results.

2. Materials and Methods

The 3D model of the humerus bone is constructed from CT scan images using Materialise Mimics software and is meshed by tetrahedral elements using Materialise 3-matic software (Fig.1). The bone consists of cortical (E=13.4 GPa, υ=0.3) and cancellous (E=2 GPa, υ=0.3) sections, with different material properties [12]. To decide which element belongs to cortical or cancellous bone, the Hounsfield Unit (HU) from CT scan images is utilized. First, a mesh sensitivity analysis was performed to study the effects of mesh size and element type (linear 4-node vs non-liner 10-node tetrahedral) on lateral stiffness of the bone. Then, different HU values were used to study the effects of cortical wall thickness (t) to bone diameter (D) on lateral stiffness.

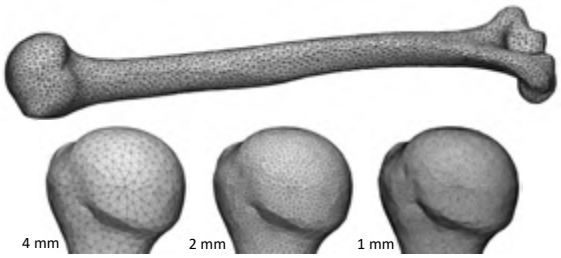

Figure 1: 3D model of the humerus bone with 4 mm meshes (top), and different mesh sizes (bottom)

3. Results

FEA results suggest that a mesh size of 1 mm and 4 mm for linear and non-linear elements, respectively; with less mesh-size sensitivity for non-linear element. To study the effects of t/D on lateral stiffness, 1 mm non-linear elements was utilized. The HU value method resulted in t/D ratios within the range of 0.3 to 1. The FE-generated points for lateral stiffness versus t/D is well fitted with a power function curve with R^2=0.97 (Fig. 2).

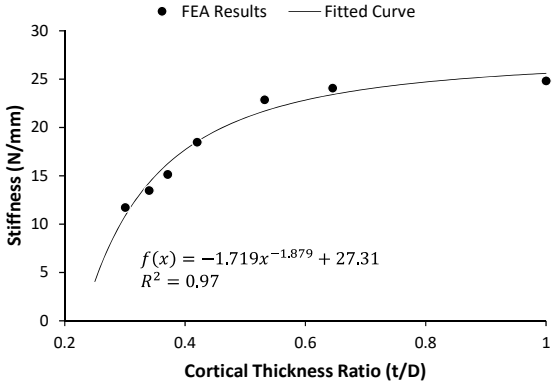

Figure 2: The effect of cortical wall thickness on lateral stiffness

4. Discussion and Conclusions

The present study indicates the minimum mesh size required to achieve mesh size independent results from FEM simulation using linear and non-linear tetrahedral elements. Moreover, it describes a novel approach to modify the wall thickness of a bone model obtained from CT images to simulate the effects of osteoporosis on the cortex wall thickness and lateral stiffness.

5. References

1. Patel, AH., et al., JSES international 6.1 (2022): 137-143.
2. He Y et al., Medicine (Baltimore). 2015; 94(41):e1775 (2015).

Acknowledgements:
"The image datasets used in this experiment were from the Laboratory of Human Anatomy and Embryology, University of Brussels (ULB), Belgium".

CMBBE2023
18th International Symposium on Computer Methods in Biomechanics and Biomedical Engineering
3 - 5 May 2023, Paris, France



Arts et Métiers Institute of Technology
Institut de Biomécanique Humaine Georges Charpak
155 boulevard de l'Hôpital 75013 Paris France
www.cmbbe-symposium.com

THE EFFECT OF VACUUM EXTRACTORS WITH DIFFERENT THICKNESS DURING DELIVERY

Kuo-Chih Su (1), Kuo-Min Su (2)

1. Taichung Veterans General Hospital, Taiwan; 2. National Defense Medical Center, Taiwan;

1. Introduction

Vacuum extractor is commonly used in surgical instruments during delivery, although many studies have carried out biomechanical analysis of vacuum extractors, but at present there is no research on the thickness size of the vacuum extractors biomechanical assessment. Thus, the effects of the vacuum extractors of different thickens on the hemispherical ball were compared through finite element analysis. The results can provide reference for medical device designers and obstetricians to improve the quality of delivery and reduce the incidence of maternal and neonatal complications.

2. Materials and Methods

These finite element vacuum extractor models are mainly hemispherical in design, with a diameter of 70 mm and thickness of 1 mm, 2 mm and 3 mm respectively (Fig. 1). The vacuum extractors were applied separately on the hemispherical ball. Fig. 2 shows the boundary and load conditions of this study [1]. This study mainly uses the finite element analysis software ANSYS Workbench for analysis.

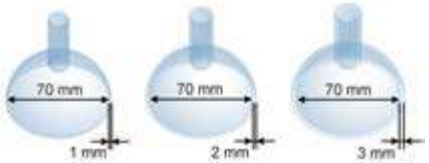

Figure 1: Vacuum extractor models with different thicknesses.

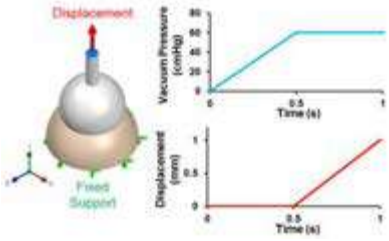

Figure 2: Boundary and load conditions.

The structure analyzed in this study is mainly divided into vacuum extractor (silicone rubber) and hemispherical ball (scalp and skull). The main observation indicators are reaction force at the fixed end of the hemispherical ball and von Mises stress on the skull structure of hemispherical ball.

3. Results

Fig.3 shows the reaction force of vacuum extractor with different thickness at the fixed end of the hemispherical ball.

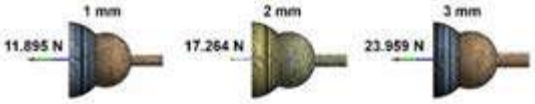

Figure 3: The reaction force at the fixed end of the hemispherical ball.

Fig. 4 shows the von Mises stress distribution of vacuum extractor acting on the skull of the hemispherical ball.

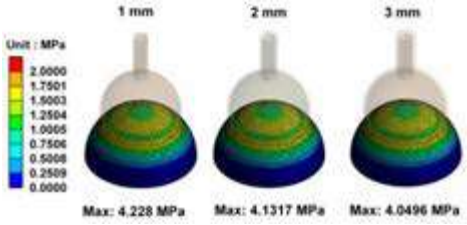

Figure 4: The von Mises stress distribution on the skull of the hemispherical ball.

4. Discussion and Conclusions

The result shows that the greater the thickness of the vacuum extractor used, the greater the reaction force of the fixed end of the hemispherical ball, and the thinner the vacuum extractor used, the higher the von Mises stress on the skull of the hemispherical ball.

5. References

1. Huang CY et al., Polymers. 2022, 14(4):723 (2022).

Acknowledgements:

We would like to thank the National Science and Technology Council of Taiwan (110-2221-E-075A-001, 111-2221-E-075A-002 and 111-2314-B-075A-005-1)

CMBBE2023
18th International Symposium on Computer Methods in Biomechanics and Biomedical Engineering
3 - 5 May 2023, Paris, France



Arts et Métiers Institute of Technology
Institut de Biomécanique Humaine Georges Charpak
155 boulevard de l'Hôpital 75013 Paris France
www.cmbbe-symposium.com

UNCERTAINTY QUANTIFICATION IN PERSONALIZED PULMONARY MECHANICS

Alice Peyraut (1, 2), Martin Genet (1, 2)

1. Laboratoire de Mécanique des Solides, École Polytechnique/IPP/CNRS, France;
2. Équipe MΞDISIM, INRIA, France

1. Introduction

Idiopathic Pulmonary Fibrosis (IPF) is an interstitial lung disease whose mechanisms of evolution are poorly understood, making it difficult to diagnose and treat. The development of a physical model of the lungs, able to integrate patient data, could prove useful for the investigation of IPF and provide doctors with an efficient tool for prognosis and diagnosis.

2. Materials and Methods

This work is based on the model of [1], and the associated personalization pipeline of [2]. One of the main challenges of the development of a personalized model is to formulate an appropriate material law representing accurately the constitutive behavior of the lungs. The constants involved in this law being highly patient-dependent, the question of their actual identifiability based on clinical data is central for the development of our personalized lung model. We therefore developed a statistical pipeline to perform a quantitative study of the identifiability of those material constants.

This pipeline relies on the construction of a cost function, measuring the difference between a synthetic displacement field (obtained with the model run with reference parameters values, to which random Gaussian noise is added) and the displacement field obtained with the model for given parameter values. The estimation is then performed by optimizing the cost function, here using the standard direct search Nelder-Mead method, starting from a random value. The optimization is performed for many realizations of noise, until convergence of the obtained distribution.

3. Results

Figure 1 illustrates our method on a simple spring under tension, where the estimated parameter is the spring stiffness—a highly identifiable problem. For any level of noise, our method provides the estimation error for the stiffness parameter: for large SNR, the optimization always converges toward the exact parameter value; whereas for small SNR, the obtained parameters are far away from the ground truth. Thus, our pipeline allows to quantify the identifiability of the different parameters depending on the noise present on the measures and to estimate the error performed during the estimation process.

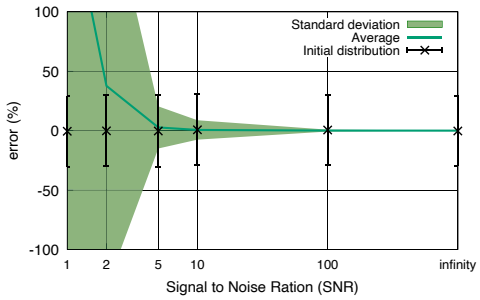

Figure 1: Distribution of the estimation error for the stiffness parameter as a function of SNR.

4. Discussion and Conclusions

Our results illustrate that the pipeline we developed can be used as a tool to improve the estimation process, and therefore our personalized lung model.

5. References

1. Patte C., Genet M., Chapelle D., Biomech. Model. Mechanobiol., 21, 2022.
2. Patte C., Brillet P.-Y., Fetita C., Gille T., Bernaudin J.-F., Nunes H., Chapelle D., Genet M., ASME J. Biomech. Eng., 144(9), 2022.

Acknowledgements:
The authors would like to thank the French National Research Agency (ANR) for providing financial support to this project (Grant no: ANR-19-CE45-0007).



PATIENT SPECIFIC SIMULATION OF UPPER AIRWAY COLLAPSE: GEOMETRY VS SOFT TISSUE STIFFNESS.

Venkat Ayyalasomayajula (1), Bjørn Skallerud (1)

1. Department of Structural Engineering, Norwegian University of Science and Technology, Trondheim, Norway.

1. Introduction

Obstructive sleep apnea (OSA) affects a large percentage of the population and is increasingly recognized as a major global health problem. Several surgical procedures exist, but their efficacy remains moderate with significant uncertainty [1]. In this study, we evaluate the influence of geometry and the mechanics of the tissues in the upper airway based on numerical simulations which could improve surgical decision making.

2. Materials and Methods

Upper airway tissues (pharyngeal wall, soft palate, tongue along with genioglossal muscle) are segmented from six patients' CT scans, approved by the Norwegian Regional Committee for Medical Research Ethics (REK). The tissue geometries are subsequently meshed in ICEM CFD and imported to abaqus for numerical simulations. Non-linear isotropic hyperelastic material models were used for all the tissues based on mechanical tests performed on bovine samples. The posterior surface of the pharyngeal wall, the anterior surfaces of the tongue and soft-palate were fixed to mimic in-vivo conditions. A ramp pressure loading was applied on the interior surfaces uniformly to simulate breathing. Figure 1 shows the image segmentation process, the tissues segmented, applied loading and boundary conditions, and an illustration of stress contours in the finite element simulation. The minimal airway space was computed for each patient to evaluate the correlation with critical airway closing pressure. Similarly, the effect of material degradation is checked by softening and stiffening the base material parameters. The skeletal muscle activation in the tongue and genioglossal muscle is not included in this study.

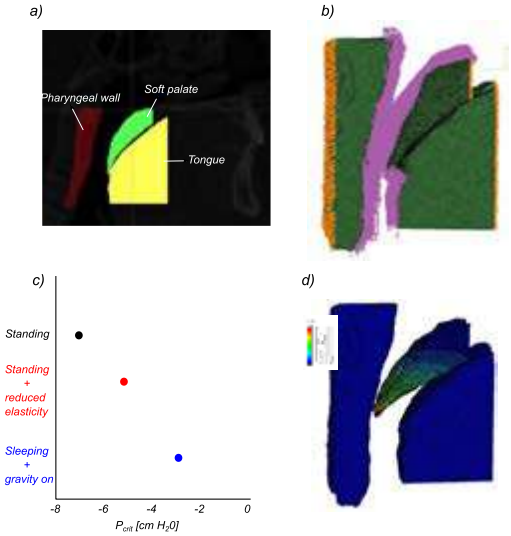

Figure 1 a) Segmented tissue regions in the CT scan images; b) Boundary conditions used in the finite element simulations; c) Pcrit obtained for different scenarios; d) An illustration of displacement contours in the model at airway closure.

3. Results

Preliminary results show that a 25 % reduction in soft tissue elasticity increased critical pressure by 15%, indicating an easier collapse as seen in figure 1c. The tongue undergoes significant displacement while sleeping, further increasing the collapsibility the response of the airway.

4. Discussion

Geometry of the upper airway was shown previously to influence the closing pressure. The aim of this paper is to categorically determine the contribution of geometry, passive mechanical properties, and muscle activation on upper airway collapsibility.

4. References

[1] Sher, Aaron E., Kenneth B. Schechtman, and Jay F. Piccirillo. "The efficacy of surgical modifications of the upper airway in adults with obstructive sleep apnea syndrome." *Sleep* 19.2 (1996): 156-177.

CMBBE2023
18th International Symposium on Computer Methods in Biomechanics and Biomedical Engineering
3 - 5 May 2023, Paris, France
Arts et Métiers Institute of Technology
Institut de Biomécanique Humaine Georges Charpak
155 boulevard de l'Hôpital 75013 Paris France
www.cmbbe-symposium.com

EVALUATION OF AIRFLOW CHANGES IN TRACHEA ACCORDING TO LEFT UPPER LOBECTOMY TYPES BASED ON CFD

Minsu Kim (1), Soojin Lee (2), Hyo Yeong Ahn (2), Chiseung Lee (1)

1. Pusan National University, South Korea 2. Pusan National University Hospital, South Korea

1. Introduction

The left upper lobectomy is an operation to resect the largest lobe of the lung. As the remaining lung expands after surgery, it induces changes in the shape of the bronchi. As a result of comparing the preoperative CT image with the postoperative CT image of the airway, the greatest change in shape was confirmed in the length, curvature, and cross-sectional area of the main bronchus [1]. Changes in curvature and cross-sectional area are caused by kinking of the main bronchus as the lung expands.

2. Materials and Methods

The changes in airflow were evaluated through computational fluid dynamics analysis by 3D modeling of the geometrical changes of the bronchi before and after surgery in various patients. Evaluation factors include the preservation or dissection of the pulmonary ligaments, the length of the main bronchus, and the volume of the left upper lobe. As for the operation method, the dissection or preservation of the pulmonary ligament covering the bronchi were compared and analyzed [2]. The anatomical characteristics of the patients differ from person to person in the size of the left upper lobe and the length of the main bronchus. Therefore, the main bronchus length and the volume of the left upper lobe were analyzed as factors.



Figure 1: 3D Modeling of the Bronchi.

Computational fluid dynamics simulation was performed by extracting a 3D model of the bronchi from each patient's CT image and simulating FEV1, a lung function measurement method. The anatomical characteristics of each patient were identified and analyzed by classifying each case to be compared by factor.

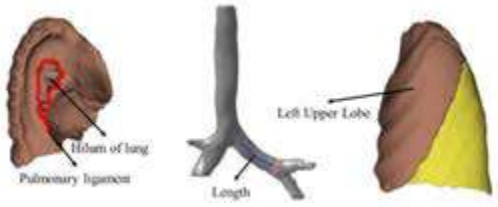

Figure 2: Factors of the Simulation.

3. Results

As a result of the simulation, it was confirmed that airflow flowed well in the change model in which kinking occurred less in the bent part of the main bronchus, and kinking was confirmed in the model with large upper lobe volume and dissected pulmonary ligaments

4. Discussion and Conclusions

Because the geometric changes depending on the left upper lobe volume and the length of the left main bronchus, it is recommended to determine pulmonary ligament dissection according to the patient's anatomical characteristics.

5. References

1. Aliboni, L., Tullio, M., Pennati, F., Lomauro, A., Carrinola, R., Carrafiello, G., ... & Aliverti, A. Scientific reports, 12(1), 1-13(2022).
2. Moon, D. H., Park, C. H., Jung, J. H., Kim, T. H., Haam, S. J., & Lee, S. Journal of Clinical Medicine, 10(18), 4033(2021).

Acknowledgements:

This work was supported by the National Rese arch Foundation of Korea (NRF) grant funded by the Korea Government (MSIT) (No. NRF-2 022R1F1A1066509; No. NRF-2020R1C1C100 5004).



DIGITAL TWINS OF BREAST TUMOURS FOR PREDICTING THE OUTCOME OF NEOADJUVANT CHEMOTHERAPY

Rose Collet (1,2), David Buckley (2,3), Zeike Taylor (2)

1. Centre for Doctoral Training in Fluid Dynamics, University of Leeds, UK;
2. Centre for Computational Imaging and Simulation Technologies in Biomedicine, University of Leeds, UK;
3. Biomedical Imaging, University of Leeds, UK

scrmc@leeds.ac.uk, Sir William Henry Bragg Building, Woodhouse Lane, LS2 9BW Leeds

1. Introduction

Neoadjuvant chemotherapy (NACT) is a treatment option for patients with locally advanced breast cancer. However, only 39% of patients achieve pathological complete response and up to 12% experience no response at all. Non-responsive patients suffer side-effects of NACT without reaping benefits. There is a need to identify non-responsive tumours as early as possible, enabling clinicians to discontinue the unsuccessful NACT and proceed with alternative treatment. For this purpose, we use digital twins: virtual replicates of a patient's tumour cellularity, which can be progressed in time, and in sync with image-based measurements, to predict evolution under NACT.

2. Materials and Methods

Digital twins are created using a mechanically-coupled reaction diffusion (MC-RD) model of tumour growth and proliferation [1] personalised with data from magnetic resonance imaging (MRI) in a process inspired by [2]. We have implemented this model in FEniCS [3], an open-source platform for solving partial differential equations.

We use diffusion-weighted (DW-) and dynamic contrast-enhanced (DCE-) MRI from the CHERNAC study [4] acquired for 37 patients before, during and after NACT. The DCE data is used to identify the tumour, fibroglandular and adipose tissues. This allows the inhibitive effect of surrounding tissue stiffness on tumour cell diffusion to be accounted for. The DW-MRI returns a measure of the apparent diffusion coefficient (ADC) of water in the tumour used to estimate cellularity. Initial tumour cellularity calculated in this manner is used to calibrate the model, and return personalised coefficients (tumour cell proliferation rate and diffusion coefficient in the absence of stress) that are used in its forward evaluation.

3. Results

This process is applied to several patients from the CHERNAC study to predict their tumour response to NACT according to the MC-RD. Model outputs are compared to images acquired after the completion of NACT. By extending to a larger cohort of patients undergoing more diverse NACT regimens, potential limitations of the underlying model can be identified.

4. References

1. Weis JA et al., Cancer Research. 75(22):4697-4707 (2015).
2. Jarrett A et al., Phys Med Biol. 63(10):105015, 5 (2018).
3. Alnaes M et al., Arch Num Soft 3 (2015).
4. Stevens W et al., Br J Radiol, 94:20201396 (2021).

Acknowledgements:
Financial support of the EPSRC (EP/S022732/1) is gratefully acknowledged.

CMBBE2023
18th International Symposium on Computer Methods in Biomechanics and Biomedical Engineering
3 - 5 May 2023, Paris, France
Arts et Métiers Institute of Technology
Institut de Biomécanique Humaine Georges Charpak
155 boulevard de l'Hôpital 75013 Paris France
www.cmbbe-symposium.com

SYSTEM BIOLOGY MEETS SINGLE-CELL MECHANOBIOLOGY: THE CASE OF LAMIN-A TURNOVER INHIBITION IN SUSPENDED CELLS

Maria Isabella Maremonti (1)* and Filippo Causa (1)

1. Interdisciplinary Research Centre on Biomaterials (CRIB) and Department of Chemical, Materials and Production Engineering of the University of Naples Federico II, Italy

*Corresponding author: Ph.D. Maria Isabella Maremonti, mariaisabella.maremonti@unina.it.

1. Introduction

The ability of cells to perform mechanosensing processes mainly relies on the cell nucleus with the related changes in envelope composition, principally constituted by the Lamin-A (Lmn-A) protein. Lmn-A provides structural support and governs nuclear deformability and fragility [1,2]. In general, its own phosphorylation promotes disassembly and turnover of the protein, with an inverse relationship respect to an increasing matrix stiffness. Particularly, from the solution of a single mathematical module modelled by system mechanobiological approaches, a power-law variation of the Lmn-A can be written as function of the rigidity of the substrate where cells are placed [1,3].

Here, we show that, regardless the formation of well-structured cytoskeletons, cells subjected to in-flow compressive stresses [4] are able to inhibit the degradation of Lmn-A, which positively regulates in turn its own gene expression.

2. Materials and Methods

Lmn-A levels were measured after in-flow compression by fluorescence intensities from confocal images (Figure 1a). A feedback-based gene circuit for Lmn-A expression [3] was employed to describe the Lmn-A scaling with the in-flow compression (Figure 1b). The used equations are [3]:

$$\frac{dm}{dt} = aP - bm, \qquad (1)$$

$$\frac{dP}{dt} = gm - k\frac{P^2}{S^2+P^2} \text{ where } S \propto Stress^n \qquad (2)$$

3. Results

We show how a single module feedback gene circuit is able to quantify the cell specific Lmn-A level scaling with respect to applied in-flow compressive stresses. In fact, after increasing in-flow compression, we verified that cells are characterized by enhanced levels of Lmn-A protein coupled with more rigid nuclei. Moreover, we show that such mechanosensitive Lmn-A changes strictly correlate with the cell line, discerning different power-law indices depending on the cell state.

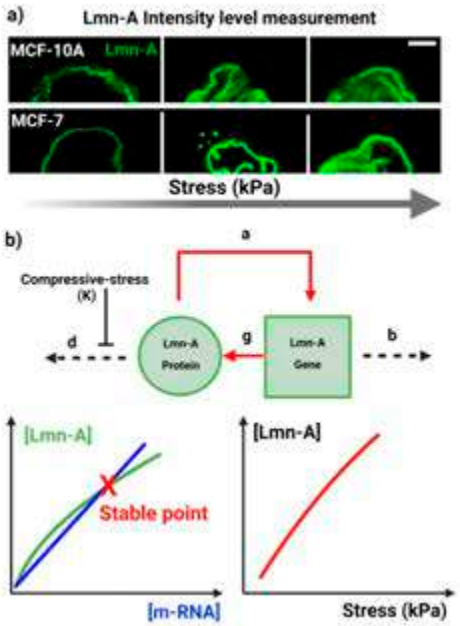

Figure 1. Lmn-A protein level scales with applied in-flow compressive forces. a) Confocal images of Lmn-A for MCF-10 (healthy cells) and MCF-7 (low-invasive cancer cells) subjected to variable levels of compression. A protein signal accumulation is revealed by increasing the applied stress. b) The Lmn-A intensity values have been collected and reported with respect to the applied stresses verifying that such reciprocal variations agree with the stability conditions (red curve) described by the single-module gene circuit model. Scale bar 5 μm.

4. References

1. Andreu I. et al., Nat. Commun., 12, 4229, 2021.
2. Davidson P.M. et al., Trends Cell Biol. 24, 247-256, 2014.
3. Swift J. et al., Science 341, 1240104, 2013.
4. Maremonti M.I. et al., J. R. Soc. Interface 19, 20210880, 2022.

CMBBE2023
18th International Symposium on Computer Methods in Biomechanics and Biomedical Engineering
3 - 5 May 2023, Paris, France
Arts et Métiers Institute of Technology
Institut de Biomécanique Humaine Georges Charpak
155 boulevard de l'Hôpital 75013 Paris France
www.cmbbe-symposium.com

SCAFFOLD PROPERTIES ON CELLULAR LOADING IN DENTAL RESTORATIONS: A MULTISCALE MODELLING APPROACH

Evangelos Karatsis (1), Livia Emmanuela Baksiova (1), Yvoni Kirmanidou (2), Leonidas Spyrou (3), Lambros Papadakis (2), Konstantinos Michalakis (4), Alexander Tsouknidas (2,4)*

1. BETA CAE Systems, Switzerland; 2. Department of Mechanical Engineering, University of Western Macedonia, Greece; 3. Centre for Research & Technology, Hellas, Greece; 4. Department of Restorative Sciences and Biomaterials, Boston University, USA
**Corresponding author: 72 East Concord Street, Room E-430, Boston, MA 02118, atsouk@bu.edu*

1. Introduction

Despite dental implants being a successful treatment modality, various pathologic conditions lead to large bone defects (e.g. jaw atrophy) and thus, insufficient bone volume for their placement [1]. In such cases, bone augmentation with cell-seeded bone grafts is necessitated prior to restoration. These constructs, allograft or autograft, are exposed to stimulus via the adjacent anatomy, which is (to some extent) transduced to the cells hosted within. The modulation of the graft's properties, to accommodate specific ranges of stimulus and promote osteointegration, would thus be of great clinical interest.

2. Materials and Methods

To determine the effect of scaffold properties on cellular loading in dental restorations, a Finite Element (FE) model of a clinically relevant scenario was reverse engineered (see Fig. 1).

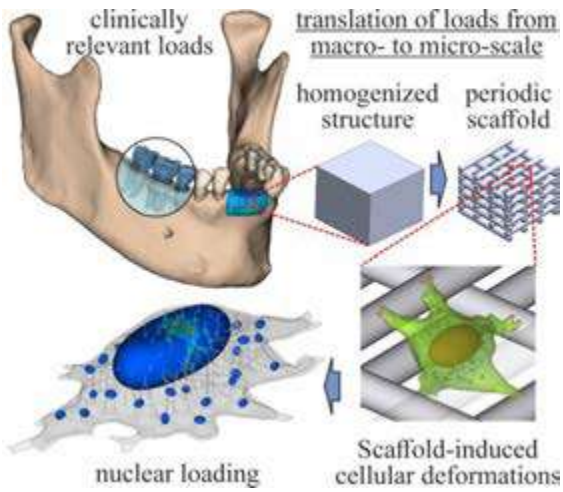

Figure 1: Schematic representation of multiscale modelling approach to assess the transduction of anatomical loads to cellular components.

The scaffold's structural periodicity, facilitated an estimation of the equivalent mechanical properties of its homogeneous solid counterpart [1], employed in this macro-scale model, considering bio-realistic tissue allocation and a dynamic masticatory scenario. The calculated deformations were then applied as boundary/loading conditions to a representative unit-cell of the actual scaffold geometry, whilst integrating the model of a osteoblast, verified and validated against experimental data obtained during cellular loading via atomic force microscopy [2].

3. Results

PCL scaffolds differing in HAA content (0-20%wt) exhibited Young's moduli varying by up to 30% (pure PCL being the most elastic at 240MPa), whereas the deformation of the more elastic graft was twice that of the stiffest one, leading to increased nuclear loading by >300%.

4. Discussion and Conclusions

The presented results, combined with proper mechanotransduction assays, could provide refined insight into the underlying mechanisms of mechanosensing, catalysing the development of "fast-healing" bone autograft alternatives.

5. References

1. Khojasteh A et al., J Oral Implantol; 39(3):386-98 (2013).
2. Luxner M et al., J Mater Sci; 40:5859–66 (2005).
3. Papadakis L et al., J Biomech; 136:111084 (2022).

Acknowledgements: The Hellenic Foundation for Research & Innovation under the 4th call of PhD Fellowships & the Fulbright Scholar Program 2022-2023.



CONTINUUM MECHANICS MODELING OF STIFFNESS SENSING BY SMOOTH MUSCLE CELLS

Ali Akbar Karkhaneh Yousefi, Claudie Petit, Stéphane Avril

Mines Saint-Etienne, Université Jean Monnet, INSERM, U 1059 SAINBIOSE, F – 42023, Saint-Etienne, France

1. Introduction

Aortic Smooth Muscle Cells (SMCs) play a vital role by regulating the wall stiffness to maintain mechanical homeostasis. However, the mechanisms that underlie the ability of SMCs to sense and respond to stiffness change are still partially unclear. Recent studies have highlighted the role of acto-myosin units in the cytoskeleton that can act as stiffness sensors [1]. Inspired by this, we develop a new computational model for the contractile behavior of SMCs that can account for the variations of cellular Traction Forces (TFs) with the surrounding stiffness [2]. To account for the inter-cellular variations, large populations of SMCs are modeled with the Finite Element (FE) method, each cell having a random number and a random arrangement of Stress Fibers (SFs).

2. Materials and Methods

In Traction Force Microscopy (TFM), SMCs are attached to the substrate, and contraction of SFs deforms of the substrate. For sufficiently compliant substrates, the deformation is large and SFs only withstand a small tensile force, but for rigid substrates, the deformation becomes negligible and SFs have to withstand large tensile forces. Therefore, TFs tend to increase with the substrate stiffness. However, experimental findings showed that the sliding between actin and myosin filaments decreases TFs on the surface of stiff substrates [2].

To model the shortening of SFs induced by myosin activation, we used the concept of thermal contraction. The contraction initially results in a gradual increase of TF to a maximum value and then, after the sliding occurrence, the TF would gradually decrease.

3. Results

We confronted our model predictions with the TFM results on the surface of substrates with different elastic moduli 4, 8, 12, and 25 kPa [2]. By considering a random arrangement, a variable number of SFs, we generated 300 cells for FE simulation. Fig. 1, shows the strain field around the focal adhesions for one of the randomly generated SMC. The strain field patterns in both figures are similar.

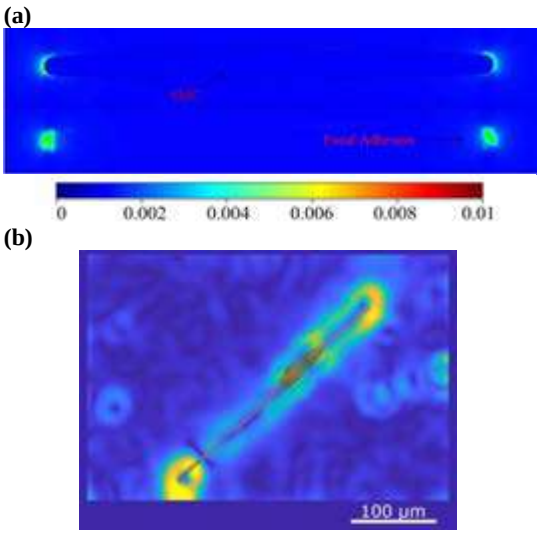

Figure 1: Predicted (a) and experimental (b) strain fields.

4. Discussion and Conclusions

We developed the first continuum mechanics model of SMCs accounting for stiffness sensing through the contractile acto-myosin units. Model predictions were in very good agreement with TFs measured on different substrates. The simplicity of the model is a promising asset for further investigation of stiffness sensing in 3-D environments. This could contribute to deciphering the effects of mechanosensitivity impairment, which are known to be at the root of aortic aneurysms.

5. References

1. Elosegui A et al., Trends in cell biology, 28(5):356-367 (2018).
2. Petit C et al., Biomechanics and Modeling in Mechanobiology, 20(2):717-731 (2021).



FRACTIONAL DIFFUSION OF MEMBRANE RECEPTORS IN ENDOCYTOSIS PATHWAY

Gianmarco Nuzzo (1), Emanuela Bologna (1), Kaushik Dayal (2), Massimiliano Zingales (1)

1. Department of Engineering, University of Palermo, Viale delle Scienze ed. 8, 90128, Palermo, Italy; 2. Center for Nonlinear Analysis, Carnegie Mellon University, Pittsburgh, PA 15213, USA

Correspondence: gianmarco.nuzzo@unipa.it

1. Abstract

Endocytosis is one of the main processes by which the cells of the human body receive substances and nutrients from the extracellular matrix, but it is also the route whereby viruses enter host cells to reproduce [1,2].

The first step in this process involves contact between virus ligands and membrane receptors, which diffuse to the membrane region where endocytosis will be performed [3].

In the past decade many models have been made to describe how these receptors diffuse across the membrane and bind to the virus [4,5,6]. But these works have only dealt with the free diffusion of the receptors on the membrane, neglecting important phenomena such as the attractive influence exerted by the virus on the receptor's movement.

Recently the fractional calculus tool has provided excellent results to describe tissue biomechanics [7,8], proving its usefulness in describing tissue behaviour.

Therefore, in this study we have reported a model of receptor diffusion exploiting Stefan's fractional problem, in which we have considered a flow of receptors that diffuses under the virus, with a certain frontier evolving over time. To consider the attractive potential of the virus and the chemical potential of membrane, instead of using the classical Fick's law, we used Smoluchoski's equation in its fractional shape.

2. References

[1] Joseph JG, Liu AP. 2020. Mechanical Regulation of Endocytosis: New Insights and Recent Advances. Adv Biosyst. 4(5):1–15.

[2] Shang J, Wan Y, Luo C, Ye G, Geng Q, Auerbach A, Li F. 2020. Cell entry mechanisms of SARS-CoV-2. Proc Natl Acad Sci USA. 117(21).

[3] Zhang S, Gao H, Bao G. 2015. Physical Principles of Nanoparticle Cellular Endocytosis. ACS Nano. 9(9):8655–8671.

[4] Gao H, Shi W, Freund LB. 2005. Mechanics of receptor-mediated endocytosis. 102(27):3–8.

[5] Nguyen H, Dayan P, Goodhill GJ. 2014. How receptor diffusion influences gradient sensing. J R Soc Interface. 12(102).

[6] Napoli G, Goriely A. 2020. Elastocytosis. J Mech Phys Solids. 145.

[7] Deseri L, Pollaci P, Zingales M, Dayal K. 2016. Fractional hereditariness of lipid membranes: Instabilities and linearized evolution. J Mech Behav Biomed Mater. 58:11–27.

[8] Bologna E, Di Paola M, Dayal K, Deseri L, Zingales M. 2020. Fractional-order nonlinear hereditariness of tendons and ligaments of the human knee: FOH for fibrous tissues. Philos Trans R Soc A Math Phys Eng Sci. 378(2172).

CMBBE2023
18th International Symposium on Computer Methods in Biomechanics and Biomedical Engineering
3 - 5 May 2023, Paris, France



Arts et Métiers Institute of Technology
Institut de Biomécanique Humaine Georges Charpak
155 boulevard de l'Hôpital 75013 Paris France
www.cmbbe-symposium.com

IMPLEMENTATION OF A GRADIENT ENHANCED BONE REMODELLING MODEL IN ABAQUS

Fynn Bensel (1), Marlis Reiber (1), Philipp Junker (2), Udo Nackenhorst (1)

1. Leibniz University Hannover, Institute of Mechanics and Computational Mechanics, Germany. 2. Leibniz University Hannover, Institute of Continuum Mechanics, Germany.

Corresponding authors: fynn.bensel@ibnm.uni-hannover.de; marlis.reiber@ibnm.uni-hannover.de

1. Introduction

Bones are living tissue and are able to adapt their structure to changes in the mechanical loading situation. Mathematical models are used to simulate this bone remodelling process. In the simulation results numerical instabilities, the checkerboard phenomenon, can occur. Several approaches to mitigate these instabilities are present e.g. smoothing techniques or higher order ansatz functions. We propose a new approach for mitigating the checkerboarding in bone remodelling simulations which has been introduced in damage mechanics and topology optimisation [1-2].

2. Materials and Methods

The bone remodelling process is calculated using a User Element Routine in Abaqus incorporating a thermodynamic consistent constitutive law for stress adaptive bone remodelling using a gradient enhanced free energy for regularisation.

Assuming a non-linear constitutive relation between the bone mass density (BMD) and the Young's modulus [3] and applying the gradient enhancement approach the free energy yields

$$\psi(\varepsilon, \varrho, \varphi) = \left(\frac{\varrho}{\varrho_0}\right)^2 \psi^{\mathrm{LE}} + \frac{\alpha}{2}(\varphi - \varrho)^2 + \frac{\beta}{2}|\nabla\varphi|^2 \,.$$

The second additional term penalises gradients of the global BMD but the first additional term couples it to the local BMD, which indirectly penalises the checkerboarding.

3. Results

The computational results of a plate under compression are depicted in Figure 1. Furthermore, the method is applied for a human femur.

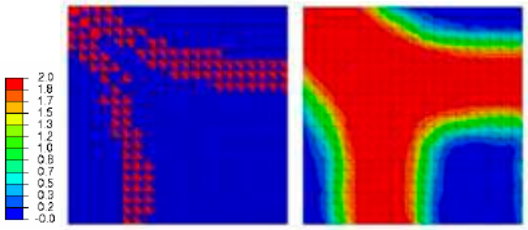

Figure 1: Results of bone remodelling simulation for a plate under compression without gradient enhancement for BMD ϱ in g/cm^3 (left) and with gradient enhancement for BMD φ in g/cm^3 (right)

4. Discussion and Conclusions

A new computational approach for stress adaptive bone remodelling simulation to avoid the checkerboard phenomenon is presented. A new degree of freedom is introduced which increases the computational effort.

5. References

1. Dimitrijevic, B.J., Hackl, K.: A method for gradient enhancement of continuum damage models. Technische Mechanik-European Journal of Engineering Mechanics 28(1), 43–52 (2008)

2. Junker, P., Hackl, K.: A variational growth approach to topology optimization. Structural and Multidisciplinary Optimization 52(2), 293–304 (2015).

3. Lutz, A., Nackenhorst, U.: Numerical investigations on the biomechanical compatibility of hip-joint endoprostheses. Archive of Applied Mechanics 80(5), 503–512 (2010).

Acknowledgements:

The funding of the DFG of the IRTG 2657 grant 433082294 and the SFB/TRR-298-SIIRI – Project-ID 426335750 are gratefully acknowledged.

CMBBE2023
18th International Symposium on Computer Methods in Biomechanics and Biomedical Engineering
3 - 5 May 2023, Paris, France
Arts et Métiers Institute of Technology
Institut de Biomécanique Humaine Georges Charpak
155 boulevard de l'Hôpital 75013 Paris France
www.cmbbe-symposium.com

GROWTH AND REMODELING STUDY OF MECHANO-IMMUNO-DRIVEN ENDOGENOUS TISSUE RESTORATION

Hadi Shirazi, Thibault Vervenne, Lauranne Maes, Nele Famaey

Department of Mechanical Engineering, KU Leuven, Belgium

1. Introduction

Endogenous Tissue Restoration (ETR) is a promising technique to provide tissue restoration by the patient's own body. During ETR, neo-tissue gradually replaces a biodegradable scaffold. This study aims at providing insights into the roles of mechano- and immuno-mediated mechanisms in the ETR.

2. Materials and Methods

A theoretical framework was employed to model a tissue-engineered vascular graft. In addition to an analytical study, a FE solver (ABAQUS) was utilized with a user material subroutine (UMAT). To model growth and remodeling (G&R), we used the homogenized constrained mixture theory (HCMT) which states that the elastic deformation gradient of constituent j can be written as:

$$\boldsymbol{F}_{\boldsymbol{e}}^{\boldsymbol{j}} = \boldsymbol{F}\left(\boldsymbol{F}_{\boldsymbol{g}}\right)^{-1}\left(\boldsymbol{F}_{\boldsymbol{r}}^{\boldsymbol{j}}\right)^{-1} \quad (1)$$

Here $\boldsymbol{F}$ is the deformation gradient of the mixture, $\boldsymbol{F}_{\boldsymbol{g}}$ and $\boldsymbol{F}_{\boldsymbol{r}}$ are the growth and remodeling deformation gradients, respectively. The densities of every constituent j evolve as [1]:

$$\dot{\rho}^{j} = \dot{\rho}_{+}^{j} + \dot{\rho}_{-}^{j} \quad (2)$$

where subscripts + and – represent the production and removal. The values of the parameters and the mass turnover equations were borrowed from [2] with some modifications. For the scaffold, the degradation rate was dependent on time (t) and degradation rate, shape and modifier parameters [2]. For the fibers, *i.e.* collagen and smooth muscle cells (SMCs), the rates of deposition and degradation were divided into two parts: stress-induced (SI) and immuno-driven. The former corresponds *e.g.* to the deviation of the fiber stress with respect to the homeostatic fiber stress. The latter is governed by four key inflammatory parameters [2]. A neo-Hookean model and an anisotropic exponential model were considered for the scaffold and fiber families, respectively.

3. Results

Fig.1 provides the G&R results over time for our example case. A good agreement can be observed between the analytical and FE results (normalized root mean square error (NRMSE) < 0.05).

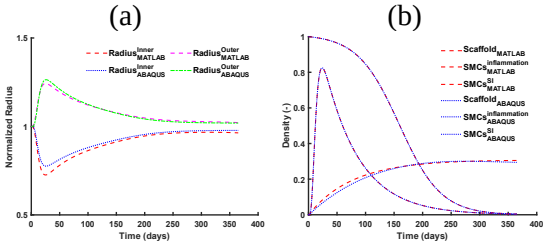

Figure 1: Changes in the (a) inner and outer radii, (b) scaffold and SMCs densities over time.

4. Discussion and Conclusions

At the beginning of the simulation, *i.e.* right after implantation, the initial ρ values of the fiber families are equal to 0. As shown, the inflammatory response is more prominent than the SI one when the scaffold starts degrading. However, the inflammatory response subsides over time and then, the SI response plays a key role in the mass turnover. Whereas the current work provided a verification of our model implementation, the next step will be to calibrate the model parameters and validate the approach using experimental data that is currently being collected in a sheep study in the framework of the H2020 SimInSitu project.

5. References

1. Braeu, F et al., Biomech Model Mechnobiol. 16(3):889-906 (2017).
2. Drews, J et al., Sci Transl Med. 12(537): eaax6919 (2020).

Acknowledgments:

The authors would like to thank the European Commission and its Horizon 2020 funding program (Grant ID: 101017523) for providing financial support to the SimInSitu project.



A CELL-BASED MATHEMATICAL MODEL OF TISSUE REGENERATION AND ITS NUMERICAL TREATMENT

Elise Grosjean (1), Nishith Mohan (1), Bernd Simeon (1), Christina Surulescu (1)

1. Department of Mathematics, RPTU Kaiserslautern-Landau, 67657, Deutschland

1. Introduction

We propose a PDE-ODE system modeling the dynamics of two cell populations (adipose derived stem cells and chondrocytes) involved in the production of cartilage tissue.
They are supposed to migrate, proliferate, and differentiate within an artificial scaffold impregnated with a chemoattractant and contained in a perfusion chamber. We investigate some model variants in terms of cell pattern formation and numerical treatment.
Concerning the numerical simulations, we aim at identifying the parameters of interest. In this context, several methods exist. When dealing with discretized solutions of parameter-dependent PDEs, the sensitivities with respect to certain parameters of interest may be directly computed from the original problem but it requires solving a new system for each parameter of interest. Thus, when dealing with a large number of parameters, the adjoint method may be a good alternative [1]. We will present efficient ways of combining reduced basis techniques [2] and the computation of the sensitivities with both methods in order to further reduce the computational time. These adaptations will be numerically illustrated with several results on our model problem with finite elements.

2. References

1. JF. Sykes and JL. Wilson, Adjoint sensitivity theory for the finite element method, Finite Elements in Water Resources, Springer, p3-12, 1984.
2. R. Chakir and Y. Maday, A two-grid finite-element/reduced basis scheme for the approximation
of the solution of parameter dependent PDE., 9e Colloque national en calcul des structures, CSMA, 2009.

Acknowledgements:
This work is supported by the SPP2311 program.

A cell-based mathematical model of tissue regeneration and its numerical treatment

Élise Grosjean, TU Kaiserslautern

Nishith Mohan, Bernd Simeon, Christina Surulescu, TU Kaiserslautern

We propose a PDE-ODE system modeling the dynamics of two cell populations (adipose derived stem cells and chondrocytes) involved in the production of cartilage tissue. They are supposed to migrate, proliferate, and differentiate within an artificial scaffold impregnated with a chemoattractant and contained in a perfusion chamber. We investigate some model variants in terms of cell pattern formation and numerical treatment.
Concerning the numerical simulations, we aim at identifying the parameters of interest. In this context, several methods exist. When dealing with discretized solutions of parameter-dependent PDEs, the sensitivities with respect to certain parameters of interest may be directly computed from the original problem but it requires solving a new system for each parameter of interest. Thus, when dealing with a large number of parameters, the adjoint method may be a good alternative [1]. We will present an efficient way of combining reduced basis techniques [2] and the computation of the sensitivities with this method in order to further reduce the computational time. This adaptation will be numerically illustrated with several results on our model problem with finite elements.

Références

[1] JF. Sykes and JL. Wilson, *Adjoint sensitivity theory for the finite element method*, Finite Elements in Water Resources, Springer, p3-12, 1984.

[2] R. Chakir and Y. Maday, *A two-grid finite-element/reduced basis scheme for the approximation of the solution of parameter dependent PDE.*, 9e Colloque national en calcul des structures, CSMA, 2009.

Élise Grosjean, Felix-Klein-Zentrum für Mathematik, TU Kaiserslautern
grosjean@mathematik.kl-uni.de

CMBBE2023
18th International Symposium on Computer Methods in Biomechanics and Biomedical Engineering
3 - 5 May 2023, Paris, France
Arts et Métiers Institute of Technology
Institut de Biomécanique Humaine Georges Charpak
155 boulevard de l'Hôpital 75013 Paris France
www.cmbbe-symposium.com

MECHANOBIOLOGY OF A MULTI-CELL UTERINE WALL MODEL

Yael Shlomo (1), Mark Gavriel (1), Ariel J Jaffa (2), Dan Grisaru (2), David Elad (1)

(1) Department of Biomedical Engineering, Tel Aviv University, Tel Aviv, ISRAEL
(2) Lis Maternity Hospital, Tel Aviv Medical Center, Tel Aviv, Israel

E-mail: elad@tauex.tau.ac.il

1. Introduction

The non-pregnant uterus is characterized by spontaneous myometrial contractions that induce intra-uterine peristaltic flows [1]. The human uterine wall is composed of endometrial epithelial cells (EEC), endometrial stromal cells (ESC) and myometrial smooth muscle cells (MSMC) without a separating layer. Many *in vitro* models were developed to study molecular aspects of the uterine wall. Recently, we developed a layer-by-layer co-culture model of the uterine wall and exposed it to peristaltic wall shear stresses (WSS) [2]. In nature, tissue development is the outcome of spontaneous organization of different layers of cells due to cellular and molecular signals. Accordingly, in the present study we developed a new *in vitro* model by co-culture of all the cells together and exposed it to steady WSS.

2. Materials and Methods

We seeded an equal mixture of EEC (RL95-2, ATCC), ESC (T0533, ABM) and MSMC (ATCC® PCS-460-11™) at once on the collagen coated PTFE membrane using our custom-designed wells. Immunofluorescence staining with specific antibodies was used to validate the barrier model. Then, we exposed the *in vitro* model to steady WSS of 0.5 dyne/cm^2 for durations of 10 and 30 minutes.

3. Results

The results demonstrated a three-dimensional (3D) structure (Fig. 1A) with the 3 different cells arranged into three different layers and very similar to the results of seeding layer-by-layer model [2]. Further confirmation for the multi-layer model of the EMI is shown in the projection and Z-section (Fig. 1B). The model thickness was 50±20 µm whereas the EEC layer was 25±10 µm and the MSMC layer was 15±5 µm. We also exposed this *in vitro* model to steady wall shear stresses. Examination of confocal images revealed cellular alterations in both layers of the EEC and MSMC.

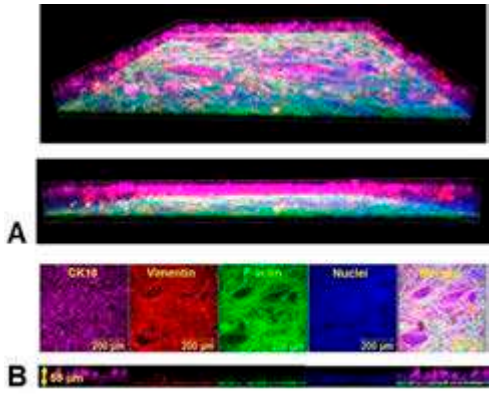

Figure 1: Confocal images of the uterine wall model cultured of a mixture of EEC, ESC and MSMC: A) Three-dimensional plot; B) Projection of all cells and Z-section. Antibodies: for EEC - Anti-Cytokeratin 18 antibody AB-ab206269 [EPR1626] (Alexa Fluor® 647) 1:100 in 1% BSA; for ESC - conjugated Anti-Vimentin antibody [EPR3776] AB-ab202504 (Alexa Fluor® 568) 1:500 in 1% BSA; for all nuclei - DAPI nucleic acid staining (D9542).

4. Discussion and Conclusions

We successfully developed a complex *in vitro* 3D model of the uterine wall with cellular layers that mimic the *in vivo* structure. Seeding all the cells together revealed that the wall layers evolved as in nature. In addition, application of WSS on the outer layer of EEC is also affecting the inner layer of MSMC. This new *in vitro* model may be implement in studies of reproduction physiology and pathophysiology.

5. References

1. Myers K, Elad, D. Wiley Interdiscip Rev: Syst Biol Med 9, e1388 (2017).
2. Elad D et al. APL Bioengineering 4, 026107 (2020).



BIOMIMETICS OF STRUCTURAL MOTIFS IN SOFT FIBROUS TISSUES

Mirit Sharabi
Department of Mechanical engineering and Mechatronics, Ariel University, Ariel 407000, Israel

1. Introduction

Through years of evolution, biological soft fibrous tissues have developed outstanding structural motifs that result in extremely efficient mechanical behaviors and, most notably, large deformations. From a mechanical point of view, these tissues are built as composite materials made of repeated building blocks (e.g., collagen, proteoglycans, and elastin) consisting of diverse structural motifs such as fiber fraction and orientation, hierarchy, crimping, and weak interfaces [1].

The unique properties of soft fibrous tissues stem from their structural complexity, which, unfortunately, also hinders our ability to generate adequate synthetic analogs, such that autografts remain the "gold standard" materials for soft-tissue repair and replacement.

Whereas the structure-function relationship is well-studied in natural hard materials, soft materials are not getting similar attention, despite their high prevalence in nature.

Reverse biomimetics of these materials and structural motifs in soft composites holds valuable insights that could be exploited to generate the next generation of biomaterials for soft tissue repair and also provide a better understanding of the structure-function relationship in these biological tissues.

2. Materials and Methods

We have developed new biomimetic composite material systems based on silk and collagen fibers reinforced alginate hydrogels and reverse-engineered different structural motifs, such as fiber fraction and orientation, crimping, and multi-scale hierarchy, and investigated their mechanical influence.

Moreover, we generated dedicated 3D hyperelastic and heterogeneous finite-element models to simulate the mechanical behavior of the composite laminates under physiological conditions.

3. Results

Our novel material systems demonstrated hyperelastic and anisotropic mechanical behavior with large deformations, including toe, heel, and linear regions. The tensile strength and modulus of the longitudinal composites reached 18MPa and 178MPa, respectively, and the strain and toughness to 0.3 and 3.7 MJ/m^3, respectively. Furthermore, a wide range of mechanical behaviors could be tailor-designed using different variations of the structural motifs.

4. Discussion and Conclusions

Our biomimetic soft composites demonstrated similar large-deformation behavior to different functional tissue structures, such as the annulus fibrosus in the intervertebral disc [2,3] and the knee meniscus [4].

Mimicking the native structural motifs in simpler material systems can provide a better understanding of the soft-tissue structure-function relationship in very complex systems (such as the cumulative influence of controlled fiber crimping, orientation, and fraction). This would lead to the design of next-generation materials with custom-made mechanical behavior for future soft-tissue repair applications by creating mechanically biocompatible native tissue behaviors.

References

1. Sharabi M., Structural mechanisms in soft fibrous tissues: A review. Front. Mater. (2022) 8: 793647.
2. Sharabi, M., Wertheimer, S., Wade, K. R., Galbusera, F., Benayahu, D., Wilke, H. J., & Haj-Ali, R. Towards intervertebral disc engineering: bio-mimetics of form and function of the annulus fibrosus lamellae. JMBBM. (2019). 94, 298-307.
3. Mordechai HS, Aharonov A, Sharon SE Bonshtein I, Simon C, Sivan SS, Sharabi M. A novel combined annulus fibrosus-nucleus pulposus biomimetic construct for intervertebral disc engineering. Submitted.
4. Aharonov A, Mordechai HS, Sharon SE and Sharabi M. The Mechanical Behavior of Silk-Fibroin Reinforced Alginate Hydrogel Biocomposites - Toward Functional Tissue Biomimetics. Submitted.

CMBBE2023
18th International Symposium on Computer Methods in Biomechanics and Biomedical Engineering
3 - 5 May 2023, Paris, France
Arts et Métiers Institute of Technology
Institut de Biomécanique Humaine Georges Charpak
155 boulevard de l'Hôpital 75013 Paris France
www.cmbbe-symposium.com

MORPHING IN PLANT TISSUES:

BIOMIMETICS OF STRUCTURE AND FUNCTION

Gital Shteinberg and Mirit Sharabi
Department of Mechanical engineering and Mechatronics, Ariel University, Ariel 407000, Israel

1. Introduction

In nature, various plants such as seedpods, pinecones and wheat awns transform their shape in response to humidity changes [1]. This ability of shape transformation is known as morphing [2]. Plants tissues are multi-scaled soft composite materials with a hierarchical structure based on stiff cellulose fibers embedded in a soft hemicellulose matrix [3]. The shape-morphing mechanism of plants is due to asymmetrical fiber alignment, which allows a coupling effect for in-plane/bending/twisting deformations [4].

2. Materials and Methods

Soft biocomposite was designed and fabricated using silk fibers that reinforced an alginate hydrogel matrix. The biocomposite was constructed from two asymmetrical fiber layers. The silk fibers were aligned in different orientations of 0°, 30°, 45°, 60° and 90°. The biocomposites were tested mechanically using uniaxial tension testing and their morphing ability was investigated.

3. Results

The biocomposite materials demonstrated nonlinear, hyperelastic mechanical behavior with large deformations, as shown in Fig. 1. They present a wide range of elasticity moduli (3.20-92.44MPa) and strength (0.38-10.78 Mpa).

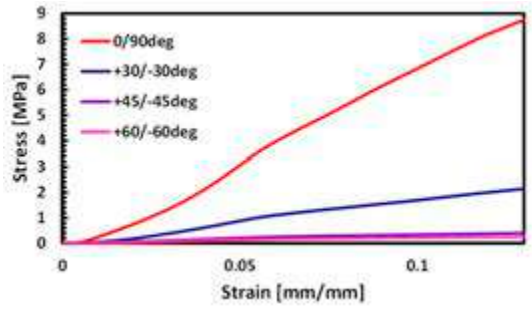

Figure 1: The mechanical behavior of biocomposite laminates as a function of fiber orientations

Moreover, by mimicking plant structure principles, we achieved shape transformations similar to those of plants with the same structures as in nature. Thus, the wheat awn mimic demonstrated the opening of its stalks upon bending, the pinecone showed bending of its scales and the seedpod presented twisting of its valves, as shown in Fig. 2.



Figure 2: Biomimetics of plant morphing

4. Discussion and Conclusions

Our novel material system demonstrated multifunctional capabilities such as shape transformation, large deformations, and robust mechanical properties. Hence, these biocomposites have the potential to affect the future of smart materials with new applications in soft robotics, sensing, biomedical engineering, drug delivery and tissue engineering.

5. References

[1] Studart, A. R., & Erb, R. M. **(2014)**. *Soft matter*, 10(9), 1284-1294.
[2] Ren, L. *et al.*, **(2021)** *Frontiers in Materials,* 90
[3] Burgert, I., & Fratzl, P. **(2009)**,*Integr. Comp. Biol.*, 49(1), 69–79.
[4] Ahn *et al.*, **(2012)**. *Int. J. Precis. Eng. Manuf.*13(4), 631-634

Acknowledgements:
The authors would like to thank Ariel University for their support to this project**.**

CMBBE2023
18th International Symposium on Computer Methods in Biomechanics and Biomedical Engineering
3 - 5 May 2023, Paris, France
Arts et Métiers Institute of Technology
Institut de Biomécanique Humaine Georges Charpak
155 boulevard de l'Hôpital 75013 Paris France
www.cmbbe-symposium.com

BIOMIMETICS OF THE MENISCUS TISSUE: STRUCTURE AND FUNCTION RELATIONSHIP

Adi Aharonov and Mirit Sharabi

Department of Mechanical engineering and Mechatronics, Ariel University, Ariel 407000, Israel

1. Introduction

The knee meniscus is a load-bearing and -transferring structure that is essential for the normal function of the knee joint. The high prevalence of meniscal injuries led to the growing need for meniscus substitutes that could replace damaged native tissue. Biomimetics of the meniscal structure-function relationship remains a significant challenge due to the tissue's structural complexity and anisotropic nature.

2. Materials and Methods

Soft biocomposite laminates were fabricated using silk-fibroin fibers-reinforced alginate hydrogel matrix and tested mechanically using unidirectional tensile tests. The fiber orientations were selected based on the main fiber directions of the meniscus tissue. A three-dimensional finite element model of the knee joint containing structural representations of the menisci as fiber-reinforced composite material was generated. The influence of the meniscal composite structure on various contact mechanics variables and meniscal geometrical changes were examined under axial compression at full extension of the knee.

3. Results

The biocomposite laminates demonstrated nonlinear, anisotropic hyperelastic mechanical behavior with large deformations, shown in Fig. 1. They presented substantial stiffness (101.73-178.55 MPa) and strength (8.29-18.47 MPa), similar to high stiffness functional soft tissues such as the meniscus. The FE composite meniscal model presented better contact results than an isotropic model (Fig. 2). All the meniscal components, the matrix, and the circumferential and radial fibers function under axial loading. Without the radial fibers, considerable shape deformation and peak contact pressure on the tibial cartilage were obtained.

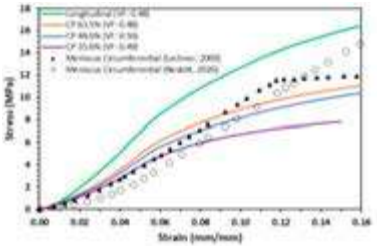

Figure 1: The mechanical behavior of the biocomposite laminates as a function of fiber VFs, and meniscus tissue from previous studies [1,2].

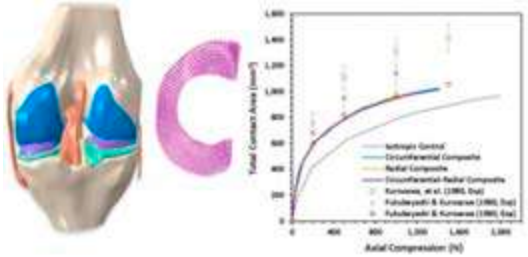

Figure 2: FE model of the knee joint, including a refined composite structure of the meniscus using circumferential and radial fibers and validation of the model against experimental results [3,4].

4. Discussion and Conclusions

Our silk-based biocomposites have the potential to mimic the meniscal tissue mechanical behavior toward novel repair and replacement solutions. Composite biomimetic models may be more appropriate for representing the meniscus in healthy knee joints. The deformations, contact mechanics, and stresses within the meniscus are affected by changes in the internal structure.

5. References

[1] K. Lechner, M.L. Hull, S.M. Howell, J. Orthop. Res. 18 (2000) 945–951.
[2] D.Q. Nesbitt, D.N. Siegel, S.J. Nelson, T.J. Lujan, J. Biomech. (2020) 110126.
[3] H. Kurosawa, T. Fukubayashi, H. Nakajima, Clin. Orthop. Relat. Res. 149 (1980) 283–290.
[4] T. Fukubayashi, H. Kurosawa, Acta Orthop. Scand. 51 (1980) 871–879.

Acknowledgments:
The authors would like to thank Ariel University for supporting this project**.**

CMBBE2023
18th International Symposium on Computer Methods in Biomechanics and Biomedical Engineering
3 - 5 May 2023, Paris, France



Arts et Métiers Institute of Technology
Institut de Biomécanique Humaine Georges Charpak
155 boulevard de l'Hôpital 75013 Paris France
www.cmbbe-symposium.com

FROM POPULATION TO INDIVIDUAL. DERIVATION OF AN AGENT BASED MODEL FOR GLIOBLASTOMA EVOLUTION IN VITRO.

Raquel B. Arroyo-Vázquez (1), Marina Pérez-Aliacar (1), Jacobo Ayensa-Jiménez (1,2), Manuel Doblaré (1,2)

1. Engineering Research Institute of Aragon (I3A), University of Zaragoza, Spain;
2. Health Research Institute of Aragon (IISA), Spain.

1. Introduction

Glioblastoma (GBM) is a very aggressive and invasive brain cancer, with an average survival time for the patient of only 15 months after diagnosis. This lethality is due to its resistance to radiotherapeutic and chemotherapeutic treatments, and the inability to perform surgery to eliminate all the tumor tissue in the brain [1].

GBM evolution is characterized by a high proliferation around blood vessels, that ends up generating hypoxic areas and the migration of cellular clusters towards more oxygenated areas (pseudopalisades); and areas where cells die from anoxia, known as necrotic cores [2].

In this work, the objective is to develop an Agent-Based Model (ABM) that reproduces the evolution of GBM, and then incorporate new parameters related to cell - cell mechanical interactions and analyze whether this phenomena contribute to better reproducing experimental results.

2. Methodology

To develop the ABM model, we use the software PhysiCell [4]. The starting point is a continuous model of GBM evolution validated with previous experimental in our group [5].

Due to the difference in scales between the two models, the way of modeling the phenomena and their associated parameters in both models are different and it is necessary to establish mathematical equivalences that relate the population parameters (continuum) to the individual parameters (ABM). To establish these equivalences, we isolate the different biological phenomena composing the problem.

3. Results

The obtained ABM can replicate the results of the continuous model to reproduce the formation of the different cell structures, that is, the pseudopalisade and the necrotic core (Fig. 1) and to incorporate cell – cell interactions not captured by the continuum models.

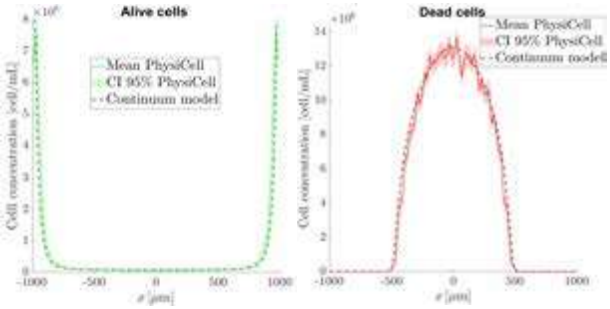

Figure 1: Necrotic core. Cell concentration.

4. Conclusions

ABMs are very useful tools to study complex biological processes, allowing us to study certain aspects that could not be studied with other methodologies. The developed ABM reproduces GBM evolution and may allow us to test hypothesis and incorporate new local phenomena for enriching the system physics.

5. References

1. Lah TT et al. Semin. Cancer Viol. 60:262-273.2020.
2. Ayuso et al. Neuro-oncology.19.4:503-513.2017.
3. Metzcar et al. JCO CCI. 3:1-13.2019.
4. Ghaffarizadeh et al. PLOS Comp. Biol. Vol.14, 2018.
5. Ayensa-Jiménez et al. Sci. Rep. 10,21193, 2020

Acknowledgements:
The authors gratefully acknowledge the financial support from the Spanish Ministry of Science and Innovation and the Research State Agency (AEI), (PID2021-126051OB-C41).

CMBBE2023
18th International Symposium on Computer Methods in Biomechanics and Biomedical Engineering
3 - 5 May 2023, Paris, France
Arts et Métiers Institute of Technology
Institut de Biomécanique Humaine Georges Charpak
155 boulevard de l'Hôpital 75013 Paris France
www.cmbbe-symposium.com

SHIFT OF LOAD DISTRIBUTION WITH LUMBAR DISC REPLACEMENT-A SIMULATION STUDY

Regina Guth (1), Maria Hammer (1,2), Syn Schmitt (1,2)

1. Institute for Modelling and Simulation of Biomechanical Systems, University of Stuttgart, Germany;
2. Stuttgart Center for Simulation Science (SC SimTech), University of Stuttgart, Germany

Correspondence: Maria Hammer, maria.hammer@imsb.uni-stuttgart.de

1. Introduction

In case of instability, injuries or very advanced wear of intervertebral discs, the natural supporting structures in the spinal column are damaged to such an extent that strong pain can occur. In this case, stiffening of intervertebral joints, mostly L4|5, by inserting screws to reposition slipped vertebrae, or replacement of intervertebral discs by implants, is unavoidable for an increasing number of patients. Within only few postoperative years, patients often suffer back pain again due to progressing degeneration in surrounding intervertebral levels. Biomechanical simulations can assist in gaining more knowledge about the impact of disc replacement. With the help of a physiological spine model [1,2,3], we compare the static and dynamic behavior of spine models with disc implants at lumbar level L4|5 to healthy lumbar spine kinetics in static as well as dynamic situations.

2. Materials and Methods

A detailed, generic neuromusculoskeletal model of the thoracolumbar spine [1,3] was used as reference for a healthy spine in this study. It bases on the lumbar spine model of [2], revised and validated for passive motions, and is fully articulated in the spinal column, i.e. with free intervertebral joints (six degree of freedom joints) on every spinal level. While intervertebral discs are represented by Bushing elements, the 192 ligament strands and 294 muscles fascicles are implemented as line actuators. The healthy model was modified by inserting L4|5 disc implants: i) stiffening the level L4|5 and ii) an artificial disc prothesis (Maverick Disc, Medtronic), allowing for rotational movements. The internal forces of all models were compared for forward dynamic simulations in an upright posture and during active forward flexion.

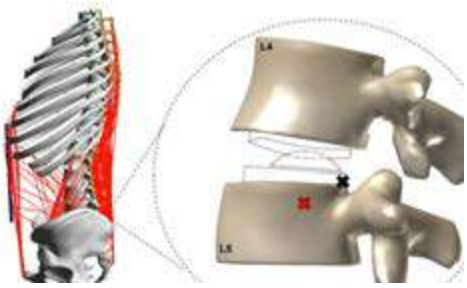

Figure 1: Detailed spine model with intervertebral disc replacement in L4|5 exhibits a shift of the flexion rotation axis from healthy (black dot) to the implant center of rotation (red dot).

3. Results

In the simulations with different disc replacements, we observed a shift of the rotation center in the sagittal plane and in the distribution of loads, especially in surrounding levels and towards larger ligament and muscle forces in the operated level for the Maverick Disc.

4. Discussion

With the presented generic spine model, we were able to study how lumbar disc replacements affect the spine stiffness and internal forces in the entire spinal column. In combination with patient-specific models, such spine simulations serve as a novel, objective method to support the clinical decision-making process by predicting postoperative internal forces and, therewith, possible secondary damage.

5. References

1. http://www.get-demoa.com
2. Mörl et al., *Biomech Model Mechan,* 19(6):2015- 2047 (2020).
3. Meszaros-Beller er al. *BMMB (under review)*.

Acknowledgements: Funded by Deutsche Forschungsgemeinschaft (DFG, German Research Foundation) under Germany's Excellence Strategy - EXC 2075 – 390740016.

CMBBE2023
18th International Symposium on Computer Methods in Biomechanics and Biomedical Engineering
3 - 5 May 2023, Paris, France
Arts et Métiers Institute of Technology
Institut de Biomécanique Humaine Georges Charpak
155 boulevard de l'Hôpital 75013 Paris France
www.cmbbe-symposium.com

MEASURMENT OF BULK MODULUS OF SOFT TISSUES USING DIGITAL IMAGE CORRELATION IN TENSILE TEST

Amin Kazemi, Nima Etemadi, Mohammad Ali Nazari

School of Mechanical Engineering, College of Engineering, University of Tehran, Tehran, Iran

1. Introduction

The volumetric part of deformation has crucial role in characterizing mechanical response of soft tissues. Experimental measurement of volumetric part of strain is very challenging. Usually, a hydrostatic chamber is used to measure the change in volume due to the induced pressure [1]. The porous structure of the soft tissues makes the results erroneous. Another solution is measuring the strains in the planes normal to the stretch direction in tensile test simultaneously. This allows us to obtain the volumetric strain. The purpose of this research is the measurement of bulk moduli of soft tissues using tensile test with digital image correlation (DIC) technique. Then the equivalent Poisson's ratio is computed.

2. Materials and Methods

Tensile experiments are performed on mucous membrane of bovine tongue. The strains are measured using digital image correlation. The geometric irregularity of a sample highly impacts the results of tensile test. Thus, a device is deigned to extract the dog-bone specimens with uniform thickness using 3D printed mould. Samples were spotted with black alkyd paint such that appropriately distributed speckles are generated. Manual spraying is used in this study. The alkyd paint exhibits acceptable bonding to soft tissue samples. Two cameras were used to measure the strain field in frontal and lateral view. The displacement field is then extracted from images.

3. Results

The displacement field in both lateral (X and Z) and longitudinal (Y) directions (Figs. 1, 2) presents sufficient uniformity as expected by the assumption of uniaxial stress. This observation conforms the suitability of dog-bone shape samples. The value of computed Poisson's ratios during loading are given in Table 1.

4. Discussion and Conclusions

The effectiveness of the DIC method to measure the bulk moduli and the corresponding Poisson's ratios is evaluated. The computed values show some compressibility in tissues.

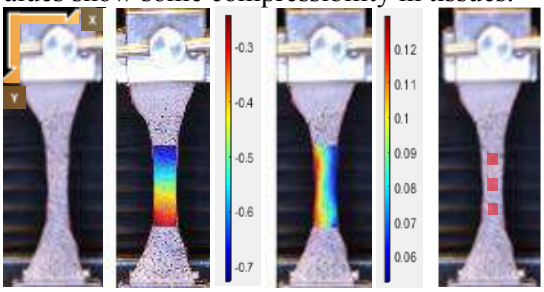

(a) (b) (c) (d)

Figure 1: a) The frontal view of bovine mucous membrane sample mounted on the tensile test machine. b) Displacement in the Y direction. c) Displacement in the X direction. d) Three locations at the gauge region where the average Poisson's ratios were calculated

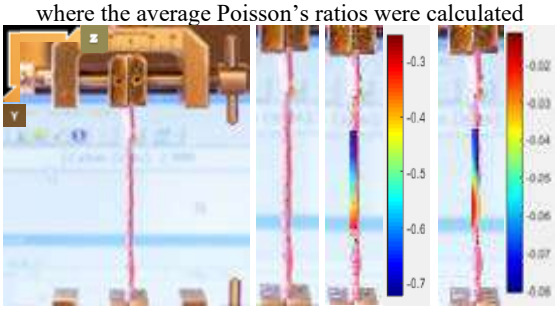

(a) (b) (c) (d)

Figure 2: a) The lateral view of mucous membrane sample. c) Displacement in the Y direction. d) Displacement in the Z direction.

Table 1: Poisson's ratio calculated at locations specified in Fig.1d

Location	Poisson's ratio
Top	0.478
Middle	0.483
Bottom	0.439

5. References

[1] Kanzenbach, L., et al. "Development of a compression chamber for the determination of the bulk modulus." Materials Today: Proceedings 4.5, p 5839-5842, 2017

[2] M. Scholze *et al.*, "Standardized tensile testing of soft tissue using a 3D printed clamping system," *HardwareX*, vol. 8, p. e00159, Oct. 2020.

CMBBE2023
18th International Symposium on Computer Methods in Biomechanics and Biomedical Engineering
3 - 5 May 2023, Paris, France
Arts et Métiers Institute of Technology
Institut de Biomécanique Humaine Georges Charpak
155 boulevard de l'Hôpital 75013 Paris France
www.cmbbe-symposium.com

CLASSIFICATION OF COGNITIVELY NORMAL AND ALZHEIMER BRAIN MR IMAGES USING MULTISCALE TEXTURE AND EXTREME LEARNING MACHINE

Amrutha Veluppal[1], Deboleena Sadhukhan[2], Ramakrishnan Swaminathan[1]
1. Indian Institute of Technology Madras, India; 2. Institut Langevin, Paris, France

1. Introduction

Computer-assisted systems incorporating MR neuroimaging data are gaining prominence as a diagnostic aid for detecting Alzheimer's Disease (AD). AD-related abnormal protein aggregation can cause degeneration in multiple brain regions manifesting as textural changes in images. Advanced texture analysis techniques are required to characterize these imperceptible changes. Multi Scale Entropy (MSE) features have been recently introduced to characterize subtle changes occurring across multiple image scales [1]. The current study explores the utility of whole-brain MSE features to classify AD from Cognitively Normal (CN) subjects.

2. Materials and Methods

The pre-processed mid-sagittal brain MR images of 92 cognitively normal (CDR=0) and 92 AD (CDR=0.5,1) subjects are retrieved from OASIS database [2]. The images are coarse grained to form the scaled versions of original image. Subsequently, MSE values of each scaled image are evaluated by comparing the patterns within a specific window length. The MSE features are extracted from sagittal slices across spatial scales ranging from 1 to 5 at three varying window lengths. For classification model, single hidden layer neural network namely Extreme Learning Machine (ELM) classifier with sigmoid activation function and 10-fold cross validation is employed.

3. Results

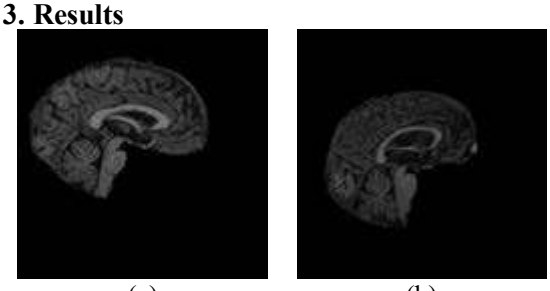

(a) (b)

Figure 1: Representative sagittal view T1-weighted brain MR images of (a)CN and (b)AD subjects

Fig.1 shows the representative mid-sagittal MR images. All MSE features are found to be statistically significant ($p<0.05$)among obtained CN and AD subjects. These features are also found to be distinct at each spatial scale, as observed in Fig.2. The MSE values are found to be most distinguishable at window length 2.

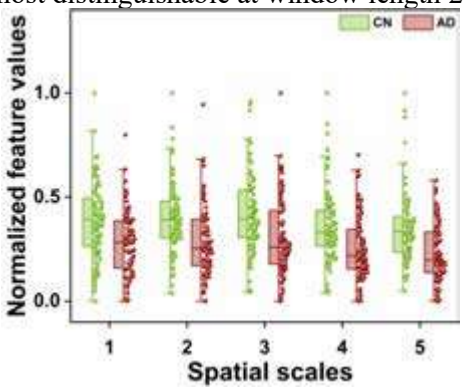

Figure 2: Variation of MSE features for CN and AD groups across multiple spatial scales for representative window length of 2.

ELM classifier achieves an accuracy of 82.46% and F-measure of 80.12% for AD detection indicating a robust model.

4. Discussion and Conclusions

MSE texture features captures the irregularities occurring at multiple spatial scales of the sagittal MR brain images to differentiate CN and AD. These features are found to be high in CN, which may be due to fact that healthy systems have higher complexities compared to pathological ones [3]. Bidimensional MSE features with ELM classifier provides good results in detecting AD subjects with a single MR slice. Thus, the proposed pipeline could contribute towards automated AD diagnosis which would benefit physicians in clinical milieu.

5. References

1. Silva et al., Signal process. ;147: 224-232 (2018).
2. Marcus et al., J. Cogn. Sci ;19(9):1498-1507 (2007).
3. Hilal M et al., IEEE Trans on BioMed Imaging; 67(7):2015-2022 (2019).

CMBBE2023
18th International Symposium on Computer Methods in Biomechanics and Biomedical Engineering
3 - 5 May 2023, Paris, France
Arts et Métiers Institute of Technology
Institut de Biomécanique Humaine Georges Charpak
155 boulevard de l'Hôpital 75013 Paris France
www.cmbbe-symposium.com

MECHANICS OF AAA TISSUE FOR PERSONALIZED CALCULATION OF THE RISK OF ITS RUPTURE

Lipovka Anna(1), Tikhvinsky Denis(1), Volkova Irina(1,2); Maus Maria(1,2), Karpenko Andrey(1,2), Besov Alexey(1), Chupakhin Alexander P(1), Parshin Daniil V (1)

1. Novosibirsk State University,Russia 2. E.N. Meshalkin National Medical Research Center, Russia

1. Introduction

Abdominal aortic aneurysm is an important and widespread disease. Statistically, smoking men over 60 years of age are most predisposed to them[1]. Despite decades of study and hundreds of works in this direction, the mechanisms of aneurysm growth and models of degradation of its wall have not yet been developed.

2. Materials and Methods

In this study, testing of aortic tissue was performed in several ways: a uniaxial test on an INSTRON 5944 tensile testing machine with a thermostatic biobath, as well as on an ANTON PAAR rheometer. Both normal tissue and tissues with aneurysmal or atherosclerotic lesions were studied. In addition, intraluminal thrombotic masses were subjected to rheological tests. The obtained data on the viscoelastic properties of materials were used in the ANSYS Mechanical 2020R2 software package to simulate the contact with the spine of the aortic wall with intraluminal thrombotic masses.

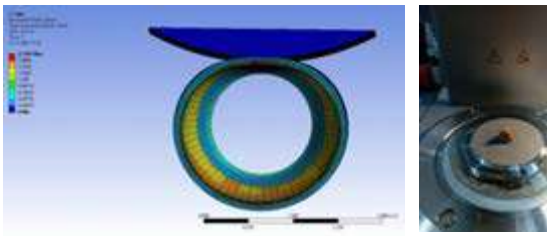

Figure 1: Contact simulation of aorta with thrombus (left), thrombus rheology test (right).

3. Results

Samples of almost 100 patients with lesions of the abdominal aortic wall were characterized, about 20 rheometric tests with aortic tissue, its aneurysm, and intraluminal thrombi were performed. The viscoelastic properties of these materials are obtained and ordered. A numerical model of the contact of the spine and aorta with an intraluminal thrombus was implemented, and a statistical analysis of the distribution of strains and stresses depending on the volume occupied by the thrombus, as well as its localization was performed.

4. Discussion and Conclusions

The work carried out for the first time represents a huge array of experimental data [2] on the viscoelastic properties of the aortic walls; this material can be extremely useful for developing models [3] of fatigue deformation and, subsequently, for models of degradation of the aortic wall.

5. References

1. P.E. Norman and J.T. Powell Circulation. 2007;115:2865–2869
2. A.I. Lipovka, A.A. Karpenko, A.P. Chupakhin, D. V.Parshin, Journal of Applied Mechanics and Technical Physics, 2022, Vol. 63, No. 2, pp. 251–258.
3. Andrey A. Karpenko, and Daniil V. Parshin Russ. J. Numer. Anal. Math. Modelling 2022; 37(5):311–329

Acknowledgements:
This study was supported by a grant from Russian Science Foundation (No 21-15-00091)



DIGITAL VOLUME CORRELATION ASSOCIATED WITH OPTICAL COHERENCE TOMOGRAPHY FOR SKELETAL MUSCLE MECHANICAL CHARACTERIZATION

ESCOBAR JUAN F. [A,B]*, TRABELSI OLFA[A], GARZÓN DIEGO[B]

[a]Université de Technologie de Compiègne, CNRS, Biomechanics and Bioengineering, Centre de Recherche Royallieu, CS 60 319 - 60 203 Compiègne Cedex, France [b]Numerical Methods and Modeling Research Group (GNUM), Universidad Nacional de Colombia

1. Introduction

Optical Coherence Tomography (OCT) is a non-invasive optical technique based on the Michelson interferometry principle. OCT measurements can reach 1µm lateral resolution and 2mm in measuring depth and it is the first non-invasive and in-vivo imaging technique that enable to image biological tissue in depth with such lateral solution [1]. According to [2], muscle type IID/X fiber is about 63±1.0µm, so that OCT acquisition enhanced with optical clearing might enable to distinguish muscle fibres. This morphological non-destructive imaging technique is associated to Digital Volume Correlation DVC to perform multiscale mechanical characterization throughout the muscle depth. A mapping of three-dimensional strain measurements, and normal and shear stresses in skeletal muscle is obtained. Tissue anisotropy and volume changes under physiological and pathological conditions are thus determined. This work can be used to evaluate treatments, such as the injection of utrophin, to assess their effects on the muscle fibres, better understand degenerative pathologies whose pathophysiology has not been precisely described, and help to discover new therapeutic targets and to increase the chances of developing effective therapies.

2. Materials and Methods

OCT imaging was performed on Extensor Digitorum Longum (EDL) muscle extracted from 6-month-old wistar rats (398±35g). Rats were sacrificed by isoflurane induction followed by exagon injection. Before imaging, muscles were thawed overnight at 4°C, and immersed for one hour in a solution of 80% (v/v) PG in Phosphate Buffered Saline. An OCT system (Thorlabs OCT-TEL220C1, central wavelength: 1,300nm, focal length: 18mm, maximum sensitivity range: 111dB at 5.5kHz) was used for imaging. Lateral and vertical resolution were set to 3µm and 2.45µm. For morphological architecture analysis, histology using azorubine is made on EDL rat muscle [3]. DaVis® software was used to extract three-dimensional strain measurements, and derive normal and shear stresses in skeletal muscle. Mechanical properties were then identified

3. Results

OCT imaging enable to distinguish the different components of muscle. A similar structure is observed on histological images. fibers diameter has been measured. Mean ± standard variation fiber diameter measured on OCT images is d_{OCT}=45±12µm on that of histological images is d_{hist}=32±7µm. Both are within the same order of magnitude but d_{OCT} is higher than d_{hist}. A volumetric mapping of the mechanical properties of the muscle was derived.

4. Discussion and Conclusions

OCT enable to accurately image skeletal muscle structure, and preserve it for mechanical testing. This technique associated with DVC permit to study the local mechanical properties of skeletal muscle [4]. This combination can be used to develop effective therapies for degenerating diseases.

5. References

1. J. G. Fujimoto et al, Neoplasia, 2(1-2):9-25, 2000
2. M. D. Delp et al, J. Appl. Physiol., 80(1):261-270, 1996.
3. M. Kammoun, et al, Eur. J. Histochem., 58(2):163–168, 2014.
4. V. A. Acosta Santamaría, Front. Mech. Eng. 4:1-14, 2018.

CMBBE2023
18th International Symposium on Computer Methods in Biomechanics and Biomedical Engineering
3 - 5 May 2023, Paris, France
Arts et Métiers Institute of Technology
Institut de Biomécanique Humaine Georges Charpak
155 boulevard de l'Hôpital 75013 Paris France
www.cmbbe-symposium.com

USING MACHINE LEARNING FOR DRUG DISCOVERY IN IBD

Sarah Kidwai (1), David Rojas-Velazquez (1,2), Dora Kožinec(1), Péter Tőzsér(1), Lukas Vaišvilas(1), Paula Perez-Pardo(1), Alejandro Lopez-Rincon (1,2)

1. Utrecht University, Pharmacology, Netherlands; 2. Julius Center UMC Utrecht, Netherlands

1. Introduction

Inflammatory Bowel Disease (IBD) refers to two conditions: ulcerative colitis (UC) and Crohn disease (CD) [1]. IBD has a range of clinical symptoms including abdominal pain, diarrhoea, weight loss, constipation, and fatigue [2]. The main cause of IBD is unknown, but it is the result of a weakened immune system. The possible causes of IBD involve genetic and environmental factors. Unfortunately, with conventional diagnostic methods it is hard to predict therapeutic responsiveness of patients beforehand [3]. Genetic expression may be a valuable prediction tool to determine patient' responsiveness to treatment.

2. Materials and Methods

mRNA data from *Arijs et al* [4] was analysed with Recursive Ensemble Feature Selection (REFS). The data has 120 colonic biopsies of patients and 12 healthy controls. The REFS algorithm uses 8 classifiers from the sci-kit toolbox [5] in a nested 10-fold cross-validation and then we validate our results with 5 new classifiers to avoid overfitting. Finally, as a measure for diagnostic accuracy we used the ROC curve[6].

3. Results

5 resulting features were selected from the original 33252: 7922994 (*FAM5C)*, 7905881 (*ADAM15)*, 7894470 (N/A), 7995803 (*MT1JP)* and 7927288 (*SHLD2P3)*.

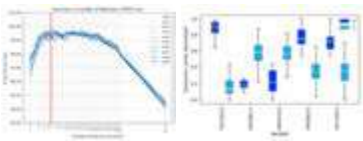

Figure 1: 10 runs of REFS algorithm, with best answer at 5 genes (left). Boxplot of the 5 selected features comparison between healthy controls and IBD (right).

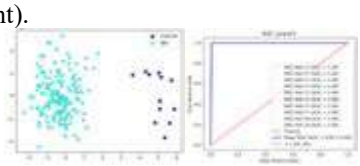

Figure 2: PCA plot of IBD and control groups (left), ROC Curve with an AUC of 0.99 using the 5 selected features(right).

4. Discussion and Conclusions

FAM5C is the most important gene found by REFS to differentiate IBD patients compared to healthy controls. In colonic tissue, gene expression sites are mainly located in the cytoskeleton region of the brush border membrane. Smith et al. suggested that *FAM5C* under expression may cause membrane damage in patients, therefore serving as a susceptibility factor for IBD [7]. *FAM5C* expression is upregulated by inflammatory stimuli such as TNF-α [8]. By inhibiting proinflammatory pathways such as NF-κB, increased *FAM5C* expression could be reversed. These results correlate with new IBD therapy, Cyclosporine's effects. Cyclosporine decreases the expression of *FAM5C*, and it is also a NF-κB and JNK inhibitor [9].

5. References

[1] Sairenji, T., Collins, K. L., & Evans, D. V. (2017). An Update on Inflammatory Bowel Disease. Primary Care: Clinics in Office Practice, 44(4), 673–692. https://doi.org/10.1016/j.pop.2017.07.010

[2] Flynn, S., & Eisenstein, S. (2019). Inflammatory Bowel Disease Presentation and Diagnosis. Surgical Clinics of North America, 99(6), 1051–1062. https://doi.org/10.1016/j.suc.2019.08.001

[3] Wang, M. H., Friton, J. J., Raffals, L. E., Leighton, J. A., Pasha, S. F., Picco, M. F., Cushing, K. C., Monroe, K., Nix, B. D., Newberry, R. D., & Faubion, W. A. (2019). Novel Genetic Risk Variants Can Predict Anti-TNF Agent Response in Patients with Inflammatory Bowel Disease. Journal of Crohn's & colitis, 13(8), 1036–1043. https://doi.org/10.1093/ecco-jcc/jjz017

[4] Arijs, I., De Hertogh, G., Lemmens, B., Van Lommel, L., de Bruyn, M., Vanhove, W., ... & Vermeire, S. (2018). Effect of vedolizumab (anti-α4β7-integrin) therapy on histological healing and mucosal gene expression in patients with UC. Gut, 67(1), 43-52.

[5] Pedregosa, F., Varoquaux, G., Gramfort, A., Michel, V., Thirion, B., Grisel, O., ... & Duchesnay, E. (2011). Scikit-learn: Machine learning in Python. The Journal of machine Learning research, 12, 2825-2830.

[6] Šimundić, A. M. (2009). Measures of diagnostic accuracy: basic definitions. ejifcc, 19(4), 203.

[7] Smith, P. J., Levine, A. P., Dunne, J., Guilhamon, P., Turmaine, M., Sewell, G. W., O'Shea, N. R., Vega, R., Paterson, J. C., Oukrif, D., Beck, S., Bloom, S. L., Novelli, M., Rodriguez-Justo, M., Smith, A. M., & Segal, A. W. (2014). Mucosal transcriptomics implicates under expression of BRINP3 in the pathogenesis of ulcerative colitis. Inflammatory Bowel Diseases, 20(10), 1802–1812. https://doi.org/10.1097/MIB.0000000000000169

[8] Sato, J., Kinugasa, M., Satomi-Kobayashi, S., Hatakeyama, K., Knox, A. J., Asada, Y., Wierman, M. E., Hirata, K. I., & Rikitake, Y. (2014). Family with Sequence Similarity 5, Member C (FAM5C) Increases Leukocyte Adhesion Molecules in Vascular Endothelial Cells: Implication in Vascular Inflammation. PLOS ONE, 9(9), e107236. https://doi.org/10.1371/JOURNAL.PONE.0107236

[9] Weissman, S., Chris-Olaiya, A., Mehta, T. I., Aziz, M., Alshati, A., Berry, R., Fatima, R., Kolli, S., Hassan, A., & Sciarra, M. A. (2019). A novel player: cyclosporine therapy in the management of inflammatory bowel disease. Translational Gastroenterology and Hepatology, 4. https://doi.org/10.21037/TGH.2019.08.08